Formation and migration histories of giant exoplanets in multi-stellar systems

Thesis by

Henry Hoang Khoi Ngo

In Partial Fulfillment of the Requirements for the
Degree of
Doctor of Philosophy

CALIFORNIA INSTITUTE OF TECHNOLOGY
Pasadena, California

2017
Defended 19 May 2017

Henry Hoang Khoi Ngo
ORCID: 0000-0001-5172-4859

For Mom, Dad,
Laura and our little chip

"Decide in your heart of hearts what really excites and challenges you, and start moving your life in that direction. Every decision you make, from what you eat to what you do with your time tonight, turns you into who you are tomorrow, and the day after that. Look at who you want to be, and start sculpting yourself into that person. You may not get exactly where you thought you'd be, but you will be doing things that suit you in a profession you believe in. Don't let life randomly kick you into the adult you don't want to become."

—Chris Hadfield, Commander, Expedition 35, International Space Station

ACKNOWLEDGEMENTS

I am grateful for everyone who has supported me as I worked towards this dissertation. I want to thank my advisor, Heather Knutson, for her scientific advice and mentorship during the past five years. She encourages her students to pursue interesting research opportunities, to become excellent colleagues, and to have a healthy work-life balance. Heather will continue to be a role model for me in years to come. I also want to thank Dimitri Mawet, who agreed to join my thesis committee during his first weeks at Caltech, for providing an opportunity to work with the vortex coronagraph and for entrusting an exciting new planet finding project with me.

I have benefited from the Planetary Science faculty's open-door policy, which has made it easy to build a mentoring network. I am thankful for the advice from my committee members: Mike Brown, Geoff Blake and Konstantin Batygin. I appreciate the friendship and mentorship from the postdocs, especially Courtney Dressing, Gary Ruane, Björn Benneke, Brendan Bowler, and Sasha Hinkley. I am also thankful for friends, collaborators and advisors at the University of British Columbia and Queen's University.

Many people in the GPS Division and Planetary Science Department have improved my graduate student life. I am proud to be a member of the "Captains Planet", with Lu Pan, Mike Wong, Danielle Piskorz, and Joe O'Rourke. Thank you for working with me on homework, studying with me for quals and providing moral support. I also appreciate scientific and life advice from grad students that went through before me: Alex Lockwood, Aaron Wolf, Josh Kammer, and Miki Nakajima. I have enjoyed fun scientific and not-so-scientific discussions with Peter Buhler, Chris Spalding, Nancy Thomas, and Peter Gao. Extra thanks to Peter Gao for your friendship over the last 10 years over two academic programs. Although I cannot name all the awesome students in our Division here, I am thankful for our dodgeball team ("The Late Heavy Bombardment"), our softball team ("Strike-slip"), and all the social events we do together. Special thanks to Mike Wong for collaborating with me on many of these projects. Finally, I am extremely grateful for the wonderful and caring staff members that have helped me along the way, both in the Division and the department, especially Dian Buchness, Liz Boyd, Julie Lee, Julia Zuckerman, Aleen Boladian, Margaret Carlos, Ulrika Terrones, Irma Black, and Mike Black.

Moving to Caltech was a big change for Laura and me, but there were many wonderful

people that helped us feel at home. Thank you to Laura Flower Kim and Daniel Yoder at the International Student Office; Natalie Gilmore, Felicia Hunt, and Kate McAnulty at the Graduate Office; and Kurt Murdoch and Kevin Lee at Human Resources. I am also grateful for the opportunity to improve graduate student life with the Graduate Student Council. Thank you to all of my colleagues on the Board of Directors over the past four years.

I am very grateful for my parents' love and support over the past 30 years. After the Vietnam War, they took great risks and made huge sacrifices. They left everything they knew behind to immigrate to Canada as refugees to create a better life for themselves and their future children. They taught me the importance of education and hard work, which has helped me become the person I am today.

Finally, and most importantly, none of this would have been possible without Laura. Thank you for always being there for me. When I feel overwhelmed by a challenge, I know I can always count on your unconditional love and support. No words can capture how much love I have for you and how fortunate I feel to have you as my life partner in every sense of the word. Over the past 15 years, we have had many adventures and I am looking forward to many more in the years to come.

ABSTRACT

The first planets discovered outside of our solar system were very different from the solar system planets. These discoveries raised new challenges to planet formation models, which were designed to explain the origin of the solar system planets. One particularly intriguing population, the "hot Jupiters" were some of the first planets discovered. These gas giant planets have masses similar to Jupiter and Saturn, however, they were found on orbits 100 times closer to their star than Jupiter is to the sun. Proposed formation scenarios involve models that argue for formation at presently observed locations, but these are challenged by the lack of planet-building materials so close to the host star. Other models assume these planets form at more moderate locations, perhaps in a manner similar to Jupiter and Saturn, followed by inward migration via some other mechanism. These models are challenged by the lack of a known migration mechanism.

This dissertation compiles three studies conducted over the past five years to investigate the formation and migration histories of gas giant exoplanets. After the discovery of the first hot Jupiter, additional discoveries revealed some population characteristics that could provide evidence for certain formation or migration scenarios. A large fraction of hot Jupiters were found to have eccentric orbits and/or misaligned orbits relative to the star's spin axis. These properties suggest that a gravitational interaction with an additional massive object may have played a role in the dynamical history of these hot Jupiters. Studies of stellar multiplicity for nearby, sun-like stars have also revealed that multi-stellar systems are common.

The studies presented in this dissertation investigate whether stellar companions to giant planet systems influence the planets. In the first and second study, we conduct a survey for stellar companions around stars that host hot Jupiters detected by the transiting method. The first study examines whether stars hosting misaligned planets are more likely to host a companion star. We found no such correlation, suggesting that stellar companions do not play a dominant role in causing planetary misalignment. In the second study, we look at the population of stellar companions as a whole to quantify the fraction of hot Jupiters that might have migrated due to stellar interactions. We find that less than 20% of hot Jupiters might have experienced this migration scenario. However, we do find that hot Jupiters are three times more likely to be in a wide multi-stellar system compared to nearby stars that do not host hot Jupiters, suggesting some other connection between the companion

star and the giant planet.

In the third study, we search for stellar companions around stars that host giant planets over a wide range of separations, from the close-in hot Jupiters to giant planets as far away as Jupiter is to our sun. These planets were found via the radial velocity method. We compare the giant planets' orbital properties for single- and multi-stellar systems to determine whether planets in multi-stellar systems show some evidence for star-planet interactions. With the current dataset, we find no evidence to support the hypothesis that planets in multi-stellar systems have a different set of orbital properties.

Finally, we present preliminary results of an ongoing survey to understand giant planet formation on the other extreme end. Instead of hot Jupiters on close-in orbits, this survey seeks to explain the origin of the very distant giant planetary mass objects found by direct imaging surveys. These objects are often found on separations that are ten to one hundred times farther away than Neptune is to our sun. Due to their distance and size, it's not certain if these objects are some of the biggest planets in existence or if they are the smallest stars. This new survey will search for planets to serve as the link between known giant exoplanets and these unknown directly imaged objects.

PUBLISHED CONTENT AND CONTRIBUTIONS

Ngo, H., H. Knutson, S. Hinkley, et al. (2015). *The Astrophysical Journal* **800**, 138. DOI: 10.1088/0004-637X/800/2/138.

H. Ngo conducted the observations, processed the data, analyzed the results and wrote the manuscript. H. Knutson advised this project. Reproduced with permission from the American Astronomical Society (copyright holder).

Ngo, H., H. A. Knutson, S. Hinkley, et al. (2016). *The Astrophysical Journal* **827**, 8. DOI: 10.3847/0004-637X/827/1/8.

H. Ngo conducted the observations, processed the data, analyzed the results and wrote the manuscript. H. Knutson advised this project. Reproduced with permission from the American Astronomical Society (copyright holder).

Ngo, H., H. A. Knutson, M. L. Bryan, et al. (2017). *The Astronomical Journal* **153**, 242. DOI: 10.3847/1538-3881/aa6cac.

H. Ngo conducted the observations, processed the data, analyzed the results and wrote the manuscript. H. Knutson advised this project. Reproduced with permission from the American Astronomical Society (copyright holder).

TABLE OF CONTENTS

LIST OF ILLUSTRATIONS

LIST OF TABLES

Chapter 1

INTRODUCTION

1.1 Exoplanet discoveries challenge planet formation models

In the early 1990s, the first confirmed detections of exoplanets—planets around other stars—revealed planets that were unlike any of the objects in our own solar system. Wolszczan and Frail (1992) reported that the pulsar PSR B1257+12 hosts two planets, at orbital separations of 0.36 au (astronomical unit; equal to the average distance between the earth and the sun, or 1.5×10^{11} m) and the other at 0.46 au, corresponding to orbital periods of 66.5 days and 98.2 days, respectively. These distances are similar to the closest planet in our solar system, Mercury, which has a mean orbital separation of 0.39 au and an orbital period of 88 days. The planetary masses are about four times as massive as the earth, which is unlike any other planet in our solar system. A few years later, Wolszczan (1994) announced a third planet in the system, at a separation of 0.19 au, or an orbital period of 25.3 days. This third planet is smaller than any planet in our solar system, with a mass similar to those of Ganymede and Titan, the largest moons around Jupiter and Saturn, respectively. The detection of this planetary system and its planets with masses unlike our solar system planets and separations smaller than Mercury raises interesting questions about planet formation processes. And perhaps most surprisingly, all three planets orbit around a pulsar, instead of a hydrogen-burning main-sequence star like our Sun. Pulsars are the remnant cores of massive stars which exploded in a supernova. Therefore, planets around pulsars must either somehow survive this catastrophic event, or their formation happens after the pulsar is formed. If this is the case, these "second-generation" planets must have formed in a very different environment, and potentially via a different mechanism than the planets in our solar system (see review by Martin et al., 2016).

The next planetary system discovered raised even more questions than the first. Mayor and Queloz (1995) presented 51 Pegasi b, a giant planet and the first confirmed exoplanet found around a sun-like star. At half the mass of Jupiter, this new planet's size is not too different from the solar system giant planets. However, its orbital separation was even more surprising than the PSR B1257+12 planets. 51 Pegasi b has an orbital separation of 0.05 au, eight times smaller than Mercury's orbit,

corresponding to an orbital period of only 4.2 days. These extreme levels of stellar irradiance results in a planetary temperature of 1300 K. This discovery prompted a new class of planet not seen in our solar system, the "hot Jupiters". More hot Jupiters were discovered in the coming years and these planets challenged giant planet formation models based on Jupiter and Saturn. For example, would there be enough materials at separations less than 0.1 au available to form into a rocky core massive enough to accrete the giant planet's gaseous envelope? Would the conditions close the star allow a planet to gravitationally retain an envelope? Or, did these hot Jupiters originally form further away from their star, at locations similar to Jupiter and Saturn and then migrate inwards to their present-day locations? If so, what are the driving forces behind this migration? Classical core accretion models based on the solar system (e.g. Lissauer and Stewart, 1993; Pollack et al., 1996; Kokubo and Ida, 1996; Ward, 1997; Boss, 1997; Kokubo and Ida, 1998; Duncan et al., 1998) did not anticipate the existence of hot Jupiters, suggesting that our understanding of planet formation and migration was (and perhaps still is) incomplete.

1.2 Exoplanet detection methods

Figure 1.1 shows all confirmed exoplanets from the NASA Exoplanet Archive[1] as of May 2017 with mass and semi-major axis measurements. The majority of confirmed planets, 3358 out of 3483, are found via the transiting and radial velocity (RV) methods. This dissertation examines the formation and migration histories of giant exoplanets discovered by these two methods. A brief explanation of these two methods follows; the remaining methods are beyond the scope of this work.

The radial velocity detection method

The radial velocity (RV) method was responsible for the discovery of 51 Pegasi b and many of the initial planet discoveries around sun-like stars. In a distant planetary system, the target star orbits around the system's center of mass. From the point of view of an observer on earth, the star's 3-dimensional motion can be separated into components along the observer's line of sight and components in the plane of the sky. The RV method infers the existence of planets based on this line-of-sight motion. Another method, astrometric planet detection, uses the components of motion in the sky's plane, however this method will not be discussed in this dissertation. Although the line-of-sight motion of a planet-hosting star is small, it

[1] https://exoplanetarchive.ipac.caltech.edu/

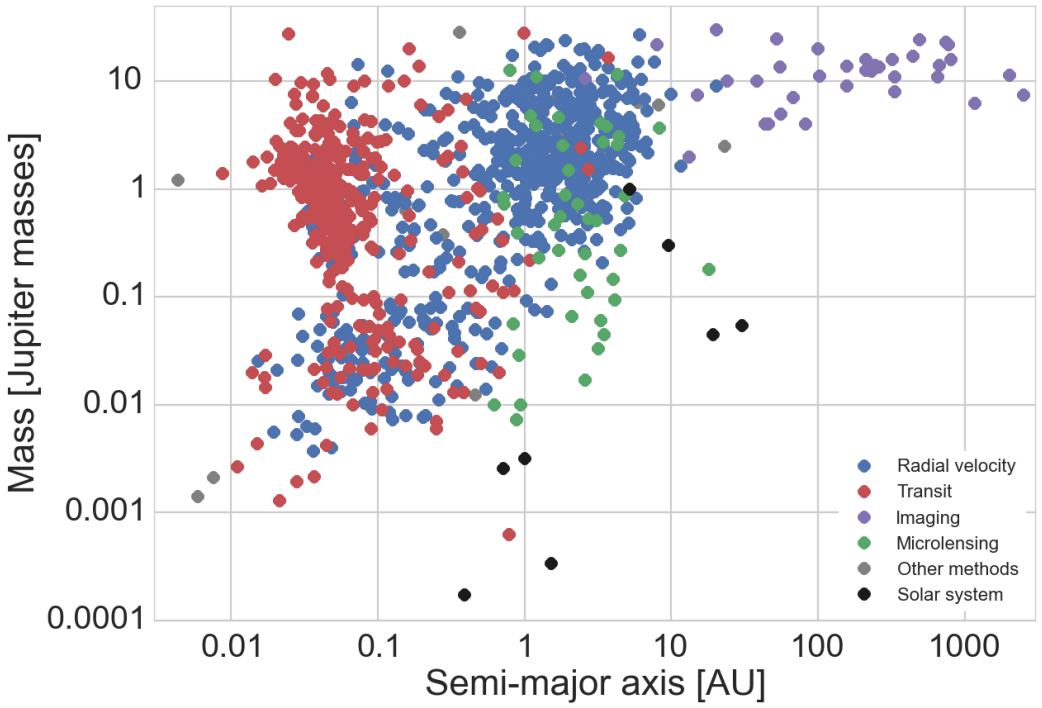

Figure 1.1: Masses and orbital semi-major axes of confirmed exoplanets with known measurements as of May 2017. The color of each point indicates the detection method: transit (red), radial velocity (blue), microlensing (green), imaging (purple), and all other methods (gray). The eight solar system planets are also shown as black points.

creates a periodic Doppler effect on the star's spectral signature. With a properly calibrated spectrograph, an observer can measure the relative shift in wavelength of certain spectral lines due the star's motion and calculate the relative RV of this motion. Since the motion is periodic, repeat observations allow an observer to map the change in measured RV over the course of the planet's orbit. The period of this RV curve is the period of the planet's orbit, the shape indicates the planetary eccentricity (circular orbits generate sinusoidal curves, more eccentric orbits add more skewness) and the RV semi-amplitude K depends on planetary properties as

$$K = \frac{28.4329\,\mathrm{m\,s^{-1}}}{\sqrt{1-e^2}} \frac{m_2 \sin i}{\mathrm{M_{Jup}}} \left(\frac{m_1 + m_2}{\mathrm{M_\odot}}\right)^{-2/3} \left(\frac{P}{1\,\mathrm{yr}}\right)^{-1/3}, \tag{1.1}$$

where e is the planet's orbital eccentricity, P is the planet's orbital period, i is the orbital inclination, and m_1 and m_2 are the star's and planet's masses, respectively. The inclination i follows a convention where a face-on orbit (entirely in the plane of the sky) is defined as $i = 0°$, which produces zero RV signal as all of the motion is in the plane of the sky. Therefore, characterizing the RV curve's semi-amplitude can only reveal the minimum mass of a planet, $m_2 \sin i$, as the orbit's orientation is

unknown. A review of this technique can be found in Lovis and Fischer (2010).

As of May 2017, the NASA Exoplanet Archive reports 632 confirmed exoplanets first discovered with the RV technique, and, at this time, the main contributors are the HARPS surveys (Lagrange et al., 2009) and the California Planet Survey (Howard et al., 2010) using the Keck HIRES instrument. Large planets that are close to stars generate larger RV signals which make them easier to detect, so hot Jupiters account for a large number of RV detected planets, especially in the beginning. Equation 1.1 shows that a Jupiter-mass planet orbiting at 1 au around a solar-mass star will generate a signal of 28.4 $\mathrm{m\,s^{-1}}$ while the same planet at 0.1 au will generate a 89.8 $\mathrm{m\,s^{-1}}$ signal. On the other hand, a Neptune-mass object at 1 au or a super-Earth at 0.1 au produce signals of a few $\mathrm{m\,s^{-1}}$, which is currently the limit of our sensitivity. RV signals from Earth-mass planets at Earth-like separations are still at least one order of magnitude smaller than the detection limits of current spectrographs. These limits cause RV planet surveys to be biased towards finding more massive planets closer in to their host stars. They are also biased towards nearby stars, up to a few hundred parsecs (pc; 3.1×10^{16} m) away and brighter stars, because the sensitivity to the spectral lines is better with more photons collected. Finally, RV surveys mostly target solar-type stars. Stars hotter than the sun tend to have relatively featureless spectra and are often rapidly rotating, and cooler stars are more active and have relatively large starspot coverage which generate additional periodic signals that can mask the planetary signal. Cooler stars are also very faint in the optical bandpasses used by most current RV instruments.

Previous RV planet surveys mostly operated in optical bandpasses. However, future instrumentation can improve RV precision in both optical and near-infrared bandpasses. In a review by Fischer et al. (2016), they identify potential avenues for achieving higher precision RV observations. These include higher spectral resolution to distinguish line shifts from changes in the line shape, increased instrumental stability, and better wavelength calibrators. They also recommend RV surveys in infrared bandpasses to better study the coolest stars and to minimize noise from star spots.

The transit detection method

The transit method has, to date, produced the largest number of confirmed exoplanets, accounting for 2726 out of 3483 confirmed exoplanets on the NASA Exoplanet Archive. For some distant planetary systems, the planet's orbit may be edge-on,

with $i = 90°$, so that the planet will pass directly between the observer and the target star. Although we cannot directly image the planet as it crosses the face of the star, observers can detect a dimming of starlight while the planet is transiting the star. The periodicity of this signal allows observers to infer the existence of a planet orbiting at the same period. If the planet also emits or reflects a small amount of light when the planet passes behind the star, known as an occultation or a secondary eclipse, there is a much smaller dimming of light as well. The duration of the transit and occultation leads to an estimate of orbital eccentricity, as a circular orbit would have the same duration for both events. Neglecting small effects such as light from the planet's nightside and limb-darkening due to the fact that stellar disks are brighter in the center compared to the limbs, the transit depth, δ, corresponding to the maximum amount of light loss is

$$\delta = \left(\frac{R_\mathrm{p}}{R_\mathrm{s}}\right)^2. \tag{1.2}$$

This ratio of planetary radius to stellar radius allows for a direct measurement of the planet's size if the stellar properties are well constrained. Unlike the RV method, the transit method does not provide any estimate of planetary mass, but RV instruments often follow up transiting planet detections in order to make mass estimates. The inclinations of transiting systems are well constrained, as they must be close to edge-on, so the measured $m_2 \sin i$ from RV characterization can be converted to the planet's true mass. Combining RV and transit observations allow for planetary density measurements, which constrain the planet's bulk composition. However, transiting systems require fortunate geometry. Allowing for grazing transits, in which the planet's cross section does not fully transit the star, the probability of a transit, p_transit, is

$$p_\mathrm{transit} = \frac{R_\mathrm{s} + R_\mathrm{p}}{a(1 - e^2)}, \tag{1.3}$$

where a is the planet's orbital semi-major axis and e is the planet's orbital eccentricity. Winn (2010) provides a full review of the transiting planet detection technique.

Transiting planet surveys are more sensitive to planets on shorter orbital periods, such as hot Jupiters. A planet on a 0.1 au circular orbit around a sun-like star has a transit probability of only 0.5%, and this probability drops off as $1/a$, much faster than the RV semi-amplitude signal, which drops off as $1/\sqrt{a}$. In addition, transiting surveys are more sensitive to larger planets. A Jupiter-radius planet around a sun-like star would dim the star's light by 1%. As transit depth is proportional to the

square of the ratio of planetary radius to stellar radius, this signal drops off quickly for smaller planets. An earth-radius planet, at one-tenth the radius of a Jupiter-sized planet, would produce a transit depth 100 times smaller. Therefore, like RV surveys, transiting planet surveys are strongly biased towards finding larger, closer-in planets such as hot Jupiters. However, unlike RV surveys, it is possible to survey a large number of stars simultaneously as only photometry is required. The *Kepler* space telescope (Borucki et al., 2010) took this concept to its logical end and became the most successful planet-finding machine to date. *Kepler* stared at one dense region of sky and continuously surveyed over 150,000 stars over the course of its four year mission. Therefore, while RV planet surveys target nearby stars in all directions, the majority of transiting planets come from a brightness-limited survey in one single direction, and these stars have a large range of distances, up to 1000 pc. After *Kepler's* reaction wheels failed in 2013, the same telescope was repurposed for the K2 mission, which served as a transiting-planet finder at various points in the ecliptic plane for 90 days at a time, allowing detection of closer-in planets but from different parts of the galaxy. From the ground, the HATNet (Bakos et al., 2004) and WASP (Pollacco et al., 2006) surveys have been the most productive ground-based transiting surveys to date, but are primarily to short-period gas giant planets around nearby sun-like stars.

Future transiting planet surveys include CHEOPS (Fortier et al., 2014) and TESS (Ricker et al., 2014), both with planned launch dates in 2018. CHEOPS will target bright stars already known to host planets for planet characterization, specifically those hosting small planets detected by RV surveys and transiting Neptune-sized planets found by ground-based surveys. Although *Kepler* found a large number of transiting planets, many of them will be very challenging to characterize with RV followup. On the other hand, TESS will be a new two-year all-sky mission to detect new exoplanets around nearby stars via the transiting technique. TESS has a specific goal of finding small rocky planets around bright stars, which can then be further characterized by ground-based spectrometers and other missions such as CHEOPS. Like future RV planet surveys, TESS will also search for planets around smaller M-stars.

1.3 Population properties of gas giant exoplanets

Figure 1.2 shows the distribution of planetary radii for confirmed exoplanets with measured planetary radii. Without correcting for detection effects, the super-Earth planet type is the most common, even though there are no currently known super-

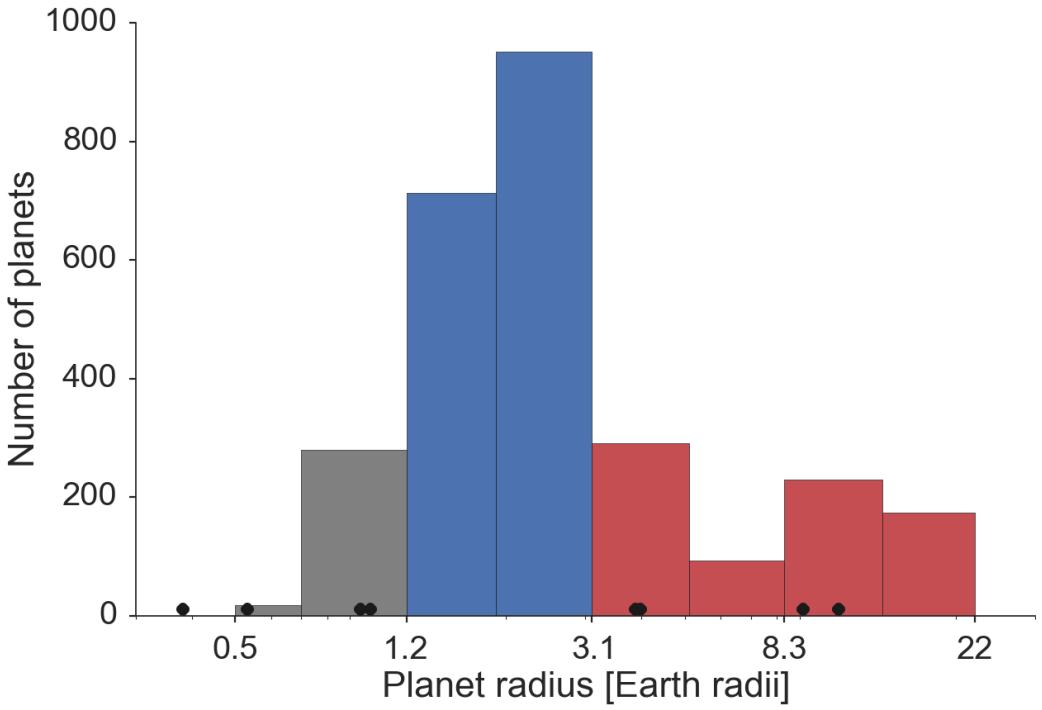

Figure 1.2: Distribution of planetary radii for confirmed exoplanets. The histogram bars are colored to show three rough size classes: Earth-like (gray), super-Earths (blue) and giant planets (red). Black circles indicate solar system planets, of which there are no super-Earths.

Earths in our solar system. Super-Earths are planets more massive than Earth, but smaller than the solar system's next largest planets, Uranus and Neptune. Giant planets are also numerous but this is a result of the selection bias towards detecting giant planets discussed in the previous section. Fressin et al. (2013) corrected for these factors and determined that giant planets with radii of 4-22 times earth's radius and orbital periods of 0.8-418 days occur in about 10% of sun-like stars. For giant planets with orbital periods of less than 10 days (i.e. hot Jupiters), earlier surveys of solar neighborhood stars reported that hot Jupiters have a 1% occurrence rate around sun-like stars, however, *Kepler* survey results estimate an occurrence rate of 0.5% (Howard et al., 2012).

Previous studies have considered whether there is a link between host star properties and the presence of giant planets. Fischer and Valenti (2005) conducted a spectroscopic survey to model the stellar properties of 850 sun-like stars targeted in RV planet search surveys at that time. They ensured that their sample included all stars with RV measurements capable of detecting an RV semi-amplitude signal of $30\,\mathrm{m\,s^{-1}}$ or larger, to ensure that no close-in Jupiter-mass planets would be missed.

They found that 25% of stars with metallicities[2] of [Fe/H] greater than 0.3 dex host a giant planet and that higher metallicity stars are much more likely to host giant planets. They conclude that giant planets are more likely to form in higher metallicity environments due to the increased surface density of solid materials in the disk, which are required to form the massive cores of giant planets. Recent analysis by Thorngren et al. (2016) also show that most giant planets appear to be enriched in heavy elements as compared to their host stars, with Neptune-sized planets having a larger fractional core size than their Jovian counterparts. These results support the core accretion model of giant planet formation, where a solid core forms first, followed by accretion of the gaseous envelope.

Orbital eccentricity provides another clue to the dynamical history of gas giant exoplanets. Wright et al. (2009) first suggested a correlation between the distribution of orbital eccentricity and planetary mass. They considered all RV-detected giant planets with semi-major axes greater than 0.1 au to avoid the effects of tidal circularization and found that planets with minimum masses above 1 M_{Jup} have a mean eccentricity of 0.34 while planets below this mass limit have a mean eccentricity of 0.19. Figure 1.3 repeats this analysis for the current confirmed exoplanet list. The giant planets' eccentricity distributions show more systems at higher eccentricities than the subgiant planets. The corresponding average eccentricity values are 0.27 and 0.19, for giant and sub-giant planets, respectively. Non-zero eccentricities could indicate that these planet histories included interactions with other planets or other stars.

The final property of giant planets relevant to this dissertation is the sky-projected spin-orbit angle λ. For a given planetary orbit, this angle measures the misalignment between the star's spin axis and the planet's orbital angular momentum vector, as projected onto the sky-plane. A retrograde orbit has $\lambda > 90°$. In the nebular hypothesis, planetary systems form from dense clouds of gas, collapsing into a spinning disk which forms the star and planets. In this simple model, conservation of angular momentum requires the disk to be aligned to the star's spin, so λ should be zero. However, dynamical interactions with other objects, such as a passing star or a companion star, could either alter the disk's alignment or knock the planets out of the disk, causing misaligned orbits. Interactions between planets forming in a disk could also cause a similar effect. Therefore, a non-zero measurement of

[2] [Fe/H] is a measure of the ratio of the amount of iron to hydrogen present in a star relative to the Sun's ratio. It is a logarithmic measure, so [Fe/H]=0 corresponds to a star with the same ratio as the Sun while [Fe/H]=1 corresponds to a ratio ten times greater than the Sun's.

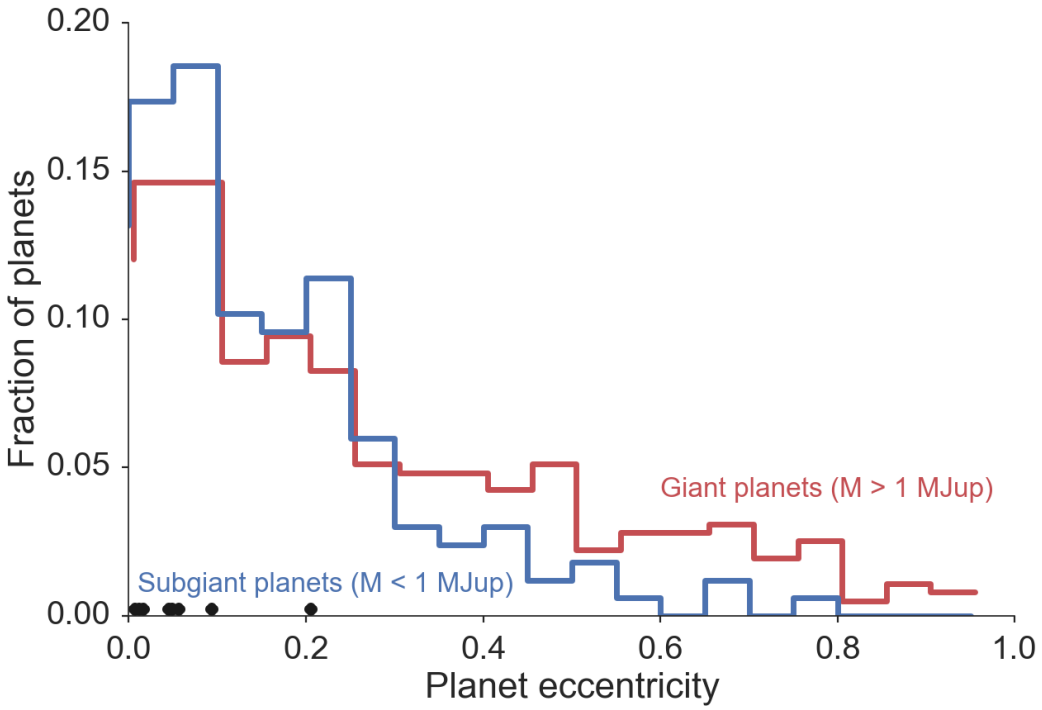

Figure 1.3: Distribution of orbital eccentricity of RV-detected giant ($M > 1\mathrm{M_{Jup}}$, red) and sub-giant($M < 1\mathrm{M_{Jup}}$, blue) planets with semi-major axes greater than 0.1 au. These distributions show more likelihood of larger eccentricities for giant planets, as first suggested by Wright et al. (2009). Black circles show the solar system planets (Mercury is the most eccentric) for comparison.

λ suggests that the planetary system may have encountered a stellar companion in the past. Winn et al. (2010) noted that a significant fraction of hot Jupiters are on misaligned orbits, and in particular, hotter stars are more likely to host misaligned hot Jupiters. For hot Jupiters with measured spin-orbit angles, Figure 1.4 plots λ against host star temperature, recreating the plot from Winn et al. (2010) with additional planets.

1.4 Finding stellar companions through Keck direct imaging

Studies of nearby, solar-neighborhood (within 25 pc) sun-like stars reveal that almost half of all stars have at least one stellar companion (Duquennoy and Mayor, 1991; Raghavan et al., 2010). Although our solar system is not in a multi-stellar system, the ubiquity of stellar companions suggests that stellar companions may have dynamically influenced the giant planets orbiting the host star. This dissertation collects three direct imaging surveys to find these stellar companions, characterize them, and constrain their potential effects on giant planets.

In our surveys, we target sun-like stars known to host giant planets to search for

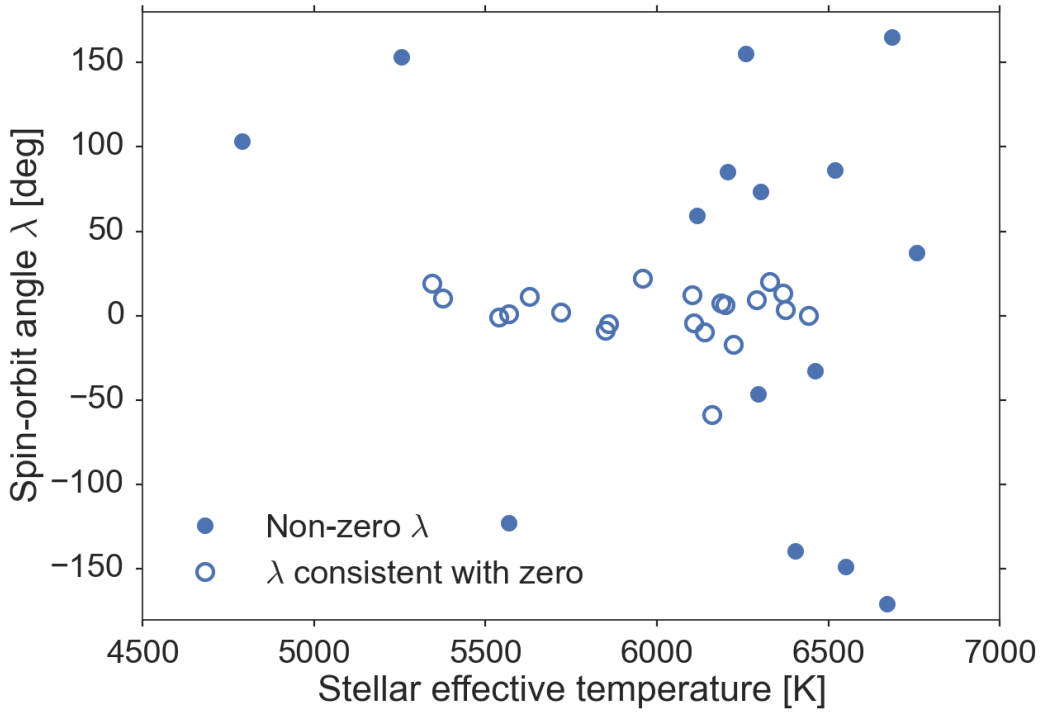

Figure 1.4: Distribution of hot Jupiter spin-orbit angles and stellar effective temperature. Planets having λ that are 3σ away from zero are plotted with solid symbols, while planets having λ consistent with zero within 3σ are plotted as open symbols.

companion stars. These companion stars are M-stars, which are smaller stars than the planet host and emit light redder than planet host. An infrared imager, such as the NIRC2 camera at the Keck Observatory, is most sensitive to the redder light emitted by the companion stars. Although archival images of stars are often used to identify stellar companions, in order to find companions close enough to dynamically influence planets, surveys require the ability to resolve light from the stellar companions at small on-sky angular separations. For a circular aperture, a telescope's resolving power is approximately $1.22\lambda/D$ where λ is the operating wavelength of the instrument and D is the telescope's diameter. With this approximation, Keck's NIRC2 Ks-band filter and large telescope diameter has a resolving power of about 50 milliarcseconds. However, the earth's atmosphere distorts the incoming starlight and reduces the telescope's spatial resolution. As starlight travels through the earth's atmosphere, each atmospheric layer is at a different temperature and refracts light a little differently, spreading the point source of light over a wide area. The atmosphere may also absorb photons, reducing the amount of light received by the camera. These effects make it difficult to detect and resolve stellar companions. In order to overcome the atmospheric effects, we make use of Keck's

adaptive optics (AO) system, which includes a deformable mirror that can adjust its shape to cancel out the atmospheric distortions in the incoming starlight. This is an automatic closed-loop system that uses the optical light entering the telescope to measure the distortions and correct them in real time, while the infrared light is sent to the science instruments. Use of the AO system greatly improves our ability to resolve stars, however, due to the glare from the bright target star, it is difficult to find companion stars closer than 0.3 arcseconds (or 300 millarcseconds). It is possible to use coronagraphs to block out incoming starlight, however, this increases the amount of telescope time required per target and the coronagraph itself would block light within some radius of the target star. The surveys presented in this dissertation did not use a coronagraph to enable a larger sample size in order to draw statistically significant conclusions.

With Keck/NIRC2 and adaptive optics, it is possible to image companions with contrasts up to six magnitudes in K-band at separations around 0.3 arcseconds. A typical companion star near this limit would be a $0.2 M_{\odot}$ star at a separation of 50 au. While RV and transit methods used to find stellar companions have been successful in finding larger and closer-in binary star systems in the past, the typical companion in this dissertation would be beyond the reach of these techniques. Although Equation 1.1 shows that the semi-amplitude of this nominal companion would be large, at over $700\,\mathrm{m\,s^{-1}}$, the period of the signal would be several hundred years, much longer than RV monitoring surveys. Similarly, although a stellar companion would create a very large transiting signal (Equation 1.2), at 50 au, the probability of a transit is 100 times smaller than a hot Jupiter's already low transit probability (Equation 1.3). The probability is even further reduced when considering the short length of the transit compared to the very long period of the stellar orbit. Thus, direct imaging with near-infrared detectors on large telescopes with adaptive optics systems is the best way to search for stellar companions that may have influenced the history of giant planetary systems.

1.5 Organization of this dissertation

In this dissertation, I present three previously published studies to detect and characterize stellar companions to giant planet host stars using the Keck Observatory NIRC2 instrument. These studies investigated the effects of stellar companions on the formation and migration of giant planets. In Chapter 2, we examine the link between transiting hot Jupiters with spin-orbit misalignment and the presence of a companion star. In Chapter 3, we test whether the population of stellar com-

panions to transiting hot Jupiter systems could induce Kozai-Lidov migration in these planets. In Chapter 4, we search for stellar companions around stars hosting RV-detected giant planets on a wide range of separations to determine whether the planetary orbital properties are influenced by the presence of stellar companions. Finally, in Chapter 5, I summarize our major results and propose some additional work motivated by the results of this dissertation.

References

Bakos, G., R. W. Noyes, G. Kovács, et al. (2004). *Publications of the Astronomical Society of the Pacific* **116**, 266. DOI: 10.1086/382735.

Borucki, W. J., D. Koch, G. Basri, et al. (2010). *Science* **327**, 977. DOI: 10.1126/science.1185402.

Boss, A. P. (1997). *Science* **276**, 1836–1839.

Duncan, M. J., H. F. Levison, and M. H. Lee (1998). *The Astronomical Journal* **116**, 2067–2077.

Duquennoy, A. and M. Mayor (1991). *Astronomy & Astrophysics* **248**, 485.

Fischer, D. A., G. Anglada-Escude, P. Arriagada, et al. (2016). *Publications of the Astronomical Society of the Pacific* **128**.964, 066001. DOI: 10.1088/1538-3873/128/964/066001.

Fischer, D. A. and J. Valenti (2005). *The Astrophysical Journal* **622**, 1102–1117. DOI: 10.1086/428383.

Fortier, A., T. Beck, W. Benz, et al. (2014). *Space Telescopes and Instrumentation 2014: Optical, Infrared, and Millimeter Wave*. Vol. 9143, 91432J. DOI: 10.1117/12.2056687.

Fressin, F., G. Torres, D. Charbonneau, et al. (2013). *The Astrophysical Journal* **766**, 81. DOI: 10.1088/0004-637X/766/2/81.

Howard, A. W., J. A. Johnson, G. W. Marcy, et al. (2010). *The Astrophysical Journal* **721**, 1467. DOI: 10.1088/0004-637X/721/2/1467.

Howard, A. W., G. W. Marcy, S. T. Bryson, et al. (2012). *The Astrophysical Journal Supplement Series* **201**, 15. DOI: 10.1088/0067-0049/201/2/15.

Kokubo, E. and S. Ida (1996). *Icarus* **123**, 180–191.

Kokubo, E. and S. Ida (1998). *Icarus* **131**, 171–178.

Lagrange, A.-M., M. Desort, F. Galland, S. Udry, and M. Mayor (2009). *Astronomy and Astrophysics* **495**, 335. DOI: 10.1051/0004-6361:200810105.

Lissauer, J. J. and G. R. Stewart (1993). *Protostars and Planets III*. Ed. by E. H. Levy and J. Lunine. University of Arizona Press, p. 1061.

Lovis, C. and D. Fischer (2010). *Exoplanets*. Ed. by S. Seager, p. 27.

Martin, R. G., M. Livio, and D. Palaniswamy (2016). *The Astrophysical Journal* **832**, 1. DOI: 10.3847/0004-637X/832/2/122.

Mayor, M. and D. Queloz (1995). *Nature* **378**, 355. DOI: 10.1038/378355a0.

Pollacco, D., I. Skillen, A. Cameron, et al. (2006). *Astrophysics and Space Science* **304**, 253. DOI: 10.1007/s10509-006-9124-x.

Pollack, J. B., O. Hubickyj, P. Bodenheimer, et al. (1996). *Icarus* **124**.1, 62–85. DOI: 10.1006/icar.1996.0190.

Raghavan, D., H. A. McAlister, T. J. Henry, et al. (2010). *The Astrophysical Journal Supplement Series* **190**, 1. DOI: 10.1088/0067-0049/190/1/1.

Ricker, G. R., J. N. Winn, R. Vanderspek, et al. (2014). *Journal of Astronomical Telescopes, Instruments, and Systems* **1**. Ed. by J. M. Oschmann, M. Clampin, G. G. Fazio, and H. A. MacEwen, 014003. DOI: 10.1117/1.JATIS.1.1.014003.

Thorngren, D. P., J. J. Fortney, R. A. Murray-Clay, and E. D. Lopez (2016). *The Astrophysical Journal* **831**, 64. DOI: 10.3847/0004-637X/831/1/64.

Ward, W. R. (1997). *The Astrophysical Journal* **482**.2, L211–L214. DOI: 10.1086/310701.

Winn, J. N. (2010). *Exoplanets*. Ed. by S. Seager. University of Arizona Press, p. 55.

Winn, J. N., D. Fabrycky, S. Albrecht, and J. A. Johnson (2010). *The Astrophysical Journal* **718**, L145. DOI: 10.1088/2041-8205/718/2/L145.

Wolszczan, A. (1994). *Science* **264**, 538. DOI: 10.1126/science.264.5158.538.

Wolszczan, A. and D. A. Frail (1992). *Nature* **355**, 145. DOI: 10.1038/355145a0.

Wright, J. T., S. Upadhyay, G. W. Marcy, et al. (2009). *The Astrophysical Journal* **693**, 1084. DOI: 10.1088/0004-637X/693/2/1084.

Chapter 2

NO CORRESPONDENCE BETWEEN HOT-JUPITER SPIN-ORBIT MISALIGNMENT AND THE INCIDENCE OF DIRECTLY IMAGED STELLAR COMPANIONS

This chapter is adapted from work previously published as

Ngo, H., H. A. Knutson, S. Hinkley, et al. (2015). *The Astrophysical Journal* **800**, 138. DOI: 10.1088/0004-637X/800/2/138.

2.1 Abstract

Multi-star systems are common, yet little is known about a stellar companion's influence on the formation and evolution of planetary systems. For instance, stellar companions may have facilitated the inward migration of hot Jupiters towards their present day positions. Many observed short period gas giant planets also have orbits that are misaligned with respect to their star's spin axis, which has also been attributed to the presence of a massive outer companion on a non-coplanar orbit. We present the results of a multi-band direct imaging survey using Keck NIRC2 to measure the fraction of short period gas giant planets found in multi-star systems. Over three years, we completed a survey of 50 targets ("Friends of Hot Jupiters") with 27 targets showing some signature of multi-body interaction (misaligned or eccentric orbits) and 23 targets in a control sample (well-aligned and circular orbits). We report the masses, projected separations, and confirmed common proper motion for the 19 stellar companions found around 17 stars. Correcting for survey incompleteness, we report companion fractions of 48% ± 9%, 47% ± 12%, and 51% ± 13% in our total, misaligned/eccentric, and control samples, respectively. This total stellar companion fraction is 2.8 σ larger than the fraction of field stars with companions approximately 50 − 2000 au. We observe no correlation between misaligned/eccentric hot Jupiter systems and the incidence of stellar companions. Combining this result with our previous radial velocity survey, we determine that 72% ± 16% of hot Jupiters are part of multi-planet and/or multi-star systems.

2.2 Introduction

Surveys of solar-like stars within 25 pc indicate that approximately 44% are found in multiple star systems (Raghavan et al., 2010). At the same time, recent surveys have sought to quantify planet occurrence rates around solar-type FGK stars (e.g. Howard et al., 2012b; Fressin et al., 2013). However, the effects of additional stellar companions on the formation and subsequent evolution of planetary systems are not well understood. A stellar companion might disrupt planet formation by stirring up the disk (e.g. Mayer et al., 2005), truncating the disk (e.g. Pichardo et al., 2005; Kraus et al., 2012), or ejecting planets (e.g Kaib et al., 2013; Zuckerman, 2014). Numerical simulations often fail to produce planets in binary star systems (e.g. Pichardo et al., 2005; Mayer et al., 2005; Thébault et al., 2006; Fragner et al., 2011), suggesting that a stellar companion can indeed hinder planet formation. On the other hand, analytic calculations predict that stellar companions would have little effect on planetesimal growth (e.g. Batygin et al., 2011; Rafikov, 2013a; Rafikov, 2013b) and current surveys have found a number of planets in binary star systems (e.g. Eggenberger et al., 2007; Raghavan et al., 2010; Kaib et al., 2011; Orosz et al., 2012a; Orosz et al., 2012b). In addition, a stellar companion might cause planets to migrate via three-body interactions, such as the Kozai-Lidov mechanism or via other secular interactions, resulting in very small orbital distances (e.g. Malmberg et al., 2007a; Malmberg et al., 2007b; Fabrycky and Tremaine, 2007; Morton and Johnson, 2011; Naoz et al., 2012; Naoz et al., 2013; Teyssandier et al., 2013; Petrovich, 2015; Storch et al., 2014). However, the Kozai-Lidov mechanism is suppressed in multi-planet systems because planet-planet interactions tend to prohibit the libration of the argument of perihelion characteristic of the Kozai-Lidov resonance (Wu and Murray, 2003; Batygin et al., 2011). Finally, stellar companions can also bias our estimates of the properties of transiting planet systems by diluting the measured transit depth, resulting in an underestimate of the planet's radius and a corresponding overestimate of its density.

In this study we focus on a class of short-period gas giant planets known as "hot Jupiters." These planets could not have formed at their current locations, but must have migrated in from beyond the ice lines of their natal disks (e.g. Lin et al., 1996). However, the mechanism(s) responsible for hot Jupiter migration remain controversial. Current migration models include disk interactions (e.g. Goldreich and Tremaine, 1980; Tanaka et al., 2002; Lin and Papaloizou, 1986) and gravitational interaction with a third body, such as another planet (e.g. Chatterjee et al., 2008; Nagasawa et al., 2008; Wu and Lithwick, 2011; Beaugé and Nesvorný, 2012;

Lithwick and Wu, 2014) or a stellar companion. In general, isolated simple disk migration models produce hot Jupiters on circular orbits that are well aligned with the primary star's spin axis, while migration due to a third body leads to hot Jupiters that are often eccentric and/or misaligned with the primary's star spin axis.

Surveys from the past few years (e.g. Winn et al., 2010; Albrecht et al., 2012) indicate misaligned hot Jupiters are common–18 out of the 53 hot Jupiters surveyed to date have obliquities that are inconsistent with zero at the three sigma level or higher. As a result, it has been argued that a significant fraction of hot Jupiters may have migrated via three-body interactions such as the the Kozai-Lidov effect, which naturally results in large orbital inclinations (e.g. Morton and Johnson, 2011; Li et al., 2014). If stellar tides can bring misaligned hot Jupiters back into alignment with the star's spin axis (Dawson, 2014), this fraction may be even higher than the current rate suggests. Conversely, Dawson et al. (2015) argue that the lack of high eccentricity Jupiters at intermediate periods in the overall *Kepler* sample places a strict upper limit on the fraction of hot Jupiters that might have migrated via three-body processes. Misaligned hot Jupiters may also result from migration in a tilted disk, which could be caused by torque from a distant stellar companion (Batygin, 2012). Moreover, significant star-disk misalignments may naturally arise from the physical evolution of the star and the disk in a perturbed system (Batygin and Adams, 2013; Spalding and Batygin, 2014a). This suggests that a hot Jupiter's obliquity, which can be measured with the Rossiter-McLaughlin effect (Winn et al., 2005) or via Doppler tomography (e.g. Collier Cameron et al., 2010; Brown et al., 2012), might provide a clue to whether or not a third body has influenced the planetary system.

Alternatively, planet-planet scattering could produce misaligned hot Jupiters without requiring the presence of a stellar companion. Dawson and Murray-Clay (2013) also find evidence that high-eccentricity proto-hot Jupiters are more common around metal-rich stars, which presumably are more likely to have formed multiple gas giant planets. Other studies have also suggested that protoplanetary disks in isolation might in fact be tilted by the chaotic nature of star formation (Bate et al., 2010), the primary star's magnetic torques (Lai et al., 2011), and stellar surface modulation by internal gravity waves (Rogers et al., 2012; Rogers et al., 2013).

If a significant fraction of hot Jupiters migrate inward and acquire spin-orbit misalignments via three-body interactions, then this necessarily requires the presence of a massive outer planetary or stellar companion in these systems. However, there

have not been any studies published to date that have provided a well-constrained estimate of the frequency of bound stellar companions in hot Jupiter systems. A few stellar companions to transiting planet host stars were discovered serendipitously as part of studies intended to better characterize the transiting planet and its host star (e.g. Collier Cameron et al., 2007; Crossfield et al., 2012; Sing et al., 2013). Some other works, such as Narita et al. (2010a) and Narita et al. (2012) report directly imaged stellar companions from adaptive optics (AO) follow-up of known planets but only for one or two transiting gas giant planetary systems. The first systematic surveys for stellar companions to transiting planet systems used the "lucky imaging" method. These studies focused exclusively on transiting hot Jupiter systems and their sample sizes were small: 14 in Daemgen et al. (2009), 16 in Faedi et al. (2013) and 21 in Bergfors et al. (2013). In addition, many of these surveys observed overlapping target lists.

More recently, there have been a series of studies focusing on the sample of *Kepler* transiting planet candidate host stars. The two surveys by Lillo-Box et al. (2012) and Lillo-Box et al. (2014), covering 174 *Kepler* planet host candidates, is the largest "lucky imaging" search to date. Current state-of-the-art direct imaging surveys use adaptive optics to achieve diffraction-limited imaging to allow for better detection and survey efficiency. Adams et al. (2012), Adams et al. (2013), Dressing et al. (2014), and Wang et al. (2014) obtained infrared AO images of 90, 12, 87, and 56 *Kepler* planet candidate hosts, respectively. Adams et al., 2013 also searched around 15 transiting planet hosts. Law et al. (2014) recently published the first part of an optical campaign to search for companions around all *Kepler* planet candidate hosts using the Robo-AO instrument, with an initial sample size of 715 stars. Gilliland et al. (2015) searched for companions around 23 *Kepler* planet candidate hosts using optical images from the Hubble Space Telescope WFC3 instrument. Finally, Horch et al. (2014) used differential speckle imaging in two optical bandpasses to search for companions around 623 *Kepler* planet candidate hosts.

Unlike previous surveys of hot Jupiters detected by ground-based transit surveys, these imaging surveys were intended to confirm the planetary nature of the transits detected by *Kepler* and to correct the transit light curves for any dilution due to nearby stars, therefore ensuring accurate planetary radius estimates. Because the typical proper motions of the *Kepler* stars are quite small, these studies report relative brightness and projected separation for companions but do not attempt to determine whether or not they are bound companions or background objects. The planetary

systems in these surveys have a size distribution that reflects that of the *Kepler* survey as a whole, with the majority of systems consisting of sub-Neptune-sized transiting planets.

In this work, we present a diffraction-limited direct imaging survey of close-in transiting gas giant planets orbiting bright, nearby stars, as part of the "Friends of Hot Jupiters" campaign. These systems are among the most favorable targets for the Rossiter-McLaughlin technique, and the majority of our targets have published measurements of their spin-orbit alignment. By focusing on this sample, we can directly test current hot Jupiter migration models and investigate the origin of their observed spin-orbit misalignments by searching for massive, distant companions in these systems. Our survey uses multiple bandpasses and repeated observations spanning a several year baseline in order to determine whether any directly imaged companions are physically bound. We also use these same data to estimate companion masses and projected physical separations, which are required in order to evaluate the likelihood of specific dynamical evolution scenarios for these systems.

The Friends of Hot Jupiters survey uses multiple companion detection modes to search for planetary and stellar companions around exoplanetary systems. Our sample consists of 51 exoplanetary systems that are known to host a transiting gas giant planet with a mass of $0.06 - 11\,M_{Jup}$ and a period of $0.7 - 11$ days. We divide this sample into two sub-samples, consisting of planets that are on misaligned and/or eccentric orbits and a control sample of planets on apparently circular, well-aligned orbits (see Knutson et al., 2014, for a full description of the sample selection for this survey). We consider targets to be "misaligned" if they host planets with an eccentricity or spin-orbit alignment more than three standard deviations away from zero. In Knutson et al. (2014), we presented our search for long-term radial velocity (RV) accelerations due to distant massive planetary or stellar companions in these systems. We found a total companion occurrence rate of $51\% \pm 10\%$ for companions with masses of $1 - 13\,M_{Jup}$ and orbital semimajor axes of $1 - 20$ au, with no evidence for a higher frequency of radial velocity companions in systems with eccentric and/or misaligned gas giant planets. In a future paper we will present the results of a complementary search for close-in stellar companions using high resolution K band spectroscopy, which is primarily sensitive to K and M stars within $0.5''$of the primary.

In this paper, we present the results of our diffraction-limited direct imaging search. In Section 2.3, we describe our observations. In Section 2.4, we summarize the

point spread function (PSF) fitting method used to calculate the brightness ratio and positions of the candidate stellar companions, as well as upper limits for companions in systems with non-detections. We then determine whether or not the candidate companions share common proper motion with the primary, and estimate their projected physical separations and masses. In Section 2.5, we discuss each system individually. In Section 2.6, we compare our estimated frequency for stellar companions to the results from previous surveys of planet-hosting and field star samples. Finally, in Section 2.7, we summarize our findings and discuss the implications of our measured companion fraction for the formation of hot Jupiter systems.

2.3 Observations

During the AO phase of our survey, we collected data for 50 out of 51 FHJ systems with the NIRC2 instrument (instrument PI: Keith Matthews) on Keck II using K band natural guide star adaptive optics imaging. We were not able to image one target, WASP-19, because its declination, $-45.7°$, was too far south to observe with Keck AO. Two of our target systems, HAT-P-8 and WASP-12, turned out to be triple systems, which we previously reported in Bechter et al. (2014). We obtained observations between February 2012 and October 2014 and our observations are summarized in Table 2.1. We used the full array (1024x1024 pixel field of view) on the narrow camera setting ($10\,\mathrm{mas\,pixel^{-1}}$) to maximize our spatial resolution. However, for several bright targets (as noted in Table 2.1), we used a subarray to reduce integration times and avoid saturation. We used a three-point dither pattern to reduce the effects of the NIRC2 array's noisier lower left quadrant and instrumental noise levels while also preserving our sensitivity to companions with higher spatial separations. We aimed for a total of two minutes of on-target integration time per system in position angle mode, where the orientation of the image is kept constant on the detector as the telescope tracks. This technique allows us to detect companions with ΔK of approximately 8 at separations of approximately $1''$. For targets where a potential companion object is seen, we repeat the observations in at least one other filter, such as J or H, in order to obtain color information. We also follow up on targets with detected companions approximately one or more years later to obtain K band astrometric measurements necessary to confirm that the companion is gravitationally bound via a common proper motion analysis. We elect to use K band rather than J or H band for our astrometry because the AO correction is superior at longer wavelengths.

Table 2.1: Summary of NIRC2 AO observations

Target	N_c	UT Obs. Date	Filter	Array	$T_{\rm int}$	$N_{\rm fit}$	$N_{\rm stack}$
GJ-436	0	2012 Feb 02	K'	256	5	···	18
HAT-P-2	0	2012 May 29	K'	512	13.3	···	9
HAT-P-4	0	2012 Feb 02	K'	1024	15	···	9
HAT-P-6	0	2012 Jul 27	K'	1024	9	···	30
HAT-P-7	1	2012 Jul 27	J	1024	9	10	10
		2012 Jul 27	H	1024	9	10	10
		2012 Jul 27	K'	1024	9	10	10
		2013 May 31	K_s	1024	9	8	8
		2013 Jun 22	H	1024	9	12	12
		2013 Jun 22	K_s	1024	9	12	12
		2014 Jul 12	K_s	1024	15	15	15
HAT-P-8	2	2012 Jul 27	J	1024	9	10	15
		2012 Jul 27	H	1024	9	13	15
		2012 Jul 27	K'	1024	9	15	15
		2013 Aug 19	H	512	12.5	6	6
		2013 Aug 19	K'	1024	9	12	12
		2013 Aug 19	K_s	1024	9	12	12
HAT-P-10	1	2012 Feb 02	J	1024	9	9	9
		2012 Feb 02	K'	1024	10	9	9
		2013 Aug 19	H	1024	9	6	6
		2013 Aug 19	K'	1024	9	12	12
		2013 Aug 19	K_s	1024	9	12	12
HAT-P-11	0	2012 Jul 27	K'	512	5	···	18
		2013 Aug 19	K_c	1024	9	···	12
HAT-P-12	0	2012 Feb 02	K'	1024	15	···	9
HAT-P-13	0	2012 Feb 02	K'	1024	9	···	9
HAT-P-14	1	2012 Jun 05	K'	512	5	33	33
		2013 Mar 26	H	1024	9	5	6
		2013 Mar 26	K_s	1024	10	6	6
		2014 Jul 07	K_s	1024	20	5	5
HAT-P-15	0	2012 Feb 02	K'	1024	15	···	9
		2014 Oct 03	K_s	1024	20	···	12
HAT-P-16	1	2012 Feb 02	J	1024	10	14	15
		2012 Feb 02	K'	1024	15	15	15
		2013 Aug 19	H	1024	18	6	6
		2013 Aug 19	K_s	1024	9	12	12
HAT-P-17	0	2012 May 07	K'	1024	0.9	···	18
HAT-P-18	0	2012 May 29	K'	1024	30	···	9
HAT-P-20	0	2012 Feb 02	K'	512	2.5	···	18
		2013 Nov 17	K_c	1024	10	···	12
HAT-P-22	0	2012 Feb 02	K'	512	10	···	18
HAT-P-24	1	2012 Feb 02	K'	1024	15	6	9
		2014 May 13	J	1024	10	12	12
		2014 May 13	H	1024	20	6	6
		2014 May 13	K_s	1024	10	12	12
HAT-P-26	0	2012 Feb 02	K'	1024	15	···	9
HAT-P-29	0	2012 Feb 02	J	1024	10	···	9
		2012 Feb 02	K'	1024	15	···	9
HAT-P-30	1	2012 Feb 02	K'	1024	10	9	27

Continued on next page

Table 2.1 – continued from previous page

Target	N_c	UT Obs. Date	Filter	Array	$T_{\rm int}$	$N_{\rm fit}$	$N_{\rm stack}$
		2014 May 13	J	1024	10	12	12
		2014 May 13	H	512	10	12	12
		2014 May 13	K_s	1024	10	12	12
HAT-P-31	0	2012 May 07	K'	1024	8	···	17
HAT-P-32	1	2012 Feb 02	J	1024	10	9	9
		2012 Feb 02	K'	1024	15	15	15
		2013 Mar 02	H	1024	5	9	9
		2013 Mar 02	K_s	1024	15	15	15
HAT-P-33	1	2012 Feb 02	J	1024	15	8	9
		2012 Feb 02	K'	1024	15	9	9
		2013 Mar 02	H	1024	10	12	12
		2013 Mar 02	K_s	1024	10	12	12
HAT-P-34	0	2012 Jul 27	K'	1024	9	···	30
HD-149026	0	2012 Jun 05	K'	256	1	···	39
		2013 Mar 26	K_s	256	9	···	12
		2013 Jul 04	H	128	10	···	9
		2013 Jul 04	K_s	256	10	···	12
TrES-2	1	2012 Jul 27	J	1024	9	15	15
		2012 Jul 27	H	1024	9	15	15
		2012 Jul 27	K'	1024	9	15	15
		2013 May 31	H	1024	9	12	12
		2013 May 31	K_s	1024	9	6	6
TrES-3	0	2012 Jul 27	K'	1024	9	···	30
TrES-4	1	2012 Jul 27	J	1024	9	15	15
		2012 Jul 27	H	1024	9	18	18
		2012 Jul 27	K'	1024	9	18	18
		2013 Jul 04	H	1024	9	9	9
		2013 Jul 04	K_s	1024	10	12	12
WASP-1	1	2012 Jul 27	K'	1024	20	20	20
		2013 Aug 19	H	1024	9	6	6
		2013 Aug 19	K_s	1024	12.5	12	12
		2014 Jul 12	K_s	1024	15	15	15
		2014 Oct 03	K_s	1024	15	12	12
WASP-2	1	2012 Jul 27	J	1024	10	15	15
		2012 Jul 27	H	1024	9	15	15
		2012 Jul 27	K'	1024	9	30	30
		2013 Jun 22	H	1024	9	11	11
		2013 Jun 22	K_s	1024	9	12	12
WASP-3	1	2012 Jun 05	K'	1024	5	30	30
		2012 Jul 27	J	1024	9	14	15
		2012 Jul 27	H	1024	9	15	15
		2012 Jul 27	K'	1024	9	30	30
		2013 May 31	H	512	5	5	6
		2013 May 31	K_s	1024	9	12	12
WASP-4	0	2012 Jul 27	K'	1024	20	···	15
WASP-7	0	2012 Aug 29	K'	1024	9	···	48
WASP-8	1	2012 Jul 27	J	1024	9	10	15
		2012 Jul 27	H	1024	9	10	15
		2012 Jul 27	K'	1024	9	20	30
		2013 Aug 19	K_s	512	12.5	8	8

Continued on next page

Table 2.1 – continued from previous page

Target	N_c	UT Obs. Date	Filter	Array	$T_{\rm int}$	$N_{\rm fit}$	$N_{\rm stack}$
WASP-10	0	2012 Jul 04	J	1024	20	···	9
		2012 Jul 04	K'	1024	20	···	9
WASP-12	2	2012 Feb 02	J	1024	15	9	9
		2012 Feb 02	K'	1024	15	9	9
		2013 Mar 02	K_s	1024	10	15	15
WASP-14	1	2012 Jul 27	J	1024	9	15	15
		2012 Jul 27	H	1024	9	15	15
		2012 Jul 27	K'	1024	9	33	33
		2013 Mar 26	K'	1024	9	12	12
		2013 Mar 26	K_s	1024	9	12	12
WASP-15	0	2012 Feb 02	K'	1024	15	···	9
WASP-16	0	2012 Feb 02	K'	1024	15	···	18
		2012 Jul 27	H	1024	9	···	15
		2012 Jul 27	K'	1024	9	···	33
WASP-17	0	2012 May 07	K'	1024	10	···	18
WASP-18	0	2012 Aug 28	K'	1024	9	···	32
WASP-22	0	2012 Aug 26	K'	1024	10	···	9
WASP-24	0	2012 Feb 02	K'	1024	15	···	9
		2012 Jun 03	K'	1024	15	···	12
WASP-34	0	2012 Feb 02	K'	1024	10	···	18
WASP-38	0	2012 Jun 04	K'	1024	30	···	4
XO-2	0	2012 Feb 02	K'	1024	10	···	27
XO-3	0	2012 Feb 02	J	512	2.5	···	9
		2012 Feb 02	K'	512	2.5	···	9
		2013 Mar 02	H	1024	15	···	12
		2013 Mar 02	K'	1024	15	···	9
XO-4	0	2012 Feb 02	K'	1024	9	···	9
XO-5	0	2012 Feb 02	K'	1024	15	···	16

Notes. The N_c columns indicate the number of confirmed common proper motion companions found for each target. The "Array" column denotes the horizontal width, in pixels, of the section of the NIRC2 detector used to capture the image. The array dimensions used in this survey were 1024x1024 (the full NIRC2 array), 512x512, 256x264, or 128x152. These dimensions are constrained by NIRC2's readout software. The $T_{\rm int}$ column indicates the total integration time of a single exposure, in seconds. For targets with detected companions, the $N_{\rm fit}$ column indicates the number of exposures used to make our photometric and/or astrometric measurements of companions. The $N_{\rm stack}$ column indicates the number of exposures used to compute the final stacked image for contrast curve measurements. The last column is only given for images taken in the K', K_s, or K_c bandpasses because we only compute contrast curves in these bands. $N_{\rm fit}$ and $N_{\rm stack}$ may differ because the companion may not be visible at all dither positions and/or poor conditions prevented acquisition of useful data.

We calibrate our images using dome flat fields and dark frames. We also find and remove image artifacts. We flag flat field pixels that are less than 0.1 times the median as dead pixels and dark frame pixels that are more than 10σ from the median as hot pixels. For each frame, we identify the remaining bad pixels as those with counts that are 8σ outliers compared to the counts in pixels in the surrounding 5x5 box. We replace all the flagged pixels' values with the median of the 5x5 box

centered on the flagged pixel. We use these calibrated individual frames in all of our photometric and astrometric analyses. We limit our integrations to stay just below the nonlinear regime for the NIRC2 detector, and use Poisson statistics to determine the uncertainty in our counts. We also create a single, reduced image by aligning the individual frames so that the target star is in the same position and then combine using a median stack. We use the stacked image for our sensitivity calculations.

2.4 Analysis of companion properties

Detections

We find 15 binary systems and 2 triple systems, for a total of 17 multi-star systems, out of the 50 systems with AO observations. We show one median-stacked K-band image for each of these detections in Figure 2.1. Table 2.2 summarizes the stellar parameters for all Friends of Hot Jupiters survey targets and the number of companions found around each star.

To measure the flux ratio and on-sky separations for each system, we fit a multiple-source point spread function (PSF) to each calibrated frame. Following Bechter et al. (2014), we choose to model the PSF with as a Moffat function with a Gaussian component,

$$I(x,y) = \sum_{i=1}^{N_*} \left(\alpha_i \left[1 + \left(\frac{r_i}{r_s} \right)^2 \right]^{-\beta} + \gamma_i \exp\left[-\frac{r_i^2}{w^2} \right] \right) + b, \tag{2.1}$$

where N_* is the number of stars in the image (either 2 or 3); $r_i = \sqrt{x_i^2 + y_i^2}$ is the distance from the i-th star; $x_i, y_i, \alpha_i, \gamma_i$ are parameters that vary with each star and determine the position of the star and the amplitude of the PSF; β takes a single value for all stars and sets the exponent of the Moffat contribution; r_s and w each take a single value for all stars and determine the width of the Moffat and Gaussian portions of the PSF, respectively; and b is the background sky level. Hence, the total number of free parameters is $4N_* + 4$. We also only fit a circular aperture of radius 10 pixels around each star. From experimenting with different aperture sizes, we find this radius covered most of the star's flux (the full width half maximum, FWHM, is about 5 pixels) while remaining small enough to avoid counting any remaining bad pixels in the background. We also explored some alternative PSF fitting schemes using a smaller sample from our survey. We tried a Moffat function combined with an elliptical Gaussian model, a purely Gaussian model, and a sinc^2 model. From examining the Bayesian information criteria, we find that the best model is the Moffat function with a radially symmetric (circular) Gaussian component.

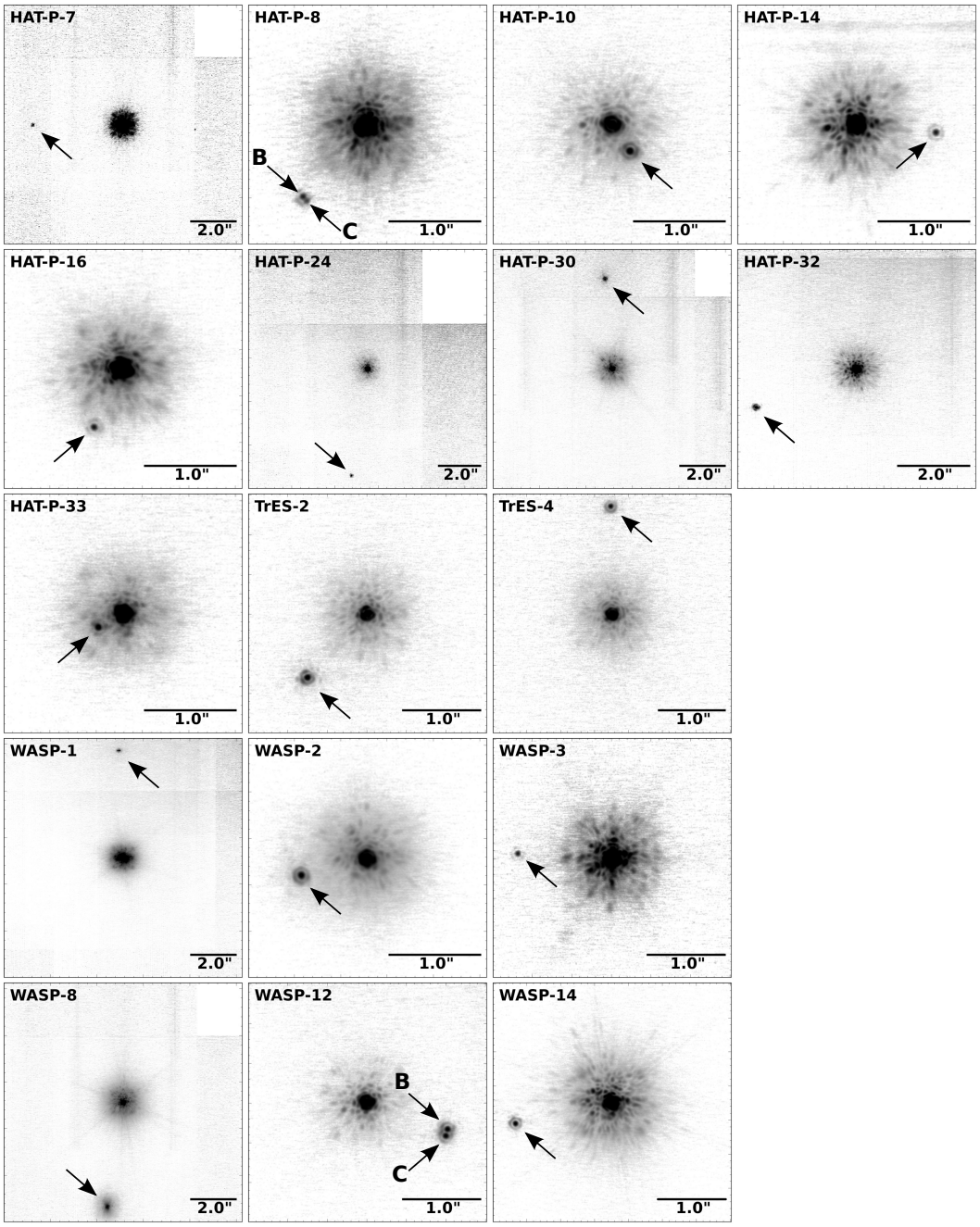

Figure 2.1: Median-stacked K-band images showing the Friends of Hot Jupiters survey targets with detected and confirmed stellar companions (marked with arrows). The first epoch observation (see Table 2.1) for each target was used.

We find the best fit parameters using a maximum likelihood estimation routine. These best fit parameters determine an analytic form for our PSF model. We compute the flux ratio by integrating the best-fit PSF model over the same circular aperture used in the PSF fitting for each star. We use the difference in the stellar position parameters to compute the horizontal and vertical separation as projected onto the NIRC2 array. We then adjust these separations to account for the well characterized distortion and rotation of the NIRC2 array using the astrometric corrections presented in Yelda et al. (2010).

We compute the flux ratio and corrected one-dimensional separations for each frame. Our best estimate of these measurements for each observation is the median value from all of the frames. We calculate the standard error on the mean and use that as our measurement error. Using the best estimate for the one-dimensional separations and the corrected NIRC2 plate scale (Yelda et al., 2010), we then compute the projected on-sky separation ρ and position angle PA for each detected companion. The NIRC2 astrometric corrections include uncertainties on the distortion, plate scale, and the orientation of the NIRC2 array. Therefore, we include these uncertainties in our total error budget for our measured ρ and PA.

We complete the above analysis to determine the photometry for all detected companions in all bandpasses (J, H, K', K_s) and find the best fitting flux ratio between primary and companion stars in each band, reported as a difference in magnitudes in Table 2.3. We then compute the apparent magnitudes of the companion stars in all bands as well as the colors of the companion stars. In order to do this, we require the apparent magnitudes of the primary star, which we obtained from the 2MASS catalog (Skrutskie et al., 2006). Table 2.4 shows the full multiband photometry of our detected companion stars. For our astrometric analysis, we only use K-band data and report the best fit separations and position angles in Table 2.5.

Table 2.2: Target stellar parameters

Target	N_c	Sample	$T_{\rm eff}$ (K)	M ($M_\odot$)	$\log g$ (cgs)	D (pc)	References for... T	M, $\log g$	D
GJ 436	0	Misaligned	3416 ± 54	0.507 ± 0.070	4.83 ± 0.03	10.14 ± 0.24	1	1	2
HAT-P-2	0	Misaligned	6290 ± 60	1.36 ± 0.04	4.138 ± 0.035	125.3 ± 13.1	3	3	2
HAT-P-4	0	Control	5890 ± 67	1.26 ± 0.10	4.12 ± 0.03	293.5 ± 19.4	4	5,6	2
HAT-P-6	0	Misaligned	6687 ± 71	1.29 ± 0.06	4.188 ± 0.035	277.8 ± 19.1	4	7	2
HAT-P-7	1	Misaligned	6259 ± 32	1.361 ± 0.021	4.98 ± 0.13	320^{+50}_{-40}	8	8	2
HAT-P-8	2	Control	6223 ± 67	1.192 ± 0.075	4.177 ± 0.022	230 ± 15	4	9	2
HAT-P-10	1	Control	4974 ± 65	0.83 ± 0.03	4.56 ± 0.02	121.7 ± 4.2	4	10	10
HAT-P-11	0	Misaligned	4792 ± 69	0.81 ± 0.03	4.59 ± 0.03	38.0 ± 1.3	4	11	11
HAT-P-12	0	Control	4650 ± 60	0.733 ± 0.018	4.61 ± 0.01	139.1 ± 9.6	12	12	2
HAT-P-13	0	Misaligned	5720 ± 69	1.320 ± 0.062	4.070 ± 0.020	214 ± 12	4	13	14
HAT-P-14	1	Misaligned	6671 ± 75	1.418 ± 0.054	4.187 ± 0.025	205 ± 11	4	7	15
HAT-P-15	0	Misaligned	5640 ± 69	1.013 ± 0.043	4.38 ± 0.03	190 ± 8	4	16	16
HAT-P-16	1	Misaligned	6140 ± 72	1.218 ± 0.039	4.34 ± 0.03	235 ± 10	4	17	17
HAT-P-17	0	Misaligned	5345 ± 70	0.857 ± 0.039	4.52 ± 0.02	90 ± 3	4	18	18
HAT-P-18	0	Control	4790 ± 72	0.770 ± 0.031	4.57 ± 0.04	166 ± 9	4	19	19
HAT-P-20	0	Misaligned	4619 ± 72	0.756 ± 0.028	4.63 ± 0.02	70 ± 3	4	20	21
HAT-P-22	0	Control	5367 ± 67	0.916 ± 0.035	4.36 ± 0.04	82 ± 3	4	20	21
HAT-P-24	1	Control	6329 ± 67	1.191 ± 0.042	4.27 ± 0.04	396 ± 20	4	22	22
HAT-P-26	0	Control	5142 ± 69	0.816 ± 0.033	4.56 ± 0.06	134^{+18}_{-8}	4	23	23
HAT-P-29	0	Control	6086 ± 69	1.207 ± 0.046	4.34 ± 0.06	322^{+35}_{-21}	4	24	24
HAT-P-30	1	Misaligned	6304 ± 88	1.242 ± 0.041	4.36 ± 0.03	193 ± 8	25	25	25
HAT-P-31	0	Misaligned	6065 ± 100	1.218 ± 0.070	$4.26^{+0.11}_{-0.13}$	354^{+74}_{-51}	26	26	26
HAT-P-32	1	Misaligned	6207 ± 88	1.160 ± 0.041	4.33 ± 0.01	283 ± 5	27	27	27
HAT-P-33	1	Control	6446 ± 88	1.375 ± 0.040	4.15 ± 0.01	387 ± 9	27	27	27
HAT-P-34	0	Misaligned	6442 ± 88	1.392 ± 0.047	4.21 ± 0.06	257^{+22}_{-17}	28	28	28
HD149026	0	Control	6103 ± 66	1.345 ± 0.020	4.189 ± 0.020	80.8 ± 4.0	4	29	2

Continued on next page

Table 2.2 – continued from previous page

Target	N_c	Sample	$T_{\rm eff}$ (K)	M ($M_\odot$)	$\log g$ (cgs)	D (pc)	References for... T	M, $\log g$	D
TrES-2	1	Control	5850 ± 50	0.94 ± 0.05	4.45 ± 0.01	220 ± 10[a]	30	31	2
TrES-3	0	Misaligned	5514 ± 69	0.928 ± 0.038	4.57 ± 0.01	258.5 ± 16.1[a]	4	32	2
TrES-4	1	Control	6200 ± 75	1.339 ± 0.086	4.030 ± 0.033	476 ± 26[a]	32	7	2
WASP-1	1	Control	6160 ± 64	1.265 ± 0.054	4.209 ± 0.051	380 ± 38[a]	4	7	2
WASP-2	1	Misaligned	5255 ± 71	0.851 ± 0.050	4.537 ± 0.017	140 ± 10[a]	4	7	2
WASP-3	1	Control	6375 ± 63	1.20 ± 0.01	4.33 ± 0.03	220 ± 20[a]	4	33	2
WASP-4	0	Control	5540 ± 55	0.927 ± 0.056	4.487 ± 0.010	280.9 ± 31.1	34	7	2
WASP-7	0	Misaligned	6520 ± 70	1.317 ± 0.072	4.218 ± 0.048	140 ± 15	34	7	35
WASP-8	1	Misaligned	5570 ± 85	1.04 ± 0.08	4.41 ± 0.09	87 ± 7	34	36	2
WASP-10	0	Misaligned	4735 ± 69	0.703 ± 0.070	$4.51^{+0.06}_{-0.05}$	90 ± 20	4	37	37
WASP-12	2	Misaligned	6118 ± 64	1.38 ± 0.19	4.159 ± 0.024	427 ± 90[a]	4	7	2
WASP-14	1	Misaligned	6462 ± 75	1.350 ± 0.121	4.126 ± 0.042	160 ± 20[a]	4	7	2
WASP-15	0	Misaligned	6405 ± 80	1.305 ± 0.051	4.189 ± 0.021	256 ± 32[b]	36	38	See note[b]
WASP-16	0	Control	5630 ± 70	0.980 ± 0.054	4.357 ± 0.022	174 ± 14[b]	36	38	See note[b]
WASP-17	0	Misaligned	6550 ± 100	1.286 ± 0.079	4.149 ± 0.014	476 ± 36[a]	39	39	2
WASP-18	0	Control	6368 ± 66	1.274 ± 0.060	4.365 ± 0.022	122.6 ± 6.7[a]	4	7	2
WASP-22	0	Control	5958 ± 98	1.109 ± 0.026	4.31 ± 0.03	300 ± 30[c]	40	40	41[c]
WASP-24	0	Control	6107 ± 77	1.184 ± 0.027	4.263 ± 0.017	332.5 ± 23.8[a]	4	42	2
WASP-34	0	Control	5700 ± 100	1.01 ± 0.07	4.5 ± 0.1	120 ± 15	43	43	43
WASP-38	0	Misaligned	6187 ± 77	1.23 ± 0.04	4.267 ± 0.030	110 ± 20	4	44	45
XO-2	0	Control	5377 ± 79	0.924 ± 0.173	4.436 ± 0.042	156.0 ± 8.8	4	7	2
XO-3	0	Misaligned	6759 ± 79	1.213 ± 0.066	4.244 ± 0.041	185.7 ± 11.8	4	46	2
XO-4	0	Misaligned	6297 ± 72	1.32 ± 0.02	4.18 ± 0.07	308.2 ± 19.6	4	47	2
XO-5	0	Control	5370 ± 70	0.88 ± 0.03	4.31 ± 0.03	260 ± 12	48	48	48

Continued on next page

Table 2.2 – continued from previous page

Target	N_c	Sample	$T_{\rm eff}$ (K)	M ($M_\odot$)	$\log g$ (cgs)	D (pc)	References for... T	M, $\log g$	D

Notes. N_c is the number of confirmed common proper motion companions found for each target. "Sample" shows whether we placed the target in the "misaligned" (planets on misaligned or eccentric orbits) or the "control" (planets on well-aligned and circular orbits) subsamples. With the exception of GJ 436 and HAT-P-2, our stars do not have directly measured parallax estimates. We take our distance estimates from the referenced papers, which combine estimates of the stellar surface gravity, effective temperature, and metallicity from high-resolution optical spectroscopy and (in some cases) constraints on the stellar density from fits to the transit light curve in order to constrain the mass, radius, and age of the host star. The measured apparent magnitudes in V, J, H, and K bands can then be used to estimate the distance to the star given these known properties. The final three columns lists references for our temperature; mass and $\log g$; and distance measurements, respectively.

[a] This distance estimate has been updated from the values used in the first "Friends of Hot Jupiters" paper (Knutson et al., 2014). The new distances are consistent with the previously used values except for WASP-12.

[b] We could not find distance measurements for these targets so we estimated the distance based on relative brightness of the target to a reference star and used the same relative error. For WASP-15, we used WASP-14 as a reference and for WASP-16, we used WASP-8 as a reference.

[c] A distance was reported with no uncertainty, so we use a conservative estimate of 10%, based on uncertainties of other stars.

References. (1) Braun et al. (2012); (2) Triaud et al. (2014); (3) Pál et al. (2010); (4) Torres et al. (2012); (5) Kovács et al. (2007); (6) Winn et al. (2011); (7) Southworth et al. (2012b); (8) Van Eylen et al. (2012); (9) Mancini et al. (2013); (10) Bakos et al. (2009b); (11) Bakos et al. (2010); (12) Hartman et al. (2009); (13) Southworth et al. (2012a); (14) Bakos et al. (2009a); (15) Torres et al. (2010); (16) Kovács et al. (2010); (17) Buchhave et al. (2010); (18) Howard et al. (2012a); (19) Hartman et al. (2011b); (20) Bakos et al. (2011); (21) Bakos et al. (2010); (22) Kipping et al. (2010); (23) Hartman et al. (2011a); (24) Buchhave et al. (2011); (25) Johnson et al. (2011); (26) Kipping et al. (2011); (27) Hartman et al. (2011c); (28) Bakos et al. (2012); (29) Carter et al. (2009); (30) Sozzetti et al. (2007); (31) Barclay et al. (2012); (32) Sozzetti et al. (2009); (33) Miller et al. (2010); (34) Maxted et al. (2011); (35) Hellier et al. (2009); (36) Doyle et al. (2013); (37) Christian et al. (2009); (38) Southworth et al. (2013); (39) Southworth (2012); (40) Anderson et al. (2011); (41) Maxted et al. (2010); (42) Street et al. (2010); (43) Smalley et al. (2011); (44) Brown et al. (2012); (45) Barros et al. (2011); (46) Winn et al. (2008a); (47) McCullough et al. (2008); (48) Pál et al. (2009)

Table 2.3: Flux ratio measurements of confirmed common proper motion companions

Companion	UT Obs. Date	ΔJ	ΔH	$\Delta K'$	ΔK_s
HAT-P-7B	2012 Jul 27	6.562 ± 0.075	5.887 ± 0.078	5.920 ± 0.058	···
HAT-P-7B	2013 May 31	···	···	···	5.948 ± 0.040
HAT-P-7B	2013 Jun 22	···	5.926 ± 0.093	···	6.04 ± 0.12
HAT-P-7B	2014 Jul 12	···	···	···	5.827 ± 0.058
HAT-P-8B	2012 Jul 27	6.59 ± 0.12	5.671 ± 0.054	5.874 ± 0.063	···
HAT-P-8C	2012 Jul 27	7.16 ± 0.15	6.352 ± 0.065	6.447 ± 0.057	···
HAT-P-8B	2013 Aug 19	···	5.597 ± 0.036	5.841 ± 0.073	···
HAT-P-8C	2013 Aug 19	···	6.147 ± 0.077	6.310 ± 0.057	···
HAT-P-8B	2013 Aug 19	···	5.597 ± 0.036	···	5.726 ± 0.075
HAT-P-8C	2013 Aug 19	···	6.147 ± 0.077	···	6.201 ± 0.094
HAT-P-10B	2012 Feb 02	2.656 ± 0.017	···	2.960 ± 0.022	···
HAT-P-10B	2013 Aug 19	···	2.448 ± 0.014	2.763 ± 0.034	···
HAT-P-10B	2013 Aug 19	···	2.448 ± 0.014	···	2.733 ± 0.045
HAT-P-14B	2012 Jun 05	···	···	5.633 ± 0.033	···
HAT-P-14B	2013 Mar 26	···	5.237 ± 0.086	···	5.647 ± 0.096
HAT-P-14B	2014 Jul 07	···	···	···	5.844 ± 0.034
HAT-P-16B	2012 Feb 02	5.421 ± 0.039	···	5.530 ± 0.021	···
HAT-P-16B	2013 Aug 19	···	5.147 ± 0.047	···	5.382 ± 0.061
HAT-P-24B	2012 Feb 02	···	···	4.45 ± 0.12	···
HAT-P-24B	2014 May 13	4.658 ± 0.080	4.163 ± 0.052	···	3.811 ± 0.010
HAT-P-30B	2012 Feb 02	···	···	3.134 ± 0.054	···
HAT-P-30B	2014 May 13	3.4304 ± 0.0063	3.1153 ± 0.0053	···	2.975 ± 0.041
HAT-P-32B	2012 Feb 02	4.148 ± 0.028	···	3.733 ± 0.042	···
HAT-P-32B	2013 Mar 02	···	3.668 ± 0.071	···	3.500 ± 0.073
HAT-P-33B	2012 Feb 02	4.137 ± 0.054	···	3.938 ± 0.085	···
HAT-P-33B	2013 Mar 02	···	3.469 ± 0.033	···	3.415 ± 0.057
TrES-2B	2012 Jul 27	2.896 ± 0.020	2.4515 ± 0.0073	2.422 ± 0.019	···
TrES-2B	2013 May 31	···	2.4628 ± 0.0085	···	2.523 ± 0.036
TrES-4B	2012 Jul 27	3.528 ± 0.012	3.177 ± 0.013	3.301 ± 0.046	···
TrES-4B	2013 Jul 04	···	3.1841 ± 0.0084	···	3.447 ± 0.024
WASP-1B	2012 Jul 27	···	···	4.551 ± 0.077	···
WASP-1B	2013 Aug 19	···	4.766 ± 0.046	···	4.840 ± 0.055
WASP-1B	2014 Jul 12	···	···	···	4.858 ± 0.064
WASP-1B	2014 Oct 03	···	···	···	4.561 ± 0.100
WASP-2B	2012 Jul 27	2.880 ± 0.010	2.7343 ± 0.0061	2.871 ± 0.028	···
WASP-2B	2013 Jun 22	···	2.7254 ± 0.0075	···	2.687 ± 0.017
WASP-3B	2012 Jun 05	···	···	6.528 ± 0.049	···
WASP-3B	2012 Jul 27	7.27 ± 0.12	6.683 ± 0.079	6.641 ± 0.052	···
WASP-3B	2013 May 31	···	6.550 ± 0.091	···	6.552 ± 0.027
WASP-8B	2012 Jul 27	4.492 ± 0.062	3.134 ± 0.056	2.550 ± 0.021	···
WASP-8B	2013 Aug 19	···	···	···	2.560 ± 0.018
WASP-12B	2012 Feb 02	3.711 ± 0.076	···	3.32 ± 0.11	···
WASP-12C	2012 Feb 02	3.672 ± 0.021	···	3.577 ± 0.036	···
WASP-12B	2013 Mar 02	···	···	···	3.286 ± 0.030
WASP-12C	2013 Mar 02	···	···	···	3.182 ± 0.017
WASP-14B	2012 Jul 27	5.207 ± 0.020	4.788 ± 0.024	4.984 ± 0.025	···
WASP-14B	2013 Mar 26	···	···	4.765 ± 0.057	···
WASP-14B	2013 Mar 26	···	···	···	4.701 ± 0.054

Notes. ΔX is the difference in magnitude between the companion and primary stars in the X filter.

Table 2.4: Multi-band photometry of confirmed common proper motion companions

Companion	UT Obs. Date	K	m_J	m_H	m_K	$J-K$	$H-K$	$J-H$
HAT-P-7B	2012 Jul 27	K'	16.117 ± 0.075	15.231 ± 0.078	15.254 ± 0.058	0.863 ± 0.095	-0.023 ± 0.097	0.89 ± 0.11
HAT-P-7B	2013 May 31	K_s	···	···	15.282 ± 0.040	···	···	···
HAT-P-7B	2013 Jun 22	K_s	···	15.270 ± 0.093	15.37 ± 0.12	···	-0.10 ± 0.15	···
HAT-P-7B	2014 Jul 12	K_s	···	···	15.161 ± 0.058	···	···	···
HAT-P-8B	2012 Jul 27	K'	15.81 ± 0.12	14.675 ± 0.054	14.827 ± 0.063	0.98 ± 0.14	-0.152 ± 0.083	1.13 ± 0.13
HAT-P-8C	2012 Jul 27	K'	16.37 ± 0.15	15.356 ± 0.065	15.400 ± 0.057	0.97 ± 0.16	-0.044 ± 0.087	1.02 ± 0.16
HAT-P-8B	2013 Aug 19	K'	···	14.601 ± 0.036	14.794 ± 0.073	···	-0.193 ± 0.082	···
HAT-P-8C	2013 Aug 19	K'	···	15.151 ± 0.077	15.263 ± 0.057	···	-0.113 ± 0.096	···
HAT-P-8B	2013 Aug 19	K_s	···	14.601 ± 0.036	14.679 ± 0.075	···	-0.078 ± 0.083	···
HAT-P-8C	2013 Aug 19	K_s	···	15.151 ± 0.077	15.154 ± 0.094	···	-0.00 ± 0.12	···
HAT-P-10B	2012 Feb 02	K'	12.671 ± 0.017	···	12.381 ± 0.022	0.290 ± 0.027	···	···
HAT-P-10B	2013 Aug 19	K'	···	12.008 ± 0.014	12.184 ± 0.034	···	-0.176 ± 0.037	···
HAT-P-10B	2013 Aug 19	K_s	···	12.008 ± 0.014	12.154 ± 0.045	···	-0.146 ± 0.047	···
HAT-P-14B	2012 Jun 05	K'	···	···	14.484 ± 0.033	···	···	···
HAT-P-14B	2013 Mar 26	K_s	···	14.164 ± 0.086	14.498 ± 0.096	···	-0.33 ± 0.13	···
HAT-P-14B	2014 Jul 07	K_s	···	···	14.695 ± 0.034	···	···	···
HAT-P-16B	2012 Feb 02	K'	15.271 ± 0.039	···	15.083 ± 0.021	0.189 ± 0.045	···	···
HAT-P-16B	2013 Aug 19	K_s	···	14.770 ± 0.047	14.935 ± 0.061	···	-0.165 ± 0.077	···
HAT-P-24B	2012 Feb 02	K'	···	···	14.99 ± 0.12	···	···	···
HAT-P-24B	2014 May 13	K_s	15.455 ± 0.080	14.752 ± 0.052	14.354 ± 0.010	1.101 ± 0.081	0.398 ± 0.053	0.703 ± 0.096
HAT-P-30B	2012 Feb 02	K'	···	···	12.285 ± 0.054	···	···	···
HAT-P-30B	2014 May 13	K_s	12.8724 ± 0.0063	12.3353 ± 0.0053	12.126 ± 0.041	0.746 ± 0.042	0.209 ± 0.042	0.5371 ± 0.0082
HAT-P-32B	2012 Feb 02	K'	14.399 ± 0.028	···	13.723 ± 0.042	0.676 ± 0.050	···	···
HAT-P-32B	2013 Mar 02	K_s	···	13.692 ± 0.071	13.490 ± 0.073	···	0.20 ± 0.10	···
HAT-P-33B	2012 Feb 02	K'	14.400 ± 0.054	···	13.942 ± 0.085	0.46 ± 0.10	···	···
HAT-P-33B	2013 Mar 02	K_s	···	13.530 ± 0.033	13.419 ± 0.057	···	0.111 ± 0.066	···
TrES-2B	2012 Jul 27	K'	13.128 ± 0.020	12.3715 ± 0.0073	12.268 ± 0.019	0.859 ± 0.028	0.103 ± 0.021	0.756 ± 0.021
TrES-2B	2013 May 31	K_s	···	12.3828 ± 0.0085	12.369 ± 0.036	···	0.014 ± 0.037	···

Continued on next page

Table 2.4 – continued from previous page

Companion	UT Obs. Date	K	m_J	m_H	m_K	$J-K$	$H-K$	$J-H$
TrES-4B	2012 Jul 27	K'	14.111 ± 0.012	13.527 ± 0.013	13.631 ± 0.046	0.481 ± 0.048	−0.104 ± 0.048	0.584 ± 0.018
TrES-4B	2013 Jul 04	K_s	···	13.5341 ± 0.0084	13.777 ± 0.024	···	−0.243 ± 0.025	···
WASP-1B	2012 Jul 27	K'	···	···	14.827 ± 0.077	···	···	···
WASP-1B	2013 Aug 19	K_s	···	15.130 ± 0.046	15.116 ± 0.055	···	0.014 ± 0.072	···
WASP-1B	2014 Jul 12	K_s	···	···	15.134 ± 0.064	···	···	···
WASP-1B	2014 Oct 03	K_s	···	···	14.837 ± 0.100	···	···	···
WASP-2B	2012 Jul 27	K'	13.046 ± 0.010	12.4863 ± 0.0061	12.503 ± 0.028	0.543 ± 0.030	−0.016 ± 0.028	0.560 ± 0.012
WASP-2B	2013 Jun 22	K_s	···	12.4774 ± 0.0075	12.319 ± 0.017	···	0.158 ± 0.018	···
WASP-3B	2012 Jun 05	K'	···	···	15.889 ± 0.049	···	···	···
WASP-3B	2012 Jul 27	K'	16.88 ± 0.12	16.090 ± 0.079	16.002 ± 0.052	0.87 ± 0.13	0.088 ± 0.095	0.78 ± 0.15
WASP-3B	2013 May 31	K_s	···	15.957 ± 0.091	15.913 ± 0.027	···	0.044 ± 0.095	···
WASP-8B	2012 Jul 27	K'	12.993 ± 0.062	11.354 ± 0.056	10.636 ± 0.021	2.357 ± 0.065	0.719 ± 0.060	1.638 ± 0.083
WASP-8B	2013 Aug 19	K_s	···	···	10.646 ± 0.018	···	···	···
WASP-12B	2012 Feb 02	K'	14.188 ± 0.076	···	13.51 ± 0.11	0.68 ± 0.13	···	···
WASP-12C	2012 Feb 02	K'	14.149 ± 0.021	···	13.765 ± 0.036	0.384 ± 0.042	···	···
WASP-12B	2013 Mar 02	K_s	···	···	13.474 ± 0.030	···	···	···
WASP-12C	2013 Mar 02	K_s	···	···	13.370 ± 0.017	···	···	···
WASP-14B	2012 Jul 27	K'	14.076 ± 0.020	13.438 ± 0.024	13.605 ± 0.025	0.471 ± 0.032	−0.167 ± 0.034	0.638 ± 0.031
WASP-14B	2013 Mar 26	K'	···	···	13.386 ± 0.057	···	···	···
WASP-14B	2013 Mar 26	K_s	···	···	13.322 ± 0.054	···	···	···

Notes. The K column indicates whether the following columns refer to the K' or K_s bandpass, as both were used in the Friends of Hot Jupiters survey. The m_X columns refer to the secondary star's apparent magnitude in the X filter, which is computed from the primary star's apparent magnitude and the measured flux ratio as reported in Table 2.3. The last three columns show the computed color of the companion star.

References. Primary star apparent magnitudes from 2MASS (Skrutskie et al., 2006).

Common proper motion confirmation

Our next step is to determine whether or not our candidate companions share common proper motion with the primary star, indicating that they are bound companions rather than background sources in the same line of sight. If the detected companion is actually a very distant background star, it will remain effectively stationary while the closer primary star moves across the sky as dictated by its parallax and proper motion. We would therefore expect that a background object would display a time-varying separation and position angle relative to the primary star, while a bound companion will maintain a constant separation and position angle.

We calculate the "background track" (i.e. the evolution of the companion's separation and position angle as a function of time if it was a background object) as shown in Figures 2.2 and 2.3. We compute the primary star's parallactic motion using the celestial coordinates of the primary star from the SIMBAD database and the Earth ephemerides from the JPL Horizons service. The primary star's proper motion and uncertainties are also taken from the SIMBAD database. When determining the background tracks, we account for uncertainties in the primary star's celestial coordinates, proper motion, and parallax in addition to our measurement uncertainties in separation and position angle. We run a Monte Carlo routine to calculate the uncertainty in the background tracks. The 68% and 95% confidence regions for the separation and position angle evolution are shown as shaded regions in Figures 2.2 and 2.3. We use the measurement with the smallest uncertainty in separation and position angle as the starting point for our track.

After creating these background tracks, we next overplot the measured companion separation and position angle at each epoch from Tables 2.5, 2.6, and 2.7. Several of our candidate companions were detected in previous imaging surveys; when available, we also show the separations and position angles from these earlier studies. We provide a complete list of these previously published detections in Tables 2.6 and 2.7, and discuss individual systems in more detail in section 2.5. In Figures 2.2 and 2.3, measurements from this study are plotted as circles while measurements from other studies are plotted as squares.

Based on these measurements, we conclude that all but two of our detected candidate companions must be bound to the host star. The exceptions are the second candidate companion seen around HAT-P-7 and the candidate companion seen around HAT-P-15. Our followup observations determined these candidate companions to be background objects. Due to the small projected physical and angular separa-

Table 2.5: K-band astrometric measurements of confirmed common proper motion companions

Companion	UT Obs. Date	K	ρ (mas)	PA (°)
HAT-P-7B	2012 Jul 27	K'	3858.7 ± 1.8	89.958 ± 0.025
HAT-P-7B	2013 May 31	K_s	3859.3 ± 1.7	90.020 ± 0.025
HAT-P-7B	2013 Jun 22	K_s	3858.7 ± 2.0	90.020 ± 0.024
HAT-P-7B	2014 Jul 12	K_s	3858.6 ± 1.7	90.010 ± 0.024
HAT-P-8B	2012 Jul 27	K'	1037.9 ± 1.5	137.601 ± 0.084
HAT-P-8C	2012 Jul 27	K'	1047.8 ± 1.6	140.868 ± 0.089
HAT-P-8B	2013 Aug 19	K'	1040.3 ± 1.6	137.810 ± 0.084
HAT-P-8C	2013 Aug 19	K'	1045.0 ± 1.5	141.058 ± 0.083
HAT-P-8B	2013 Aug 19	K_s	1041.0 ± 1.5	137.770 ± 0.084
HAT-P-8C	2013 Aug 19	K_s	1044.7 ± 1.5	141.059 ± 0.092
HAT-P-10B	2012 Feb 02	K'	342.5 ± 1.5	214.09 ± 0.24
HAT-P-10B	2013 Aug 19	K'	355.0 ± 1.5	215.65 ± 0.24
HAT-P-10B	2013 Aug 19	K_s	355.0 ± 1.5	215.64 ± 0.24
HAT-P-14B	2012 Jun 05	K'	857.6 ± 1.5	264.10 ± 0.10
HAT-P-14B	2013 Mar 26	K_s	857.4 ± 1.5	264.24 ± 0.11
HAT-P-14B	2014 Jul 07	K_s	856.9 ± 1.6	264.38 ± 0.13
HAT-P-16B	2012 Feb 02	K'	691.6 ± 1.5	153.83 ± 0.12
HAT-P-16B	2013 Aug 19	K_s	688.6 ± 1.5	153.65 ± 0.12
HAT-P-24B	2012 Feb 02	K'	4946.1 ± 1.8	170.894 ± 0.020
HAT-P-24B	2014 May 13	K_s	4944.2 ± 1.9	170.872 ± 0.020
HAT-P-30B	2012 Feb 02	K'	3835.1 ± 1.7	4.219 ± 0.024
HAT-P-30B	2014 May 13	K_s	3836.6 ± 1.7	4.206 ± 0.024
HAT-P-32B	2012 Feb 02	K'	2935.5 ± 1.6	110.583 ± 0.030
HAT-P-32B	2013 Mar 02	K_s	2935.5 ± 1.7	110.624 ± 0.031
HAT-P-33B	2012 Feb 02	K'	307.2 ± 1.5	117.86 ± 0.29
HAT-P-33B	2013 Mar 02	K_s	306.3 ± 1.5	118.05 ± 0.29
TrES-2B	2012 Jul 27	K'	1105.4 ± 1.5	136.325 ± 0.077
TrES-2B	2013 May 31	K_s	1106.7 ± 1.5	136.357 ± 0.077
TrES-4B	2012 Jul 27	K'	1562.3 ± 1.6	0.357 ± 0.056
TrES-4B	2013 Jul 04	K_s	1563.4 ± 1.5	0.386 ± 0.055
WASP-1B	2012 Jul 27	K'	4580.0 ± 1.8	1.901 ± 0.021
WASP-1B	2013 Aug 19	K_s	4581.5 ± 1.8	1.953 ± 0.021
WASP-1B	2014 Jul 12	K_s	4582.3 ± 1.8	1.958 ± 0.021
WASP-1B	2014 Oct 03	K_s	4581.7 ± 1.8	1.917 ± 0.021
WASP-2B	2012 Jul 27	K'	734.3 ± 1.5	104.39 ± 0.12
WASP-2B	2013 Jun 22	K_s	730.0 ± 1.5	104.54 ± 0.12
WASP-3B	2012 Jun 05	K'	1192.2 ± 1.6	87.103 ± 0.077
WASP-3B	2012 Jul 27	K'	1191.0 ± 1.5	87.070 ± 0.075
WASP-3B	2013 May 31	K_s	1189.1 ± 1.6	87.169 ± 0.081
WASP-8B	2012 Jul 27	K'	4505.2 ± 1.7	170.948 ± 0.021
WASP-8B	2013 Aug 19	K_s	4507.4 ± 2.0	170.988 ± 0.021
WASP-12B	2012 Feb 02	K'	1058.8 ± 1.5	251.242 ± 0.084
WASP-12C	2012 Feb 02	K'	1067.1 ± 1.5	246.751 ± 0.083
WASP-12B	2013 Mar 02	K_s	1058.6 ± 1.5	251.444 ± 0.082
WASP-12C	2013 Mar 02	K_s	1068.4 ± 1.5	246.945 ± 0.082
WASP-14B	2012 Jul 27	K'	1450.8 ± 1.5	102.066 ± 0.059
WASP-14B	2013 Mar 26	K'	1449.1 ± 1.5	102.210 ± 0.060
WASP-14B	2013 Mar 26	K_s	1449.5 ± 1.5	102.207 ± 0.060

Notes. We use both the K' and K_s band for astrometric measurements. We imaged a few of our targets on the same night in both bands (HAT-P-8, HAT-P-10, and WASP-14) and show that the astrometry agrees to well within our uncertainties. The ρ column shows the on-sky separation between the fitted positions of the primary and companion stars, in milliarcseconds. The PA column shows the position angle, in degrees east of north.

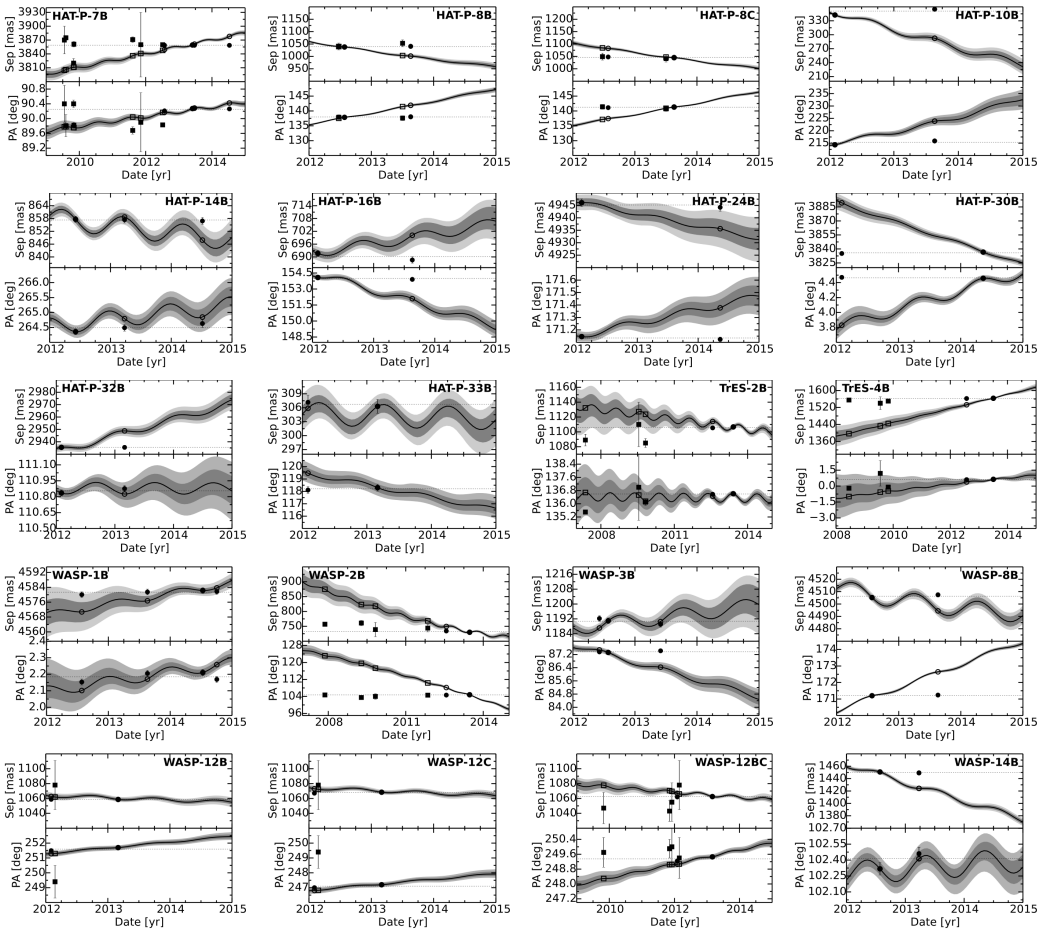

Figure 2.2: For each object, the two panels show the separation (top) and position angle (bottom) of a detected companion star relative to the primary target star. The lines show the track of a background object, as computed from our observation with the smallest uncertainty. The dark- and light-gray shaded regions indicate the 68% and 95% confidence region for this track. Filled symbols indicate measured positions of companions while open symbols indicate the position the detected source would have if it were a background source. Measurements from this work are plotted as circles and shown in Table 2.5, while measurements from previous studies are plotted as squares and shown in Table 2.6. Detected companions can be ruled out as background objects if either their separation or position angle are inconsistent with the background track. The two triple systems, HAT-P-8 and WASP-12, have each of their companion candidates plotted separately. Because the individual analysis for WASP-12B and WASP-12C cannot conclusively confirm or rule out common proper motion, we also plot the astrometric measurements for the center of mass for the combined light of both companions as WASP-12BC. All objects in this figure are determined to be common proper motion companions to their primary star.

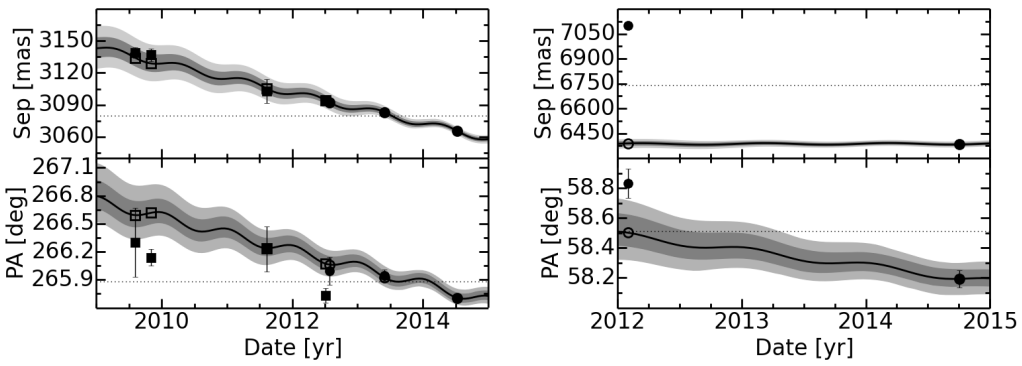

Figure 2.3: These plots are the same as Figure 2.2, except this figure shows the two candidate objects that were determined to be background objects. The measurements are reported in Table 2.7. The left plot shows the astrometric measurements for the second candidate companion to HAT-P-7, with circles showing our data and squares showing the four measurements for the "western companion" reported in Narita et al. (2012). The right plot shows the astrometric measurements for the candidate companion to HAT-P-15. The data rules out a bound companion conclusion for both of these candidates.

tions of our companion candidates, our result that the majority of our candidates are physically bound companions is consistent with other direct imaging surveys that confirm association via multi-epoch detections (e.g. Eggenberger et al., 2007; Bowler et al., 2014) or via galactic crowding estimates (e.g. Adams et al., 2012). We report confirmed common proper motion companions in Figure 2.2 and Tables 2.5 and 2.6. The two background objects are reported separately in Figure 2.3 and Table 2.7. We discuss each system individually in Section 2.5 below.

Masses and separation

For each confirmed companion-primary pair, we compute a flux ratio based on the stars' physical parameters,

$$F_r = \frac{\int_0^\infty I(\lambda, T_p, \log g_p)\, R(\lambda)\, r_p^2\, \mathrm{d}\lambda}{\int_0^\infty I(\lambda, T_c, \log g_c)\, R(\lambda)\, r_c^2\, \mathrm{d}\lambda}, \tag{2.2}$$

where the subscripts p and c refer to the primary and companion stars, respectively, $I(\lambda, T, \log g)$ is the star's specific intensity, T is the star's effective temperature, $\log g$ is a measure of the stellar surface gravity, $R(\lambda)$ is the response function of the NIRC2 filter, and r is the stellar radius. In order to determine $I(\lambda, T, \log g)$, we interpolate the gridded PHOENIX synthetic spectra (Husser et al., 2013) for solar metallicities and composition ([Fe/H]= 0 and [α/H]= 0). Although our companion host stars have [Fe/H] between -0.21 and 0.25, we found that this assumption changes our estimated companion temperatures by less than 5 K.

Table 2.6: Astrometric measurements from previous studies for confirmed common proper motion companions

Companion	UT Obs. Date	ρ (mas)	PA (°)	Reference
HAT-P-7B	2009 Jul 18-22[a]	3870 ± 30	90.4 ± 0.5	Faedi et al. (2013)
HAT-P-7B	2009 Aug 06	3875 ± 5	89.8 ± 0.3	Narita et al. (2010a)
HAT-P-7B	2009 Oct 30	3820 ± 10	90.4 ± 0.1	Bergfors et al. (2013)
HAT-P-7B	2009 Nov 02	3861 ± 6	89.8 ± 0.1	Narita et al. (2012)
HAT-P-7B	2011 Aug 12	3871 ± 6	89.7 ± 0.1	Narita et al. (2012)
HAT-P-7B	2011 Nov 09	3860 ± 70	89.9 ± 0.8	Bergfors et al. (2013)
HAT-P-7B	2012 Jul 07	3860 ± 4	89.8 ± 0.1	Narita et al. (2012)
HAT-P-8B	2012 Jun 24	1040 ± 14	137.9 ± 0.8	Bechter et al. (2014)
HAT-P-8B	2013 Jul 03	1053 ± 14	137.6 ± 0.8	Bechter et al. (2014)
HAT-P-8C	2012 Jun 24	1049 ± 14	141.4 ± 0.8	Bechter et al. (2014)
HAT-P-8C	2013 Jul 03	1041 ± 14	140.7 ± 0.8	Bechter et al. (2014)
TrES-2B	2007 May[a]	1089 ± 8	135.5 ± 0.1	Daemgen et al. (2009)
TrES-2B	2009 Jul 18-22[a]	1110 ± 30	137.0 ± 2.0	Faedi et al. (2013)
TrES-2B	2009 Oct 29	1085 ± 6	136.1 ± 0.2	Bergfors et al. (2013)
TrES-4B	2008 Jun[a]	1555 ± 5	−0.2 ± 0.1	Daemgen et al. (2009)
TrES-4B	2009 Jul 18-22[a]	1540 ± 30	1.2 ± 1.2	Faedi et al. (2013)
TrES-4B	2009 Oct 30	1550 ± 7	−0.1 ± 0.2	Bergfors et al. (2013)
WASP-2B	2007 Nov[a]	757 ± 1	104.7 ± 0.3	Daemgen et al. (2009)
WASP-2B	2009 Apr 13	761 ± 9	103.5 ± 0.2	Bergfors et al. (2013)
WASP-2B	2009 Oct 29	739 ± 24	104 ± 1.3	Bergfors et al. (2013)
WASP-2B	2011 Nov 09	744 ± 13	104.6 ± 0.7	Bergfors et al. (2013)
WASP-12BC[b]	2009 Oct 30	1047 ± 21	249.7 ± 0.8	Bergfors et al. (2013)
WASP-12BC[b]	2011 Nov 8-9[a]	1043 ± 14	249.9 ± 0.5	Bergfors et al. (2013)
WASP-12BC[b]	2011 Dec 04	1055 ± 26	250.0 ± 1.0	Crossfield et al. (2012)
WASP-12BC[b]	2012 Feb 25	1078 ± 33	249.4 ± 1.1	Crossfield et al. (2012)

Notes. Astrometric measurements of Friends of Hot Jupiters companions reported in previous studies. Unless otherwise stated, only studies reporting a numerical value with uncertainties for both separation and position angle of all companions are included in this table and plotted in Figure 2.2.

[a] A specific date was not reported. We report the date to the same precision as it appears in original work.

[b] This study did not resolve the two companions. Thus, the measurement for the center of light of both companions is reported here and only used in the plots for the combined light of WASP-12BC.

Table 2.7: Astrometric measurements from previous studies for candidate companions determined to be background objects

UT Obs. Date	ρ (mas)	PA (°)	Reference
For the second candidate companion to HAT-P-7			
2009 Aug 06	3139 ± 5	266.30 ± 0.37	Narita et al. (2010a)
2009 Nov 02	3137 ± 6	266.14 ± 0.09	Narita et al. (2012)
2011 Aug 12	3103 ± 11	266.23 ± 0.24	Narita et al. (2012)
2012 Jul 07	3095 ± 4	265.73 ± 0.08	Narita et al. (2012)
2012 Jul 27	3091.5 ± 3.3	266.00 ± 0.15	this work
2013 May 31	3083.0 ± 2.7	265.947 ± 0.059	this work
2014 Jul 12	3065.5 ± 1.7	265.705 ± 0.044	this work
For the candidate companion to HAT-P-15			
2012 Feb 02	7099.3 ± 9.9	58.834 ± 0.097	this work
2014 Oct 03	6382.6 ± 7.70	58.193 ± 0.058	this work

Notes. These measurements are used to generate the plots in Figure 2.3.

We use previously published measurements for the primary star's mass, radius, effective temperature and distances as listed in Table 2.2 and fit for the companion star's effective temperature, T_c, by matching the observed flux ratio with the computed flux ratio from Equation 2.2. In order to calculate the flux from a companion with a given effective temperature, we use the zero-age main sequence models from Baraffe et al. (1998) to match each effective temperature with a corresponding radius and surface gravity, and then calculate the corresponding flux ratio using Equation 2.2. After determining the best-fit companion temperature, we calculate the corresponding uncertainty as the sum in quadrature of the uncertainties contributed by the flux ratio measurement error and the reported primary star temperature, surface gravity, and radius. We determine uncertainties for these parameters from uncertainties in our flux ratio measurement and primary star's temperature, radius, and $\log g$. We do not include any uncertainties introduced through use of the stellar model or the PHOENIX model spectra.

Finally, we convert our measured projected on-sky separations to projected spatial separations using the stellar distance. Unfortunately most of our stars don't have measured parallaxes; for these systems we generally used a spectroscopic distance estimate based on the derived stellar properties combined with the star's apparent magnitude.

We calculate an estimated temperature for each candidate companion using either the J, H, or K band photometry, and find that these three independent temperature estimates are consistent with a late-type main sequence star in each filter. This indicates that all of the detected companions have infrared colors consistent with their inferred effective temperatures. In Table 2.8, we report the error-weighted averages of the companion stellar parameters from all three bands as well as temperature estimates using data from individual bands. We conclude that our detected companion stars have colors consistent with a late-type main sequence star in the same system rather than being a distant early-type star in the background.

Table 2.8: Derived stellar parameters of confirmed common proper motion companions

Companion	UT Obs. Date	$T_{\rm eff}$ (K)	M ($M_\odot$)	$\log g$ (cgs)	D (au)	J-band $T_{\rm eff}$ (K)	H-band $T_{\rm eff}$ (K)	K-band $T_{\rm eff}$ (K)
HAT-P-7B	2012 Jul 27	3321 ± 28	0.215 ± 0.016	5.047 ± 0.018	1238 ± 67	3291^{+14}_{-15}	3357^{+16}_{-14}	$3316.7^{+11}_{-9.8}$
HAT-P-7B	2013 May 31	3307 ± 10	0.2089 ± 0.0043	5.0563 ± 0.0047	1238 ± 67	···	···	3307.0 ± 6.5
HAT-P-7B	2013 Jun 22	3320 ± 30	0.214 ± 0.018	5.047 ± 0.019	1238 ± 67	···	3351^{+18}_{-17}	3291^{+23}_{-24}
HAT-P-7B	2014 Jul 12	3328 ± 11	0.2215 ± 0.0066	5.0428 ± 0.0070	1238 ± 67	···	···	$3328.1^{+11}_{-9.8}$
HAT-P-8B	2012 Jul 27	3216 ± 59	0.168 ± 0.020	5.102 ± 0.029	236 ± 13	3153^{+31}_{-33}	$3293.2^{+9.8}_{-11}$	3208^{+16}_{-15}
HAT-P-8B	2013 Aug 19	3252 ± 41	0.182 ± 0.017	5.086 ± 0.022	237 ± 13	···	$3306.2^{+5.7}_{-6.5}$	3216^{+20}_{-18}
HAT-P-8C	2012 Jul 27	3058 ± 63	0.131 ± 0.011	5.167 ± 0.023	239 ± 13	2989^{+50}_{-42}	3136^{+19}_{-18}	3055^{+16}_{-18}
HAT-P-8C	2013 Aug 19	3130 ± 44	0.146 ± 0.010	5.139 ± 0.018	238 ± 13	···	3188^{+20}_{-18}	3092^{+17}_{-15}
HAT-P-10B	2012 Feb 02	3483 ± 43	0.344 ± 0.047	4.922 ± 0.038	41.7 ± 1.4	$3525.4^{+3.9}_{-3.3}$	···	$3443.1^{+3.3}_{-2.6}$
HAT-P-10B	2013 Aug 19	3494 ± 37	0.362 ± 0.035	4.913 ± 0.031	43.2 ± 1.5	···	$3545.0^{+3.3}_{-2.6}$	$3469.2^{+5.2}_{-3.9}$
HAT-P-14B	2012 Jun 05	3310 ± 17	0.211 ± 0.010	5.054 ± 0.011	175.8 ± 9.4	···	···	$3310.2^{+5.7}_{-6.5}$
HAT-P-14B	2013 Mar 26	3356 ± 57	0.232 ± 0.037	5.021 ± 0.039	175.8 ± 9.4	···	3413^{+15}_{-13}	3302^{+18}_{-16}
HAT-P-14B	2014 Jul 07	3263 ± 20	0.1873 ± 0.0087	5.082 ± 0.011	175.7 ± 9.4	···	···	$3263.1^{+7.3}_{-6.5}$
HAT-P-16B	2012 Feb 02	3255 ± 67	0.182 ± 0.027	5.081 ± 0.035	162.5 ± 6.9	3319.2 ± 7.3	···	$3194.8^{+5.7}_{-4.9}$
HAT-P-16B	2013 Aug 19	3269 ± 51	0.188 ± 0.023	5.076 ± 0.028	161.8 ± 6.9	···	$3315.1^{+8.9}_{-8.1}$	3225 ± 15
HAT-P-24B	2012 Feb 02	3434 ± 26	0.298 ± 0.026	4.968 ± 0.022	1959 ± 99	···	···	3434^{+16}_{-19}
HAT-P-24B	2014 May 13	3499 ± 29	0.373 ± 0.030	4.908 ± 0.025	1958 ± 99	$3474.4^{+13}_{-9.8}$	$3498.8^{+8.9}_{-8.1}$	3523.2 ± 1.6
HAT-P-30B	2012 Feb 02	3634 ± 29	0.489 ± 0.020	4.808 ± 0.020	740 ± 31	···	···	3634^{+13}_{-11}
HAT-P-30B	2014 May 13	3692 ± 40	0.519 ± 0.019	4.777 ± 0.019	740 ± 31	3709.3 ± 2.4	3692.2 ± 1.6	3674^{+15}_{-13}
HAT-P-32B	2012 Feb 02	3516 ± 12	0.393 ± 0.012	4.8930 ± 0.0098	831 ± 15	$3524.0^{+5.7}_{-4.9}$	···	3508.6 ± 6.5
HAT-P-32B	2013 Mar 02	3551 ± 10	0.4243 ± 0.0085	4.8677 ± 0.0070	831 ± 15	···	3555^{+15}_{-14}	3548^{+16}_{-15}
HAT-P-33B	2012 Feb 02	3653 ± 54	0.493 ± 0.031	4.800 ± 0.031	118.9 ± 2.8	3705^{+20}_{-18}	···	3604^{+20}_{-18}
HAT-P-33B	2013 Mar 02	3776 ± 32	0.557 ± 0.014	4.740 ± 0.013	118.5 ± 2.8	···	3800^{+13}_{-11}	3753^{+21}_{-20}
TrES-2B	2012 Jul 27	3669 ± 29	0.509 ± 0.013	4.787 ± 0.014	216 ± 13	$3651.6^{+7.3}_{-4.9}$	3701.2 ± 2.4	$3655.7^{+6.5}_{-5.7}$
TrES-2B	2013 May 31	3662 ± 39	0.501 ± 0.021	4.793 ± 0.021	216 ± 13	···	$3697.9^{+2.4}_{-3.3}$	3627.2 ± 8.1
TrES-4B	2012 Jul 27	3985 ± 93	0.626 ± 0.028	4.677 ± 0.023	900 ± 89	4048.2 ± 6.5	4023.8 ± 6.5	3889^{+24}_{-21}

Continued on next page

Table 2.8 – continued from previous page

Companion	UT Obs. Date	$T_{\rm eff}$ (K)	M ($M_\odot$)	$\log g$ (cgs)	D (au)	J-band $T_{\rm eff}$ (K)	H-band $T_{\rm eff}$ (K)	K-band $T_{\rm eff}$ (K)
TrES-4B	2013 Jul 04	3910 ± 110	0.602 ± 0.036	4.696 ± 0.032	900 ± 89	···	$4019.8^{+4.9}_{-3.3}$	3817 ± 11
WASP-1B	2012 Jul 27	3446 ± 15	0.313 ± 0.019	4.956 ± 0.014	1587^{+160}_{-16}	···	···	$3446.0^{+11}_{-8.9}$
WASP-1B	2013 Aug 19	3420 ± 26	0.285 ± 0.023	4.978 ± 0.021	1587^{+160}_{-16}	···	$3441.9^{+6.5}_{-5.7}$	3398.0 ± 8.1
WASP-1B	2014 Jul 12	3395 ± 17	0.266 ± 0.014	4.998 ± 0.013	1587^{+160}_{-16}	···	···	$3394.8^{+11}_{-9.8}$
WASP-1B	2014 Oct 03	3442 ± 18	0.308 ± 0.021	4.960 ± 0.017	1587^{+160}_{-16}	···	···	3442^{+13}_{-15}
WASP-2B	2012 Jul 27	3509 ± 26	0.383 ± 0.028	4.899 ± 0.022	113.0 ± 6.1	3527.9 ± 2.2	$3523.55^{+0.72}_{-1.4}$	$3477.4^{+4.3}_{-3.6}$
WASP-2B	2013 Jun 22	3514 ± 16	0.391 ± 0.016	4.895 ± 0.013	112.3 ± 6.1	···	$3525.7^{+1.4}_{-2.2}$	3502.6 ± 2.9
WASP-3B	2012 Jun 05	2909 ± 33	0.1089 ± 0.0035	5.223 ± 0.010	300 ± 22	···	···	2909^{+17}_{-18}
WASP-3B	2012 Jul 27	2871 ± 51	0.1053 ± 0.0048	5.233 ± 0.015	299 ± 22	2825 ± 47	2924^{+24}_{-28}	2867^{+20}_{-18}
WASP-3B	2013 May 31	2922 ± 48	0.1109 ± 0.0058	5.216 ± 0.016	299 ± 22	···	2962^{+29}_{-25}	2883.6 ± 9.8
WASP-8B	2012 Jul 27	3530 ± 130	0.34 ± 0.11	4.881 ± 0.099	383 ± 48	3383.3 ± 9.6	3568 ± 12	$3666.0^{+6.4}_{-7.2}$
WASP-8B	2013 Aug 19	3657 ± 76	0.504 ± 0.043	4.793 ± 0.043	384 ± 48	···	···	$3657.2^{+5.6}_{-6.4}$
WASP-12B	2012 Feb 02	3786 ± 53	0.561 ± 0.022	4.736 ± 0.021	462 ± 39	3810^{+36}_{-28}	···	3762^{+40}_{-35}
WASP-12B	2013 Mar 02	3769 ± 44	0.554 ± 0.020	4.743 ± 0.018	462 ± 39	···	···	$3768.6^{+11}_{-9.8}$
WASP-12C	2012 Feb 02	3748 ± 90	0.540 ± 0.038	4.753 ± 0.037	466 ± 40	3828.0 ± 9.8	···	3674^{+12}_{-11}
WASP-12C	2013 Mar 02	3808 ± 49	0.571 ± 0.019	4.727 ± 0.017	466 ± 40	···	···	$3807.6^{+7.3}_{-6.5}$
WASP-14B	2012 Jul 27	3464 ± 31	0.331 ± 0.037	4.939 ± 0.028	302 ± 23	3476.0 ± 3.3	$3484.2^{+4.1}_{-3.3}$	$3432.2^{+4.9}_{-3.3}$
WASP-14B	2013 Mar 26	3464 ± 19	0.336 ± 0.024	4.939 ± 0.018	302 ± 23	···	···	$3461.4^{+8.1}_{-7.3}$

Notes. The $T_{\rm eff}$, M, $\log g$, and D columns are error weighted averages from all measurements of each target for each date. These uncertainties include measurement uncertainty, uncertainties from the primary star's stellar parameter and uncertainties on the error weighted average but do not include uncertainties arising from the stellar models and our assumptions on stellar composition. The uncertainties in the last three columns, which report $T_{\rm eff}$ for each filter, only include measurement uncertainties and thus would be underestimates of the true uncertainty. The last three columns show that the companion objects have $T_{\rm eff}$ measurements consistent with a late type main sequence star in all filters.

Contrast curves

We calculate contrast curves for our target stars as follows. First, we measure the FWHM of the central star's PSF in the stacked and combined image, taking the average of the FWHM in the x and y directions as our reference value. We then create a box with dimensions equal to the FWHM and step it across the array, calculating the total flux from the pixels within the box at a given position. The 1σ contrast limit is then defined as the standard deviation of the total flux values for boxes located within an annulus with a width equal to twice the FWHM centered at the desired radial separation. We convert our absolute flux limits to differential magnitude units by taking the total flux in a box of the same size centered on the peak of the stellar point spread function and calculating the corresponding differential magnitude at each radial distance. We show the resulting 5σ average contrast curve for these observations in Figure 2.4.

2.5 Systems with detected companions

New physically bound companions

Seven out of our 17 targets with detected companions (HAT-P-10, HAT-P-14, HAT-P-16, HAT-P-24, HAT-P-33, WASP-3, and WASP-14) have not been previously reported to have a directly imaged stellar companion. Here, we discuss each of these systems individually and report error-weighted averages of corresponding measurements in Tables 2.5 and 2.8.

HAT-P-10. HAT-P-10 hosts a transiting gas giant planet with a mass of $0.5\,M_{Jup}$ and an orbital semimajor axis of of 0.04 au (Bakos et al., 2009b). HAT-P-10b does not have a published Rossiter-McLaughlin measurement constraining its spin-orbit measurement, but its eccentricity is consistent with zero (Bakos et al., 2009b; West et al., 2009). We therefore placed this system in our control sample. We report a $0.36\,M_{\odot} \pm 0.05\,M_{\odot}$ stellar companion at a projected separation of $42\,\text{au} \pm 2\,\text{au}$. In the first paper of the Friends of Hot Jupiter survey (Knutson et al., 2014), HAT-P-10 was found to have a detected radial velocity trend that is consistent with the mass and separation of the directly imaged companion reported in this work. We show that HAT-P-10B is a common proper motion companion. Although there are three other systems with both radial velocity trends and a directly imaged stellar companion, this is the only such target where the stellar companion might plausibly explain the observed trend (Knutson et al., 2014).

HAT-P-14. Torres et al. (2010) report a transiting gas giant planet around HAT-

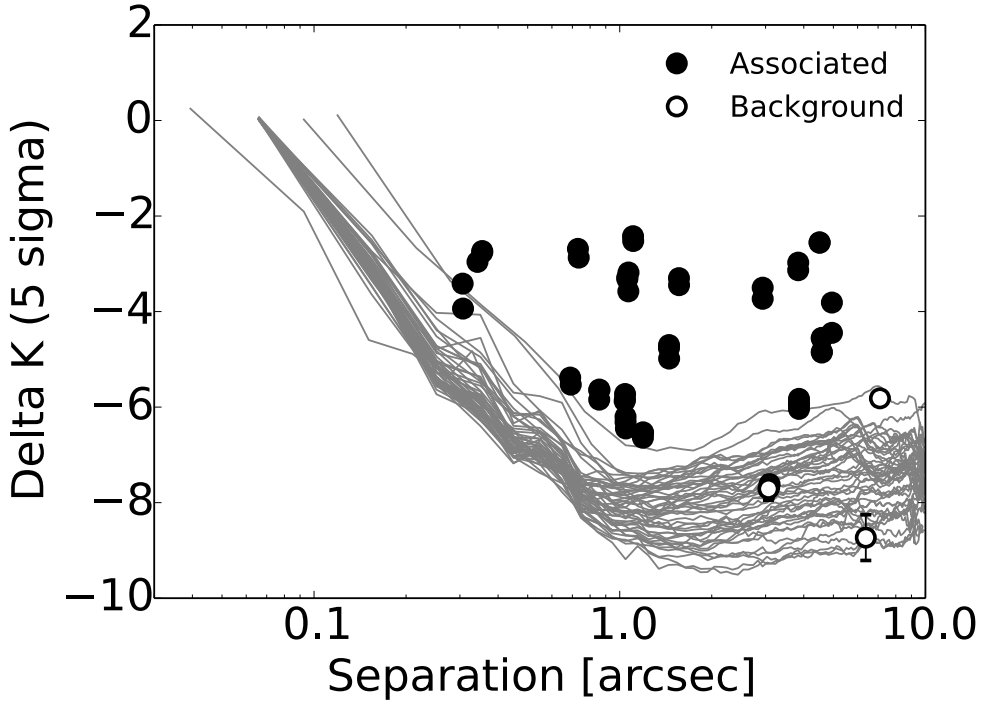

Figure 2.4: The grey lines show K band contrast curves for all 50 Friends of Hot Jupiters imaging targets. For each target, the curve with the greatest contrast was chosen. All companion stars are masked out for the computation of these curves. The points show the magnitude difference and separation for all detected candidate companions at all epochs, where filled points indicate physically associated companions (with confirmed common proper motion) and open points indicate background objects.

P-14 with a mass of 2.2 M_{Jup} and an orbital semimajor axis of 0.06 au. We placed this system in our misaligned sample because this planet has an eccentricity of 0.12 ± 0.02 (Knutson et al., 2014) and a spin-orbit angle of $-171° \pm 5°$ (Winn et al., 2011). We find a $0.20\,M_\odot \pm 0.04\,M_\odot$ stellar companion to HAT-P-14 at a projected separation of 180 au ± 10 au. Our observations in 2012 through 2014 confirm that HAT-P-14B is a common proper motion companion.

HAT-P-16. HAT-P-16 hosts a transiting gas giant planet with a mass of 4.2 M_{Jup} and an orbital semimajor axis of 0.04 au (Buchhave et al., 2010). Moutou et al. (2011) measured a spin-orbit angle consistent with zero but Knutson et al. (2014) measured a planet orbital eccentricity of 0.04 ± 0.01 so we placed this system in our misaligned sample. We report a $0.19\,M_\odot \pm 0.03\,M_\odot$ stellar companion to HAT-P-16 at a separation of 160 au ± 10 au. From our detections in February 2012 and August 2013, we are able to confirm that HAT-P-16B is a common proper motion

companion.

HAT-P-24. Kipping et al. (2010) report a transiting gas giant planet around HAT-P-24 with a mass of $0.7\,M_{Jup}$ and an orbital semimajor axis of 0.05 au. They also find the planet's eccentricity to be consistent with zero and Albrecht et al. (2012) find evidence for a well-aligned orbit, so we placed this target in our control sample. We report a $0.33\,M_{\odot} \pm 0.03\,M_{\odot}$ stellar companion to HAT-P-24 at a separation of 2000 au ± 100 au. From our detections in February 2012 and May 2013, we are able to confirm that HAT-P-24B is a common proper motion companion.

HAT-P-33. HAT-P-33 is a planetary system with a transiting gas giant planet with a mass of $0.8\,M_{Jup}$ and an orbital semimajor axis of 0.05 au (Hartman et al., 2011c). We placed this system in our control sample because HAT-P-33b has an eccentricity consistent with zero (Hartman et al., 2011c) and no published spin-orbit angle measurement. We report a $0.55\,M_{\odot} \pm 0.03\,M_{\odot}$ stellar companion to HAT-P-33 at a separation of 119 au ± 3 au. From our detections in February 2012 and March 2013, we are able to confirm that HAT-P-33B is a common proper motion companion.

WASP-3. WASP-3 hosts a transiting gas giant planet with a mass of $1.8\,M_{Jup}$ and an orbital semimajor axis of 0.03 au (Pollacco et al., 2008). WASP-3b has an eccentricity consistent with zero (Pollacco et al., 2008; Gibson et al., 2008) and a measured spin-orbit angle consistent with zero (Tripathi et al., 2010) so we placed this target in our control sample. We report a $0.108\,M_{\odot} \pm 0.006\,M_{\odot}$ stellar companion to WASP-3 at a separation of 300 au ± 20 au. From our detections in June 2012, July 2012, and May 2013, we are able to confirm that WASP-3B is a common proper motion companion.

WASP-14. Joshi et al. (2009) report a transiting gas giant planet around WASP-14 with a mass of $7.3\,M_{Jup}$ and an orbital semimajor axis of 0.04 au. This system is in our misaligned sample because the planet has an eccentricity of 0.082 ± 0.003 (Knutson et al., 2014) and a spin-orbit angle of $-33^{\circ} \pm 7^{\circ}$ (Johnson et al., 2009). We report a $0.33\,M_{\odot} \pm 0.04\,M_{\odot}$ stellar companion to WASP-14 at a separation of 300 au ± 20 au. From our detections in July 2012 and March 2013, we are able to confirm that WASP-14B is a common proper motion companion.

Companions reported in previous studies

The remaining ten stellar companions were detected in previous studies, although not all systems were confirmed to be physically bound. We discuss each system individually below, with measurements reported in Table 2.6.

HAT-P-7. HAT-P-7 hosts a transiting gas giant planet with a mass of 1.8 M_{Jup} and an orbital semimajor axis of 0.04 au (Pál et al., 2008). HAT-P-7b has a measured eccentricity consistent with zero (Pál et al., 2008) but its spin orbit angle is 160° ± 40° (Albrecht et al., 2012; Winn et al., 2009) so we placed this target in our misaligned sample. Our reported stellar companion to HAT-P-7 is consistent with the seven previous detections by Faedi et al. (2013), Narita et al. (2010a), Bergfors et al. (2013), and Narita et al. (2012) between 2009 and 2012. The study by Narita et al. (2012) determined this detected stellar companion HAT-P-7B is a common proper motion companion. Our own detections in 2012 through 2014 are also consistent with this conclusion. In addition, Narita et al. (2012) also reported a second directly imaged stellar companion (a "western companion") in four of their images (spanning the same dates as above) with a separation of 3.1″ ± 0.1″ and a position angle of 265.9° ± 0.4°. They were unable to confirm that this object is bound to the primary. We were able to image this second companion on three out of the four nights we observed HAT-P-7. Our analysis (Figure 2.3) concludes that this second companion is actually a background object and therefore not physically bound to the other two stars. This target is one of four systems with both a directly imaged stellar companion and a long term radial velocity trend, as reported in Knutson et al. (2014). However, our resolved stellar companion, at a projected separation of 1240 au ± 70 au, is too distant to explain the observed radial velocity trend.

HAT-P-8. Mancini et al. (2013) report a transiting gas giant planet around HAT-P-8 with a mass of 1.3 M_{Jup} and an orbital semimajor axis of 0.04 au. They also report the planet's eccentricity to be consistent with zero and its spin-orbit angle has been measured to be consistent with zero (Simpson et al., 2011; Moutou et al., 2011). Thus, we placed this system in our control sample. In our survey, we find two stellar companions for HAT-P-8. These companions were previously detected by Bergfors et al. (2013) in 2009 but their photometry did not resolve the two stars and they instead reported a single companion. We resolve these two stars in our Keck images, which were published in Bechter et al. (2014). Bechter et al. (2014) followed up on this target in 2012 and 2013 and find that both stellar companions have common proper motion with the primary. In this work we present a new set of observations, also taken in 2012 and 2013, which also indicate that HAT-P-8 is a physically bound triple system. We do not use the unresolved astrometric measurements from Bergfors et al. (2013) in our analysis because the resolved measurements from Bechter et al. (2014) and this survey were enough to confirm common proper motion.

HAT-P-30. HAT-P-30 is a planetary system with a transiting gas giant planet with a mass of 0.7 M_{Jup} and an orbital semimajor axis of 0.04 au (Johnson et al., 2011). Although they measure the planet's eccentricity to be consistent with zero, they also measure a spin-orbit misalignment of 74° ± 9°. We therefore placed this target in our misaligned sample. Our detected stellar companion is consistent with the companion reported by Adams et al. (2013), observed between 2011 Oct 9-11. With only one detection, they were unable to confirm common proper motion. We found this companion in 2012 and followed up in 2014. Our data confirm that the companion HAT-P-30B is indeed bound. We do not use the Adams et al. (2013) measurement in this analysis as they did not report uncertainties on their measured separation and position angle.

HAT-P-32. HAT-P-32 hosts a transiting gas giant planet with a mass of 0.9 M_{Jup} and an orbital semimajor axis of 0.03 au (Hartman et al., 2011c). HAT-P-32b has an eccentricity consistent with zero (Hartman et al., 2011c) but a mesaured spin-orbit misalignment of 85° ± 2° (Albrecht et al., 2012) so we placed this system in our misaligned sample. Our detected stellar companion is consistent with the stellar companion reported by Adams et al. (2013), observed between 2011 Oct 9-11. As with HAT-P-30, they were unable to measure the proper motion for this companion. We found this stellar companion in 2012 and followed up in 2013. Our data confirms that HAT-P-32B is indeed bound. We do not use the Adams et al. (2013) measurement in this analysis as they did not report uncertainties in the measured separation and position angle. This target is also one of four targets with both a directly imaged stellar companion and a long term radial velocity trend, as reported in Knutson et al. (2014). However, our resolved stellar companion, at a projected separation of 830 au ± 20 au, is too distant to explain the observed radial velocity trend.

TrES-2. Barclay et al. (2012) report a transiting gas giant planet around TrES-2 with a mass of 1.4 M_{Jup} and an orbital semimajor axis of 0.04 au. They also report a planet eccentricity consistent with zero and Winn et al. (2008b) report a spin-orbit angle consistent with zero so we placed this target in our control sample. Our detected stellar companion for TrES-2 is consistent with the three previous detections reported by Daemgen et al. (2009), Faedi et al. (2013), and Bergfors et al. (2013) between 2007 and 2009. These studies were not able to measure the proper motion of the companion in order to determine whether or not it was bound to TrES-2. Our measurements from 2012 and 2013 show that TrES-2B is a common

proper motion companion.

TrES-4. TrES-4 is a planetary system with a transiting gas giant planet with a mass of 0.9 M_{Jup} and an orbital semimajor axis of 0.05 au (Sozzetti et al., 2009). TrES-4b has an eccentricity consistent with zero (Sozzetti et al., 2009) and Narita et al. (2010b) measure a spin-orbit angle consistent with zero so we placed this system in our control sample. Our detected stellar companion for TrES-4 is consistent with the three previous detections reported by Daemgen et al. (2009), Faedi et al. (2013), and Bergfors et al. (2013) between 2008 and 2009. Using all the data from the prior studies, Bergfors et al. (2013) were able to confirm that TrES-4B is a common proper motion companion. Our measurements from 2012 and 2013 support this assessment.

WASP-1. WASP-1 hosts a transiting gas giant planet with a mass of 0.8 M_{Jup} (Knutson et al., 2014) and an orbital semimajor axis of 0.04 au (Torres et al., 2008). Albrecht et al., 2011 report that the eccentricity and spin-orbit angles are consistent with zero, so we placed this target in our control sample. Collier Cameron et al. (2007) observed a stellar companion to WASP-1 with a separation of 4.7″ north of the primary from observations made in 2006. They did not report any uncertainties nor did they provide a numerical positional angle. Thus, we are unable to include this observation in our analysis. However, these values are consistent with the reported separation and position angle from our observations in 2012, 2013 and 2014. Our measurements confirm that WASP-1B is a common proper motion companion.

WASP-2. There is a transiting gas giant planet around WASP-2 with a mass of 0.9 M_{Jup} (Knutson et al., 2014) and an orbital semimajor axis of 0.06 au (Torres et al., 2008). Radial velocity and secondary eclipse measurements for this planet are consistent with a circular orbit, but Triaud et al. (2010) find that the planet has spin-orbit misalignment of $150^{\circ}{}^{+10^{\circ}}_{-20^{\circ}}$. We therefore place this planet in the misaligned sample. A stellar companion for WASP-2 was reported in six separate observations from 2006 to 2011 by Collier Cameron et al. (2007), Daemgen et al. (2009), Bergfors et al. (2013), and Adams et al. (2013). These observations are all consistent with the companion we detect in our images. However, the measurements reported in 2006 by Collier Cameron et al. (2007) did not include uncertainties nor a numerical value for the position angle, so we do not use this observation in our analysis. In addition, one observation from 2011 by Adams et al. (2013) also did not include uncertainties so we omit this measurement as well. Bergfors et al. (2013) combined their observations with previous studies to conclude that the stellar companion must

be bound to the primary. Our own measurements from 2012 and 2013 also indicate WASP-2B is a common proper motion companion.

WASP-8. WASP-8 is a planetary system with a transiting gas giant planet with a mass of 2.2 M_{Jup} and an orbital semimajor axis of 0.08 au (Queloz et al., 2010). Knutson et al. (2014) report the planet's eccentricity to be 0.304 ± 0.004 and the discovery paper measures a spin-orbit misalignment of $-123^{\circ}{}^{+3^{\circ}}_{-4^{\circ}}$. Therefore, we placed this planet in the misaligned sample. This paper also reported a stellar companion for WASP-8 consistent with our own observations in 2012 and 2013. They did not provide a date for their observation, so we do not use their measurement in our analysis. However, they note that this companion was mentioned in the Washington Double Star Catalog (Mason et al., 2001) from 70 years ago at the same position. They conclude that WASP-8B is a common proper motion companion. Our data also rules out a background object and supports the conclusion of Queloz et al. (2010). This target is one of four targets with a directly imaged companion and also a long term radial velocity trend, as reported in Knutson et al. (2014). However, our resolved stellar companion, at a projected separation of 380 au ± 50 au, is too distant to explain the observed radial velocity trend.

WASP-12. WASP-12 hosts a transiting gas giant planet with a mass of 1.4 M_{Jup} and an orbital semimajor axis of 0.02 au (Hebb et al., 2009). WASP-12b has eccentricity consistent with zero (Hebb et al., 2009), however, Albrecht et al. (2012) measures a spin-orbit angle of $59^{\circ}{}^{+15^{\circ}}_{-20^{\circ}}$. Thus, we placed this system in our misaligned sample. Stellar companion(s) for WASP-12 have been seen in seven observations from 2009 to 2013 as reported by Bergfors et al. (2013), Crossfield et al. (2012), Sing et al. (2013), and Bechter et al. (2014). The first two studies were not able to resolve the two stellar companions for WASP-12 but did detect a single source at the same position. Bergfors et al. (2013) noted that the source was elongated and Crossfield et al. (2012) obtained a spectrum for the companion, which they used to estimated its effective temperature and surface gravity. They concluded that the observed source must be a foreground object as it was otherwise significantly brighter than expected for its spectral type. Sing et al. (2013) was the first to report images of the two resolved stellar companions but did not provide any astrometric measurements so we do not include this data point in our analysis. The two observations reported in Bechter et al. (2014) are part of the Friends of Hot Jupiters survey. We independently analyzed the data and our results are consistent with the measurements reported in Bechter et al. (2014). Our measurement uncertainties are lower as we account for

the NIRC2 distortion; thus we use the measurements reported in this work for our analysis. We also recently discovered a more precise distance estimate for this star in Triaud et al. (2014), which we use to replace the Bergfors et al. (2013) value from our previous papers. Despite these improvements, we find that our 2012 and 2013 data points are insufficient to rule out the possibility of a background source (see astrometric plots for WASP-12B and WASP-12C separately in Figure 2.2; these plots do not include the combined light astrometric measurements). However, when considering previously reported combined light measurements for this system our analysis indicate the center of mass of WASP-12BC has common proper motion with the primary, consistent with our conclusions in Bechter et al. (2014).

Candidates determined to be background objects

As discussed in Section 2.5, we found that the second candidate companion to HAT-P-7 reported in Narita et al. (2012) and followed up in our survey was a background object (see Figure 2.3 and Table 2.7), so HAT-P-7 is simply a binary system.

We also detect a candidate companion to HAT-P-15 on 2 February 2012 with $\Delta K' = 5.77 \pm 0.05$, a separation of $7.100'' \pm 0.002''$ and position angle of $58.6° \pm 0.1°$. Due to the large separation of this object to HAT-P-15, the object was only visible in one of our dither positions in our first epoch, resulting in relatively large astrometric uncertainties. We followed up with a second epoch on 3 October 2014 and did not find an object in the same position. However, we did find an object with $\Delta K_s = 8.2 \pm 0.9$, a separation of $6.387'' \pm 0.008''$ and position angle of $58.0° \pm 0.1°$. Physical association of these two detections is ruled out by our astrometric analysis (see Figure 2.3 and Table 2.7). In addition, the location of these detections is also inconsistent with both detections being the same object. Thus, we conclude that we imaged two different background or foreground objects in the two epochs and exclude this target from our list of bound companions.

Non-detections

For the remaining 32 targets, we did not find any candidate companions within the $5.5''$ NIRC2 field of view. For two of these targets, previous studies have found directly imaged companions at larger separations. Mugrauer et al. (2014) reports a common proper motion companion to the south of HAT-P-4 with a separation of $91.8''$. Bergfors et al. (2013) reports a candidate companion to XO-3 with a separation of $6.059'' \pm 0.047''$ and a position angle of $296.7° \pm 0.3°$. This companion is also very faint ($\Delta z' = 8.22 \pm 0.23$ and $\Delta i' = 8.57 \pm 0.24$) and Bergfors et al. (2013)

note that it is unlikely that the detected object is a bound companion. This companion would not be visible in our survey due to its faintness and our survey's FOV, given our 3-point dither pattern.

2.6 Companion fraction

We find bound stellar companions around 17 out of the 50 targets observed, corresponding to an overall raw companion fraction of 34% ± 7%. We find that 9 out of 27 stars with planets on misaligned or eccentric orbits have stellar companions, yielding a raw stellar companion fraction of 33% ± 9%. We also find that 8 out of 23 stars with planets on well-aligned or circular orbits have stellar companions, corresponding to a raw stellar companion fraction of 35% ± 9%. Figure 2.5 plots the physical separation of detected companions versus their mass ratios. Companions to stars with measured spin-orbit misalignment are shown in black, companions to stars with measured spin-orbit angles consistent with zero are shown in red, and companions to stars with no spin-orbit angle measurement (HAT-P-10 and HAT-P-33) are shown as open squares. We find no evidence for a difference in the typical mass ratios or projected separations between misaligned and well-aligned targets.

Figure 2.5 also plots lines to show the minimum companion mass necessary to excite Kozai-Lidov oscillations at a timescale short enough to overcome pericenter precession due to general relativity. For these representative lines, we use a central stellar mass of 1 $M_{\odot}$ and a planetary mass of 1 $M_{\rm Jup}$ and assume a circular orbit for both planet and companion star. We plot these limits for initial planet semimajor axis distances of 1 au, 2.5 au and 5 au (solid, dashed and dotted lines, respectively). These lines are computed by equating the timescales for the Kozai-Lidov oscillation and general relativity pericenter precession, using Equations 1 and 23 from Fabrycky and Tremaine (2007). These expressions scale as $1 - e^2$, so they are not strongly affected by our assumption of circular orbits. All companions that lie above and to the left of these lines are sufficiently massive and close enough to excite Kozai-Lidov oscillations on the planet. We find that the majority of our detected companions could potentially excite Jupiter-mass planets that form within 5 au.

Survey incompleteness correction

In order to make a reliable estimate of the companion fraction for our sample, we must correct for our survey's incompleteness. For each of our 50 targets, we determine our survey's sensitivity to companions with various mass ratios and orbital semimajor axes. We create a 50x50 grid of linearly spaced bins in mass

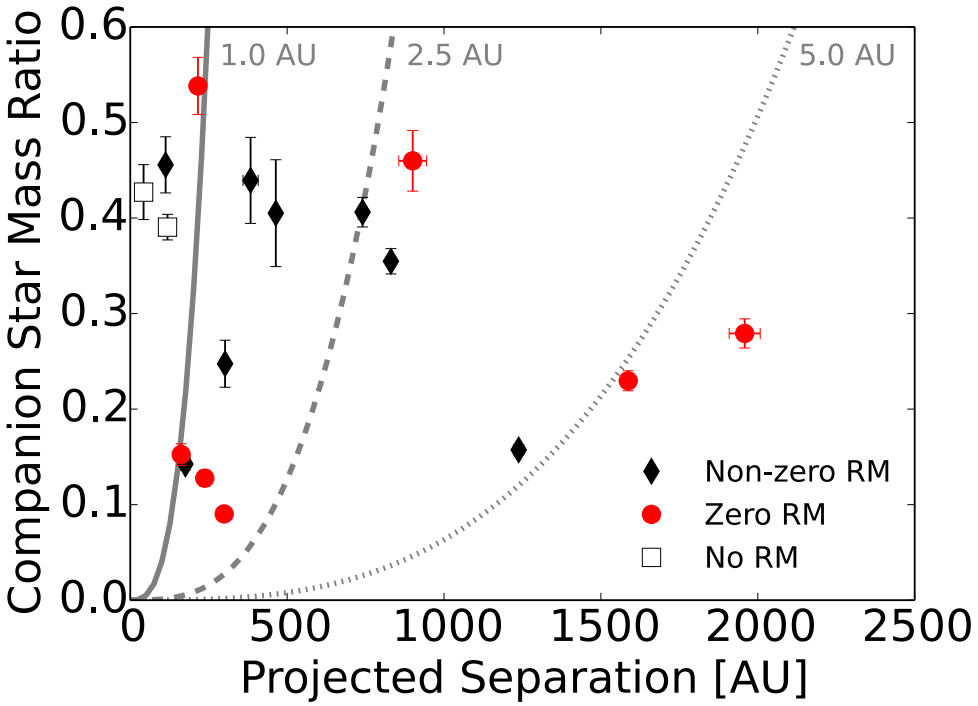

Figure 2.5: For each target, we plot the weighted average of companion masses and projected separation from all epochs reported in Table 2.8. Only one point is plotted for each of the triple systems. We plot targets with a non-zero spin-orbit angle measured using the Rossiter-McLaughlin (RM) effect as black diamonds, targets with spin-orbit angles consistent with zero as red circles, and targets without any spin-orbit angle measurement as open squares. The two objects without a RM measurement are HAT-P-10b and HAT-P-33b; both have orbital eccentricities consistent with zero so we placed them in the "control" sample. Companions that lie above and to the left of the solid, dashed, and dotted lines are sufficiently massive and close enough to excite Kozai-Lidov oscillations and overcome general relativity pericenter precession for giant planets at 1 au, 2.5 au and 5 au, respectively.

ratio and logarithmically spaced bins in semimajor axis out to the distance that corresponds to a separation of 5.5″. For each grid point, we generate 1000 fake companions with a mass and semimajor axis within the grid point limits. We draw the companion's orbital eccentricity from a uniform distribution derived from surveys of field star binaries (Raghavan et al., 2010) and we randomize the remaining orbital elements. Then, for each fake companion, we compute the projected angular separation and brightness ratio and compare to that target's 5σ contrast curve to determine whether or not our survey would have been able to detect that fake companion. Thus, we compute our survey sensitivity for star i for companions in the grid point corresponding to mass ratio m_r and semimajor axis a to be $D_i(m_r, a)$.

We then compute the total average sensitivity, or survey completeness, for star i

as S_i by taking the average of all $D_i(m_r, a)$ values weighted by the frequency of a companion with each m_r and a: $f(m_r, a)$. Raghavan et al. (2010) determine $f(m_r, a)$ to be a log-normal distribution in period (which is a function of m_r and a). We use this distribution to compute each target star's survey sensitivity as:

$$S_i = \frac{\int\int D_i(m_r, a) f(m_r, a) \mathrm{d}m_r \mathrm{d}\ln a}{\int\int f(m_r, a) \mathrm{d}m_r \mathrm{d}\ln a} \tag{2.3}$$

where we integrate over the range of our survey. We are sensitive to companions with periods between 10^4 days and $10^{7.5}$ days, which approximately correspond to semimajor axes between 50 au and 2000 au.

We use our estimate of survey completeness for each star to compute the likelihood L of obtaining our data set of N_d detected companions out of N survey targets as

$$L = \prod_{i=1}^{N_d} (S_i \eta) \prod_{j=1}^{N-N_d} (1 - S_j \eta), \tag{2.4}$$

where η is the true companion fraction and the product sum over i is for the targets with a detected companion while the product sum over j is for the targets without a detected companion. We define companion fraction as the fraction of stars with at least one stellar companion within our survey range.

We use the affine-invariant Markov chain Monte Carlo scheme implemented by the python package "emcee" (Goodman and Weare, 2010; Foreman-Mackey et al., 2013) to determine the posterior probability distribution of η. Our prior on η is uniform between $\eta = 0$ and $\eta = 1$. In addition, we assume that we are 100% complete for targets where we have detected at least one companion because we expect all triple or higher order systems to be hierarchical. That is, we set all $S_i = 1.0$ but still compute S_j as described in Equation 2.3. This assumption is supported by the two hierarchical systems detected by our survey and by previous studies (e.g. Eggleton et al., 2007).

We find that the companion fraction is $\eta_T = 49\% \pm 9\%$ for our total sample, $\eta_M = 48\% \pm 12\%$ for our misaligned sample, and $\eta_C = 51\% \pm 13\%$ for our control sample. These posterior distributions are shown in Figure 2.6. These fractions are consistent with one another and we therefore conclude that there is no evidence for a correlation between the presence of a stellar companion and the orbital properties of the transiting gas giant planet.

We compare the companion fraction for hot ($T_{\rm eff} > 6200$ K) and cool primary stars and find that hot stars have a higher companion rate, at the $2.9\,\sigma$ level. We find

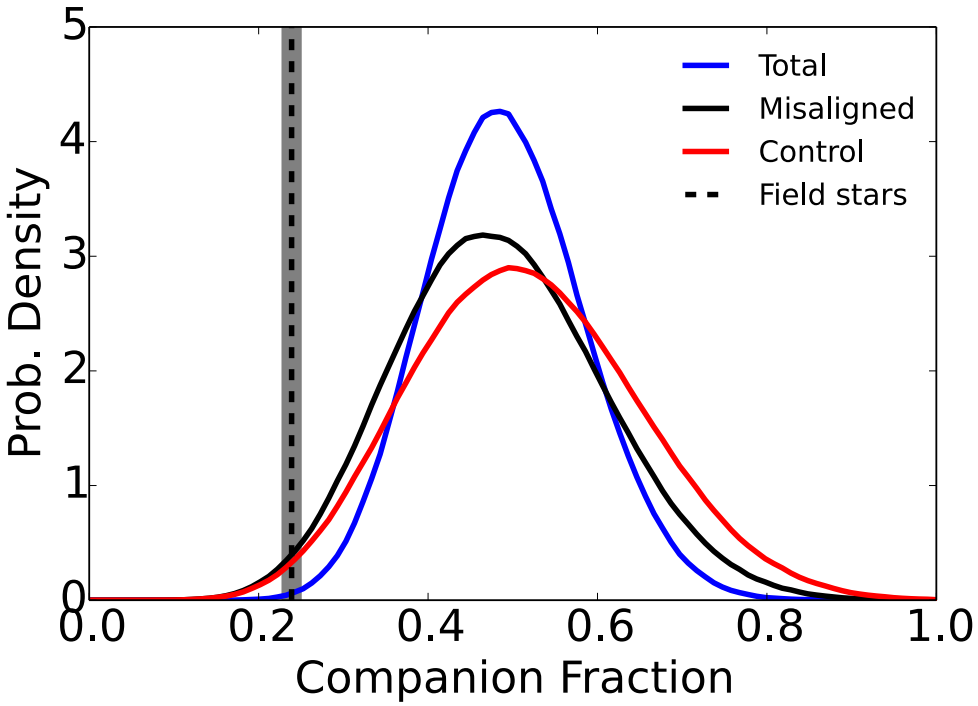

Figure 2.6: A comparison of the posterior probability density of the fraction of stars with at least one companion, η, for our total sample, our misaligned sample, our control sample, and for solar type field stars in the solar neighborhood (Raghavan et al., 2010). Only companions with periods between 10^4 days and $10^{7.5}$ days are considered.

the companion fraction for hot stars to be 75% ± 14% and the companion fraction for cool stars to be 34% ± 10%. This difference is consistent with surveys of stellar multiplicity, which indicate that more massive stars have higher binary fractions (e.g. Duchêne and Kraus, 2013). Surveys of hot Jupiter obliquities indicate that misaligned hot Jupiters are preferentially located around stars hotter than 6200 K, which may be due to more efficient tidal damping of primordial spin-orbit misalignments in systems with cooler host stars (Schlaufman, 2010; Winn et al., 2010; Albrecht et al., 2012). We test this hypothesis by recalculating the companion fractions for our two sub-samples using only stars hotter than 6200 K, where planets should still retain their primordial spin-orbit orientations. We find that hot stars in our misaligned sample have a companion fraction of 59% ± 17%, while hot stars in our control sample have a companion fraction of 83% ± 14%. These fractions are consistent at the 1.7 σ level.

We also consider the companion fractions for the 35 stars in our sample with published measurements of spin-orbit alignment from the Rossiter-McLaughlin

effect. We find the companion fraction for stars with a non-zero spin-orbit angle to be 73% ± 15% while the companion fraction for stars with a spin-orbit angle consistent with zero is 53% ± 14%. These fractions are consistent at the 1.4 σ level.

When we examined these same targets using the radial velocity technique we found that 51% ± 10% had companions with masses between $1 - 13\,M_{Jup}$ on long period orbits (Knutson et al., 2014). Aside from HAT-P-10, where the directly imaged stellar companion is consistent with the measured RV acceleration, we find no evidence for any correlation between the presence of a stellar companion and a measured RV acceleration. Approximately one-third of our target stars have a detected stellar companion and one-third have a radial velocity acceleration, so we would therefore expect to see approximately one-ninth of the stars in our sample with both types of companions. We detect four such systems including HAT-P-10. We therefore conclude that the rates of stellar and radial velocity companions appear to be independent of one another and sum the two in quadrature to obtain a combined stellar and planetary occurrence rate of 72% ± 16%.

Comparison with other direct imaging surveys

We compare this companion fraction to the results from other surveys for stellar companions to planet hosts and field stars. These surveys are summarized in Table 2.9. Our survey results are consistent with previous direct imaging surveys for stellar companions to transiting gas giant planet hosts (Daemgen et al., 2009; Faedi et al., 2013; Bergfors et al., 2013; Adams et al., 2013). These previous surveys had small sample sizes; the largest sample size was 21 stars (Bergfors et al., 2013). Our results are also consistent with the result of infrared direct imaging surveys of *Kepler* transiting planet candidate hosts (Adams et al., 2012; Adams et al., 2013; Dressing et al., 2014; Lillo-Box et al., 2012; Lillo-Box et al., 2014; Wang et al., 2014). Except for Wang et al. (2014) and Horch et al. (2014), none of the above surveys quantify their completeness and their numbers are closer to our uncorrected companion fraction. In addition, these surveys have quite widely varying sensitivities that may contribute to the large observed scatter in measured companion fraction.

Figure 2.7 compares the companions reported in this work with these diffraction-limited near-infrared AO surveys. As companion masses are not always reported, we plot the difference in magnitude versus angular separation for all reported companions. Our survey is primarily sensitive to companions within 5″ while the others

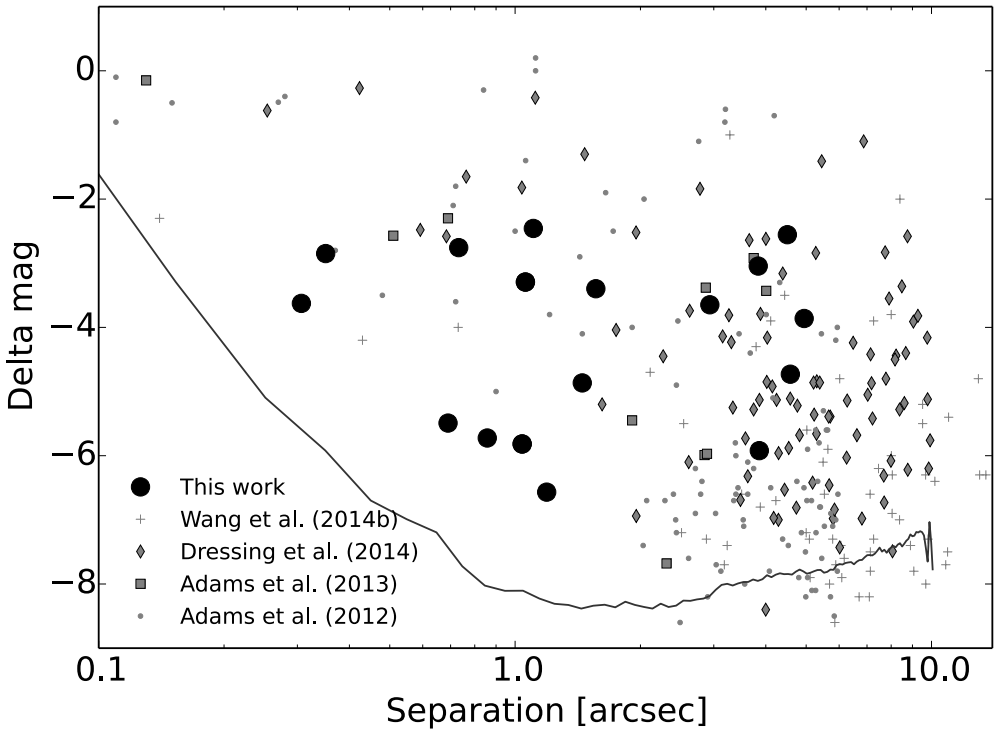

Figure 2.7: The difference in magnitude (J or K_s) for our confirmed physically associated companions compared to companion candidates from other near-infrared direct imaging surveys and a representative 5 σ contrast curve from our survey. Our survey is more sensitive to faint companions at small separations. The published surveys shown here target *Kepler* planet candidate host stars, which are on average three times more distant than our targets. Thus, our survey finds companions at smaller projected physical separations as well.

consider companions at larger separations. In addition, our survey is able to detect companions that are approximately two magnitudes fainter than these previous studies at separations less than 2″. Because the *Kepler* candidate host stars are on average significantly more distant than our target stars, these surveys were unable to distinguish between background objects and bound stellar companions. This also means that the *Kepler* surveys are less sensitive to stellar companions at small projected physical separations. We also limit our survey to systems with short-period transiting gas giant planets, while the *Kepler* planet candidate sample is dominated by much smaller planets, many of which are in compact multi-planet systems.

The direct imaging surveys conducted at visible wavelengths (Law et al., 2014; Gilliland et al., 2015; Horch et al., 2014) report smaller companion fractions than our survey and other NIR surveys. This is not surprising, as the majority of our detected companions are M stars that would be much fainter at optical wavelengths.

These surveys also have relatively small fields of view, which would also contribute to a lower detection rate for companions as compared to the wide-field infrared surveys.

We note that our results for the multiplicity rate of hot Jupiter host stars may also have implications for the ongoing debate about the origin of the discrepancy between hot Jupiter occurrence rates from radial velocity and transit surveys. Wang et al. (2015) point out that hot Jupiter occurrence rates in *Kepler* surveys are approximately two to three times smaller than hot Jupiter occurrence rates in Doppler planet surveys. Because the *Kepler* survey does not filter multi-stellar systems from its target list, Wang et al. (2015) suggest that one potential cause for the discrepancy may be that these companion stars are suppressing the formation of all planets, including hot Jupiters, in the *Kepler* sample. Wang et al. (2014) also find that planets are 1.7 ± 0.5 times less likely to form in a system with a stellar companion within 1000 au. However, we find that half of all hot Jupiters are found in stellar binaries, indicating that stellar multiplicity does not inhibit the formation of these systems for cases where the stellar companion is on an orbit approximately 50-2000 au.

Comparison with field stars

Finally, we compare our companion fraction to the measured multiplicity rate for solar-type field stars. The most recent survey (Raghavan et al., 2010) reports that $44\% \pm 2\%$ of solar-type stars within 25 pc are in multiple star systems, which is in good agreement with previous results from Duquennoy and Mayor (1991). This value is corrected for survey completeness. This fraction includes companions with separations too small to resolve with direct imaging or too wide to be found within our survey's field of view. Thus, we only consider the companions from Raghavan et al. (2010) with periods between 10^4 days and $10^{7.5}$ days, which corresponds to physical separations of approximately 50 au and 2000 au. If we select only the subset of binaries from Raghavan et al. (2010) that fall within this period range, we find that the fraction of field stars with stellar companions is $24\% \pm 1\%$. This is $2.8\,\sigma$ smaller than our estimated companion frequency for systems with short period gas giant planets, suggesting that the presence of a stellar companion increases the likelihood that a gas giant planet will migrate inward to a relatively short period orbit.

2.7 Summary

We found nineteen companions around seventeen targets, including two triple systems, HAT-P-8 and WASP-12, which we previously reported in Bechter et al.

Table 2.9: Stellar companion fractions from other surveys

Survey	η	Range	$N_{\rm targets}$	Notes
This work				
Total sample, uncorrected	34% ± 7%	5.5″	50	Diffraction-limited AO
Total sample, corrected	49% ± 9%	5.5″	50	Diffraction-limited AO
Misaligned sample, corrected	48% ± 12%	5.5″	27	Diffraction-limited AO
Control sample, corrected	51% ± 13%	5.5″	23	Diffraction-limited AO
Near-infrared direct imaging surveys of transiting gas giant planet hosts				
Daemgen et al. (2009)	21% ± 12%	Unknown[a]	14	Lucky imaging
Faedi et al. (2013)	38% ± 15%	Unknown[a]	16	Lucky imaging
Bergfors et al. (2013)	29% ± 12%	Unknown[a]	21	Lucky imaging
Adams et al. (2013)	33% ± 15%	Unknown[a]	15	Diffraction-limited AO
Near-infrared direct imaging surveys of *Kepler* planet candidate hosts				
Adams et al. (2012)	59% ± 5%	6″	90	Diffraction-limited AO
Adams et al. (2013)	33% ± 17%	Unknown[a]	12	Diffraction-limited AO
Dressing et al. (2014)	31% ± 5%	4″	87	Diffraction-limited AO
Lillo-Box et al. (2012, 2014)	33% ± 4%	6″	174	Lucky imaging
Wang et al. (2014)	45% ± 7%	6″	56	Diffraction-limited AO
Optical direct imaging surveys of *Kepler* planet candidate hosts				
Law et al. (2014)	7.4% ± 1.0%	2.5″	715	Diffraction-limited AO
	$14.0^{+5.8}_{-3.5}$%			Only hosts of planets $P < 15$ d, $R_p > R_{\rm Nep}$
Gilliland et al. (2015)	22% ± 10%	2.5″	23	Hubble Space Telescope WFC3 imaging
Horch et al. (2014), raw	7.0% ± 1.1%	1″	588	DSSI[b] on WIYN 3.5m telescope
	23% ± 8%	1″	35	DSSI[b] on Gemini-N 8.1m telescope
Horch et al. (2014), corrected	37% ± 7%	1″	588	DSSI[b] on WIYN 3.5m telescope
	47% ± 19%	1″	35	DSSI[b] on Gemini-N 8.1m telescope
Multi-modal surveys of field stars				
Raghavan et al. (2010)	44% ± 2%	varies[c]	454	Solar-like stars with 25 pc
	24% ± 1%	See note[d]	454	For comparison with our survey

Notes. Unless otherwise noted, companion fraction η reported are based on raw counts, with no correction for completeness. The uncertainties for completeness corrected companion fractions do not scale inversely with the square root of the number of targets because the completeness correction effectively multiplies both the value and uncertainty by a constant.
[a] These studies do not report a number of companions in any given range.
[b] Differential speckle survey instrument
[c] This study uses multiple techniques to find stellar companions, each with different sensitivities for companion separation.
[d] This line reports the fraction of stars with companions in the same range as our survey, as detailed in Section 2.6.

(2014). We measure the proper motions for all detected companions and confirm that they are physically bound to the planet-hosting primary stars. We report seven new multiple star systems with transiting giant planets and provide follow-up observations for ten previously reported candidate multi-star systems. Our follow-up observations allowed us to confirm the bound nature of three previously detected candidate companions and were in good agreement with the conclusions of previous studies on the bound nature of the other seven companions. We also determined the second candidate companion to HAT-P-7 found by Narita et al. (2012) to be a background object. For all systems, we provide updated astrometric measurements as well as estimated masses and physical separations for the observed companions. We find that most of the detected companions are massive enough to excite Kozai-Lidov

oscillations on giant planets forming within 5 au.

Our companion fraction is consistent with previous NIR direct imaging surveys of stellar companions around transiting planet hosts. We correct for survey sensitivity and find that close-in transiting gas giant planetary hosts are approximately twice as likely to have at least one stellar companion with 50 au $\lesssim a \lesssim$ 2000 au as compared to field stars, although the significance of this difference is only $2.8\,\sigma$. We find that the companion fraction for systems hosting a transiting gas giant planet on a misaligned or eccentric orbit is indistinguishable from the companion fraction for systems hosting a planet on a well-aligned and circular orbit. This is consistent with other results that suggest hot Jupiters may not primarily migrate via the Kozai-Lidov mechanism (Dawson et al., 2015; Naoz et al., 2012; Petrovich, 2015). We also recalculate the companion fractions for our two sub-samples using only stars hotter than 6200 K, as it has been suggested that tidal evolution might be able to remove primordial spin-orbit misalignments for planets orbiting cooler stars. We find that there is no evidence for a correlation between the presence of a stellar companion and spin-orbit misalignment of the transiting hot Jupiter, in good agreement with our results for the full sample. Finally, we calculate the companion frequency for the overall sample as a function of host star temperature and find that stars hotter than 6200 K have a companion rate that is approximately two times larger ($2.9\,\sigma$ significance) than their cool counterparts, consistent with surveys of stellar multiplicity (Duchêne and Kraus, 2013).

We conclude that the data are consistent with two possible scenarios and discuss them here. First, stellar companions may not play a role in the determination of hot Jupiter spin-orbit misalignments. This would be consistent with the planet-planet scattering scenario (e.g. Chatterjee et al., 2008; Nagasawa et al., 2008; Wu and Lithwick, 2011; Beaugé and Nesvorný, 2012; Lithwick and Wu, 2014). However, our radial velocity survey in Knutson et al. (2014) found no correlation between the presence of a long term radial velocity acceleration and the spin-orbit alignment of the inner transiting planet. Other proposed orbital obliquity excitation mechanisms that do not require a companion star include misalignment of the natal disk's angular momentum vector with respect to the stellar spin axis due to chaotic star formation (Bate et al., 2010; Thies et al., 2011; Fielding et al., 2015), magnetic warping torques due to the primary star's magnetic field (Lai et al., 2011), and modulation of stellar surfaces by internal gravity waves (Rogers et al., 2012; Rogers et al., 2013). Alternatively, primordial gravitationally bound stellar companions may have acted to perturb the

protoplanetary disks out of alignment with their host stars at the epoch of star and planet formation (e.g. Batygin, 2012; Batygin and Adams, 2013; Crida and Batygin, 2014; Storch et al., 2014). However, dynamical processing by cluster evolution would have removed or exchanged these companions, diminishing their current observational signatures (Malmberg et al., 2007b). In other words, the companions we observe today may not be the ones responsible for the facilitation of hot Jupiter misalignments.

In this scenario, a majority of planetary systems should form from disks with random alignments, regardless of whether or not there is currently a stellar companion present. This prediction can be tested by measuring the spin-orbit alignment of a large number of coplanar, multi-planet systems such as those detected by the *Kepler* survey. If a significant fraction of these systems are misaligned even when no stellar companion is present, it would provide strong support for the ubiquity of primordial disk misalignments, which could also explain the observed population of misaligned hot Jupiters. Morton and Winn (2014) present the framework for such a test.

Whatever the favored scenario may be, it must also be consistent with the increased frequency of misaligned hot Jupiters found around hot stars. If a stellar companion is not responsible for misalignment, then tidal evolution of the star-planet pair, which proceeds at an enhanced rate around cooler stars, could give rise to the observed trend (e.g. Winn et al., 2010; Lai, 2012; Valsecchi and Rasio, 2014). However, this mechanism has been recently criticized by Rogers and Lin (2013), who argue that such a process requires an unphysical set of assumptions, and would generally lead to a misalignment distribution that is inconsistent with the observed one. Alternatively, magnetically facilitated disk-star coupling may cause cooler stars to realign with their disks (Spalding and Batygin, 2014b), signaling constancy with the second scenario where protoplanetary disks are misaligned by transient stellar companions at early times.

The apparent enhancement in the companion fraction for our sample of transiting planets versus that of field stars is suggestive, and may indicate that these companions play a role in the migration process. Intriguingly, Law et al. (2014) found tentative evidence that in the *Kepler* sample, short period gas giant planets are more likely to have stellar companions than their more distant counterparts, which is also consistent with the idea that these companions play a role in planet migration. In addition, when considering the companion fraction found in our radial velocity survey (Knutson et al., 2014), we find that the overall rate of both planetary and stellar companions

in systems with close-in transiting gas giant planets is 72% ± 16%, suggesting that these systems frequently have companions that may interact dynamically with the short-period planet.

In the future, we plan to survey a larger sample of planets detected using the radial velocity technique, which will span a much broader range of semimajor axes than any of the transiting planet surveys. A number of sources show long-term Doppler accelerations indicating the presence of outer companions, and Keck AO imaging has been demonstrated as a successful technique for identifying faint stellar and substellar companions based on the existence of such "trends" (Crepp et al., 2012). These data should provide a more definitive test of the potential correlation between multiplicity and orbital semimajor axis of the inner planet. We also plan to expand our sample of hot Jupiter systems with AO imaging, in order to reduce the uncertainties in our estimate of the stellar companion rate for these systems.

2.8 Acknowledgments

This work was supported by NASA grant NNX14AD24G. HN is grateful for funding support from the Natural Sciences and Engineering Research Council of Canada. JAJ gratefully acknowledges support from generous fellowships from the David & Lucile Packard and Alfred P. Sloan foundations. We also thank Brendan Bowler for assistance with our common proper motion analysis and Rebekah Dawson and Cristobal Petrovich for helpful discussions.

This work was based on observations at the W. M. Keck Observatory granted by the California Institute of Technology. We thank the observers who contributed to the measurements reported here and acknowledge the efforts of the Keck Observatory staff. We extend special thanks to those of Hawaiian ancestry on whose sacred mountain of Mauna Kea we are privileged to be guests.

References

Adams, E. R., D. R. Ciardi, A. K. Dupree, et al. (2012). *The Astronomical Journal* **144**, 42. DOI: 10.1088/0004-6256/144/2/42.

Adams, E. R., A. K. Dupree, C. Kulesa, and D. McCarthy (2013). *The Astronomical Journal* **146**, 9. DOI: 10.1088/0004-6256/146/1/9.

Albrecht, S., J. N. Winn, J. A. Johnson, et al. (2011). *The Astrophysical Journal* **738**, 50. DOI: 10.1088/0004-637X/738/1/50.

Albrecht, S., J. N. Winn, J. A. Johnson, et al. (2012). *The Astrophysical Journal* **757**, 18. DOI: 10.1088/0004-637X/757/1/18.

Anderson, D. R., A. Collier Cameron, M. Gillon, et al. (2011). *Astronomy & Astrophysics* **534**, A16. DOI: 10.1051/0004-6361/201117597.

Bakos, G. Á., J. D. Hartman, G. Torres, et al. (2012). *The Astronomical Journal* **144**, 19. DOI: 10.1088/0004-6256/144/1/19.

Bakos, G. Á., J. Hartman, G. Torres, et al. (2011). *The Astrophysical Journal* **742**, 116. DOI: 10.1088/0004-637X/742/2/116.

Bakos, G. Á., A. W. Howard, R. W. Noyes, et al. (2009a). *The Astrophysical Journal* **707**, 446. DOI: 10.1088/0004-637X/707/1/446.

Bakos, G. Á., A. Pál, G. Torres, et al. (2009b). *The Astrophysical Journal* **696**, 1950. DOI: 10.1088/0004-637X/696/2/1950.

Bakos, G. Á., G. Torres, A. Pál, et al. (2010). *The Astrophysical Journal* **710**, 1724. DOI: 10.1088/0004-637X/710/2/1724.

Baraffe, I., G. Chabrier, F. Allard, and P. H. Hauschildt (1998). *Astronomy & Astrophysics* **412**, 403.

Barclay, T., D. Huber, J. F. Rowe, et al. (2012). *The Astrophysical Journal* **761**, 53. DOI: 10.1088/0004-637X/761/1/53.

Barros, S. C. C., F. Faedi, A. Collier Cameron, et al. (2011). *Astronomy & Astrophysics* **525**, A54. DOI: 10.1051/0004-6361/201015800.

Bate, M. R., G. Lodato, and J. E. Pringle (2010). *Monthly Notices of the Royal Astronomical Society* **401**, 1505. DOI: 10.1111/j.1365-2966.2009.15773.x.

Batygin, K., A. Morbidelli, and K. Tsiganis (2011). *Astronomy & Astrophysics* **533**, A7. DOI: 10.1051/0004-6361/201117193.

Batygin, K. (2012). *Nature* **491**, 418. DOI: 10.1038/nature11560.

Batygin, K. and F. C. Adams (2013). *The Astrophysical Journal* **778**, 169. DOI: 10.1088/0004-637X/778/2/169.

Beaugé, C. and D. Nesvorný (2012). *The Astrophysical Journal* **751**, 119. DOI: 10.1088/0004-637X/751/2/119.

Bechter, E. B., J. R. Crepp, H. Ngo, et al. (2014). *The Astrophysical Journal* **788**, 2. DOI: 10.1088/0004-637X/788/1/2.

Bergfors, C., W. Brandner, S. Daemgen, et al. (2013). *Monthly Notices of the Royal Astronomical Society* **428**, 182. DOI: 10.1093/mnras/sts019.

Bowler, B. P., M. C. Liu, E. L. Shkolnik, and M. Tamura (2014). *The Astrophysical Journal Supplement Series* **216**, 7. DOI: 10.1088/0067-0049/216/1/7.

Braun, K. von, T. S. Boyajian, S. R. Kane, et al. (2012). *The Astrophysical Journal* **753**, 171. DOI: 10.1088/0004-637X/753/2/171.

Brown, D. J. A., A. Collier Cameron, R. F. Díaz, et al. (2012). *The Astrophysical Journal* **760**, 139. DOI: 10.1088/0004-637X/760/2/139.

Buchhave, L. A., G. Á. Bakos, J. D. Hartman, et al. (2010). *The Astrophysical Journal* **720**.2, 1118–1125. DOI: 10.1088/0004-637X/720/2/1118.

Buchhave, L. A., G. Á. Bakos, J. D. Hartman, et al. (2011). *The Astrophysical Journal* **733**, 116. DOI: 10.1088/0004-637X/733/2/116.

Carter, J. A., J. N. Winn, R. Gilliland, and M. J. Holman (2009). *The Astrophysical Journal* **696**, 241. DOI: 10.1088/0004-637X/696/1/241.

Chatterjee, S., E. B. Ford, S. Matsumura, and F. A. Rasio (2008). *The Astrophysical Journal* **686**, 580. DOI: 10.1086/590227.

Christian, D. J., N. P. Gibson, E. K. Simpson, et al. (2009). *Monthly Notices of the Royal Astronomical Society* **392**, 1585. DOI: 10.1111/j.1365-2966.2008.14164.x.

Collier Cameron, A., F. Bouchy, G. Hebrard, et al. (2007). *Monthly Notices of the Royal Astronomical Society* **375**, 951. DOI: 10.1111/j.1365-2966.2006.11350.x.

Collier Cameron, A., E. Guenther, B. Smalley, et al. (2010). *Monthly Notices of the Royal Astronomical Society* **407**, 507. DOI: 10.1111/j.1365-2966.2010.16922.x.

Crepp, J. R., J. A. Johnson, A. W. Howard, et al. (2012). *The Astrophysical Journal* **761**, 39. DOI: 10.1088/0004-637X/761/1/39.

Crida, A. and K. Batygin (2014). *Astronomy & Astrophysics* **567**, A42. DOI: 10.1051/0004-6361/201323292.

Crossfield, I. J. M., T. Barman, B. M. S. Hansen, I. Tanaka, and T. Kodama (2012). *The Astrophysical Journal* **760**, 140. DOI: 10.1088/0004-637X/760/2/140.

Daemgen, S., F. Hormuth, W. Brandner, et al. (2009). *Astronomy and Astrophysics* **498**, 567. DOI: 10.1051/0004-6361/200810988.

Dawson, R. I. (2014). *The Astrophysical Journal* **790**, L31. DOI: 10.1088/2041-8205/790/2/L31.

Dawson, R. I. and R. A. Murray-Clay (2013). *The Astrophysical Journal* **767**, L24. DOI: 10.1088/2041-8205/767/2/L24.

Dawson, R. I., R. A. Murray-Clay, and J. A. Johnson (2015). *The Astrophysical Journal* **798**, 66. DOI: 10.1088/0004-637X/798/2/66.

Doyle, A. P., B. Smalley, P. F. L. Maxted, et al. (2013). *Monthly Notices of the Royal Astronomical Society* **428**, 3164. DOI: 10.1093/mnras/sts267.

Dressing, C. D., E. R. Adams, A. K. Dupree, C. Kulesa, and D. McCarthy (2014). *The Astronomical Journal* **148**, 78. DOI: 10.1088/0004-6256/148/5/78.

Duchêne, G. and A. Kraus (2013). *Annual Review of Astronomy and Astrophysics* **51**, 269. DOI: 10.1146/annurev-astro-081710-102602.

Duquennoy, A. and M. Mayor (1991). *Astronomy & Astrophysics* **248**, 485.

Eggenberger, A., S. Udry, G. Chauvin, et al. (2007). *Astronomy and Astrophysics* **474**, 273. DOI: 10.1051/0004-6361:20077447.

Eggleton, P. P., L. Kisseleva-Eggleton, and X. Dearborn (2007). *Proceedings of the International Astronomical Union* **2**.S240, 347. DOI: 10.1017/S1743921307004280.

Fabrycky, D. and S. Tremaine (2007). *The Astrophysical Journal* **669**, 1298. DOI: 10.1086/521702.

Faedi, F., T. Staley, Y. Gomez Maqueo Chew, et al. (2013). *Monthly Notices of the Royal Astronomical Society* **433**, 2097. DOI: 10.1093/mnras/stt885.

Fielding, D. B., C. F. McKee, A. Socrates, A. J. Cunningham, and R. I. Klein (2015). *Monthly Notices of the Royal Astronomical Society* **450**, 3306. DOI: 10.1093/mnras/stv836.

Foreman-Mackey, D., D. W. Hogg, D. Lang, and J. Goodman (2013). *Publications of the Astronomical Society of the Pacific* **125**, 306. DOI: 10.1086/670067.

Fragner, M. M., R. P. Nelson, and W. Kley (2011). *Astronomy & Astrophysics* **528**, A40. DOI: 10.1051/0004-6361/201015378.

Fressin, F., G. Torres, D. Charbonneau, et al. (2013). *The Astrophysical Journal* **766**, 81. DOI: 10.1088/0004-637X/766/2/81.

Gibson, N. P., D. Pollacco, E. K. Simpson, et al. (2008). *Astronomy & Astrophysics* **492**, 603. DOI: 10.1051/0004-6361.

Gilliland, R. L., K. M. S. Cartier, E. R. Adams, et al. (2015). *The Astronomical Journal* **149**, 24. DOI: 10.1088/0004-6256/149/1/24.

Goldreich, P. and S. Tremaine (1980). *The Astrophysical Journal* **241**, 425. DOI: 10.1086/158356.

Goodman, J. and J. Weare (2010). *Communications in Applied Mathematics and Computational Science* **5**, 65. DOI: 10.2140/camcos.2010.5.65.

Hartman, J. D., G. Á. Bakos, D. M. Kipping, et al. (2011a). *The Astrophysical Journal* **728**, 138. DOI: 10.1088/0004-637X/728/2/138.

Hartman, J. D., G. Á. Bakos, B. Sato, et al. (2011b). *The Astrophysical Journal* **726**, 52. DOI: 10.1088/0004-637X/726/1/52.

Hartman, J. D., G. Á. Bakos, G. Torres, et al. (2009). *The Astrophysical Journal* **706**, 785. DOI: 10.1088/0004-637X/706/1/785.

Hartman, J. D., G. Á. Bakos, G. Torres, et al. (2011c). *The Astrophysical Journal* **742**, 59. DOI: 10.1088/0004-637X/742/1/59.

Hebb, L., A. Collier Cameron, B. Loeillet, et al. (2009). *The Astrophysical Journal* **693**, 1920. DOI: 10.1088/0004-637X/693/2/1920.

Hellier, C., D. R. Anderson, M. Gillon, et al. (2009). *The Astrophysical Journal* **690**, L89. DOI: 10.1088/0004-637X/690/1/L89.

Horch, E. P., S. B. Howell, M. E. Everett, and D. R. Ciardi (2014). *The Astrophysical Journal* **795**, 60. DOI: 10.1088/0004-637X/795/1/60.

Howard, A. W., G. Á. Bakos, J. Hartman, et al. (2012a). *The Astrophysical Journal* **749**, 134. DOI: 10.1088/0004-637X/749/2/134.

Howard, A. W., G. W. Marcy, S. T. Bryson, et al. (2012b). *The Astrophysical Journal Supplement Series* **201**, 15. DOI: 10.1088/0067-0049/201/2/15.

Husser, T.-O., S. Wende-von Berg, S. Dreizler, et al. (2013). *Astronomy & Astrophysics* **553**, A6. DOI: 10.1051/0004-6361/201219058.

Johnson, J. A., J. N. Winn, G. Á. Bakos, et al. (2011). *The Astrophysical Journal* **735**, 24. DOI: 10.1088/0004-637X/735/1/24.

Johnson, J. A., J. N. Winn, S. Albrecht, et al. (2009). *Publications of the Astronomical Society of the Pacific* **121**, 1104. DOI: 10.1086/644604.

Joshi, Y. C., D. Pollacco, A. Collier Cameron, et al. (2009). *Monthly Notices of the Royal Astronomical Society* **392**, 1532. DOI: 10.1111/j.1365-2966.2008.14178.x.

Kaib, N. A., S. N. Raymond, and M. Duncan (2013). *Nature* **493**, 381. DOI: 10.1038/nature11780.

Kaib, N. A., S. N. Raymond, and M. J. Duncan (2011). *The Astrophysical Journal* **742**, L24. DOI: 10.1088/2041-8205/742/2/L24.

Kipping, D. M., G. Á. Bakos, J. Hartman, et al. (2010). *The Astrophysical Journal* **725**, 2017. DOI: 10.1088/0004-637X/725/2/2017.

Kipping, D. M., J. Hartman, G. Á. Bakos, et al. (2011). *The Astronomical Journal* **142**, 95. DOI: 10.1088/0004-6256/142/3/95.

Knutson, H. A., B. J. Fulton, B. T. Montet, et al. (2014). *The Astrophysical Journal* **785**, 126. DOI: 10.1088/0004-637X/785/2/126.

Kovács, G., G. Á. Bakos, J. D. Hartman, et al. (2010). *The Astrophysical Journal* **724**, 866. DOI: 10.1088/0004-637X/724/2/866.

Kovács, G., G. Á. Bakos, G. Torres, et al. (2007). *The Astrophysical Journal* **670**, L41. DOI: 10.1086/524058.

Kraus, A. L., M. J. Ireland, L. A. Hillenbrand, and F. Martinache (2012). *The Astrophysical Journal* **745**, 19. DOI: 10.1088/0004-637X/745/1/19.

Lai, D. (2012). *Monthly Notices of the Royal Astronomical Society* **423**, 486. DOI: 10.1111/j.1365-2966.2012.20893.x.

Lai, D., F. Foucart, and D. N. C. Lin (2011). *Proceedings of the International Astronomical Union* **S276**, 295. DOI: 10.1017/S1743921311020345.

Law, N. M., T. Morton, C. Baranec, et al. (2014). *The Astrophysical Journal* **791**, 35. DOI: 10.1088/0004-637X/791/1/35.

Li, G., S. Naoz, B. Kocsis, and A. Loeb (2014). *The Astrophysical Journal* **785**, 116. DOI: 10.1088/0004-637X/785/2/116.

Lillo-Box, J., D. Barrado, and H. Bouy (2012). *Astronomy & Astrophysics* **546**, A10. DOI: 10.1051/0004-6361/201219631.

Lillo-Box, J., D. Barrado, and H. Bouy (2014). *Astronomy & Astrophysics* **566**, A103. DOI: 10.1051/0004-6361/201423497.

Lin, D. N. C., P. Bodenheimer, and D. C. Richardson (1996). *Nature* **380**, 606. DOI: 10.1038/380606a0.

Lin, D. N. C. and J. Papaloizou (1986). *The Astrophysical Journal* **309**, 846. DOI: 10.1086/164653.

Lithwick, Y. and Y. Wu (2014). *Proceedings of the National Academy of Sciences of the United States of America* **111**, 12610. DOI: 10.1073/pnas.1308261110.

Malmberg, D., M. B. Davies, and J. E. Chambers (2007a). *Monthly Notices of the Royal Astronomical Society: Letters* **377**, L1. DOI: 10.1111/j.1745-3933.2007.00291.x.

Malmberg, D., F. De Angeli, M. B. Davies, et al. (2007b). *Monthly Notices of the Royal Astronomical Society* **378**, 1207. DOI: 10.1111/j.1365-2966.2007.11885.x.

Mancini, L., J. Southworth, S. Ciceri, et al. (2013). *Astronomy & Astrophysics* **551**, A11. DOI: 10.1051/0004-6361/201220291.

Mason, B. D., G. L. Wycoff, W. I. Hartkopf, G. G. Douglass, and C. E. Worley (2001). *The Astronomical Journal* **122**, 3466. DOI: 10.1086/323920.

Maxted, P. F. L., D. R. Anderson, M. Gillon, et al. (2010). *The Astronomical Journal* **140**, 2007. DOI: 10.1088/0004-6256/140/6/2007.

Maxted, P. F. L., C. Koen, and B. Smalley (2011). *Monthly Notices of the Royal Astronomical Society* **418**, 1039. DOI: 10.1111/j.1365-2966.2011.19554.x.

Mayer, L., J. Wadsley, T. Quinn, and J. Stadel (2005). *Monthly Notices of the Royal Astronomical Society* **363**, 641. DOI: 10.1111/j.1365-2966.2005.09468.x.

McCullough, P. R., C. J. Burke, J. A. Valenti, et al. (2008). arXiv: 0805.2921.

Miller, G. R. M., A. Collier Cameron, E. K. Simpson, et al. (2010). *Astronomy & Astrophysics* **523**, A52. DOI: 10.1051/0004-6361/201015052.

Morton, T. D. and J. A. Johnson (2011). *The Astrophysical Journal* **729**, 138. DOI: 10.1088/0004-637X/729/2/138.

Morton, T. D. and J. N. Winn (2014). *The Astrophysical Journal* **796**, 47. DOI: 10.1088/0004-637X/796/1/47.

Moutou, C., R. F. Díaz, S. Udry, et al. (2011). *Astronomy & Astrophysics* **533**, A113. DOI: 10.1051/0004-6361/201116760.

Mugrauer, M., C. Ginski, and M. Seeliger (2014). *Monthly Notices of the Royal Astronomical Society* **439**, 106. DOI: 10.1093/mnras/stu044.

Nagasawa, M., S. Ida, and T. Bessho (2008). *The Astrophysical Journal* **678**, 498. DOI: 10.1086/529369.

Naoz, S., W. M. Farr, Y. Lithwick, F. A. Rasio, and J. Teyssandier (2013). *Monthly Notices of the Royal Astronomical Society* **431**, 2155. DOI: 10.1093/mnras/stt302.

Naoz, S., W. M. Farr, and F. A. Rasio (2012). *The Astrophysical Journal* **754**, L36. DOI: 10.1088/2041-8205/754/2/L36.

Narita, N., T. Kudo, C. Bergfors, et al. (2010a). *Publications of the Astronomical Society of Japan* **62**, 779. DOI: 10.1093/pasj/62.3.779.

Narita, N., B. Sato, T. Hirano, et al. (2010b). *Publications of the Astronomical Society of Japan* **62**, 653. DOI: 10.1093/pasj/62.3.653.

Narita, N., Y. H. Takahashi, M. Kuzuhara, et al. (2012). *Publications of the Astronomical Society of Japan* **64**, L7. DOI: 10.1093/pasj/64.6.L7.

Orosz, J. A., W. F. Welsh, J. A. Carter, et al. (2012a). *Science (New York, N.Y.)* **337**, 1511. DOI: 10.1126/science.1228380.

Orosz, J. A., W. F. Welsh, J. A. Carter, et al. (2012b). *The Astrophysical Journal* **758**, 87. DOI: 10.1088/0004-637X/758/2/87.

Pál, A., G. Á. Bakos, J. Fernandez, et al. (2009). *The Astrophysical Journal* **700**, 783. DOI: 10.1088/0004-637X/700/1/783.

Pál, A., G. Á. Bakos, G. Torres, et al. (2008). *The Astrophysical Journal* **680**, 1450. DOI: 10.1086/588010.

Pál, A., G. Á. Bakos, G. Torres, et al. (2010). *Monthly Notices of the Royal Astronomical Society* **401**, 2665. DOI: 10.1111/j.1365-2966.2009.15849.x.

Petrovich, C. (2015). *The Astrophysical Journal* **799**, 27. DOI: 10.1088/0004-637X/799/1/27.

Pichardo, B., L. S. Sparke, and L. A. Aguilar (2005). *Monthly Notices of the Royal Astronomical Society* **359**, 521. DOI: 10.1111/j.1365-2966.2005.08905.x.

Pollacco, D., I. Skillen, A. Collier Cameron, et al. (2008). *Monthly Notices of the Royal Astronomical Society* **385**, 1576. DOI: 10.1111/j.1365-2966.2008.12939.x.

Queloz, D., D. R. Anderson, A. Collier Cameron, et al. (2010). *Astronomy and Astrophysics* **517**, L1. DOI: 10.1051/0004-6361/201014768.

Rafikov, R. R. (2013a). *The Astrophysical Journal* **764**, L16. DOI: 10.1088/2041-8205/764/1/L16.

Rafikov, R. R. (2013b). *The Astrophysical Journal* **765**, L8. DOI: 10.1088/2041-8205/765/1/L8.

Raghavan, D., H. A. McAlister, T. J. Henry, et al. (2010). *The Astrophysical Journal Supplement Series* **190**, 1. DOI: 10.1088/0067-0049/190/1/1.

Rogers, T. M. and D. N. C. Lin (2013). *The Astrophysical Journal* **769**, L10. DOI: 10.1088/2041-8205/769/1/L10.

Rogers, T. M., D. N. C. Lin, and H. H. B. Lau (2012). *The Astrophysical Journal* **758**, L6. DOI: 10.1088/2041-8205/758/1/L6.

Rogers, T. M., D. N. C. Lin, J. N. McElwaine, and H. H. B. Lau (2013). *The Astrophysical Journal* **772**, 21. DOI: 10.1088/0004-637X/772/1/21.

Schlaufman, K. C. (2010). *The Astrophysical Journal* **719**, 602. DOI: 10.1088/0004-637X/719/1/602.

Simpson, E. K., D. Pollacco, A. Collier Cameron, et al. (2011). *Monthly Notices of the Royal Astronomical Society* **414**, 3023. DOI: 10.1111/j.1365-2966.2011.18603.x.

Sing, D. K., A. Lecavelier des Etangs, J. J. Fortney, et al. (2013). *Monthly Notices of the Royal Astronomical Society* **436**, 2956. DOI: 10.1093/mnras/stt1782.

Skrutskie, M. F., R. M. Cutri, R. Stiening, et al. (2006). *The Astronomical Journal* **131**, 1163. DOI: 10.1086/498708.

Smalley, B., D. R. Anderson, A. Collier Cameron, et al. (2011). *Astronomy & Astrophysics* **526**, A130. DOI: 10.1051/0004-6361/201015992.

Southworth, J., L. Mancini, P. Browne, et al. (2013). *Monthly Notices of the Royal Astronomical Society* **434**, 1300. DOI: 10.1093/mnras/stt1089.

Southworth, J. (2012). *Monthly Notices of the Royal Astronomical Society* **426**, 1291. DOI: 10.1111/j.1365-2966.2012.21756.x.

Southworth, J., I. Bruni, L. Mancini, and J. Gregorio (2012a). *Monthly Notices of the Royal Astronomical Society* **420**, 2580. DOI: 10.1111/j.1365-2966.2011.20230.x.

Southworth, J., L. Mancini, P. F. L. Maxted, et al. (2012b). *Monthly Notices of the Royal Astronomical Society* **422**, 3099. DOI: 10.1111/j.1365-2966.2012.20828.x.

Sozzetti, A., G. Torres, D. Charbonneau, et al. (2007). *The Astrophysical Journal* **664**, 1190. DOI: 10.1086/519214.

Sozzetti, A., G. Torres, D. Charbonneau, et al. (2009). *The Astrophysical Journal* **691**, 1145. DOI: 10.1088/0004-637X/691/2/1145.

Spalding, C. and K. Batygin (2014a). *The Astrophysical Journal* **790**, 42. DOI: 10.1088/0004-637X/790/1/42.

Spalding, C. and K. Batygin (2014b). *American Astronomical Society, DPS meeting 46*, #501.02.

Storch, N. I., K. R. Anderson, and D. Lai (2014). *Science* **345**, 1317–21. DOI: 10.1126/science.1254358.

Street, R. A., E. Simpson, S. C. C. Barros, et al. (2010). *The Astrophysical Journal* **720**, 337. DOI: 10.1088/0004-637X/720/1/337.

Tanaka, H., T. Takeuchi, and W. R. Ward (2002). *The Astrophysical Journal* **565**, 1257. DOI: 10.1086/324713.

Teyssandier, J., S. Naoz, I. Lizarraga, and F. A. Rasio (2013). *The Astrophysical Journal* **779**, 166. DOI: 10.1088/0004-637X/779/2/166.

Thébault, P., F. Marzari, and H. Scholl (2006). *Icarus* **183**, 193. DOI: 10.1016/j.icarus.2006.01.022.

Thies, I., P. Kroupa, S. P. Goodwin, D. Stamatellos, and A. P. Whitworth (2011). *Monthly Notices of the Royal Astronomical Society* **417**, 1817. DOI: 10.1111/j.1365-2966.2011.19390.x.

Torres, G., G. Á. Bakos, J. Hartman, et al. (2010). *The Astrophysical Journal* **715**, 458. DOI: 10.1088/0004-637X/715/1/458.

Torres, G., D. A. Fischer, A. Sozzetti, et al. (2012). *The Astrophysical Journal* **757**, 161. DOI: 10.1088/0004-637X/757/2/161.

Torres, G., J. N. Winn, and M. J. Holman (2008). *The Astrophysical Journal* **677**, 1324. DOI: 10.1086/529429.

Triaud, A. H. M. J., A. Collier Cameron, D. Queloz, et al. (2010). *Astronomy & Astrophysics* **524**, A25. DOI: 10.1051/0004-6361/201014525.

Triaud, A. H. M. J., A. A. Lanotte, B. Smalley, and M. Gillon (2014). *Monthly Notices of the Royal Astronomical Society* **444**, 711. DOI: 10.1093/mnras/stu1416.

Tripathi, A., J. N. Winn, J. A. Johnson, et al. (2010). *The Astrophysical Journal* **715**, 421. DOI: 10.1088/0004-637X/715/1/421.

Valsecchi, F. and F. A. Rasio (2014). *The Astrophysical Journal* **786**, 102. DOI: 10.1088/0004-637X/786/2/102.

Van Eylen, V., H. Kjeldsen, J. Christensen-Dalsgaard, and C. Aerts (2012). *Astronomische Nachrichten* **333**, 1088. DOI: 10.1002/asna.201211832.

Wang, J., D. A. Fischer, E. P. Horch, and X. Huang (2015). *The Astrophysical Journal* **799**, 229. DOI: 10.1088/0004-637X/799/2/229.

Wang, J., D. A. Fischer, J.-W. Xie, and D. R. Ciardi (2014). *The Astrophysical Journal* **791**, 111. DOI: 10.1088/0004-637X/791/2/111.

West, R. G., A. Collier Cameron, L. Hebb, et al. (2009). *Astronomy and Astrophysics* **502**, 395. DOI: 10.1051/0004-6361/200810973.

Winn, J. N., D. Fabrycky, S. Albrecht, and J. A. Johnson (2010). *The Astrophysical Journal* **718**, L145. DOI: 10.1088/2041-8205/718/2/L145.

Winn, J. N., M. J. Holman, G. Torres, et al. (2008a). *The Astrophysical Journal* **683**, 1076. DOI: 10.1086/589737.

Winn, J. N., A. W. Howard, J. A. Johnson, et al. (2011). *The Astronomical Journal* **141**, 63. DOI: 10.1088/0004-6256/141/2/63.

Winn, J. N., J. A. Johnson, S. Albrecht, et al. (2009). *The Astrophysical Journal* **703**, L99. DOI: 10.1088/0004-637X/703/2/L99.

Winn, J. N., J. A. Johnson, N. Narita, et al. (2008b). *The Astrophysical Journal* **682**, 1283. DOI: 10.1086/589235.

Winn, J. N., R. W. Noyes, M. J. Holman, et al. (2005). *The Astrophysical Journal* **631**, 1215. DOI: 10.1086/432571.

Wu, Y. and N. Murray (2003). *The Astrophysical Journal* **589**, 605. DOI: 10.1086/374598.

Wu, Y. and Y. Lithwick (2011). *The Astrophysical Journal* **735**, 109. DOI: 10.1088/0004-637x/735/2/109.

Yelda, S., J. R. Lu, A. M. Ghez, et al. (2010). *The Astrophysical Journal* **725**, 331. DOI: 10.1088/0004-637X/725/1/331.

Zuckerman, B. (2014). *The Astrophysical Journal* **791**, L27. DOI: 10.1088/2041-8205/791/2/L27.

Chapter 3

STELLAR COMPANIONS BEYOND 50 AU MIGHT FACILITATE GIANT PLANET FORMATION, BUT MOST ARE UNLIKELY TO CAUSE KOZAI-LIDOV MIGRATION

This chapter is adapted from work previously published as

Ngo, H., H. A. Knutson, S. Hinkley, et al. (2016). *The Astrophysical Journal* **827**, 8. DOI: 10.3847/0004-637X/827/1/8.

3.1 Abstract

Stellar companions can influence the formation and evolution of planetary systems, but there are currently few observational constraints on the properties of planet-hosting binary star systems. We search for stellar companions around 77 transiting hot Jupiter systems to explore the statistical properties of this population of companions as compared to field stars of similar spectral type. After correcting for survey incompleteness, we find that 47% ± 7% of hot Jupiter systems have stellar companions with semi-major axes between 50 au-2000 au. This is 2.9 times larger than the field star companion fraction in this separation range, with a significance of 4.4σ. In the 1 au-50 au range, only $3.9^{+4.5}_{-2.0}$% of hot Jupiters host stellar companions compared to the field star value of 16.4% ± 0.7%, which is a 2.7σ difference. We find that the distribution of mass ratios for stellar companions to hot Jupiter systems peaks at small values and therefore differs from that of field star binaries which tend to be uniformly distributed across all mass ratios. We conclude that either wide separation stellar binaries are more favorable sites for gas giant planet formation at all separations, or that the presence of stellar companions preferentially causes the inward migration of gas giant planets that formed farther out in the disk via dynamical processes such as Kozai-Lidov oscillations. We determine that less than 20% of hot Jupiters have stellar companions capable of inducing Kozai-Lidov oscillations assuming initial semi-major axes of 1-5 au, implying that the enhanced companion occurrence is likely correlated with environments where gas giants can form efficiently.

3.2 Introduction

Almost half of all FGK stars are in multiple systems (Raghavan et al., 2010). Therefore, it is important to understand the role that stellar companions play in the formation and evolution of planetary systems. In addition, ongoing transit surveys have demonstrated that a majority of apparently single stars host planets, and have provided unprecedented new opportunities to compare the properties of planets located in binary star systems to those of single stars (Winn and Fabrycky, 2015).

The recent proliferation of high contrast imaging of planet hosting stars is closely linked with the *Kepler* mission, as this survey was the first to produce large numbers of transiting planet candidates for which radial velocity confirmation was impractical. For these systems, high contrast imaging is required in order to eliminate astrophysical false positives and to correct for dilution of transit light curves. Prior to *Kepler*, the first reports of stellar companions came from serendipitous discoveries from newly obtained high contrast images or archival images reported along with the planet discovery (e.g. Collier Cameron et al., 2007). Then, "lucky imaging" techniques (e.g. Daemgen et al., 2009) used adaptive optics (AO) to perform systematic surveys with small sample sizes and modest sensitivity. More recently, there have been a series of larger AO surveys targeting *Kepler* planet candidate host stars using state-of-the-art methods and large telescopes to perform diffraction-limited imaging, allowing for better survey sensitivity, especially at short wavelengths (e.g. Adams et al., 2012; Dressing et al., 2014; Wang et al., 2014). A full review of these campaigns can be found in Ngo et al. (2015).

In this work, we continue the search for stellar companions in systems with hot Jupiters transiting FGK stars in order to explore the potential role of these companions in planet formation and migration. The "Friends of Hot Jupiters" (FOHJ) campaign (Knutson et al., 2014; Ngo et al., 2015; Piskorz et al., 2015), has searched for planetary and stellar companions to a sample of 50 hot Jupiter hosts via radial velocity monitoring (Knutson et al., 2014), infrared spectral model comparison (Piskorz et al., 2015) and direct imaging (Ngo et al., 2015). This original survey sample contained two subpopulations: stars that host planets with some dynamical signature of multi-body interactions, such as a measured offset between the orientation of the planet's orbit and the host star's spin axis or a non-zero orbital eccentricity, and stars that host planets on well-aligned orbits and with orbital eccentricities consistent with zero to three sigma. Our direct imaging survey was the first to apply a statistical approach to estimate the fraction of hot Jupiter host stars with gravitationally bound

stellar companions including a correction for survey sensitivity. We found a stellar companion rate of 48% ± 9% in the 50-2000 au region, showing moderately significant (2.8σ) evidence for a larger companion fraction around solar-type hot Jupiter hosts than solar-type field stars. Our survey was also the first to systematically examine a sample of planets with spin-orbit measurements, allowing us to compare misaligned and well-aligned systems. We found no evidence for a correlation between the presence of an outer stellar or planetary companion in these systems and the orbital properties of the inner transiting hot Jupiter.

More recently, there have been four large direct imaging surveys for companions to transiting gas giant planet hosts (Wöllert et al., 2015; Wöllert and Brandner, 2015; Wang et al., 2015; Evans et al., 2016). Wöllert et al. (2015) applied stellar density arguments to estimate that 12 out of their 49 targets have bound companions while Wöllert and Brandner (2015) report candidate companions in 33 out of 74 systems. Although these studies do not confirm common proper motion or report a survey sensitivity corrected companion rate, their raw companion fractions are consistent with ours. Wang et al. (2015) and Evans et al. (2016) did check for common proper motion and correct for survey sensitivity. Wang et al. (2015) report a stellar multiplicity rate for *Kepler* hot Jupiter hosts to be 51% ± 13% and Evans et al. (2016) found a companion rate of 38^{+17}_{-13}%. Both of these results are in good agreement with our previously published value.

Although the higher binary fraction of hot Jupiter host stars suggests these stellar companions play a role in the creation of hot Jupiters, it is unclear exactly what this role might be. In one class of scenarios, the presence of a stellar companion might cause gas giant planets formed at larger separations to migrate inward via secular interactions such as the Kozai-Lidov effect (e.g. Fabrycky and Tremaine, 2007; Naoz et al., 2012; Naoz et al., 2013; Storch et al., 2014; Dawson et al., 2015; Petrovich, 2015b; Anderson et al., 2016; Muñoz et al., 2016). If stellar Kozai is the dominant migration mechanism, it should result in a population of hot Jupiters with a broad distribution of orbital inclinations that is closely correlated with the presence of companions. However, our earlier direct imaging survey finds no correlation between the orbital properties of the transiting planet and stellar multiplicity, suggesting that Kozai-Lidov migration is probably not the dominant channel for the generation of hot Jupiter spin-orbit misalignment. Instead, our results signal broad agreement with the primordial excitation of stellar obliquities (e.g., Spalding and Batygin, 2014; Spalding and Batygin, 2015; Lai, 2014; Fielding et al.,

2015).

In an alternative scenario, we consider the possibility that stellar binaries are more favorable locations for the formation of gas giant planets. Some previous studies suggested that stellar companions might suppress gas giant planet formation by exciting planetesimal velocity dispersions (Mayer et al., 2005), truncating the disk (Pichardo et al., 2005; Kraus et al., 2012; Cheetham et al., 2015), or ejecting newly formed planets (Kaib et al., 2013; Zuckerman, 2014). Other theoretical studies, however, have shown that disk self-gravity successfully shields planet-formation environments from companion-driven secular excitation of embedded orbits (Batygin et al., 2011; Rafikov, 2013). The observed enhanced binary rate for hot Jupiter host stars suggests that planet formation is indeed unhindered in these systems.

In this study we increase the sample size of our direct imaging survey from 50 transiting hot Jupiter systems to 77 systems in order to take a closer look at the properties of the observed population of stellar companions and to place improved constraints on the possible effects of these companions on hot Jupiter formation. We obtain a more precise measurement of hot Jupiter stellar multiplicity and characterize the mass ratio as well as semi-major axis distributions of the observed population of companions as compared to those of solar-type field stars. Finally, while our previous work shows that hot Jupiter migration via Kozai-Lidov oscillations is unlikely, this work uses the larger sample size to place quantitative upper limits on this migration mechanism.

This paper is structured as follows. Section 3.3 describes our observations. In Section 3.4 we characterize companion properties and determine our contrast limits. Section 3.5 describes each of the individual multistellar systems detected in our new observations. Section 3.6 reports our survey results, companion rates, and trends in the properties of the observed population of stellar companions. Section 3.7 discusses the implications of our results for hot Jupiter planet formation and constrains the fraction of systems affected by Kozai-Lidov. Section 3.8 presents a summary of this work.

3.3 Sample selection and observations

Our total sample consists of 82 systems known to host transiting gas giant planets. We divide our sample into two populations. The first population, containing 77 stars, is our "survey sample", which is the only population we use in all of the estimates of hot Jupiter companion fraction and other constraints presented in this work. The

first 50 targets in this sample are the same set of stars used in the first three FOHJ papers. For more information on the selection of these targets, see Knutson et al. (2014). The remaining 27 targets are new systems with transiting gas giant planets with masses between 0.27 M_{Jup} and 4.06 M_{Jup} and separations between 0.014 au and 0.061 au. They were selected without regard to whether or not the stars had directly imaged stellar companions reported by other imaging surveys. We also relax our previous preference for systems with published spin-orbit alignment measurements, as our initial survey results found no evidence for any correlation between this parameter and the presence of a stellar companion.

The second population is a set of five targets (HAT-P-54, WASP-36, WASP-58, WASP-76, WASP-103) that we decided to observe only after their stellar companions were reported in the published literature (Wöllert et al., 2015; Wöllert and Brandner, 2015). Therefore, they do not form a part of our survey population and we exclude them from our statistical analysis discussed in Section 3.6. We characterize the companions around these non-survey targets following the same procedure as the survey targets, to be described in Section 3.4, and report on these systems individually in Section 3.5. Although these targets cannot be fairly considered in our determination of the hot Jupiter companion rate, we are still able to confirm the existence of the companions around non-survey targets from previous studies and provide new or updated companion properties.

We obtained K band AO observations using the NIRC2 instrument (instrument PI: Keith Matthews) on Keck II between February 2012 and January 2016. These new observations are summarized in Table 3.1. We follow the procedure described in Ngo et al. (2015). We operated in the natural guide star mode using the narrow camera setting, which yields a plate scale of 10 mas pixel^{-1}. Each survey target had at least one series of K band observations with at least 105 seconds of on-sky integration time. As in our previous survey, this strategy allows us to reach contrasts of ΔK of eight magnitudes at $1''$ of separation. For targets where a companion was detected, we also take observations in J and/or H bands in order to obtain a measurement of the companion's color. We also test for common proper motion using additional epochs of K band imaging obtained one to three years after the initial detection. These followup photometric and astrometric observations may have shorter integration time.

We use dome flats and dark frames to calibrate our images and to identify hot pixels and dead pixels using the criteria described in Ngo et al., 2015. We utilize these

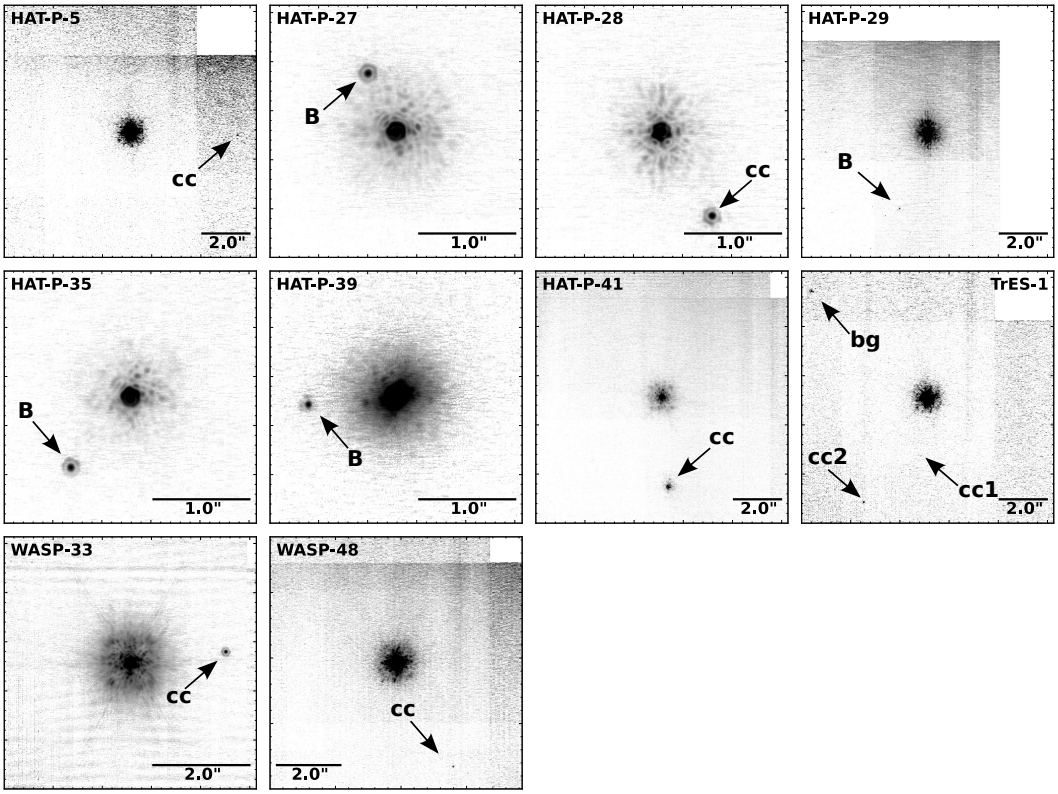

Figure 3.1: Median-stacked K band image for each detected candidate mutli-stellar system presented in this work, from our survey targets. Each image is oriented such that North points up and East to the left.

individual calibrated frames for our photometric and astrometric analysis, while we perform our sensitivity calculations on the median stack of these individual frames.

Table 3.1: Summary of NIRC2 AO observations

Target	N_{cc}	UT Obs. Date	Filter	Array	$T_{\rm int}$	$N_{\rm fit}$	$N_{\rm stack}$
Survey targets							
HAT-P-1[a]	0	2013 Oct 17	K'	1024	9.0	···	12
HAT-P-3	0	2013 May 31	K_s	1024	9.0	···	12
HAT-P-5	1	2013 Jul 04	K_s	1024	10.0	4	12
		2015 Jun 24	J	1024	12.5	12	···
		2015 Jun 24	K_s	1024	12.5	12	12
HAT-P-9	0	2013 Mar 02	K_s	1024	10.0	···	12
HAT-P-19	0	2013 Aug 19	K_s	1024	12.5	···	12
HAT-P-21	0	2013 Mar 02	K_s	1024	10.0	···	12
HAT-P-23	0	2013 Jun 22	K_s	1024	25.0	···	12
HAT-P-25	0	2014 Nov 10	K_s	1024	12.0	···	12
HAT-P-27	1	2014 Jul 12	J	1024	15.0	12	···
		2014 Jul 12	H	1024	15.0	12	···
		2014 Jul 12	K_s	1024	15.0	12	12
		2015 Jan 09	J	1024	12.5	12	···

Continued on next page

Table 3.1 – continued from previous page

Target	N_{cc}	UT Obs. Date	Filter	Array	$T_{\rm int}$	$N_{\rm fit}$	$N_{\rm stack}$
		2015 Jan 09	H	1024	12.5	12	···
		2015 Jan 09	K_s	1024	12.5	12	12
		2015 Jun 24	K_s	1024	12.5	12	12
HAT-P-28	1	2015 Jul 07	J	1024	15.0	12	···
		2015 Jul 07	K_s	1024	15.0	12	12
		2015 Jul 10	J_c	1024	25.0	6	···
		2015 Jul 10	BrG	1024	22.0	6	6
HAT-P-29[b]	1	2012 Feb 02	J	1024	10.0	9	···
		2012 Feb 02	K'	1024	15.0	9	9
		2015 Jul 05	K_s	1024	30.0	6	6
		2015 Jul 10	BrG	1024	10.0	4	6
HAT-P-35	1	2013 Mar 02	J	1024	10.0	9	···
		2013 Mar 02	K_s	1024	10.0	12	12
		2014 Nov 10	J	1024	12.0	12	···
		2014 Nov 10	H	1024	12.5	12	···
		2014 Nov 10	K_s	1024	12.0	12	12
HAT-P-36	0	2013 Mar 02	K_s	1024	10.0	···	12
HAT-P-37	0	2015 Jun 24	K_s	1024	12.0	···	12
HAT-P-38	0	2015 Jul 07	K_s	1024	15.0	···	7
HAT-P-39	1	2013 Mar 02	J	1024	10.0	12	···
		2013 Mar 02	K_s	1024	10.0	12	12
		2014 Nov 07	J	1024	10.0	11	···
		2014 Nov 07	H	1024	10.0	12	···
		2014 Nov 07	K_s	1024	10.0	12	12
HAT-P-40	0	2014 Oct 03	K_s	1024	15.0	···	12
HAT-P-41	1	2014 Oct 03	K_s	1024	12.5	6	6
		2015 Jun 24	J	1024	12.5	12	···
		2015 Jun 24	K_s	1024	12.5	12	12
HAT-P-42	0	2015 Jan 10	K_s	1024	15.0	···	12
HAT-P-43	0	2014 Nov 10	K_s	1024	12.0	···	12
TrES-1	2	2013 Jul 04	K_s	1024	9.0	4	12
		2015 Jun 24	J	1024	12.5	12	···
		2015 Jun 24	K_s	1024	12.5	12	12
WASP-5	0	2013 Oct 17	K'	1024	10.0	···	12
WASP-13	0	2015 Jan 10	K_s	1024	13.6	···	15
WASP-33	1	2013 Aug 19	J	256	9.0	6	···
		2013 Aug 19	H	256	9.0	6	···
		2013 Aug 19	K_s	512	10.6	12	12
		2014 Dec 07	K_s	512	15.0	12	12
		2015 Dec 26	K_s	512	15.9	12	12
WASP-39	0	2013 Jul 04	K_s	1024	10.0	···	12
WASP-43	0	2013 Mar 02	K_s	1024	10.0	···	12
WASP-48	1	2013 Aug 19	K_s	1024	12.5	8	12
		2015 Jun 24	J	1024	12.5	12	···
		2015 Jun 24	K_s	1024	12.5	12	12
XO-1	0	2015 Jun 24	K_s	1024	12.5	···	12
Non-survey targets							
HAT-P-54	1	2016 Jan 25	K_s	1024	15.0	12	12
WASP-36	1	2016 Jan 25	K_s	1024	15.0	9	9

Continued on next page

Table 3.1 – continued from previous page

Target	N_{cc}	UT Obs. Date	Filter	Array	$T_{\rm int}$	$N_{\rm fit}$	$N_{\rm stack}$
WASP-58	1	2015 Jul 10	J_c	1024	18.0	6	···
		2015 Jul 10	BrG	1024	12.0	6	6
WASP-76	1	2015 Jul 10	BrG	1024	1.5	3	3
		2015 Jul 10	J_c	1024	1.1	3	···
WASP-103	1	2016 Jan 25	J	1024	15.0	12	···
		2016 Jan 25	K_s	1024	15.0	12	12
		2016 Jan 25	H	1024	15.0	12	···

Notes. Column N_{cc} is the number of candidate companions detected. Column "Array" is the horizontal size, in pixel, of the NIRC2 array readout region and corresponds to subarray sizes of 1024x1024 (the full NIRC2 array), 512x512, or 256x264. Column $T_{\rm int}$ is the total integration time, in seconds, of a single frame. Column $N_{\rm fit}$ is the number of frames used in our photometric and/or astrometric analysis, and is only given when companions are present. Column $N_{\rm stack}$ is the number of frames combined to make the contrast curve measurements. We only compute contrast curves in the K', K_s, K_c, BrG bandpasses so this column is not applicable for other bandpasses. In some cases, $N_{\rm fit}$ and $N_{\rm stack}$ are not equal because the companion may not be present in all frames due to the dither pattern and/or observing conditions.

[a] HAT-P-1 has a known stellar companion (Liu et al., 2014) with a similar mass but at a separation of $11''.3$, it is outside of our survey's field of view.

[b] We originally reported no companions around HAT-P-29 in Ngo et al. (2015). However, Wöllert and Brandner (2015) reports a faint companion that we had missed earlier. We recovered this companion in our old images and also followed up with more observations in July 2015.

3.4 Analysis of companion properties

PSF fitting

We identify candidate companions around 15 of our target stars (see Figures 3.1 and 3.2). We summarize the stellar parameters for all observed stars in Table 3.2.

We measure the flux ratio and on-sky separation for each detected multi-stellar system by fitting each image with a multiple-source point spread function (PSF) modelled as a combination of Moffat and Gaussian functions. For the functional form and description of the parameters, see Ngo et al. (2015). We use a maximum likelihood estimation routine to find the best fit parameters and create an analytic form for our PSF model using these parameters. Integrating this PSF model over a circular aperture for each star yields the flux ratio. The difference in the stellar position parameters determines the separation as projected onto the NIRC2 array. To get the true on-sky separation and position angle between the stars, we use the known NIRC2 astrometric corrections (Yelda et al., 2010; Service et al., 2016) to account for the NIRC2 distortion and rotation[1]. These astrometric corrections

[1]The Yelda et al. (2010) was used for NIRC2 data taken prior to 2015 April 13. Realignment of the Keck2 AO bench caused a change in the NIRC2 distortion solution, so we use the new solution presented by Service et al. (2016) for data taken after this date.

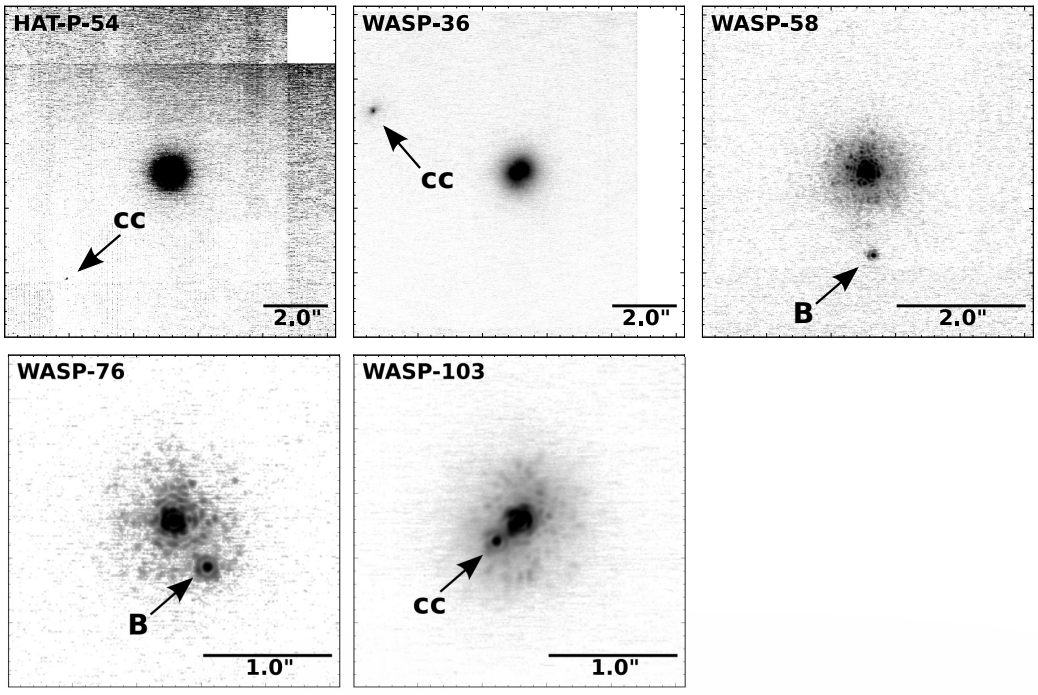

Figure 3.2: Median-stacked K band image for each detected candidate mutli-stellar system presented in this work, from our non-survey targets. Each image is oriented such that North points up and East to the left.

include uncertainties on the distortion, plate scale and orientation of the NIRC2 array and we include all of these uncertainties in our reported errorbars for our measured separation and position angle.

For each individual calibrated frame, we compute the flux ratio and separations as outlined above. We then report the best estimate for each of these values as the mean value from all of the frames. We estimate our measurement error as the standard error on the mean.

We report the best fitting flux ratio between primary and companion stars as a magnitude difference in each survey bandpass in Table 3.3. We also use apparent magnitudes of the primary star from the 2MASS catalog (Skrutskie et al., 2006) to compute the apparent magnitudes of the companion stars in all bands. Tables 3.4 and 3.5 report all computed photometry and K-band astrometry, respectively, of our detected companion stars.

Table 3.2: Target stellar parameters

Target	N_{cc}	$T_{\rm eff}$ (K)	M ($M_\odot$)	$\log g$ (cgs)	D (pc)	References for... T	M, $\log g$	D
Survey targets								
HAT-P-1	0	5980 ± 49	1.151 ± 0.052	4.359 ± 0.014	155 ± 15	1	1	2
HAT-P-3	0	5185 ± 80	0.917 ± 0.030	4.594 ± 0.041	166.4 ± 14.4	3	3	4
HAT-P-5	1	5960 ± 100	1.163 ± 0.069	4.39 ± 0.04[a]	340 ± 30	2	5	6
HAT-P-9	0	6350 ± 150	1.28 ± 0.10	4.293 ± 0.046	480 ± 60	7	7	8
HAT-P-19	0	4990 ± 130	0.842 ± 0.042	4.54 ± 0.05	215 ± 15	9	9	9
HAT-P-21	0	5588 ± 80	0.947 ± 0.042	4.33 ± 0.06	254 ± 19	10	10	10
HAT-P-23	0	5885 ± 72	1.104 ± 0.047	4.407 ± 0.018	355.0 ± 40.8	11	11	4
HAT-P-25	0	5500 ± 80	1.010 ± 0.032	4.48 ± 0.04	297^{+17}_{-13}	12	12	12
HAT-P-27	1	5300 ± 90	0.945 ± 0.035	4.51 ± 0.04	204 ± 14	13	13	13
HAT-P-28	1	5680 ± 90	1.025 ± 0.047	4.36 ± 0.06	395^{+34}_{-26}	14	14	14
HAT-P-29[b]	1	6086 ± 69	1.207 ± 0.046	4.34 ± 0.06	322^{+35}_{-21}	15	15	14
HAT-P-35	1	6178 ± 45	1.16 ± 0.08	4.40 ± 0.09	535 ± 32	16	16	17
HAT-P-36	0	5620 ± 40	1.030 ± 0.042	4.416 ± 0.011	317 ± 17	18	18	17
HAT-P-37	0	5500 ± 100	0.929 ± 0.043	4.52 ± 0.04[a]	411 ± 26	17	17	17
HAT-P-38	0	5330 ± 100	0.886 ± 0.044	$4.45^{+0.06a}_{-0.07}$	249^{+26}_{-19}	19	19	19
HAT-P-39	1	6430 ± 100	1.404 ± 0.051	4.16 ± 0.03[a]	641^{+115}_{-66}	20	20	20
HAT-P-40	0	6080 ± 100	1.512 ± 0.109	3.93 ± 0.01[a]	548 ± 36	20	20	20
HAT-P-41	1	6479 ± 51	1.28 ± 0.09	4.39 ± 0.22	311^{+36}_{-27}	21	21	20
HAT-P-42	0	5743 ± 50	1.178 ± 0.068	4.14 ± 0.07	414 ± 51	22	22	22
HAT-P-43	0	5645 ± 74	1.048 ± 0.042	4.37 ± 0.02	566^{+67}_{-37}	22	22	22
TrES-1	2	5226 ± 38	0.85 ± 0.07	4.40 ± 0.10	129.7 ± 8.7	16	16	4
WASP-5	0	5785 ± 83	1.00 ± 0.08	4.54 ± 0.14	318.6 ± 19.9	16	16	4
WASP-13	0	6025 ± 21	1.20 ± 0.08	4.19 ± 0.03	155 ± 18	16	16	23
WASP-33	1	7430 ± 100	1.495 ± 0.031	4.3 ± 0.2	123.1 ± 7.2	24	24	4
WASP-39	0	5400 ± 150	0.93 ± 0.034	4.50 ± 0.01[a]	230 ± 80	25	25	25
WASP-43	0	4400 ± 200	0.58 ± 0.05	4.64 ± 0.02[a]	106.1 ± 7.2	26	26	4
WASP-48	1	6000 ± 150	1.062 ± 0.075	4.101 ± 0.023	466.0 ± 49.0	11	11	4
XO-1	0	5754 ± 42	0.93 ± 0.07	4.61 ± 0.05	177.9 ± 10.7	16	16	4
Non-survey targets								
HAT-P-54	1	4390 ± 50	0.645 ± 0.020	4.667 ± 0.012	135.8 ± 3.5	27	27	27
WASP-36	1	5928 ± 59	1.00 ± 0.07	4.51 ± 0.09	450 ± 120	16	16	28
WASP-58	1	5800 ± 150	0.94 ± 0.1	4.27 ± 0.09	300 ± 50	29	29	29
WASP-76	1	6250 ± 100	1.46 ± 0.07	4.128 ± 0.015	120 ± 20	30	30	30
WASP-103	1	6110 ± 160	$1.220^{+0.039}_{-0.036}$	$4.22^{+0.12}_{-0.05}$	470 ± 35	31	31	31

Notes. N_{cc} is the number of candidate companions detected.

[a] The cited studies do not provide a $\log g$ measurement, so these numbers are computed from the quoted mass and radius values instead.

[b] HAT-P-29 is part of the original FOHJ sample. This line is replicated from Ngo et al. (2015).

References. (1) Nikolov et al. (2014); (2) Torres et al. (2008); (3) Chan et al. (2011); (4) Triaud et al. (2014); (5) Southworth et al. (2012); (6) Bakos et al. (2007); (7) Southworth (2012); (8) Shporer et al. (2009); (9) Hartman et al. (2011); (10) Bakos et al. (2011); (11) Ciceri et al. (2015); (12) Quinn et al. (2010); (13) Béky et al. (2011); (14) Buchhave et al. (2011); (15) Torres et al. (2012); (16) Mortier et al. (2013); (17) Bakos et al. (2012); (18) Mancini et al. (2015); (19) Sato et al. (2012); (20) Hartman et al. (2012); (21) Tsantaki et al. (2014); (22) Boisse et al. (2013); (23) Skillen et al. (2009); (24) Collier Cameron et al. (2010); (25) Faedi et al. (2011); (26) Hellier et al. (2011); (27) Bakos et al. (2015); (28) Smith et al. (2012); (29) Hébrard et al. (2013); (30) West et al. (2016); (31) Gillon et al. (2014)

Table 3.3: Flux ratio measurements of confirmed and candidate stellar companions

Companion[a]	UT Obs. Date	ΔJ	ΔH	ΔK
HAT-P-5 cc	2013 Jul 04	···	···	6.71 ± 0.15
HAT-P-5 cc	2015 Jun 24	6.84 ± 0.21	···	6.669 ± 0.073
HAT-P-27B	2014 Jul 12	3.395 ± 0.040	3.107 ± 0.021	3.519 ± 0.048
HAT-P-27B	2015 Jan 09	3.3763 ± 0.0093	3.1436 ± 0.0093	3.520 ± 0.011
HAT-P-27B	2015 Jun 24	···	···	3.380 ± 0.046
HAT-P-28 cc	2015 Jul 07	3.333 ± 0.025	···	3.168 ± 0.040
HAT-P-28 cc[b]	2015 Jul 10	3.468 ± 0.042	···	3.381 ± 0.016
HAT-P-29B[c]	2012 Feb 02	7.09 ± 0.15	···	6.92 ± 0.16
HAT-P-29B	2015 Jul 05	···	···	6.30 ± 0.16
HAT-P-29B[b]	2015 Jul 10	···	···	6.85 ± 0.18
HAT-P-35B	2013 Mar 02	4.332 ± 0.069	···	3.185 ± 0.058
HAT-P-35B	2014 Nov 10	3.726 ± 0.025	3.293 ± 0.015	3.562 ± 0.032
HAT-P-39B	2013 Mar 02	5.584 ± 0.082	···	4.17 ± 0.10
HAT-P-39B	2014 Nov 07	4.686 ± 0.050	4.058 ± 0.013	4.40 ± 0.16
HAT-P-41 cc	2014 Oct 03	···	···	2.650 ± 0.084
HAT-P-41 cc	2015 Jun 24	2.947 ± 0.017	···	2.527 ± 0.045
HAT-P-54 cc	2016 Jan 25	···	···	6.51 ± 0.17
TrES-1 cc1[d]	2013 Jul 04	···	···	···
TrES-1 cc1[d]	2015 Jun 24	···	···	···
TrES-1 cc2	2013 Jul 04	···	···	6.676 ± 0.060
TrES-1 cc2	2015 Jun 24	7.09 ± 0.21	···	6.434 ± 0.078
WASP-33 cc	2013 Aug 19	6.37 ± 0.25	5.71 ± 0.12	6.108 ± 0.016
WASP-33 cc	2014 Dec 07	···	···	6.148 ± 0.098
WASP-33 cc	2015 Dec 26	···	···	6.03 ± 0.11
WASP-36 cc	2016 Jan 25	···	···	2.74 ± 0.12
WASP-48 cc	2013 Aug 19	···	···	7.270 ± 0.064
WASP-48 cc	2015 Jun 24	7.62 ± 0.31	···	7.215 ± 0.065
WASP-58B[b]	2015 Jul 10	4.62 ± 0.14	···	4.391 ± 0.095
WASP-76B[b]	2015 Jul 10	2.738 ± 0.014	···	2.65 ± 0.14
WASP-103 cc	2016 Jan 25	2.427 ± 0.030	2.2165 ± 0.0098	1.965 ± 0.019

Notes. Except where noted, ΔK is ΔK_s.
[a] We label companions with confirmed common proper motions as "B" and as "cc" when they are candidate companions. See Section 3.5.
[b] On 2015 Jul 10, we used the J_c and BrG bandpasses instead of J and K_s, respectively. For these marked rows, J corresponds to J_c and K corresponds to BrG.
[c] On 2012 Feb 02, for HAT-P-29, we used the K' bandpass instead of K_s.
[d] This candidate companion is too faint to obtain reliable photometric measurements.

Table 3.4: Multi-band photometry of confirmed and candidate stellar companions

Companion[a]	UT Obs. Date	m_J	m_H	m_K	$J-K$	$H-K$	$J-H$
HAT-P-5 cc	2013 Jul 04	···	···	17.19 ± 0.15	···	···	···
HAT-P-5 cc	2015 Jun 24	17.68 ± 0.21	···	17.150 ± 0.073	0.53 ± 0.22	···	···
HAT-P-27B	2014 Jul 12	14.021 ± 0.040	13.356 ± 0.021	13.628 ± 0.048	0.393 ± 0.063	−0.271 ± 0.053	0.664 ± 0.045
HAT-P-27B	2015 Jan 09	14.0023 ± 0.0093	13.3926 ± 0.0093	13.629 ± 0.011	0.374 ± 0.014	−0.236 ± 0.014	0.610 ± 0.013
HAT-P-27B	2015 Jun 24	···	···	13.489 ± 0.046	···	···	···
HAT-P-28 cc	2015 Jul 07	14.894 ± 0.025	···	14.272 ± 0.040	0.623 ± 0.047	···	···
HAT-P-28 cc[b]	2015 Jul 10	15.029 ± 0.042	···	14.485 ± 0.016	0.544 ± 0.045	···	···
HAT-P-29B[c]	2012 Feb 02	17.74 ± 0.15	···	17.22 ± 0.16	0.52 ± 0.22	···	···
HAT-P-29B	2015 Jul 05	···	···	16.60 ± 0.16	···	···	···
HAT-P-29B[b]	2015 Jul 10	···	···	17.15 ± 0.18	···	···	···
HAT-P-35B	2013 Mar 02	15.690 ± 0.069	···	14.215 ± 0.058	1.475 ± 0.090	···	···
HAT-P-35B	2014 Nov 10	15.084 ± 0.025	14.365 ± 0.015	14.592 ± 0.032	0.491 ± 0.041	−0.227 ± 0.036	0.718 ± 0.029
HAT-P-39B	2013 Mar 02	17.008 ± 0.082	···	15.32 ± 0.10	1.68 ± 0.13	···	···
HAT-P-39B	2014 Nov 07	16.110 ± 0.050	15.242 ± 0.013	15.55 ± 0.16	0.56 ± 0.17	−0.31 ± 0.16	0.868 ± 0.052
HAT-P-41 cc	2014 Oct 03	···	···	12.378 ± 0.084	···	···	···
HAT-P-41 cc	2015 Jun 24	12.953 ± 0.017	···	12.255 ± 0.045	0.698 ± 0.048	···	···
HAT-P-54 cc	2016 Jan 25	···	···	16.84 ± 0.17	···	···	···
TrES-1 cc1[d]	2013 Jul 04	···	···	···	···	···	···
TrES-1 cc1[d]	2015 Jun 24	···	···	···	···	···	···
TrES-1 cc2	2013 Jul 04	···	···	16.495 ± 0.060	···	···	···
TrES-1 cc2	2015 Jun 24	17.38 ± 0.21	···	16.253 ± 0.078	1.13 ± 0.22	···	···
WASP-33 cc	2013 Aug 19	13.95 ± 0.25	13.22 ± 0.12	13.576 ± 0.016	0.38 ± 0.25	−0.35 ± 0.12	0.73 ± 0.28
WASP-33 cc	2014 Dec 07	···	···	13.616 ± 0.098	···	···	···
WASP-33 cc	2015 Dec 26	···	···	13.49 ± 0.11	···	···	···
WASP-36 cc	2016 Jan 25	···	···	14.03 ± 0.12	···	···	···
WASP-48 cc	2013 Aug 19	···	···	17.642 ± 0.064	···	···	···
WASP-48 cc	2015 Jun 24	18.25 ± 0.31	···	17.587 ± 0.065	0.66 ± 0.32	···	···
WASP-58B[b]	2015 Jul 10	15.25 ± 0.14	···	14.676 ± 0.095	0.57 ± 0.17	···	···

Continued on next page

Table 3.4 – continued from previous page

Companion[a]	UT Obs. Date	m_J	m_H	m_K	$J-K$	$H-K$	$J-H$
WASP-76B[b]	2015 Jul 10	11.279 ± 0.014	···	10.90 ± 0.14	0.38 ± 0.14	···	···
WASP-103 cc	2016 Jan 25	13.527 ± 0.030	13.0765 ± 0.0098	12.732 ± 0.019	0.795 ± 0.035	0.345 ± 0.021	0.450 ± 0.031

Notes. Except where noted, the K bandpass used is the K_s bandpass. The m_X columns report the secondary star's apparent magnitudes. The last three columns show the computed color of the companion star.

[a] We label companions with confirmed common proper motions as "B" and as "cc" when they are candidate companions. See Section 3.5.

[b] On 2015 Jul 10, we used the J_c and BrG bandpasses instead of J and K_s, respectively. For these marked rows, J corresponds to J_c and K corresponds to BrG.

[c] On 2012 Feb 02, for HAT-P-29, we used the K' bandpass instead of K_s.

[d] This candidate companion is too faint to obtain reliable photometric measurements.

References. Primary star apparent magnitudes are from 2MASS (Skrutskie et al., 2006).

Common proper motion confirmation

We are interested in determining whether or not our detected companion stars are gravitationally bound to the primary star. For our candidate mutli-stellar systems, we followed up with K-band images to verify that the companion star shares common proper motion with the primary star. Following the procedure described in Ngo et al. (2015), we calculate the evolution of the companion's separation and position angle if it were a background object and compare it to the actual measured separation and position angle at each observation date in Figures 3.3 and 3.4. When our candidate companions have been imaged in other surveys and these other surveys report a separation and position angle with uncertainties, we also include these previous measurements. Table 3.5 lists all the astrometric measurements used in our analysis.

Masses and separation

For each confirmed multi-stellar system, we compute the companion star's physical parameters using the method described in Ngo et al. (2015). In brief, we model the primary and companion star fluxes by integrating the PHOENIX synthetic spectra (Husser et al., 2013) over the observed bandpass. We use the set of models corresponding to solar metallicities and composition ([Fe/H]= 0, [α/H]= 0). For the primary star, we use previously published measurements of stellar mass, radius, effective temperature and distance as listed in Table 3.2. For the companion star, we use the same distance measurement and calculate the companion star effective temperature that would result in a companion star flux that matches the observed flux ratio. We use the zero-age main sequence models from Baraffe et al. (1998) to determine the companion star's mass and radius from the effective temperature. Our error budget includes all relevant measurement uncertainties but does not include any model dependent uncertainties from the PHOENIX spectra or the zero-age main sequence model. We calculate effective temperatures for each candidate companion based on the measured flux ratios in the J, H, and K bands, and ask whether the brightness ratios across all three bands are consistent with the same stellar effective temperature. We report these individual effective temperatures values as well as the average across all three bands in Table 3.6.

The projected spatial separations are computed using our measured projected on-sky separations and the stellar distance. Because the majority of our stars do not have measured parallaxes, we use a spectroscopic distance estimated derived from the spectral type and the star's apparent magnitude.

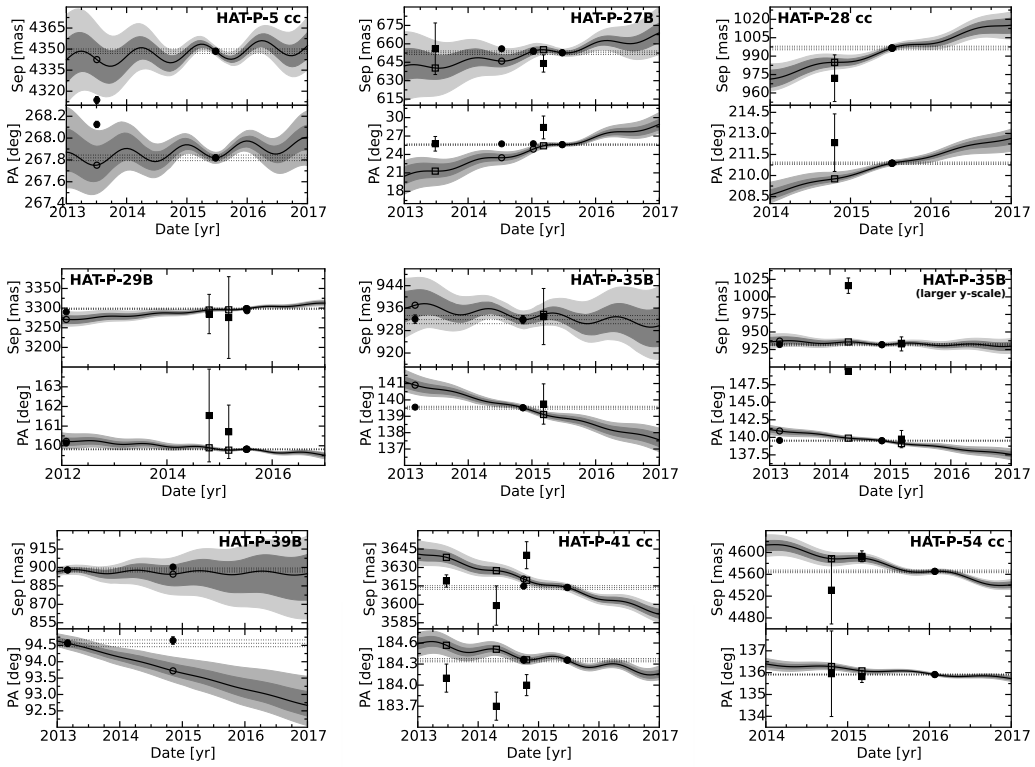

Figure 3.3: Common proper motion confirmation for each candidate companion. The top and bottom panels show the separation and position angle of a candidate companion relative to the primary star. The background track (solid line) starts at the observation with the smallest uncertainty in separation and position angle. The shaded regions indicate the 68% and 95% confidence regions. We use uncertainties in our separation and position angle measurement as well as the uncertainties in the primary star's celestial coordinates, proper motion, and parallax in our Monte Carlo routine to determine these confidence regions. The filled symbols show measured positions of companions (listed in Table 3.5) and open symbols show the expected position if the candidate object were a very distant background object. Circles are measurements from our campaign while squares are measurements from other studies. When the solid symbols and open symbols differ and when the measurement values are consistent with each other at all observation epochs, then we can conclude our detected object is a physically bound companion. Objects labeled as "B" have common proper motion, as "cc" are candidate companions, and as "bg" are background objects. See Section 3.5. Continued in Figure 3.4.

Table 3.5: Astrometric measurements of all candidate stellar companions

Candidate[a]	UT Obs. Date	Band	ρ (mas)	PA (°)	Reference
HAT-P-5 cc	2013 Jul 04	K_s	4313.7 ± 2.7	267.873 ± 0.030	this work
HAT-P-5 cc	2015 Jun 24	K_s	4348.5 ± 2.4	267.557 ± 0.032	this work
HAT-P-27B	2013 Jun 27	i', z'	656 ± 21	25.7 ± 1.2	Wöllert and Brandner (2015)
HAT-P-27B	2014 Jul 12	K_s	656.0 ± 1.5	25.48 ± 0.13	this work
HAT-P-27B	2015 Jan 09	K_s	653.9 ± 1.5	25.50 ± 0.13	this work
HAT-P-27B	2015 Mar 09	i', z'	644 ± 7	28.4 ± 1.9	Wöllert and Brandner (2015)
HAT-P-27B	2015 Jun 24	K_s	652.8 ± 1.5	25.34 ± 0.13	this work
HAT-P-28 cc	2014 Oct 24	i', z'	972 ± 19	212.3 ± 2.0	Wöllert and Brandner (2015)
HAT-P-28 cc	2015 Jul 07	K_s	996.6 ± 1.5	210.611 ± 0.086	this work
HAT-P-28 cc	2015 Jul 10	BrG	996.2 ± 1.6	210.614 ± 0.088	this work
HAT-P-29B	2012 Feb 02	K'	3290.3 ± 2.3	159.892 ± 0.032	this work
HAT-P-29B	2014 Oct 21	i', z'	3285 ± 50	161.5 ± 2.4	Wöllert and Brandner (2015)
HAT-P-29B	2015 Mar 06	i', z'	3276 ± 104	160.7 ± 1.4	Wöllert and Brandner (2015)
HAT-P-29B	2015 Jul 05	K_s	3298.4 ± 2.2	159.558 ± 0.033	this work
HAT-P-29B	2015 Jul 10	BrG	3293.2 ± 4.0	159.572 ± 0.040	this work
HAT-P-35B	2013 Mar 02	K_s	932.1 ± 1.5	139.306 ± 0.092	this work
HAT-P-35B	2014 Apr 22	r_{TCI}[b]	1016 ± 11	194.4 ± 0.2	Evans et al. (2016)
HAT-P-35B	2014 Nov 10	K_s	931.9 ± 1.5	139.270 ± 0.090	this work
HAT-P-35B	2015 Mar 09	i', z'	933 ± 10	139.8 ± 1.2	Wöllert and Brandner (2015)
HAT-P-39B	2013 Mar 02	K_s	898.0 ± 1.6	94.31 ± 0.10	this work
HAT-P-39B	2014 Nov 07	K_s	900.4 ± 1.7	94.40 ± 0.12	this work
HAT-P-41 cc	2013 Jun 26	i', z'	3619 ± 5	184.1 ± 0.2	Wöllert et al. (2015)
HAT-P-41 cc	2013 Apr 21	r_{TCI}[b]	3599 ± 16	183.7 ± 0.2	Evans et al. (2016)
HAT-P-41 cc	2014 Oct 03	K_s	3614.8 ± 1.7	184.102 ± 0.026	this work
HAT-P-41 cc	2014 Oct 21	i', z'	3640 ± 11	184.0 ± 0.1	Wöllert and Brandner (2015)
HAT-P-41 cc	2015 Jun 24	K_s	3613.7 ± 2.1	184.094 ± 0.031	this work
HAT-P-54 cc	2014 Oct 21	i', z'	4531 ± 62	135.95 ± 1.96	Wöllert and Brandner (2015)
HAT-P-54 cc	2015 Mar 06	i', z'	4593 ± 10	135.82 ± 0.27	Wöllert and Brandner (2015)
HAT-P-54 cc	2016 Jan 25	K_s	4565.4 ± 3.1	135.652 ± 0.035	this work
TrES-1 bg	2009 Jul 18-22[c]	i'	6190 ± 30	47.4 ± 0.2	Faedi et al. (2013)
TrES-1 bg	2013 Jul 04	K_s	6355.2 ± 2.1	47.309 ± 0.017	this work
TrES-1 bg	2015 Jun 24	K_s	6436.9 ± 3.1	47.321 ± 0.024	this work
TrES-1 cc1	2013 Jul 04	K_s	2345.4 ± 9.8	172.91 ± 0.11	this work
TrES-1 cc1	2015 Jun 24	K_s	2325.3 ± 4.7	171.71 ± 0.078	this work
TrES-1 cc2	2009 Jul 18-22[c]	i'	4950 ± 30	149.6 ± 0.5	Faedi et al. (2013)
TrES-1 cc2	2013 Jul 04	K_s	4940.2 ± 2.2	148.152 ± 0.026	this work
TrES-1 cc2	2015 Jun 24	K_s	4946.5 ± 2.6	147.441 ± 0.028	this work
WASP-33 cc	2010 Nov 29	K_c	1961 ± 3	276.4 ± 0.2	Moya et al. (2011)
WASP-33 cc	2013 Aug 19	K_s	1939.7 ± 1.5	276.247 ± 0.045	this work
WASP-33 cc	2014 Oct 21	i', z'	1920 ± 12	275.9 ± 0.7	Wöllert and Brandner (2015)
WASP-33 cc	2014 Dec 07	K_s	1934.3 ± 1.6	276.206 ± 0.045	this work
WASP-33 cc	2015 Dec 26	K_s	1931.2 ± 1.9	276.350 ± 0.058	this work
WASP-36 cc	2014 Apr 23	r_{TCI}[b]	4872 ± 19	66.5 ± 0.2	Evans et al. (2016)
WASP-36 cc	2015 Mar 09	i', z'	4845 ± 17	67.2 ± 0.9	Wöllert and Brandner (2015)
WASP-36 cc	2016 Jan 25	K_s	4871.0 ± 2.6	66.921 ± 0.028	this work
WASP-48 cc	2013 Aug 19	K_s	3571.9 ± 2.6	208.315 ± 0.035	this work
WASP-48 cc	2015 Jun 24	K_s	3525.4 ± 2.4	209.053 ± 0.037	this work
WASP-58B	2013 Jun 25	i', z'	1275 ± 15	183.2 ± 0.4	Wöllert et al. (2015)
WASP-58B	2015 Jul 10	BrG	1286.0 ± 1.6	183.359 ± 0.071	this work
WASP-76B	2014 Aug 20	i'	443.8 ± 5.3	214.92 ± 0.56	Ginski et al. (2016)
WASP-76B	2014 Oct 21	i', z'	425 ± 12	216.9 ± 2.9	Wöllert and Brandner (2015)
WASP-76B	2015 Jul 10	BrG	442.5 ± 1.5	215.51 ± 0.19	this work
WASP-103 cc	2015 Mar 07	i', z'	242 ± 16	132.7 ± 2.7	Wöllert and Brandner (2015)
WASP-103 cc	2016 Jan 25	K_s	239.7 ± 1.5	131.41 ± 0.35	this work

Notes. Separations (ρ) and position angle (PA) measurements of candidate companions in this work and other studies with published uncertainties. These values are plotted in Figures 3.3 and 3.4.

[a] We label companions with confirmed common proper motions as "B", as "cc" when they are candidate companions, and as "bg" when they are confirmed background objects. See Section 3.5.

[b] The red filter used by Evans et al. (2016) is described as a combination of the Sloan i' and z' filters.

[c] Faedi et al. (2013) did not provide a specific date for their observations. Here, we report the range of dates given and use the median value in our analysis.

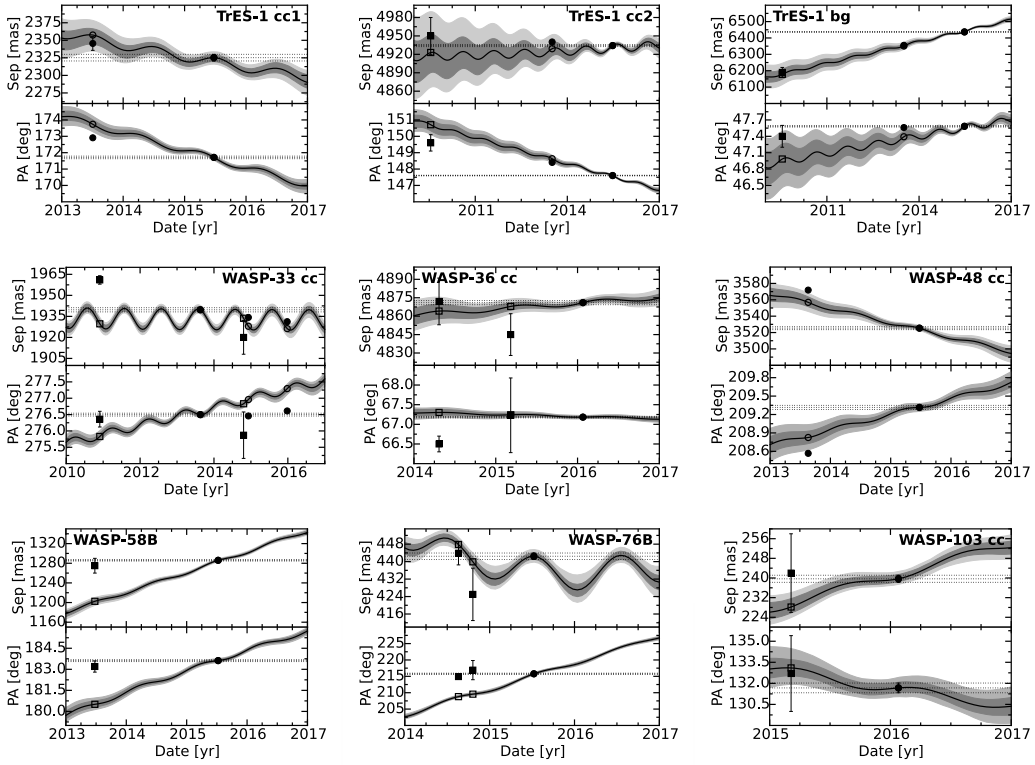

Figure 3.4: Continued from Figure 3.3.

Table 3.6: Derived stellar parameters of confirmed and candidate stellar companions

Companion[a]	UT Obs. Date	$T_{\rm eff}$ (K)	M ($M_\odot$)	$\log g$ (cgs)	D (au)	J-band $T_{\rm eff}$ (K)	H-band $T_{\rm eff}$ (K)	K-band $T_{\rm eff}$ (K)
HAT-P-5 cc	2013 Jul 04	2738 ± 73	0.0957 ± 0.0043	5.268 ± 0.017	718 ± 62	···	···	2738^{+70}_{-58}
HAT-P-5 cc	2015 Jun 24	2814 ± 72	0.1009 ± 0.0054	5.248 ± 0.019	724 ± 63	2879^{+77}_{-70}	···	2754^{+32}_{-30}
HAT-P-27B	2014 Jul 12	3460 ± 45	0.323 ± 0.049	4.941 ± 0.039	133.8 ± 9.2	$3477.0^{+6.6}_{-5.9}$	$3496.0^{+2.9}_{-3.7}$	$3409.6^{+8.8}_{-7.3}$
HAT-P-27B	2015 Jan 09	3459 ± 44	0.323 ± 0.048	4.942 ± 0.038	133.4 ± 9.2	3479.9 ± 1.5	3490.2 ± 1.5	$3409.6^{+2.2}_{-1.5}$
HAT-P-27B	2015 Jun 24	3433 ± 23	0.298 ± 0.023	4.968 ± 0.019	133.2 ± 9.1	···	···	$3433.1^{+6.6}_{-7.3}$
HAT-P-28 cc	2015 Jul 07	3579 ± 54	0.444 ± 0.043	4.847 ± 0.039	394^{+34}_{-26}	3609.3 ± 5.7	···	3549.2 ± 8.1
HAT-P-28 cc[b]	2015 Jul 10	3542 ± 57	0.409 ± 0.050	4.875 ± 0.043	394^{+34}_{-26}	$3583.3^{+9.8}_{-8.9}$	···	3502.9 ± 2.4
HAT-P-29B[c]	2012 Feb 02	2804 ± 94	0.1001 ± 0.0069	5.251 ± 0.025	1059^{+120}_{-69}	2862^{+59}_{-50}	···	2749^{+72}_{-60}
HAT-P-29B	2015 Jul 05	2955 ± 78	0.115 ± 0.011	5.206 ± 0.028	1062^{+120}_{-69}	···	···	2955^{+54}_{-46}
HAT-P-29B[b]	2015 Jul 10	2710 ± 110	0.0942 ± 0.0066	5.274 ± 0.027	1060^{+120}_{-69}	···	···	2713^{+89}_{-69}
HAT-P-35B	2013 Mar 02	3525 ± 76	0.383 ± 0.070	4.889 ± 0.059	499 ± 30	$3469.5^{+9.8}_{-8.9}$	···	3583^{+13}_{-12}
HAT-P-35B	2014 Nov 10	3563 ± 70	0.428 ± 0.059	4.859 ± 0.051	499 ± 30	3580.9 ± 5.7	3602.8 ± 3.3	$3508.6^{+4.9}_{-5.7}$
HAT-P-39B	2013 Mar 02	3477 ± 72	0.324 ± 0.068	4.926 ± 0.060	576^{+100}_{-59}	3413 ± 13	···	3548^{+21}_{-20}
HAT-P-39B	2014 Nov 07	3558 ± 52	0.422 ± 0.044	4.862 ± 0.038	577^{+100}_{-59}	3558 ± 11	$3614.2^{+2.4}_{-3.3}$	3504^{+32}_{-24}
HAT-P-41 cc	2014 Oct 03	3783 ± 67	0.561 ± 0.028	4.737 ± 0.026	1124^{+130}_{-98}	···	···	3783^{+35}_{-29}
HAT-P-41 cc	2015 Jun 24	3873 ± 83	0.593 ± 0.028	4.707 ± 0.024	1124^{+130}_{-98}	$3914.1^{+8.9}_{-8.1}$	···	3834^{+21}_{-20}
HAT-P-54 cc[d]	2016 Jan 25	1941 ± 75	0.07428 ± 0.00090	5.3996 ± 0.0083	619 ± 16	···	···	1941^{+78}_{-62}
TrES-1 cc1[e]	2013 Jul 04	···	···	···	···	···	···	···
TrES-1 cc1[e]	2015 Jun 24	···	···	···	···	···	···	···
TrES-1 cc2	2013 Jul 04	2550 ± 140	0.0874 ± 0.0047	5.307 ± 0.025	641 ± 43	···	···	2554^{+27}_{-26}
TrES-1 cc2	2015 Jun 24	2580 ± 170	0.0884 ± 0.0061	5.301 ± 0.031	642 ± 43	2507^{+110}_{-86}	···	2661^{+32}_{-30}
WASP-33 cc	2013 Aug 19	3256 ± 59	0.183 ± 0.024	5.081 ± 0.030	239 ± 14	3276^{+52}_{-47}	3316^{+22}_{-20}	3181.0 ± 4.1
WASP-33 cc	2014 Dec 07	3171 ± 29	0.1560 ± 0.0084	5.124 ± 0.012	238 ± 14	···	···	3171^{+25}_{-24}
WASP-33 cc	2015 Dec 26	3201 ± 31	0.1650 ± 0.0093	5.111 ± 0.013	238 ± 14	···	···	3201^{+29}_{-25}
WASP-36 cc	2016 Jan 25	3583 ± 67	0.451 ± 0.053	4.846 ± 0.048	2190 ± 580	···	···	3583^{+28}_{-24}
WASP-48 cc	2013 Aug 19	2768 ± 51	0.0974 ± 0.0030	5.261 ± 0.012	1660 ± 180	···	···	2768^{+28}_{-26}

Continued on next page

Table 3.6 – continued from previous page

Companion[a]	UT Obs. Date	$T_{\rm eff}$ (K)	M ($M_\odot$)	$\log g$ (cgs)	D (au)	J-band $T_{\rm eff}$ (K)	H-band $T_{\rm eff}$ (K)	K-band $T_{\rm eff}$ (K)
WASP-48 cc	2015 Jun 24	2810 ± 50	0.1001 ± 0.0036	5.251 ± 0.013	1640 ± 170	2830^{+120}_{-110}	···	2792^{+28}_{-27}
WASP-58B[b]	2015 Jul 10	3396 ± 53	0.265 ± 0.042	4.997 ± 0.040	384 ± 64	3419^{+23}_{-22}	···	3374^{+16}_{-18}
WASP-76B[b]	2015 Jul 10	4310 ± 170	0.712 ± 0.042	4.608 ± 0.030	53.0 ± 8.8	$4486.3^{+9.8}_{-8.1}$	···	4155^{+98}_{-80}
WASP-103 cc	2016 Jan 25	4330 ± 100	0.721 ± 0.024	4.604 ± 0.016	112.4 ± 8.4	4369 ± 21	4252.2 ± 6.5	4374 ± 16

Notes. For each date, we report error weighted averages of all measurements on $T_{\rm eff}$, M, $\log g$, and D. Our uncertainties account for uncertainties arising from the measurements, the primary star's stellar parameters and the error weighted average calculation. However, they do not include uncertainties from the stellar models and our assumptions on stellar composition. All uncertainties are thus underestimates of the true uncertainty, especially for the final three columns, as these only include measurement uncertainties. The last three columns also show that if our candidate companions are comoving, their temperatures are consistent with a late type main sequence star in all filters. Except where noted, K corresponds to K_s.

[a] We label companions with confirmed common proper motions as "B" and as "cc" when they are candidate companions. See Section 3.5.

[b] On 2015 Jul 10, we used the J_c and BrG bandpasses instead of J and K_s, respectively. Therefore, for these marked rows, the seventh and ninth columns report the effective temperature for these bandpasses instead.

[c] On 2012 Feb 02, for HAT-P-29, we used the K' bandpass instead of K_s.

[d] For this target, the companion temperature is below the lower limit of the PHOENIX models (2300 K), so we assumed a blackbody for both primary and secondary stars.

[e] This candidate companion is too faint to obtain reliable photometric measurements.

Contrast curves

We calculate contrast curves for all targets imaged, regardless of whether or not a companion was detected. Our algorithm is described in Ngo et al. (2015). Figure 3.5 shows the K-band 5σ contrast limit, in magnitudes, for all targets discussed in this paper. We are able to reach a 5σ contrast of $\Delta K = 8$ for most of the targets surveyed. When considering our survey's sensitivity for each target we use its individual contrast curve as discussed in Section 3.6, below.

3.5 Notes on detected companions

We find 17 candidate stellar companions around 15 of the systems observed, of which 3 are reported for the first time in this paper. In this section, we discuss each system individually and categorize them according to whether or not the companion is bound as confirmed by common proper motion measurements. For targets where our astrometric measurements are inconclusive we consider whether or not the companion has colors consistent with the expected spectral type for a bound companion. Our analysis confirms 6 companions as gravitationally bound, identifies 10 candidate companions with inconclusive astrometric measurements and colors consistent with those of a bound companion, and finds 1 candidate companion to be a background object. For each candidate companion, we report the differential magnitude ΔK, separation ρ and position angle (PA) from our first detection epoch for comparison with detections from other studies. We also discuss any observations previously reported by other studies.

Bound companions

HAT-P-27 (WASP-40). We find a companion with $\Delta K_s = 3.52 \pm 0.05$, $\rho = 0''.656 \pm 0''.002$ and PA $= 25°.5 \pm 0°.1$. Wöllert and Brandner (2015) also found a candidate stellar companion at the same separation, however they note that the companion was too dim for them to reliably measure its flux. Our three astrometric measurements show that this companion is physically bound, an argument that is strengthened by the inclusion of the single epoch of astrometry by Wöllert and Brandner (2015). Evans et al. (2016) also imaged this system but reported that this companion is below their survey sensitivity.

HAT-P-29. We find a companion with $\Delta K' = 6.9 \pm 0.2$, $\rho = 3''.290 \pm 0''.002$ and PA $= 159°.89 \pm 0°.03$. Due to our dithering pattern, this faint companion only appeared in a subset of our dithered images. As a result, we failed to identify it in our original 2012 images. After Wöllert et al. (2015) pointed this out, we revisited

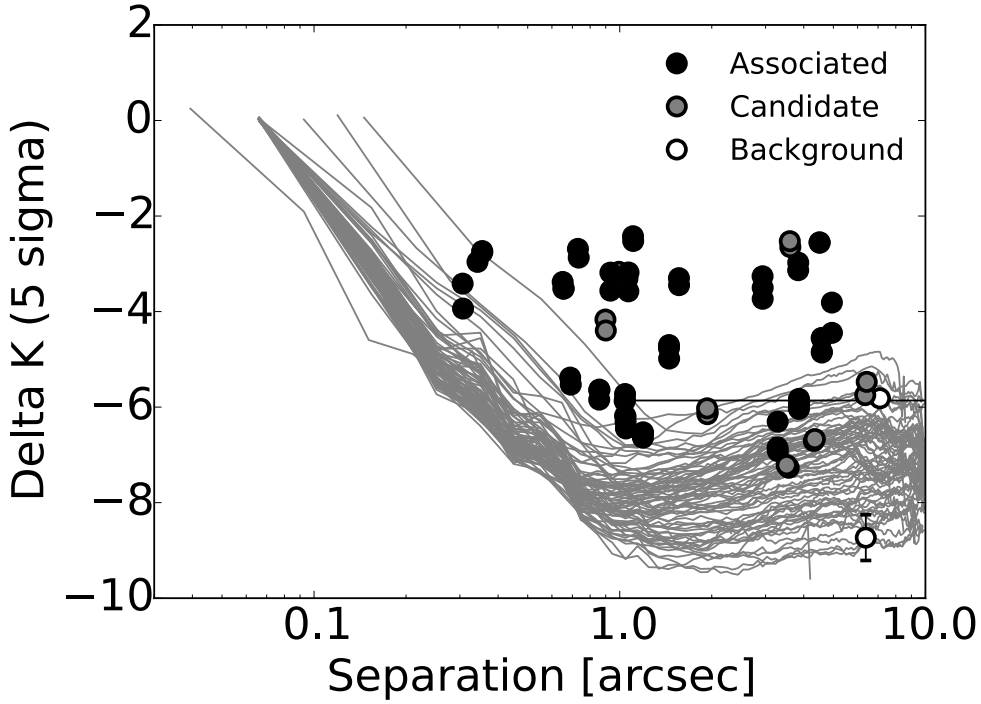

Figure 3.5: 5σ K band contrast curve computed from stacked images for all observed targets. The curve with the best contrast for each target is shown. For these curves, all companion stars are masked out. Detections of bound companions, candidate companions, and background objects as overplotted as filled black, grey, and open circles, respectively.

our old observations and found that the companion was indeed present in a subset of the frames. Inspection of the contrast curve for this system from Ngo et al. (2015) confirms that the companion fell below our formal 5σ detection limit, and is therefore consistent with the non-detection reported in Ngo et al. (2015). We obtained new images of the system in 2015, in which we planned our dither pattern to make sure that the companion remained in the frame in all images. Although the Wöllert et al. (2015) astrometric uncertainties were too large to verify common proper motion, our measurements from 2012 and 2015 show the candidate is consistent with a bound stellar companion.

HAT-P-35. We find a companion with $\Delta K_s = 3.19 \pm 0.06$, $\rho = 0''.932 \pm 0''.002$ and PA = $139°.31 \pm 0°.09$. Wöllert and Brandner (2015) also found a companion at the same position but could not confirm common proper motion with only one epoch. Our measurements in 2013 and 2014 confirm this candidate as bound stellar companion. Evans et al. (2016) report a companion in their 2014 images with a similar brightness difference but with separation $\rho = 1''.016 \pm 0''.011$ and PA

= 149°.4 ± 0°.2. This measurement is discrepant at the 10σ level to both of our measurements and at 7σ to the Wöllert and Brandner (2015) measurement.

HAT-P-39. We find a companion with $\Delta K_s = 4.2 \pm 0.1$, $\rho = 0''.898 \pm 0''.002$ and PA = 94°.3 ± 0°.1. Our observations in early 2013 and late 2014 show that this candidate companion has the same proper motion as the primary star. The color of this candidate companion is also consistent with a late-type main sequence star. We therefore consider this candidate to be a bound stellar companion.

This system was also imaged by Wöllert et al. (2015) but they did not report a companion. Their detection limit at 1″ was $\Delta z' = 4.9$. Our temperature estimate indicates the companion is an early M dwarf, therefore, this candidate may have been below the detection limit of these observations.

WASP-58. We find a companion with $\Delta BrG = 4.4 \pm 0.1$, $\rho = 1''.281 \pm 0''.002$ and PA = 183°.37 ± 0°.07. This companion was originally reported in Wöllert et al. (2015), and when we combine our single epoch of imaging with the single epoch from their paper we find clear evidence that this candidate is a gravitationally bound companion.

WASP-76. We find a companion with $\Delta BrG = 2.7 \pm 0.1$, $\rho = 0''.441 \pm 0''.002$ and PA = 215°.6 ± 0°.2. This companion was first discovered by Wöllert and Brandner (2015) and also followed up by Ginski et al. (2016). When combined with the single-epoch astrometry from these two papers our new epoch of astrometry indicates that this companion is gravitationally bound.

Candidate companions

HAT-P-5. We find a companion with $\Delta K_s = 6.7 \pm 0.2$, $\rho = 4''.314 \pm 0''.003$ and PA = 267°.83 ± 0°.03. Our astrometric analysis is not well matched by models for either a bound companion or a background object. Because the color of this candidate companion is consistent with a late-type main sequence star, we tentatively consider HAT-P-5 to be a candidate multi-stellar system for the our companion fraction analysis.

This system was also imaged by Daemgen et al. (2009) and Faedi et al. (2013). Daemgen et al. (2009) did not find this companion, but they restricted their binary search to companions within 2″. Faedi et al. (2013) noted a potential companion around HAT-P-5 with a separation of 4″.25 and position angle of 266°, but classified it as a non-detection because the companion's brightness was below their 4σ

detection limit. We do not use their astrometric point in our analysis because there is no uncertainty reported on their separation.

HAT-P-28. We find a companion with $\Delta K_s = 3.17 \pm 0.04$, $\rho = 0''.994 \pm 0''.002$ and PA = $210°.7 \pm 0°.1$. Wöllert and Brandner (2015) previously reported a candidate stellar companion at a position consistent with our measurement. We include this previous astrometric measurement but it is not precise enough to allow us to distinguish between comoving and bound tracks. Since both our study and Wöllert and Brandner (2015) find the color of the candidate companion to be consistent with a late type main sequence star, we consider this to be a candidate multi-stellar system in our analysis.

HAT-P-41. We find a companion with $\Delta K_s = 2.65 \pm 0.08$, $\rho = 3''.615 \pm 0''.002$ and PA = $184°.10 \pm 0°.03$. Hartman et al. (2012) reported a candidate companion along with the discovery of HAT-P-41b at a similar separation, however they do not report a position angle. Wöllert et al. (2015), Wöllert and Brandner (2015), and Evans et al. (2016) all report finding a companion at a similar position. When all observations are taken in account, the astrometric measurements are not well-matched by models for either a bound companion or a background object. Our companion color and effective temperature as well the previous studies' color measurements indicate this companion is consistent with a late type main sequence star at the same distance as the primary star. So, we consider HAT-P-41 to be a candidate multi-stellar system.

HAT-P-54. We find a companion with $\Delta K_s = 6.5 \pm 0.2$, $\rho = 4''.557 \pm 0''.003$ and PA = $135°.54 \pm 0°.03$. Because the central star has a spectral type of K7, the measured flux ratio predicts a companion temperature below 2300 K, the lower limit on the PHOENIX models. Therefore, we used a blackbody to model the spectral energy distribution of both the central star and companion. This candidate companion was originally reported in Wöllert and Brandner (2015). Their 2014 measurements are consistent with both our 2016 measurement and the background track. Their 2015 measurement has a separation measurement that differs from ours by 3σ but a consistent position angle. Our measured ΔK_s magnitudes correspond to an effective temperature of 1941 K $\pm$ 75 K for this candidate companion, indicating that it may be a brown dwarf. The $\Delta i'$ and $\Delta z'$ measurements from Wöllert and Brandner (2015) are also consistent with a brown dwarf candidate.

TrES-1. We find three objects around TrES-1. The object closest to the primary has $\rho = 2''.340 \pm 0''.01$ and PA = $172°.9 \pm 0°.1$. This object is too faint for us to get a reliable flux measurement. Our images show a range of differential magnitudes

between ΔK_s from 7.5 to 9.0. Adams et al. (2013) imaged this system in 2011 and reported a companion with $\Delta K_s = 7.7, \rho = 2''.31$ and PA = 174°. Although they do not report any uncertainties, these photometric and astrometric values are consistent with our detection. They also do not detect any additional objects. Our two epochs are consistent with neither the background and comoving tracks. This object remains a candidate companion and we label it as TrES-1 cc1.

The next closest object has $\Delta K_s = 6.67 \pm 0.06, \rho = 4''.940 \pm 0''.002$ and PA = 148°.15 ± 0°.02. Faedi et al. (2013) found a companion consistent with this detection. We include this previous measurement with our two epochs and find that the positions are consistent with both a comoving and background track. Our study shows the companion color is consistent with a late type main sequence star at the same distance as the primary star. We label this candidate companion as TreS-1 cc2.

The furthest object has $\Delta K_s = 5.7 \pm 0.1, \rho = 6''.355 \pm 0''.002$ and PA = 47°.31 ± 0°.02. Faedi et al. (2013) found a companion consistent with this detection. We include this previous measurement with our two epochs and find that the positions are consistent with the background track only. Therefore, we do not include this object in further analysis and we label it TrES-1 bg.

Finally, this system was also imaged by Daemgen et al. (2009), but they did not report any companions to TrES-1. They restricted their search to companions within 2″, which would miss all three objects discussed here. In our multiplicity analysis, we count this as a candidate multi-stellar system.

WASP-33. We find a companion with $\Delta K_s = 6.11 \pm 0.02, \rho = 1''.940 \pm 0''.002$ and PA = 276°.25 ± 0°.05. Moya et al. (2011) find a companion at a consistent position angle but at a separation of $1''.961 \pm 0''.003$, which is 6σ larger than our measurement. However, they report applying a rotation correction but not a NIRC2 distortion correction. Our mass and temperature estimates are also consistent with their mass (between 0.1 $M_\odot$and 0.2 $M_\odot$) and temperature (3050 K ± 250 K) estimates. They also show that the candidate companion and primary star lie on the same isochrone and argue that these objects are bound. Adams et al. (2013) also found a companion but do not report astrometric uncertainties. Wöllert and Brandner (2015) also report finding a companion at a position consistent with our three measurements. The separations measured over our three epochs are consistent with both a common proper motion track and a background track. However, the position angle measurements from this work and Moya et al. (2011) are inconsistent with

a background track. With this astrometric evidence and colors and temperatures consistent with a late type main sequence star, we consider WASP-33 to be a candidate multi-stellar system.

WASP-36. We find a companion with $\Delta K_s = 2.7 \pm 0.1$, $\rho = 4''.869 \pm 0''.002$ and PA $= 66°.98 \pm 0°.02$. This candidate companion was reported in Wöllert and Brandner (2015) and Evans et al. (2016). We obtained an additional epoch in 2016. All measurements are consistent with each other and also with the background track. We expect that another epoch of Keck imaging in the next one to two years should allow us to determine whether or not the companion is bound.

WASP-48. We find a companion with $\Delta K_s = 7.3 \pm 0.1$, $\rho = 3''.571 \pm 0''.003$ and PA $= 208°.32 \pm 0°.04$. Our astrometric measurements are not well-matched by models for either a bound companion or a background object. For now, we consider this a candidate multi-stellar system because the companion's color is consistent with a late type main sequence star.

This system was also imaged by Wöllert et al. (2015) but they did not report a companion. They only report detection limits out to $2''$, which was at $\Delta z' = 6.1$ for this target. Our temperature estimate indicates the companion is an early M dwarf, therefore this candidate may have been below the detection limit of these previous observations.

WASP-103. We find a companion with $\Delta K_s = 1.97 \pm 0.02$, $\rho = 0''.239 \pm 0''.002$ and PA $= 131°.3 \pm 0°.4$. The position measurements from our study and Wöllert and Brandner (2015) are consistent with each other, but the large uncertainty from the previous study prevents us from ruling out a background object. In addition, our companion color and effective temperature estimates are consistent with a late type main sequence star at the same distance. Evans et al. (2016) also imaged this system but reported that this companion is below their survey sensitivity.

3.6 Survey results

We combine our new companion search sample of 27 systems (see Section 3.3 for a description of the sample selection) with the original sample of 50 systems surveyed in Ngo et al. (2015) in order to derive an updated estimate of the stellar multiplicity of these stars. We include all confirmed and candidate multi-stellar systems in this analysis. Although we reserve the label of confirmed companion for systems where we can demonstrate that the companion has the same proper motion as the primary, we expect that most if not all of our candidate companions are also likely to be

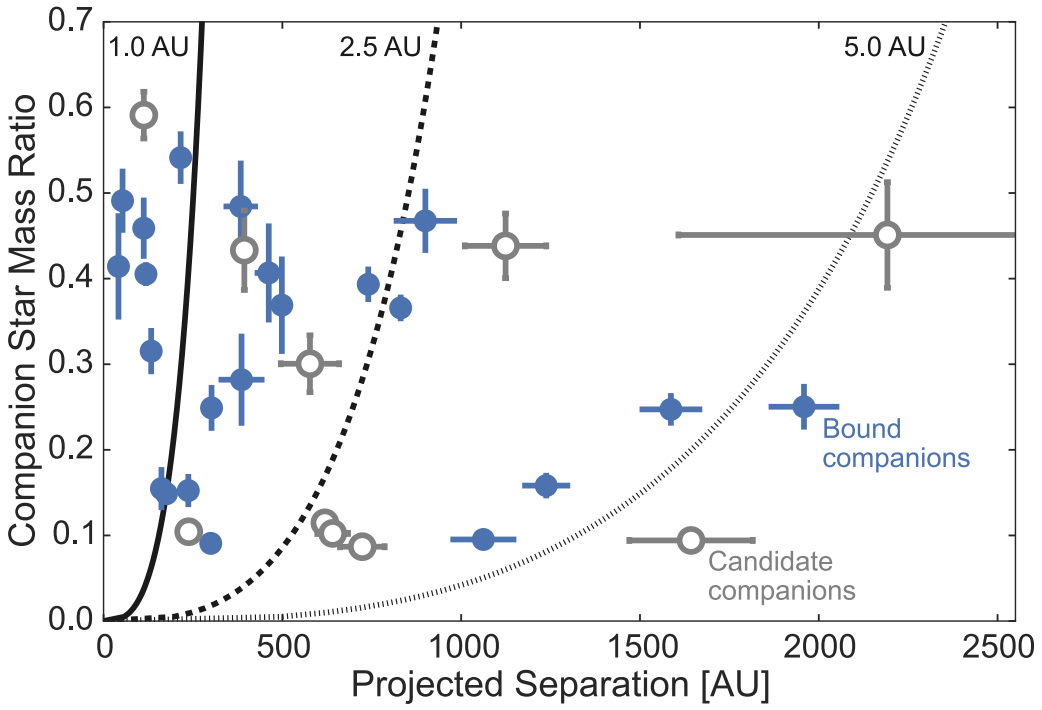

Figure 3.6: For each companion in our survey sample, we plot the companion's mass and projected separation. Each point represents the weighted average from all observations in Table 3.6. The lines represent the minimum companion mass necessary to excite Kozai-Lidov oscillations at a timescale short enough to overcome general relativity pericenter precession. These representative lines assume a primary stellar mass of 1.0 $M_{\odot}$, a planetary mass of 1.0 M_{Jup}, a circular planetary orbit and a stellar companion eccentricity of 0.5. The three lines (solid, dashed, and dotted) represent the difference in pericenter precession timescales for a hot Jupiter starting at 1 au, 2.5 au and 5 au, respectively. Companions must be above and to the left of these lines to overcome general relativity pericenter precession timescales.

bound. We base this argument on the fact that they have colors consistent with those of a bound companion, and also that their projected separations and contrast ratios make them unlikely to be a background object (e.g. see Ngo et al., 2015; Bowler et al., 2014). For some candidate companions, Evans et al. (2016) have suggested that a background red giant star at a moderate distance would have photometric and astrometric measurements consistent with both background and bound object tracks. Additional measurements would help to distinguish these two cases. We report a total raw stellar companion fraction of 27 out of 77 stars, or 35 % ± 7 %. Figure 3.6 shows the distribution of projected separations and mass ratios for the confirmed and candidate companions from this study and Ngo et al. (2015).

AO survey incompleteness correction

We correct our raw companion fraction for survey completeness following the procedure described in Ngo et al. (2015) for each of our 77 targets. In brief, we generate 2.5 million simulated companions over a 50x50 grid in mass and semi-major axis. Each simulated companion has an orbital eccentricity drawn from a uniform distribution (Raghavan et al., 2010) and randomized orbital elements. If the simulated companion's brightness ratio is above the 5σ contrast limit as computed in Section 3.4 at the projected on-sky separation, then we count it as a detection. We then calculate the average sensitivity over all grid cells where we weight each cell according to the probability that a field star would have a companion in the stated mass and semi-major axis range according to Raghavan et al. (2010). The i-th target's survey sensitivity is called S_i and it represents the fraction of stellar companions between 50 au and 2000 au (our survey phase space) that our observations could have detected.

Next, we can use our estimate of survey completeness for each star, S_i, to compute the true companion fraction, η, for any arbitrary set of stars in our survey sample. We write the likelihood L of observing N_d detected companions out of a set of N stars as:

$$L = \prod_{i=1}^{N_d} (S_i \eta) \prod_{j=1}^{N-N_d} (1 - S_j \eta), \tag{3.1}$$

where the product sum over i is for the targets with a detected companion while the product sum over j is for the targets without a detected companion. We define the companion fraction η as the fraction of stars with one or more stellar companions in our survey phase space. Thus, we also make the assumption that $S_i = 1$ for all systems with at least one detected companion. This is equivalent to assuming that there are no further companions within our survey phase space around targets with at least one companion already detected. This assumption is supported by our observational results and previous studies such as Eggleton et al. (2007).

We determine the posterior probability distribution of η by maximizing the above likelihood via the Affine-Invariant Markov Chain Monte Carlo scheme implemented by the "emcee" python package (Goodman and Weare, 2010; Foreman-Mackey et al., 2013). We use a uniform prior on η between the possible values of $\eta = 0$ and $\eta = 1$. We report the 68% confidence interval on η as the uncertainties on our best estimate of η for each of the following set of targets in our survey sample. For more details on our calculation of S_i, L, and η, see Ngo et al. (2015).

Stellar companion fraction for hot Jupiter hosts vs. field stars

First, we report the companion fraction of the entire survey sample to be 47% ± 7% (47% ± 12% for the new targets presented in this work) for companions with separations between 50 au and 2000 au. This overall companion fraction is consistent with our previously reported companion fraction of 49% ± 9% in Ngo et al. (2015). We next use the results of our long term radial velocity monitoring survey (Knutson et al., 2014; Bryan et al., 2016) to constrain the population of stellar companions within 50 au. Following the procedure in Section 3.5 of Bryan et al. (2016), we compute the sensitivity to stellar companions (masses greater than 0.08 $M_{\odot}$) for the 50 targets in our sample with long term radial velocity data. Figure 3.7 shows the resulting average sensitivity contours for AO imaging and radial velocity data sets as a function of companion semi-major axis. With the exception of one target, our radial velocity monitoring rules out stellar companions within 50 au. The only exception is the stellar companion to HAT-P-10, detected by both our radial velocity survey (Knutson et al., 2014) and our AO survey (Ngo et al., 2015) with a projected separation of 42 au. Although the current data for this companion are also consistent with orbital semi-major axes beyond 50 au, we count it as interior to 50 au for the purposes of our statistical analysis. Following the same completeness-correction procedure as for our AO companion fraction, we use the RV sensitivity curves of a sample of 51 transiting hot Jupiters (Knutson et al., 2014; Bryan et al., 2016) and find that $3.9^{+4.5}_{-2.0}$% of these hot Jupiters have stellar companions between 1 au and 50 au.

We also compare our overall companion fraction for hot Jupiter host stars with that of solar-type field stars. In Ngo et al. (2015), we were sensitive to stellar companions with periods as short as 10^4 days for some of our nearby targets, which corresponds to separations of 10 au. Without a constraint on potential stellar companions within 50 au from radial velocity monitoring, we made the conservative choice to compare our AO detected companion fraction to the field star population with periods between 10^4 days and $10^{7.5}$ days (corresponding to separations between 10 au and 2000 au for solar-like stars). However, surveys of star-forming regions indicate that binaries with separations less than 50 au have significantly shorter disk lifetimes while binaries with larger separations appear to have disk lifetimes comparable to those of single stars (e.g. Kraus et al., 2012). In addition, Kraus et al. (2016) surveyed 382 *Kepler* planet host stars and found that there is a 4.6σ deficit in stars with binaries closer than 50 au compared to field stars, suggesting that these close binaries negatively influence planet formation (see also Wang et al., 2015). We therefore change our

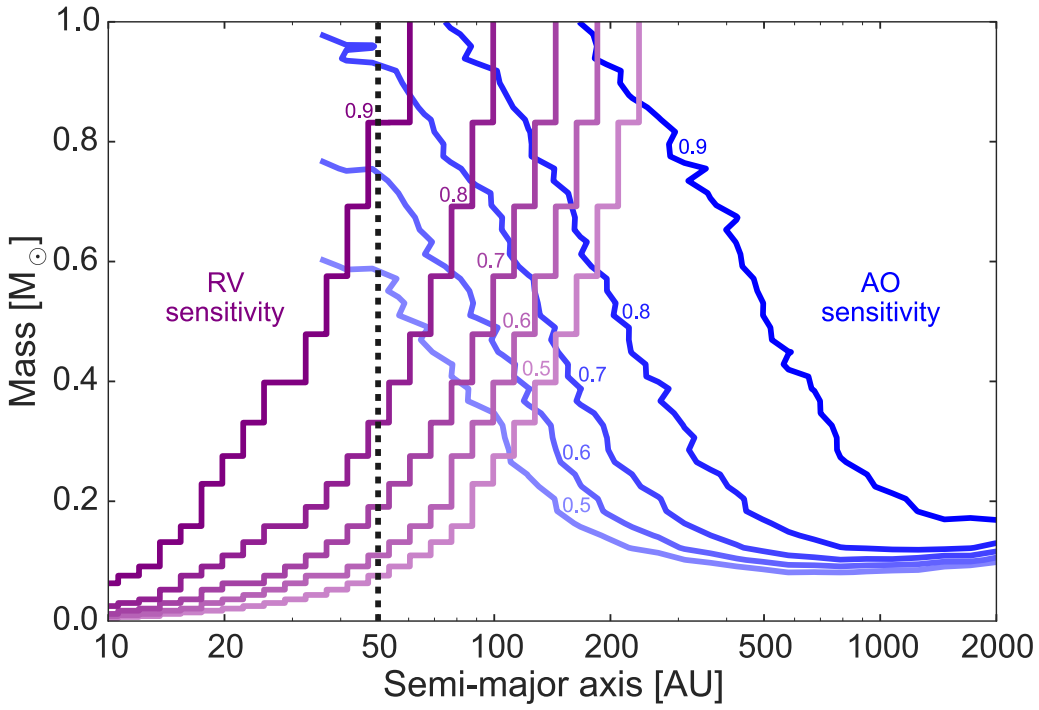

Figure 3.7: Contours of overall sensitivity to stellar companions from long term radial velocity surveys (purple) and our AO survey (blue). These sensitivities are averaged over all targets and computed for a typical 1 $M_\odot$ target. The dashed line marks a semi-major axis of 50 au.

approach in this analysis to consider the multiplicity rate for companions interior and exterior to 50 au separately.

We compute the field star companion fraction for companions with periods between 10^5 days and $10^{7.5}$ days (corresponding to separations between 50 au and 2000 au for solar-like stars) to be 16% ± 1%. Thus, we find that hot Jupiters have 2.9 times as many companions in this phase space as field stars, where the difference is significant at the 4.4σ level. In contrast, there is a lack of stellar companions to transiting hot Jupiter host stars with separations less than 50 au. On the other hand, only $3.9^{+4.5}_{-2.0}$% of hot Jupiters have stellar companions with separations between 1 au and 50 au, while 16.4% ± 0.7% of field stars have stellar companions in this range, corresponding to a 2.7σ difference. We choose a lower limit of 1 au to avoid systems where the stellar companion could eject the hot Jupiter (Mardling and Aarseth, 2001; Petrovich, 2015a). We note that if we relax this lower limit and consider all companions with separations less than 50 au, we find that hot Jupiter hosts have a companion fraction of $3.9^{+4.6}_{-2.0}$% while field stars have a companion fraction of 22% ± 1%, which is a difference of 3.8σ. These values are consistent with the results of Kraus et al. (2016).

In a recent study, Evans et al. (2016) use a sample of 101 systems observed with lucky imaging to derive a completeness-corrected estimate of 38^{+17}_{-13}% for the multiplicity rate of hot Jupiter host stars. This number is in good agreement with our value, but Evans et al. (2016) differ from our study in their calculation of the equivalent field star multiplicity rate. Although their imaging survey is only sensitive to companions beyond 200 au, they integrate over field star binaries with separations greater than 5 au, resulting in a field star multiplicity rate of 35% ± 2%. However, we argued above, this conflates two regions with apparently distinct companion occurrence rates. If we instead take 200 au, or periods of $10^{5.9}$ days, as our lower limit for field star binaries and re-calculate the corresponding field star multiplicity rate we find a value of 15% ± 1%, which is $1.8\,\sigma$ lower than the hot Jupiter multiplicity rate reported by Evans et al. (2016). We therefore conclude that their results are consistent with our finding that hot Jupiters a higher multiplicity rate than field stars at wide separations. In order to facilitate comparisons between our study and those of Evans et al. (2016) and Wang et al. (2015), we re-calculate our hot Jupiter companion fraction for separations between 200 auand 2000 au. We find a value of 32% ± 6% in this regime, in good agreement with both of these studies. This companion fraction is also 3.8σ higher than the field star companion fraction of 9.0% ± 0.4% for companions separated between 200 au and 2000 au.

Distribution of companion mass ratios and semi-major axes

Next, we compare the observed distribution of companion mass ratios and semi-major axes with those of field stars. Figure 3.8 shows the survey's observed companion fraction, the survey's completeness corrected companion fraction η_M, and the completeness corrected field star companion fraction (Raghavan et al., 2010) as a function of companion star mass ratio. We find that distribution of mass ratios for the stellar companions detected in our survey is concentrated towards small values, unlike the relatively uniform distribution observed for field stars. It is possible that our distribution is shaped at least in part by observational biases in ground-based transit surveys, where binary companions with separations less than 1″ are likely to be blended with the primary in the survey photometry, therefore diluting the observed transit depths in these systems. Equal mass binaries with projected separations of less than 0″.5 are also challenging targets for radial velocity follow-up due to the blended nature of the stellar lines, and it is possible that these kinds of systems might receive a lower priority for follow-up as compared to apparently single stars or those with relatively faint companions. Wang et al. (2015) found three stellar

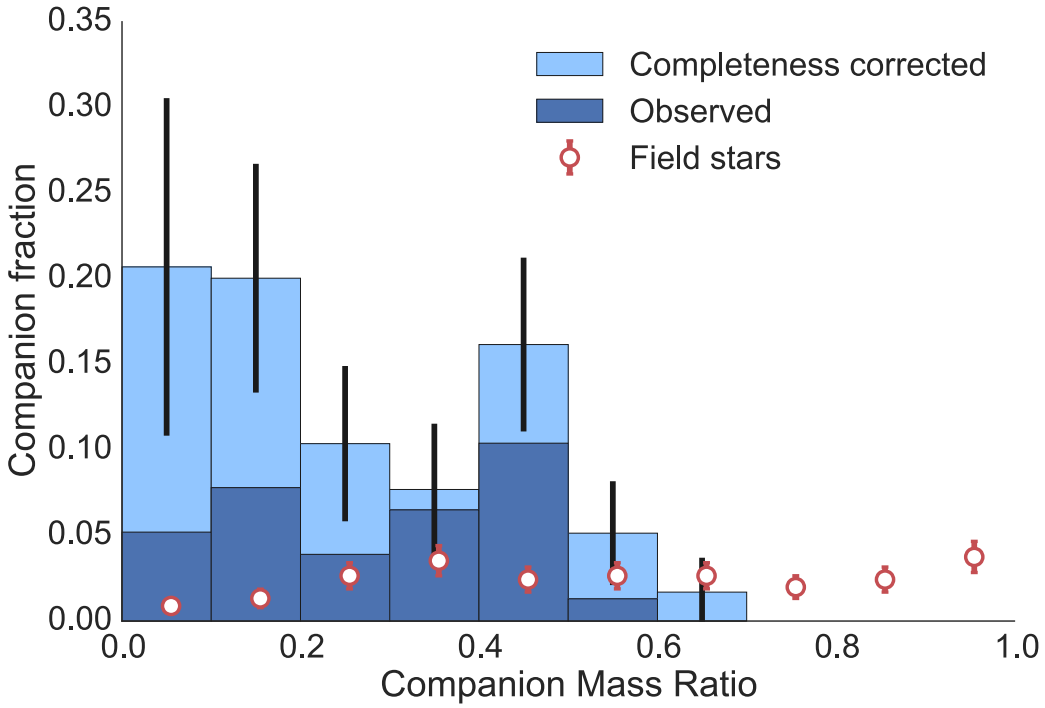

Figure 3.8: Companion fraction as a function of companion mass ratio for targets in the completeness corrected survey sample (light blue), the uncorrected survey sample (dark blue), and the field star sample (open red symbols). The field star values (open red circles) are from Raghavan et al. (2010) and are also completeness corrected.

companions to *Kepler* short-period ($P < 10$ days) giant planet hosts with $\Delta K \lesssim 0.5$, corresponding to mass ratios greater than 0.8. While this is consistent with the idea that ground-based transit surveys might be biased against detecting hot Jupiters orbiting equal mass binaries, the current transiting sample is missing this population of hot Jupiters, and the current sample sizes are too small to apply a correction.

While the field star companion fraction rises up to mass ratios of 0.3, our survey companion fraction is largest for mass ratios less than 0.2. Although Raghavan et al. (2010) corrected their field star sample to account for survey incompleteness at the lowest mass ratios, it is possible that their correction underestimated the true incompleteness at small mass ratios. Because this trend is seen in the completeness corrected companion fraction but not the observed companion fraction, we considered whether it could be an artifact introduced by our completeness correction calculation. We generate simulated companions down to a mass of 0.08 $M_{\odot}$, which is a mass ratio of 0.05 for our most massive survey target and less than 0.1 for all but one of our survey targets (for WASP-43, this limit corresponds to a mass ratio of 0.13). Therefore, while the smallest mass ratio bin may have unequal sizes for each

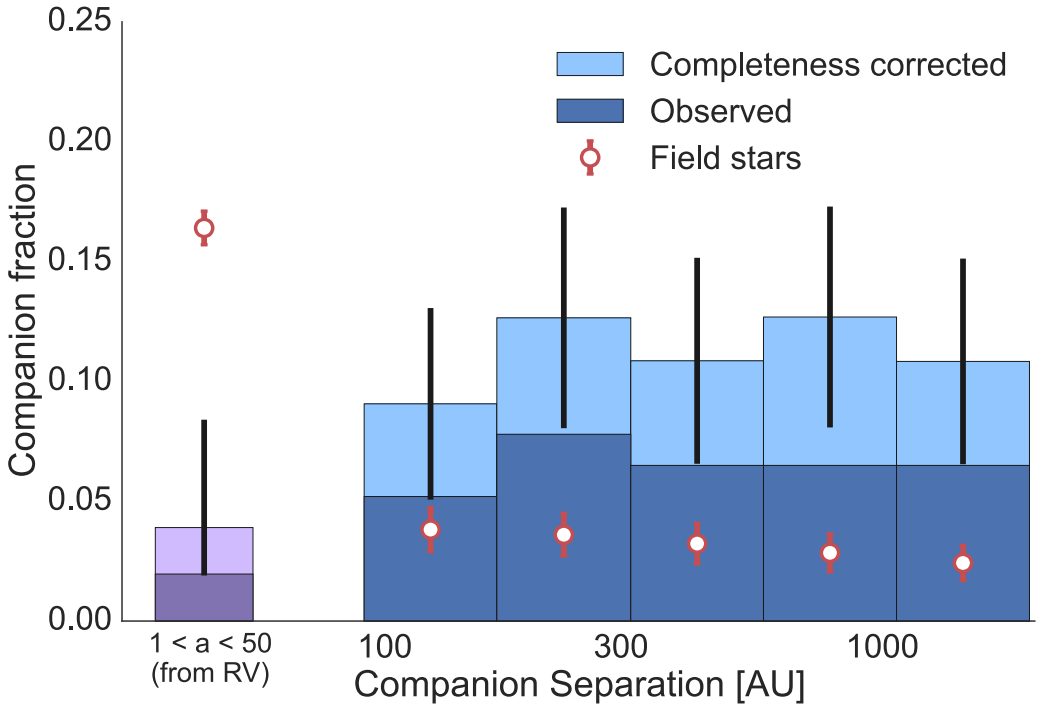

Figure 3.9: Companion fraction as a function of companion separation, in logarithmic bins, for targets in the completeness corrected survey sample (light blue), the uncorrected survey sample (dark blue), and the field star sample (open red symbols). The leftmost bin represents the corrected (light purple) and uncorrected (dark purple) companion fraction from 1 au to 50 au, computed from long term RV sensitivity surveys. The field star values (open red circles) are from Raghavan et al. (2010) and are also completeness corrected.

target, the second smallest bin is the same for all targets and also shows an enhanced companion fraction relative to that of field stars. Although our correction is more uncertain at lower masses, the difference between our completeness corrected companion fraction and the field star distribution in the 0.1-0.2 mass ratio bin is greater than the uncertainty by 2.8σ.

Figure 3.9 shows the survey's observed companion fraction, the survey's completeness corrected companion fraction η_S, and the completeness corrected field star companion fraction (Raghavan et al., 2010) as a function of companion star projected separation. The comparison is made in logarithmic space for projected separation as Raghavan et al. (2010) found that the periods of companion stars follow a log-normal distribution. This plot shows a higher companion fraction in our survey than in the field star sample. However, we find that the relative distribution of companion separations in our sample is in good agreement with those of the field star sample. Although our distribution appears to be effectively uniform, this is consistent with the log-normal distribution reported in Raghavan et al. (2010) since

our survey space spans a relatively small fraction of the separations considered in Raghavan et al. (2010).

Multiplicity and host star metallicity

We next investigate whether our measured companion fraction could be affected by differences in the metallicities of the stars in our sample as compared to the field star sample. Raghavan et al. (2010) found tentative evidence for a rise in the multiplicity rate for metal-poor ([Fe/H] < -0.3) stars and a uniform multiplicity rate for metallicities between -0.3 and +0.4. Our targets have metallicities ranging from -0.29 to +0.45. We therefore conclude that the increased companion fraction for our sample of hot Jupiter hosts is unlikely to be due to the higher metallicities of our stars as compared to the field star sample.

We also considered whether the presence of companions in our sample is correlated with the metallicities of the host stars, although we would not expect such a correlation based on the results from the field star sample. If we simply compare the host star metallicity distribution of single and multi-stellar systems, we find that they are consistent with each other. This is not surprising, as the typical metallicity uncertainties are between 0.1 dex and 0.2 dex, which is a significant fraction of the total metallicity range spanned by our sample.

3.7 Discussion

Our survey results show that stellar companions are found in hot Jupiter systems at a rate which is higher than the rate for field stars, that these companions tend to have low mass ratios, and that their distribution of projected separations is similar to that of field stars over the range of separations considered here (50 au to 2000 au). Here, we discuss two potential ways in which companion stars might influence hot Jupiter formation. We first consider whether these wide stellar companions could enhance the global gas giant planet formation rate, and then consider whether or not they might preferentially enable the inward migration of gas giant planets formed at larger separations.

Are multi-stellar systems more favorable for gas giant planet formation?

One possible explanation for the higher multiplicity rate of hot Jupiter host stars is that these systems are more favorable sites for gas giant planet formation than single stars. For example, a stellar companion could raise spiral arms in a protoplanetary disk. These spiral arms are regions of high particle and gas density, which may be

conducive to giant planet formation (e.g. dust traps as in Marel et al., 2013). Indeed, planetesimal formation through the streaming instability (Youdin and Goodman, 2005; Johansen et al., 2007) as well as subsequent core growth through pebble accretion (Lambrechts et al., 2014; Lambrechts and Johansen, 2014) exhibit a strong dependence on the local density of solids (Carrera et al., 2015). Recent high contrast VLT/SPHERE imaging of the protoplanetary disk around HD 100453, which has an M dwarf companion located at a distance of 120 au, revealed the presence of spiral structures (Wagner et al., 2015). Dong et al. (2016) showed that these structures are best explained as perturbations from this companion rather than processes intrinsic to the disk. HD 141569 is part of a triple system and also hosts an asymmetric disk (for a summary of these features see Biller et al., 2015, and references therein) with a structure that can plausibly be attributed to perturbations from these stellar companions (Augereau and Papaloizou, 2004; Quillen et al., 2005). The mass ratios and separations of these two systems are similar to those of the binaries in our study, suggesting that the presence of a stellar companion can facilitate planet formation in these systems.

Alternatively, protoplanetary disks around wide binaries might be more massive than those around single stars, and therefore would have more material available for giant planet formation. Although current observations suggest that close (< 50 au separation) binaries have shorter disk lifetimes, disks in wide binaries appear to have lifetimes comparable to those of isolated stars (Kraus et al., 2012). Planet formation simulations predict that higher-mass disks will form higher-mass planets (e.g. Thommes et al., 2008; Mordasini et al., 2012). In addition, Duchêne and Kraus (2013) suggest that the timing of fragmentation in protostellar disks could create an asymmetric mass distribution resulting in a low mass ratio companion with a relatively small disk as compared to that of the primary star. These scenarios assume that the companion stars formed at the same time as the primary star, rather than being captured.

High contrast imaging and radial velocity surveys of planet-hosting stars in the *Kepler* sample suggest that binary star systems are less likely to host small, close-in planets than their single counterparts (Wang et al., 2014). Although this might be interpreted as an argument against the massive disk scenario, it might conversely be argued that rocky cores embedded in a more massive disk are more likely to reach runaway accretion and turn into gas giants (e.g. Ikoma et al., 2000; Lee and Chiang, 2015). These gas giant planets could then become hot Jupiters via

Type II disk migration (e.g. Lin et al., 1996) or via interactions with the stellar companion as described below. Additionally, cores that reside in close proximity to the host star may also undergo runaway accretion, leading to *in-situ* formation of hot Jupiters (Bodenheimer et al., 2000; Batygin et al., 2016; Boley et al., 2016).

Are binary systems causing planets to migrate inwards via Kozai-Lidov oscillations?

We next consider a scenario in which gas giants form at the same rate around both single and binary stars, but the presence of a stellar companion causes these planets to migrate inward from their formation locations via three-body interactions such as Kozai-Lidov oscillations (e.g. Fabrycky and Tremaine, 2007; Naoz et al., 2012). We compute representative minimum mass ratios as a function of companion separation required for the stellar companion to excite Kozai-Lidov oscillations on a $1\,M_{Jup}$ mass planet. In single planet systems, this constraint is set by the planet pericenter precession timescale caused by general relativity. We therefore calculate the companion mass and separation such that the Kozai-Lidov oscillation timescale is equal to the pericenter precession timescale, following Equations 1 and 23 in Fabrycky and Tremaine (2007). For these representative limits, we assume a primary star mass of $1\,M_{\odot}$, a companion star orbital eccentricity of 0.5 and a circular orbit for the planet. These expressions scale with the companion star's orbital eccentricity as $(1-e^2)^{1/2}$ and with the planet's orbital eccentricity as $(1-e^2)^{-1/3}$, so the effect of a non-zero planetary eccentricity is mild. We choose 0.5 as the representative stellar eccentricity as previous studies of stellar companions around FGK stars in our solar neighborhood show that stellar companions with periods longer than 12 days have eccentricities uniformly distributed between 0 and 1 (Raghavan et al., 2010). We compute three different representative limits for planets with starting semimajor axis distances of 1 au, 2.5 au and 5 au, and compare these limits to the masses and projected separations of our observed population of stellar companions in Figure 3.6.

We next compute the completeness corrected fraction of hot Jupiter systems with stellar companions that are capable of inducing Kozai-Lidov oscillations. Unlike the calculation of representative cases above, we now use actual system parameters for each target, including the primary star mass and planet mass. Unfortunately the orbital parameters of the companion star, such as eccentricity and inclination, are unknown because our baselines are not currently long enough to detect orbital motion in these systems. Because the Kozai-Lidov timescale depends only weakly

on the eccentricity of the companion for values less than 0.9, we obtain equivalent results if we set the eccentricities of the companions to 0.5 in our distributions as compared to sampling from a uniform distribution. We assume that if a companion is present, its mutual inclination will be greater than the critical angle required to induce Kozai-Lidov oscillations. We do not account for suppression of the stellar Kozai-Lidov due to interactions with other planetary or brown dwarf companions, which are known to exist in a subset of these systems (Wu and Murray, 2003; Batygin et al., 2011; Knutson et al., 2014).

The resulting numbers therefore represent an upper limit on the fraction of hot Jupiter systems that have experienced Kozai-Lidov in the most optimistic case. We compute these fractions for three different initial planetary semimajor axes, at 1 au, 2.5 au, and 5.0 au, and we find that the upper limits to be 16% ± 6%, 34% ± 7%, and 47% ± 7%, respectively. We also average over all potential initial planetary semimajor axes between 1 au to 5 au by sampling from the Cumming et al. (2008) power law distribution fit to the population of known RV-detected gas giant planets. We find that the upper limit on the fraction of hot Jupiter systems that formed via Kozai-Lidov migration in this case is 32% ± 7%.

We also consider a more realistic case in which we account for the fact that the presence of additional gas giant planetary companions would act to disrupt Kozai-Lidov oscillations (Wu and Murray, 2003; Batygin et al., 2011). Knutson et al. (2014) found that 51% ± 10% of hot Jupiter systems have long period RV-detected companions so we multiply our optimistic Kozai-Lidov upper limits by a factor of 0.49 and find that our realistic upper limit on the fraction of hot Jupiter systems that formed via Kozai-Lidov migration is 16% ± 5%. Although a critical mutual inclination, which depends on the planet's initial eccentricity, is required for this mechanism, we do not know the stellar companion inclination distribution for hot Jupiter systems or the eccentricity distribution of proto-hot Jupiters. If we assume an isotropic distribution of stellar companions, then our corresponding upper limit on the fraction of Kozai-Lidov systems will decrease by a factor of 0.37, to 6% ± 2%. However, if Kozai-Lidov migration is a strong contributor to hot Jupiter migration, then it is possible that the inclination distribution for hot Jupiter companions are not isotropic. In addition, Martin et al. (2016) show that planet-disc interactions in binary star systems can act to tilt the planet's orbit so that the angle between the planet and companion is greater than the critical angle. We therefore conclude that the inclusion of a geometric correction for companion inclination is not currently

justified, leaving us with an estimate of 16% ± 5% for the fraction of hot Jupiters that might have migrated via Kozai-Lidov oscillations induced by a stellar companion.

These upper limits are consistent with a range of recent theoretical work constraining the frequency of Kozai-Lidov oscillations in hot Jupiter systems. Simulations of binary star planet hosting systems considering the eccentric Kozai-Lidov mechanism to octopole order find that the eccentric Kozai-Lidov mechanism can account for the formation of up to 30% of hot Jupiter systems (Naoz et al., 2012). Dawson et al. (2015) estimate the 2σ upper limit on the fraction of hot Jupiters with periods greater than 3 days that could have migrated in via Kozai-Lidov interactions with a stellar companion to be 44%, based on the relatively long circularization timescales in these systems and the corresponding absence of a large population of high eccentricity gas giants at intermediate separations in the Kepler sample. This calculation implicitly assumes that all systems have an outer planetary or stellar companion capable of inducing a high eccentricity in the proto-hot Jupiter, but does not specifically require that this occur via Kozai-Lidov oscillations. Petrovich (2015b) performed simulations similar to Naoz et al. (2012) with a more restrictive value for the tidal disruption distance, that is, the pericenter distance where an inwardly migrating planet would be tidally disrupted instead of forming a hot Jupiter. When he considers the currently observed hot Jupiter occurrence rate and semi-major axis distribution, he finds that at most 23% of observed hot Jupiters could have been formed via Kozai-Lidov migration. We note tha3t both Naoz et al. (2012) and Petrovich (2015b) assumed that hot Jupiter host stars have companions at the same rate as field stars, which means their limits are underestimated by a factor of two. However, they also assume that the proto-hot Jupiter is the only planet in the system, resulting in a factor of two over-estimate which effectively cancels the under-estimate due to the enhanced binary rate in these systems. Anderson et al., 2016 and Muñoz et al. (2016) performed an analytical calculation of the fraction of hot Jupiters created via a Kozai-Lidov migration scenario and found values ranging from 12% to 15%, depending on initial planet masses from 0.3 to 3 Jupiter masses and varying tidal dissipation strength.

As demonstrated in Figure 3.6, the upper limit we derive here is primarily sensitive to our assumptions about the starting semi-major axes of the proto-hot Jupiters. Because the stellar companions detected in our survey typically have low masses and large projected separations, many of them require large initial semi-major axes for the planet in order to achieve the required inward migration. In addition, if

hot Jupiter survey selection biases exclude hot Jupiters in equal mass binaries (see Section 3.6), then our sample may not be representative of the entire population of hot Jupiters. Nevertheless, Kozai-Lidov oscillations cannot be the dominant migration mechanism for transiting hot Jupiter systems from ground-based surveys.

It is worth noting that there are other ways in which a stellar companion might affect the dynamical evolution of planetary systems beyond the Kozai-Lidov migration scenario considered here. For example, Batygin (2012) and Spalding and Batygin (2014) and Spalding and Batygin (2015) have proposed that the presence of a companion could change the orientation of the protoplanetary disk relative to the star's spin axis. It is our hope that the observations described here will serve to motivate new studies of the effects of the observed population of stellar companions on the dynamical evolution of these systems. We expect that future observations, e.g. by *Gaia*, may also provide additional constraints on the orbital properties of these stellar companions, at least in the subset of systems for which it is possible to detect astrometric motion of the secondary on several year timescales.

3.8 Summary

We conducted a direct imaging search for stellar companions around 77 transiting gas giant planet hosts and combine our results with a radial velocity stellar companion surveys to determine the occurrence of stellar companions around hot Jupiter hosts. We detected a total of 27 candidate stellar companions, including three companions reported for the first time in this study. We also followed up on five systems with known candidate companions identified in published surveys. For all detected companions, we measure their flux ratios and positions to characterize the companion properties and evaluate the likelihood that they are physically bound to their host stars. We also provide updated photometric and astrometric measurements for all systems, including previously published candidate companions. We confirm common proper motion for six new multi-stellar systems while the other nine examined in this study remain candidate multi-stellar systems.

Overall, we find that hot Jupiters have a stellar companion rate of 47% ± 7% for companions between 50 au and 2000 au. This is 4.4σ larger than the equivalent companion rate for field stars, which is 16% ± 1%. For companions between 1 au and 50 au we find that only $3.9^{+4.5}_{-2.0}$% of hot Jupiter systems host stellar companions while field stars have a companion rate of 16.4% ± 0.7%, corresponding to a difference of 2.7σ. We suggest that there may be a connection between the presence of a

companion star beyond 50 au and processes that either favor giant planet formation or facilitate the inward migration of planets in these systems.

We examine the companion fraction as a function of companion mass and companion separation and compare these distributions to those of field star binaries. We find that the mass ratio distribution for binaries hosting hot Jupiters peaks at small mass ratios, unlike the relatively uniform distribution of mass ratios observed for field star binaries. Although this may in part reflect a bias against equal mass binaries in photometric transit surveys, it is also plausible that higher mass companions might actively suppress planet formation by disrupting the protoplanetary disk. As discussed in Section 3.7, the more subtle effects of a low-mass companion on the disk structure could instead aid in planet formation by creating regions of locally enhanced density. Alternatively, protoplanetary disk masses in binary star systems may be higher than those of their isolated counterparts, resulting in globally enhanced disk densities. We also find that the companion fraction does not depend strongly on companion separation for semi-major axes greater than 50 au.

We additionally use our sample of resolved stellar binaries to calculate an upper limit on the fraction of hot Jupiter systems that might have migrated inward via Kozai-Lidov oscillations. We evaluate this number as a function of the planet's initial semi-major axis and find that the upper limits are 16% ± 6%, 34% ± 7%, and 47% ± 7%, for initial semi-major axes of 1 au, 2.5 au, and 5 au, respectively. When averaged over 1-5 au using the best-fit power law distribution for RV-detected planets and accounting for the presence of radial velocity companions in a subset of the systems observed, this upper limit is 16% ± 5%. These observational constraints are in good agreement with published theoretical models and simulations of hot Jupiter formation via the Kozai-Lidov mechanism, which also suggest that Kozai-Lidov driven migration can only account for a small fraction of the known hot Jupiter systems.

3.9 Acknowledgments

This work was supported by NASA grant NNX14AD24G. HN is grateful for funding support from the Natural Sciences and Engineering Research Council of Canada and the NASA Earth and Space Science Fellowship Program grant NNX15AR12H.

This work was based on observations at the W. M. Keck Observatory granted by the California Institute of Technology. We thank the observers who contributed to the measurements reported here and acknowledge the efforts of the Keck Observatory

staff. We extend special thanks to those of Hawaiian ancestry on whose sacred mountain of Mauna Kea we are privileged to be guests.

Facility: Keck:II (NIRC2)

References

Adams, E. R., D. R. Ciardi, A. K. Dupree, et al. (2012). *The Astronomical Journal* **144**, 42. DOI: 10.1088/0004-6256/144/2/42.

Adams, E. R., A. K. Dupree, C. Kulesa, and D. McCarthy (2013). *The Astronomical Journal* **146**, 9. DOI: 10.1088/0004-6256/146/1/9.

Anderson, K. R., N. I. Storch, and D. Lai (2016). *Monthly Notices of the Royal Astronomical Society* **456**, 3671. DOI: 10.1093/mnras/stv2906.

Augereau, J. C. and J. C. B. Papaloizou (2004). *Astronomy and Astrophysics* **414**, 1153. DOI: 10.1051/0004-6361:20031622.

Bakos, G. Á., J. D. Hartman, W. Bhatti, et al. (2015). *The Astronomical Journal* **149**, 149. DOI: 10.1088/0004-6256/149/4/149.

Bakos, G. Á., J. D. Hartman, G. Torres, et al. (2012). *The Astronomical Journal* **144**, 19. DOI: 10.1088/0004-6256/144/1/19.

Bakos, G. Á., J. Hartman, G. Torres, et al. (2011). *The Astrophysical Journal* **742**, 116. DOI: 10.1088/0004-637X/742/2/116.

Bakos, G. Á., A. Shporer, A. Pál, et al. (2007). *The Astrophysical Journal* **671**, L173. DOI: 10.1086/525022.

Baraffe, I., G. Chabrier, F. Allard, and P. H. Hauschildt (1998). *Astronomy & Astrophysics* **412**, 403.

Batygin, K., A. Morbidelli, and K. Tsiganis (2011). *Astronomy & Astrophysics* **533**, A7. DOI: 10.1051/0004-6361/201117193.

Batygin, K. (2012). *Nature* **491**, 418. DOI: 10.1038/nature11560.

Batygin, K., P. H. Bodenheimer, and G. P. Laughlin (2016). *The Astrophysical Journal* **829**.2, 114. DOI: 10.3847/0004-637X/829/2/114.

Béky, B., G. Á. Bakos, J. Hartman, et al. (2011). *The Astrophysical Journal* **734**, 109. DOI: 10.1088/0004-637X/734/2/109.

Biller, B. A., M. C. Liu, K. Rice, et al. (2015). *Monthly Notices of the Royal Astronomical Society* **450**, 4446. DOI: 10.1093/mnras/stv870.

Bodenheimer, P., O. Hubickyj, and J. J. Lissauer (2000). *Icarus* **143**, 2. DOI: 10.1006/icar.1999.6246.

Boisse, I., J. D. Hartman, G. Á. Bakos, et al. (2013). *Astronomy & Astrophysics* **558**, A86. DOI: 10.1051/0004-6361/201220993.

Boley, A. C., A. P. G. Contreras, and B. Gladman (2016). *The Astrophysical Journal* **817**, L17. DOI: 10.3847/2041-8205/817/2/L17.

Bowler, B. P., M. C. Liu, E. L. Shkolnik, and M. Tamura (2014). *The Astrophysical Journal Supplement Series* **216**, 7. DOI: 10.1088/0067-0049/216/1/7.

Bryan, M. L., H. A. Knutson, A. W. Howard, et al. (2016). *The Astrophysical Journal* **821**, 89. DOI: 10.3847/0004-637X/821/2/89.

Buchhave, L. A., G. Á. Bakos, J. D. Hartman, et al. (2011). *The Astrophysical Journal* **733**, 116. DOI: 10.1088/0004-637X/733/2/116.

Carrera, D., A. Johansen, and M. B. Davies (2015). *Astronomy & Astrophysics* **579**, A43. DOI: 10.1051/0004-6361/201425120.

Chan, T., M. Ingemyr, J. N. Winn, et al. (2011). *The Astronomical Journal* **141**, 179. DOI: 10.1088/0004-6256/141/6/179.

Cheetham, A. C., A. L. Kraus, M. J. Ireland, et al. (2015). *The Astrophysical Journal* **813**, 83. DOI: 10.1088/0004-637X/813/2/83.

Ciceri, S., L. Mancini, J. Southworth, et al. (2015). *Astronomy & Astrophysics* **577**, A54. DOI: 10.1051/0004-6361/201425449.

Collier Cameron, A., F. Bouchy, G. Hebrard, et al. (2007). *Monthly Notices of the Royal Astronomical Society* **375**, 951. DOI: 10.1111/j.1365-2966.2006.11350.x.

Collier Cameron, A., E. Guenther, B. Smalley, et al. (2010). *Monthly Notices of the Royal Astronomical Society* **407**, 507. DOI: 10.1111/j.1365-2966.2010.16922.x.

Cumming, A., R. P. Butler, G. W. Marcy, et al. (2008). *The Publications of the Astronomical Society of the Pacific* **120**, 531. DOI: 10.1086/588487.

Daemgen, S., F. Hormuth, W. Brandner, et al. (2009). *Astronomy and Astrophysics* **498**, 567. DOI: 10.1051/0004-6361/200810988.

Dawson, R. I., R. A. Murray-Clay, and J. A. Johnson (2015). *The Astrophysical Journal* **798**, 66. DOI: 10.1088/0004-637X/798/2/66.

Dong, R., Z. Zhu, J. Fung, et al. (2016). *The Astrophysical Journal* **816**, L12. DOI: 10.3847/2041-8205/816/1/L12.

Dressing, C. D., E. R. Adams, A. K. Dupree, C. Kulesa, and D. McCarthy (2014). *The Astronomical Journal* **148**, 78. DOI: 10.1088/0004-6256/148/5/78.

Duchêne, G. and A. Kraus (2013). *Annual Review of Astronomy and Astrophysics* **51**, 269. DOI: 10.1146/annurev-astro-081710-102602.

Eggleton, P. P., L. Kisseleva-Eggleton, and X. Dearborn (2007). *Proceedings of the International Astronomical Union* **2**.S240, 347. DOI: 10.1017/S1743921307004280.

Evans, D. F., J. Southworth, P. F. L. Maxted, et al. (2016). *Astronomy & Astrophysics* **589**, A58. DOI: 10.1051/0004-6361/201527970.

Fabrycky, D. and S. Tremaine (2007). *The Astrophysical Journal* **669**, 1298. DOI: 10.1086/521702.

Faedi, F., S. C. C. Barros, D. R. Anderson, et al. (2011). *Astronomy & Astrophysics* **531**, A40. DOI: 10.1051/0004-6361/201116671.

Faedi, F., T. Staley, Y. Gomez Maqueo Chew, et al. (2013). *Monthly Notices of the Royal Astronomical Society* **433**, 2097. DOI: 10.1093/mnras/stt885.

Fielding, D. B., C. F. McKee, A. Socrates, A. J. Cunningham, and R. I. Klein (2015). *Monthly Notices of the Royal Astronomical Society* **450**, 3306. DOI: 10.1093/mnras/stv836.

Foreman-Mackey, D., D. W. Hogg, D. Lang, and J. Goodman (2013). *Publications of the Astronomical Society of the Pacific* **125**, 306. DOI: 10.1086/670067.

Gillon, M., D. R. Anderson, A. Collier-Cameron, et al. (2014). *Astronomy & Astrophysics* **562**, L3. DOI: 10.1051/0004-6361/201323014.

Ginski, C., M. Mugrauer, M. Seeliger, et al. (2016). *Monthly Notices of the Royal Astronomical Society* **457**, 2173. DOI: 10.1093/mnras/stw049.

Goodman, J. and J. Weare (2010). *Communications in Applied Mathematics and Computational Science* **5**, 65. DOI: 10.2140/camcos.2010.5.65.

Hartman, J. D., G. Á. Bakos, B. Béky, et al. (2012). *The Astronomical Journal* **144**, 139. DOI: 10.1088/0004-6256/144/5/139.

Hartman, J. D., G. Á. Bakos, B. Sato, et al. (2011). *The Astrophysical Journal* **726**, 52. DOI: 10.1088/0004-637X/726/1/52.

Hébrard, G., A. Collier Cameron, D. J. A. Brown, et al. (2013). *Astronomy & Astrophysics* **549**, A134. DOI: 10.1051/0004-6361/201220363.

Hellier, C., D. R. Anderson, A. Collier Cameron, et al. (2011). *Astronomy & Astrophysics* **535**, L7. DOI: 10.1051/0004-6361/201117081.

Husser, T.-O., S. Wende-von Berg, S. Dreizler, et al. (2013). *Astronomy & Astrophysics* **553**, A6. DOI: 10.1051/0004-6361/201219058.

Ikoma, M., K. Nakazawa, and H. Emori (2000). *The Astrophysical Journal* **537**, 1013. DOI: 10.1086/309050.

Johansen, A., J. S. Oishi, M.-M. M. Low, et al. (2007). *Nature* **448**, 1022. DOI: 10.1038/nature06086.

Kaib, N. A., S. N. Raymond, and M. Duncan (2013). *Nature* **493**, 381. DOI: 10.1038/nature11780.

Knutson, H. A., B. J. Fulton, B. T. Montet, et al. (2014). *The Astrophysical Journal* **785**, 126. DOI: 10.1088/0004-637X/785/2/126.

Kraus, A. L., M. J. Ireland, L. A. Hillenbrand, and F. Martinache (2012). *The Astrophysical Journal* **745**, 19. DOI: 10.1088/0004-637X/745/1/19.

Kraus, A. L., M. J. Ireland, D. Huber, A. W. Mann, and T. J. Dupuy (2016). *The Astronomical Journal* **152**.1, 8. DOI: 10.3847/0004-6256/152/1/8.

Lai, D. (2014). *Monthly Notices of the Royal Astronomical Society* **440**, 3532. DOI: 10.1093/mnras/stu485.

Lambrechts, M. and A. Johansen (2014). *Astronomy & Astrophysics* **572**, A107. DOI: 10.1051/0004-6361/201424343.

Lambrechts, M., A. Johansen, and A. Morbidelli (2014). *Astronomy & Astrophysics* **572**, A35. DOI: 10.1051/0004-6361/201423814.

Lee, E. J. and E. Chiang (2015). *The Astrophysical Journal* **811**, 41. DOI: 10.1088/0004-637X/811/1/41.

Lin, D. N. C., P. Bodenheimer, and D. C. Richardson (1996). *Nature* **380**, 606. DOI: 10.1038/380606a0.

Liu, B., D. J. Munoz, and D. Lai (2014). *Monthly Notices of the Royal Astronomical Society* **447**, 747. DOI: 10.1093/mnras/stu2396.

Mancini, L., M. Esposito, E. Covino, et al. (2015). *Astronomy & Astrophysics* **579**, A136. DOI: 10.1051/0004-6361/201526030.

Mardling, R. A. and S. J. Aarseth (2001). *Monthly Notices of the Royal Astronomical Society* **321**, 398. DOI: 10.1046/j.1365-8711.2001.03974.x.

Marel, N. van der, E. F. van Dishoeck, S. Bruderer, et al. (2013). *Science* **340**, 1199. DOI: 10.1126/science.1236770.

Martin, R. G., S. H. Lubow, C. Nixon, and P. J. Armitage (2016). *Monthly Notices of the Royal Astronomical Society* **458**, 4345. DOI: 10.1093/mnras/stw605.

Mayer, L., J. Wadsley, T. Quinn, and J. Stadel (2005). *Monthly Notices of the Royal Astronomical Society* **363**, 641. DOI: 10.1111/j.1365-2966.2005.09468.x.

Mordasini, C. A., Y. Alibert, W. Benz, H. H. Klahr, and T. Henning (2012). *Astronomy and Astrophysics* **541**, 97. DOI: 10.1051/0004-6361/201117350.

Mortier, A., N. C. Santos, S. G. Sousa, et al. (2013). *Astronomy & Astrophysics* **558**, A106. DOI: 10.1051/0004-6361/201322240.

Moya, A., H. Bouy, F. Marchis, B. Vicente, and D. Barrado (2011). *Astronomy & Astrophysics* **535**, A110. DOI: 10.1051/0004-6361/201116889.

Muñoz, D. J., D. Lai, and B. Liu (2016). *Monthly Notices of the Royal Astronomical Society* **1093**, 8. DOI: 10.1093/mnras/stw983.

Naoz, S., W. M. Farr, Y. Lithwick, F. A. Rasio, and J. Teyssandier (2013). *Monthly Notices of the Royal Astronomical Society* **431**, 2155. DOI: 10.1093/mnras/stt302.

Naoz, S., W. M. Farr, and F. A. Rasio (2012). *The Astrophysical Journal* **754**, L36. DOI: 10.1088/2041-8205/754/2/L36.

Ngo, H., H. A. Knutson, S. Hinkley, et al. (2015). *The Astrophysical Journal* **800**, 138. DOI: 10.1088/0004-637X/800/2/138.

Nikolov, N., D. K. Sing, F. Pont, et al. (2014). *Monthly Notices of the Royal Astronomical Society* **437**, 46–66. DOI: 10.1093/mnras/stt1859.

Petrovich, C. (2015a). *The Astrophysical Journal* **805**, 75. DOI: 10.1088/0004-637X/805/1/75.

Petrovich, C. (2015b). *The Astrophysical Journal* **799**, 27. DOI: 10.1088/0004-637X/799/1/27.

Pichardo, B., L. S. Sparke, and L. A. Aguilar (2005). *Monthly Notices of the Royal Astronomical Society* **359**, 521. DOI: 10.1111/j.1365-2966.2005.08905.x.

Piskorz, D., H. A. Knutson, H. Ngo, et al. (2015). *The Astrophysical Journal* **814**, 148. DOI: 10.1088/0004-637X/814/2/148.

Quillen, A. C., P. Varnière, I. Minchev, and A. Frank (2005). *The Astronomical Journal* **129**, 2481. DOI: 10.1086/428954.

Quinn, S. N., G. Á. Bakos, J. Hartman, et al. (2010). *The Astrophysical Journal* **745**, 80. DOI: 10.1088/0004-637X/745/1/80.

Rafikov, R. R. (2013). *The Astrophysical Journal* **765**, L8. DOI: 10.1088/2041-8205/765/1/L8.

Raghavan, D., H. A. McAlister, T. J. Henry, et al. (2010). *The Astrophysical Journal Supplement Series* **190**, 1. DOI: 10.1088/0067-0049/190/1/1.

Sato, B., J. D. Hartman, G. Á. Bakos, et al. (2012). *Publications of the Astronomical Society of Japan* **64**, 97. DOI: 10.1093/pasj/64.5.97.

Service, M., J. R. Lu, R. Campbell, et al. (2016). *Publications of the Astronomical Society of the Pacific* **128**, 095004. DOI: 10.1088/1538-3873/128/967/095004.

Shporer, A., G. Á. Bakos, F. Bouchy, et al. (2009). *The Astrophysical Journal* **690**, 1393–1400. DOI: 10.1088/0004-637X/690/2/1393.

Skillen, I., D. Pollacco, A. Collier Cameron, et al. (2009). *Astronomy & Astrophysics* **502**, 391. DOI: 10.1051/0004-6361/200912018.

Skrutskie, M. F., R. M. Cutri, R. Stiening, et al. (2006). *The Astronomical Journal* **131**, 1163. DOI: 10.1086/498708.

Smith, A. M. S., D. R. Anderson, A. Collier Cameron, et al. (2012). *The Astronomical Journal* **143**, 81. DOI: 10.1088/0004-6256/143/4/81.

Southworth, J. (2012). *Monthly Notices of the Royal Astronomical Society* **426**, 1291. DOI: 10.1111/j.1365-2966.2012.21756.x.

Southworth, J., L. Mancini, P. F. L. Maxted, et al. (2012). *Monthly Notices of the Royal Astronomical Society* **422**, 3099. DOI: 10.1111/j.1365-2966.2012.20828.x.

Spalding, C. and K. Batygin (2014). *The Astrophysical Journal* **790**, 42. DOI: 10.1088/0004-637X/790/1/42.

Spalding, C. and K. Batygin (2015). *The Astrophysical Journal* **811**, 82. DOI: 10.1088/0004-637X/811/2/82.

Storch, N. I., K. R. Anderson, and D. Lai (2014). *Science* **345**, 1317–21. DOI: 10.1126/science.1254358.

Thommes, E. W., S. Matsumura, and F. A. Rasio (2008). *Science* **321**, 814. DOI: 10.1126/science.1159723.

Torres, G., D. A. Fischer, A. Sozzetti, et al. (2012). *The Astrophysical Journal* **757**, 161. DOI: 10.1088/0004-637X/757/2/161.

Torres, G., J. N. Winn, and M. J. Holman (2008). *The Astrophysical Journal* **677**, 1324. DOI: 10.1086/529429.

Triaud, A. H. M. J., A. A. Lanotte, B. Smalley, and M. Gillon (2014). *Monthly Notices of the Royal Astronomical Society* **444**, 711. DOI: 10.1093/mnras/stu1416.

Tsantaki, M., S. G. Sousa, N. C. Santos, et al. (2014). *Astronomy & Astrophysics* **570**, A80. DOI: 10.1051/0004-6361/201424257.

Wagner, K., D. Apai, M. Kasper, and M. Robberto (2015). *The Astrophysical Journal* **813**, L2. DOI: 10.1088/2041-8205/813/1/L2.

Wang, J., D. A. Fischer, J.-W. Xie, and D. R. Ciardi (2014). *The Astrophysical Journal* **791**, 111. DOI: 10.1088/0004-637X/791/2/111.

Wang, J., D. A. Fischer, J.-W. Xie, and D. R. Ciardi (2015). *The Astrophysical Journal* **806**, 248. DOI: 10.1088/0004-637X/813/2/130.

West, R. G., C. Hellier, J.-M. Almenara, et al. (2016). *Astronomy & Astrophysics* **585**, A126. DOI: 10.1051/0004-6361/201527276.

Winn, J. N. and D. C. Fabrycky (2015). *Annual Review of Astronomy and Astrophysics* **53**, 409. DOI: 10.1146/annurev-astro-082214-122246.

Wöllert, M. and W. Brandner (2015). *Astronomy & Astrophysics* **579**, A129. DOI: 10.1051/0004-6361/201526525.

Wöllert, M., W. Brandner, C. Bergfors, and T. Henning (2015). *Astronomy & Astrophysics* **575**, A23. DOI: 10.1051/0004-6361/201424091.

Wu, Y. and N. Murray (2003). *The Astrophysical Journal* **589**, 605. DOI: 10.1086/374598.

Yelda, S., J. R. Lu, A. M. Ghez, et al. (2010). *The Astrophysical Journal* **725**, 331. DOI: 10.1088/0004-637X/725/1/331.

Youdin, A. N. and J. Goodman (2005). *The Astrophysical Journal* **620**, 459. DOI: 10.1086/426895.

Zuckerman, B. (2014). *The Astrophysical Journal* **791**, L27. DOI: 10.1088/2041-8205/791/2/L27.

Chapter 4

NO DIFFERENCE IN ORBITAL PARAMETERS OF RV-DETECTED GIANT PLANETS BETWEEN 0.1 AND 5 AU IN SINGLE VS MULTI-STELLAR SYSTEMS

This chapter is adapted from work previously published as

Ngo, H., H. A. Knutson, M. L. Bryan, et al. (2017). *Astronomical Journal* **153**, 242. DOI: 10.3847/1538-3881/aa6cac.

4.1 Abstract

Our Keck/NIRC2 imaging survey searches for stellar companions around 144 systems with radial velocity (RV) detected giant planets to determine whether stellar binaries influence the planets' orbital parameters. This survey, the largest of its kind to date, finds eight confirmed binary systems and three confirmed triple systems. These include three new multi-stellar systems (HD 30856, HD 86081, and HD 207832) and three multi-stellar systems with newly confirmed common proper motion (HD 43691, HD 116029, and HD 164509). We combine these systems with seven RV planet-hosting multi-stellar systems from the literature in order to test for differences in the properties of planets with semimajor axes ranging between 0.1-5 au in single vs multi-stellar systems. We find no evidence that the presence or absence of stellar companions alters the distribution of planet properties in these systems. Although the observed stellar companions might influence the orbits of more distant planetary companions in these systems, our RV observations currently provide only weak constraints on the masses and orbital properties of planets beyond 5 au. In order to aid future efforts to characterize long period RV companions in these systems, we publish our contrast curves for all 144 targets. Using four years of astrometry for six hierarchical triple star systems hosting giant planets, we fit the orbits of the stellar companions in order to characterize the orbital architecture in these systems. We find that the orbital planes of the secondary and tertiary companions are inconsistent with an edge-on orbit in four out of six cases.

4.2 Introduction

Gas giant exoplanets have been found to orbit their host stars over a wide range of orbital separations, spanning more than four orders of magnitude from close-in "hot Jupiters" to distant directly imaged planetary mass companions (Fischer et al., 2014a; Bowler, 2016). Conventional core accretion models (e.g. Pollack et al., 1996) have argued that giant planet formation is most favorable just beyond the water ice line, where the increased density of solids allows for the rapid formation of cores large enough to accrete a significant gas envelope. If correct, this would suggest that most short period gas giant planets formed at intermediate separations and then migrated inwards to their present-day locations (e.g. Lin et al., 1996). However, new modeling work motivated by the numerous close-in super-Earth exoplanetary systems (e.g. Fressin et al., 2013; Mulders et al., 2015) has suggested that it may be possible to form close-in gas giant planets *in situ*, providing an alternative to the migration-driven hypothesis (Bodenheimer et al., 2000; Boley et al., 2016; Batygin et al., 2016). We note that the conglomeration of the rocky core itself is a separate process from the accretion of the gaseous envelope. In other words, local formation of the core, followed by extended gas accretion as well as long range migration of the core followed by rapid gas accretion at close-in separations both represent viable *in situ* formation scenarios. It is unclear what role, if any, stellar companions might play in these processes. However, the fact that approximately 44% of field stars (Duquennoy and Mayor, 1991; Raghavan et al., 2010) are found in multiple star systems makes this a crucial question for studies of giant planet formation and/or migration.

There had been many recent imaging surveys carried out to determine the frequency of outer stellar companions in systems with close-in ($a < 0.1$ au) transiting giant planets (Wang et al., 2015a; Wöllert et al., 2015; Wöllert and Brandner, 2015; Ngo et al., 2015; Ngo et al., 2016; Evans et al., 2016). However, there are relatively few studies that have examined the architectures of systems with intermediate separation ($0.1 - 5$ au) planets. Giant planets at these intermediate separations have a different migration history than their their short-period counterparts. Some dynamical interactions depend strongly on orbital separations. For example, close-in planets are more tightly coupled to the host star and would therefore experience more rapid tidal circularization than planets on more distant orbits. In addition, the environment of the protoplanetary disk varies as a function of radial separation so these intermediate planets may be the product of different formation pathways. Therefore, it is important to study formation and migration processes on a wide range of planetary

separations.

Eggenberger et al. (2007) carried out the most comprehensive survey thus far, searching around 56 known RV-planet host stars as well as a control group of 74 stars without a planetary signal. Both their planet-hosting and control samples were from a CORALIE RV planet survey (Udry et al., 2000). Considering only companion candidates they have assessed as likely or truly bound, the planet sample had a companion rate of 6/56 while the control group had a larger companion rate of 13/74. Since this study, there have only been a few other surveys (Ginski et al., 2012; Mugrauer and Ginski, 2015; Ginski et al., 2016) searching for companion stars to RV-detected planet hosts, all with similar sample sizes and target lists. In total, these surveys found 17 systems with RV-detected giant planets and stellar companions within 6″.

In this work, we used the Keck Observatory to conduct the largest stellar companion search around RV-detected giant planet host stars to date. These stars host giant planets with orbital semimajor axes ranging from 0.01 to 5 au, including hot Jupiters, warm Jupiters, and cool Jupiters. Because Eggenberger et al. (2007) and Mugrauer and Ginski (2015) conducted their diffraction-limited AO surveys with the VLT in the southern hemisphere, our sample of 144 targets contains 119 unique new targets without previous diffraction-limited imaging from observatories similar in size to Keck. Ginski et al. (2012) and Ginski et al. (2016) carried out a "lucky imaging" survey with the 2.2m Calar Alto observatory in the northern hemisphere. Although lucky imaging surveys are less sensitive to close stellar companions, our sample contains 72 unique targets not present in either the VLT or Calar Alto surveys. In Bryan et al. (2016), we searched for long term RV trends around the same stars to find planetary companions; however, we excluded 23 stars with fewer than 12 Keck RV measurements in order to ensure good constraints on detected RV trends. For the three triple star systems in our sample, we combine our new astrometric measurements with previous measurements in order to fit the orbits of the binary star companions around their center of mass. We also include additional observations of three triple systems with transiting planets which were detected in previous surveys. Unlike the relatively wide separation binaries in our sample, the secondary and tertiary companions in these hierarchical triple systems have a much shorter mutual orbital period, allowing us to detect orbital motion with a several year baseline. For transiting planet systems, we show that imaging of these triple systems can constrain the inclination of the stellar orbits relative to that of the planetary orbit.

In Section 4.3, we describe our observational campaign. In Section 4.4, we describe our photometric and astrometric analysis of candidate stellar companions and provide detection limits for all observed stars. In Section 4.5, we discuss each detected multi-stellar system individually. In Section 4.6, we compare our results to other surveys, discuss the implications on giant planet formation and characterize the orbits of companion stars in our hierarchical triple systems. Finally, we present a summary in Section 4.7.

4.3 Observations

We obtained infrared AO images of 144 stars with RV-detected giant planets in order to search for stellar companions. This sample includes the set of AO images used to constrain the masses and orbits of the RV detected companions described in Bryan et al. (2016), except for two systems. We exclude HD 33636 and HD 190228 because subsequent studies revealed that their companions are actually stars on very close orbits. The companion to HD 33636 is a M-dwarf star on a 2117 day orbit (Bean et al., 2007) and the companion to HD 190228 is a brown dwarf on a 1146 day orbit (Sahlmann et al., 2011). All target stars are part of the California Planet Survey (Howard et al., 2010). We conducted our survey with the NIRC2 instrument (instrument PI: Keith Matthews) on Keck II using Natural Guide Star AO (Wizinowich, 2013) from August 2013 to September 2016. The observations are listed in Table 4.1. We follow the procedure in Ngo et al. (2015), which we briefly describe here. We operated NIRC2 in natural guide star mode and used the narrow camera setting which has a pixel scale of 10 mas pixel^{-1}. A majority of our targets were bright enough (K magnitudes from 1.8 to 8.1) to saturate the NIRC2 detector in $K_s$band, so we used the narrower K_c bandpass (2.2558 – 2.2854 μm) instead to search for companions. For systems where we detected a candidate companion we also obtained J_c images to measure a $J_c - K_c$ color. We determine whether each candidate companion is physically bound using a second epoch of K_c images taken one to three years later, which allows us to check for common proper motion. We flat-field and dark-subtract our data as well as applying a spatial filer to remove bad pixels, as described in Ngo et al., 2015. We made photometric and astrometric measurements using individually calibrated frames and computed contrast curves using a median stack of these individually calibrated frames.

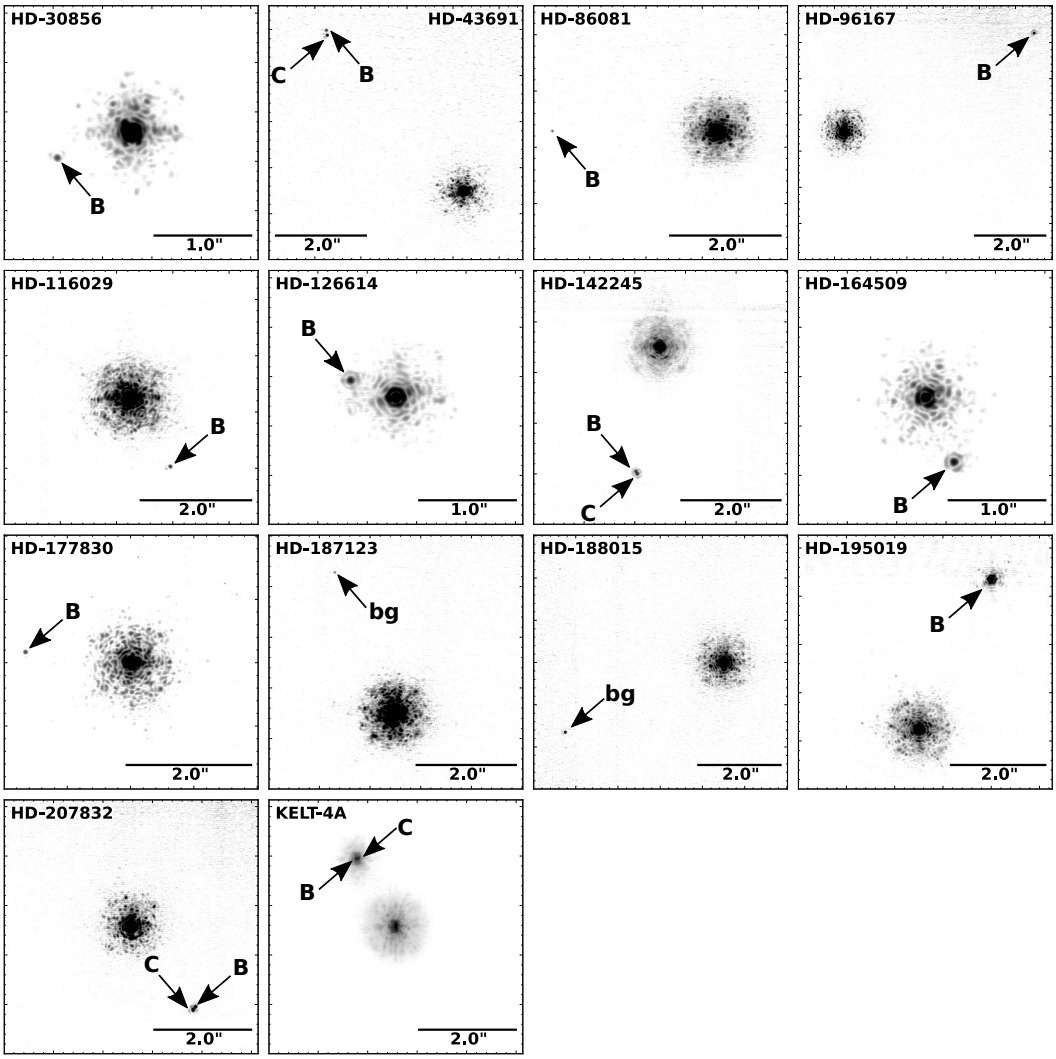

Figure 4.1: Median-stacked K band image for each candidate mutli-stellar system. Each image is oriented such that North points up and East to the left. Confirmed comoving companions are indicated by capital letters while candidates determined to be background objects are labelled as "bg". The KELT-4A triple system was not part of our main survey (see Section 4.3).

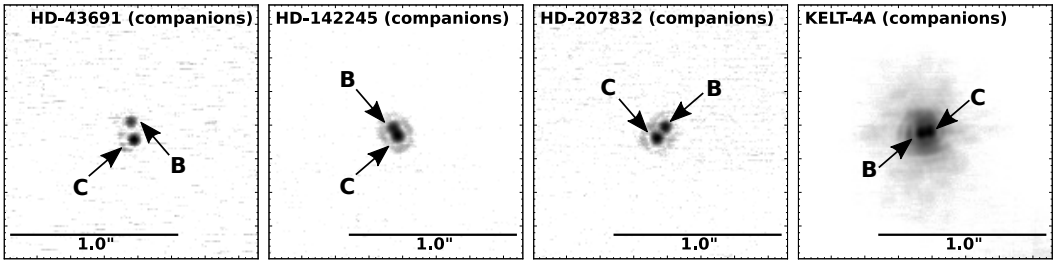

Figure 4.2: Same as Figure 4.1, but only showing a close-up view of the secondary and tertiary components of the three triple systems from our survey and a newly reported triple system, KELT-4A.

Table 4.1: Summary of NIRC2 AO observations

Target	N_{cc}	UT Obs. Date	Filter	Array	$T_{\rm int}$ (s)	$N_{\rm fit}$	$N_{\rm stack}$
RV planet host stars							
GJ 317	0	2014 Nov 07	K_c	1024	12.0	···	12
GJ 433	0	2015 Jan 09	K_c	1024	13.6	···	12
GJ 667C	0	2014 Jul 12	K_c	1024	13.6	···	12
GJ 876	0	2013 Aug 19	K_c	512	10.6	···	12
		2013 Oct 17	J_c	512	10.6	···	···
		2013 Oct 17	K_c	512	10.6	···	12
HD 1461	0	2014 Jul 12	K_c	512	15.9	···	12
HD 1502	0	2013 Aug 19	K_c	1024	9.0	···	12
HD 3651	0	2013 Aug 19	K_c	256	9.0	···	12
HD 4203	0	2013 Aug 19	K_c	1024	9.0	···	12
HD 4208	0	2013 Nov 17	K_c	1024	10.0	···	15
HD 4313	0	2013 Oct 17	K_c	512	10.6	···	12
HD 5319	0	2014 Jul 12	K_c	1024	13.6	···	12
HD 5891	0	2013 Oct 17	J_c	512	10.6	···	···
		2013 Oct 17	K_c	512	10.6	···	12
		2015 Dec 19	K_s	1024	15.0	···	12
HD 7924	0	2014 Oct 03	K_c	1024	13.6	···	12
HD 8574	0	2015 Jan 09	K_c	1024	13.6	···	12
HD 10697	0	2015 Dec 19	K_c	1024	15.0	···	···
HD 11506	0	2013 Nov 17	K_c	1024	10.0	···	15
HD 11964A	0	2013 Nov 17	K_c	512	10.6	···	12
HD 12661	0	2013 Aug 19	K_c	1024	9.0	···	12
HD 13931	0	2015 Jan 09	K_c	1024	13.6	···	12
HIP 14810	0	2013 Oct 17	K_c	1024	9.0	···	10
HD 16141	0	2013 Aug 19	K_c	512	10.6	···	12
HD 17156	0	2014 Oct 03	K_c	1024	15.0	···	12
HD 22049	0	2016 Sep 13	K_c	512	15.9	···	12
HIP 22627	0	2015 Jan 10	K_c	1024	15.0	···	12
HD 24040	0	2015 Jan 10	K_c	1024	13.6	···	12
HD 28678	0	2014 Oct 04	K_c	1024	13.6	···	12
HD 30856	1	2014 Oct 04	J_c	1024	13.6	12	···
		2014 Oct 04	K_c	1024	13.6	12	12
		2014 Dec 07	J_c	1024	15.0	11	···
		2014 Dec 07	K_c	1024	13.6	12	12
		2015 Oct 26	K_c	1024	15.0	12	12
HD 32963	0	2014 Oct 04	K_c	1024	13.6	···	12
HD 33142	0	2014 Oct 04	K_c	1024	13.6	···	12
HD 33283	0	2014 Oct 04	K_c	1024	12.5	···	12
HD 34445	0	2014 Nov 07	K_c	1024	13.6	···	12
HD 37124	0	2014 Jan 12	K'	1024	10.0	···	10
		2014 Dec 07	K_c	1024	15.0	···	12
HD 37605	0	2014 Jan 12	K'	1024	9.0	···	12
		2014 Dec 07	K_c	1024	12.5	···	12
HD 38529	0	2015 Jan 10	K_c	512	13.2	···	12
HD 38801	0	2014 Jan 12	K'	1024	9.0	···	9
		2014 Jan 12	K_c	1024	10.0	···	11
		2014 Dec 07	K_c	1024	12.5	···	12
HD 40979	0	2014 Nov 10	K_c	512	12.0	···	12

Continued on next page

Table 4.1 – continued from previous page

Target	N_{cc}	UT Obs. Date	Filter	Array	$T_{\rm int}$ (s)	$N_{\rm fit}$	$N_{\rm stack}$
HD 43691	2	2013 Dec 18	K_c	1024	10.0	4	12
		2014 Dec 04	K_c	1024	10.0	10	12
		2014 Dec 04	J_c	1024	10.0	5	···
		2015 Oct 26	K_c	1024	25.0	12	12
		2016 Sep 13	K_c	1024	45.0	12	12
HD 45350	0	2013 Oct 17	K_c	1024	9.0	···	12
HD 46375	0	2013 Oct 17	K_c	1024	9.0	···	12
HD 49674	0	2013 Oct 17	K_c	1024	9.0	···	12
HD 50499	0	2014 Nov 07	K_c	1024	13.6	···	12
HD 50554	0	2013 Dec 18	K_c	1024	10.0	···	12
HD 52265	0	2013 Oct 17	K_c	512	10.6	···	12
HIP 57050	0	2014 May 21	K_c	1024	12.5	···	12
HIP 57274	0	2014 May 21	K_c	1024	12.5	···	12
		2015 Dec 20	K_c	1024	15.0	···	12
HD 66428	0	2013 Dec 18	K_c	1024	10.0	···	12
HD 68988	0	2013 Dec 18	K_c	1024	10.0	···	12
HD 69830	0	2014 Jan 12	K_c	1024	9.0	···	8
		2014 Dec 05	K_c	512	13.2	···	12
HD 72659	0	2014 Jan 12	K_c	1024	9.0	···	15
		2014 Nov 10	K_c	1024	13.6	···	12
HD 73256	0	2014 Nov 10	K_c	1024	12.5	···	12
HD 73534	0	2014 Jan 12	K_c	1024	9.0	···	15
		2014 Dec 05	K_c	1024	13.6	···	12
HD 74156	0	2014 Nov 07	K_c	1024	13.6	···	12
HIP 74995	0	2013 Jul 04	K_c	1024	9.0	···	12
HD 75732	0	2014 May 21	K_c	256	10.0	···	12
HD 75898	0	2014 May 21	J_c	1024	12.5	···	12
		2014 May 21	K_c	1024	12.5	···	12
		2015 Dec 20	K_c	1024	15.0	···	12
HIP 79431	0	2013 Jul 04	K_c	1024	9.0	···	12
HD 80606	0	2014 Jan 12	K_c	1024	10.0	···	12
		2014 Dec 07	K_c	1024	15.0	···	12
HD 82886	0	2014 Jan 12	K_c	1024	9.0	···	15
		2014 May 21	K_c	512	13.2	···	12
HD 82943	0	2015 Jan 10	K_c	1024	15.0	···	12
		2016 Jan 25	K_c	1024	15.0	···	12
HIP 83043	0	2013 Jul 04	K_c	1024	9.0	···	12
HD 83443	0	2015 Jan 09	K_c	1024	12.5	···	12
HD 86081	1	2013 Dec 18	K_c	1024	10.0	9	12
		2014 Dec 05	K_c	1024	12.0	10	12
HD 87883	0	2015 Jan 10	K_c	1024	13.6	···	12
HD 88133	0	2013 Dec 18	K_c	1024	10.0	···	12
HD 90043	0	2014 Jan 12	K_c	512	10.6	···	12
		2014 May 21	K_c	512	13.2	···	12
		2014 May 21	J_c	256	13.5	···	6
HD 92788	0	2014 Dec 05	K_c	1024	13.6	···	12
HD 95089	0	2014 Dec 05	K_c	1024	13.6	···	12
HD 95128	0	2014 May 21	K_c	256	15.0	···	12
HD 96063	0	2014 May 21	K_c	1024	12.5	···	12
HD 96167	1	2014 Jan 12	K_c	1024	10.0	4	12

Continued on next page

Table 4.1 – continued from previous page

Target	N_{cc}	UT Obs. Date	Filter	Array	$T_{\rm int}$ (s)	$N_{\rm fit}$	$N_{\rm stack}$
		2014 Dec 07	J_c	1024	15.0	12	···
		2014 Dec 07	K_c	1024	15.0	12	12
		2015 Jan 09	J_c	1024	13.6	12	···
		2015 Jan 09	K_c	1024	15.0	12	12
HD 97658	0	2013 Dec 18	K_c	1024	9.0	···	12
HD 99109	0	2014 May 21	K_s	1024	18.1	···	12
		2016 Jan 25	K_c	1024	15.0	···	12
HD 99492	0	2014 May 21	K_c	512	13.2	···	12
HD 99706	0	2014 May 21	K_c	512	13.2	···	12
HD 102195	0	2014 May 21	K_c	1024	12.5	···	12
HD 102329	0	2014 May 21	K_c	1024	13.6	···	12
HD 102956	0	2014 May 21	K_c	1024	12.5	···	12
BD-103166	0	2014 Jan 12	K_c	1024	20.0	···	12
		2015 Jan 09	K_c	1024	15.0	···	12
HD 104067	0	2014 May 21	K_c	1024	12.0	···	12
HD 106270	0	2014 May 21	K_c	1024	12.5	···	12
HD 107148	0	2014 May 21	K_c	1024	12.5	···	12
HD 108863	0	2014 Jun 09	K_c	1024	13.6	···	12
HD 108874	0	2015 Jan 09	K_c	1024	12.0	···	12
		2015 Dec 20	K_c	1024	15.0	···	12
HIP 109388	0	2014 Nov 07	K_c	1024	13.6	···	12
HD 109749	0	2014 Jun 09	K_c	1024	12.5	···	12
HD 114729	0	2015 Jan 09	K_c	512	12.0	···	12
HD 114783	0	2014 Jun 09	K_c	1024	13.6	···	12
HD 115617	0	2014 Jun 09	K_c	256	13.5	···	13
HD 116029	1	2013 Jul 04	K_c	512	10.0	11	12
		2014 Jun 09	K_c	1024	13.6	12	12
		2014 Jun 09	J_c	512	13.2	11	···
		2015 Jan 09	K_c	512	12.0	12	12
		2015 Jan 09	J_c	512	12.7	12	···
HD 117176	0	2013 Jul 04	K_c	256	18.0	···	12
HD 117207	0	2014 Jun 09	K_c	1024	12.5	···	14
HD 125612	0	2014 Jun 09	K_c	1024	15.0	···	12
		2015 Jun 24	K_c	1024	15.0	···	12
HD 126614	1	2014 Jun 09	K_s	1024	13.6	12	12
		2015 Jan 09	K_c	1024	12.5	12	12
		2015 Jun 24	K_c	1024	12.5	12	12
		2015 Jun 24	J_c	1024	12.5	12	···
HD 128311	0	2014 Jul 07	K_c	512	10.6	···	12
HD 130322	0	2014 Jul 12	K_c	1024	13.6	···	12
HD 131496	0	2013 Jul 04	K_c	512	10.0	···	12
HD 134987	0	2016 Jun 09	K_c	1024	15.0	···	12
		2016 Jun 09	J_c	1024	15.0	···	···
HD 141399	0	2014 May 21	K_c	1024	13.6	···	12
HD 141937	0	2013 Jul 04	K_c	1024	9.0	···	12
HD 142245	2	2013 Jul 04	K_c	512	10.6	15	15
		2014 Jun 09	K_c	512	13.2	11	12
		2014 Jun 09	J_c	512	13.2	10	···
		2015 Jun 24	K_c	768	12.7	12	12
		2016 Jun 09	K_c	512	15.9	11	12

Continued on next page

Table 4.1 – continued from previous page

Target	N_{cc}	UT Obs. Date	Filter	Array	$T_{\rm int}$ (s)	$N_{\rm fit}$	$N_{\rm stack}$
HD 143761	0	2014 Jun 09	K_c	256	13.5	···	12
HD 145675	0	2014 Jul 12	K_c	512	15.9	···	12
HD 145934	0	2014 May 21	K_c	1024	12.5	···	12
HD 149143	0	2013 Jul 04	K_c	1024	9.0	···	12
HD 152581	0	2013 Jul 04	K_c	1024	9.0	···	12
HD 154345	0	2014 Jul 12	K_c	512	15.9	···	12
HD 156279	0	2013 Aug 19	K_c	1024	9.0	···	12
HD 156668	0	2013 Jul 04	K_c	1024	9.0	···	12
HD 158038	0	2015 Jun 24	K_c	768	12.7	···	12
HD 163607	0	2013 Aug 19	K_c	1024	9.0	···	12
HD 164509	1	2014 Jun 09	J_c	1024	12.5	11	···
		2014 Jun 09	K_c	1024	12.5	12	12
		2015 Jun 24	K_c	1024	12.5	12	12
		2016 Jun 09	J_c	512	15.9	12	···
		2016 Jun 09	K_c	1024	15.0	12	12
HD 164922	0	2015 Jun 24	K_c	768	12.7	···	12
HD 168443	0	2013 Aug 19	J_c	512	10.6	···	···
		2013 Aug 19	K_c	512	10.0	···	12
HD 168746	0	2013 Aug 19	K_c	1024	9.0	···	12
HD 169830	0	2013 Aug 19	K_c	512	10.6	···	12
HD 170469	0	2013 Jul 04	K_c	1024	9.0	···	12
HD 175541	0	2013 Jul 04	K_c	1024	9.0	···	12
HD 177830	1	2014 Jun 09	J_c	512	13.2	9	···
		2014 Jun 09	K_c	512	13.2	12	12
		2015 Jul 05	K_c	512	13.2	12	12
		2016 Jun 09	J_c	512	15.9	12	···
		2016 Jun 09	K_c	512	15.9	12	12
HD 178911B	0	2013 Aug 19	K_c	1024	9.0	···	12
HD 179079	0	2013 Aug 19	K_c	1024	9.0	···	12
HD 179949	0	2013 Aug 19	K_c	512	10.6	···	12
HD 180902	0	2014 Jul 12	K_c	1024	13.6	···	12
HD 181342	0	2013 Aug 19	K_c	512	10.6	···	12
HD 183263	0	2015 Jul 05	K_c	1024	15.0	···	···
HD 186427B	0	2013 Aug 19	K_c	512	10.6	···	12
HD 187123	1	2013 Aug 19	K_c	1024	9.0	9	12
		2015 Jun 24	K_c	1024	15.0	12	12
HD 188015	1	2013 Aug 19	J_c	1024	9.0	6	···
		2013 Aug 19	K_c	1024	9.0	8	12
		2014 Jul 12	J_c	1024	15.0	12	···
		2014 Jul 12	K_c	1024	15.0	12	12
HD 189733	0	2013 Jun 22	K_s	128	0.4	···	12
		2013 Aug 19	K_c	1024	9.0	···	12
HD 190360	0	2014 Jul 12	K_c	512	15.9	···	12
HD 192263	0	2013 Aug 19	K_c	512	10.6	···	12
HD 192310	0	2013 Aug 19	K_c	256	9.0	···	6
HD 195019	1	2013 Aug 19	K_c	704	12.4	12	12
		2013 Aug 19	J_c	512	10.6	6	···
		2014 Jun 09	K_c	1024	13.6	12	12
		2014 Jul 12	K_c	1024	13.6	12	12
		2014 Jul 12	J_c	512	15.9	12	···

Continued on next page

Table 4.1 – continued from previous page

Target	N_{cc}	UT Obs. Date	Filter	Array	$T_{\rm int}$ (s)	$N_{\rm fit}$	$N_{\rm stack}$
		2015 Jun 03	K_c	768	12.7	12	12
HD 200964	0	2013 Aug 19	K_c	512	10.6	···	12
HD 206610	0	2013 Aug 19	K_c	1024	9.0	···	12
HD 207832	2	2013 Aug 19	K_c	1024	12.5	12	12
		2013 Aug 19	K_s	512	10.6	9	9
		2013 Aug 19	J_c	1024	9.0	5	···
		2014 Jul 12	K_c	1024	15.0	12	12
		2014 Jul 12	J_c	1024	15.0	9	···
		2015 Jul 05	K_c	1024	20.0	12	12
		2015 Jul 05	J_c	1024	20.0	12	···
		2015 Oct 26	K_c	1024	15.0	12	12
		2016 Sep 13	K_c	1024	12.5	3	3
HD 209458	0	2013 Jun 22	K_s	256	9.0	···	12
HD 210277	0	2014 Nov 07	K_c	1024	13.6	···	15
HD 212771	0	2013 Aug 19	K_c	512	12.5	···	12
HD 217014	0	2013 Aug 19	K_c	256	9.0	···	12
HD 217107	0	2013 Nov 17	K_c	512	10.6	···	15
HD 222582	0	2013 Dec 18	K_c	1024	9.0	···	12
HD 224693	0	2013 Aug 19	K_c	1024	3.6	···	12
HD 231701	0	2013 Aug 19	K_c	1024	12.5	···	11
		2014 Jun 09	K_c	1024	12.0	···	12
		2015 Jul 05	K_c	1024	15.0	···	15
HD 285968	0	2013 Oct 17	K_c	512	10.6	···	12
Transiting planet host stars in triple systems							
HAT-P-8	2	2014 Oct 03	K_s	1024	25.0	12	11
		2015 Jul 07	K_s	1024	13.6	12	12
		2016 Sep 12	K_s	1024	12.0	12	12
KELT-4A	2	2015 Dec 20	K_s	1024	15.0	12	12
WASP-12	2	2014 Dec 04	K_s	1024	12.0	13	13
		2015 Dec 26	K_s	1024	15.0	12	12
		2016 Sep 13	K_s	1024	30.0	4	4

Notes. Column N_{cc} is the number of candidate companions detected. Column "Array" is the horizontal size, in pixels, of the NIRC2 array readout region and corresponds to subarray sizes of 1024x1024 (the full NIRC2 array), 768x760, 512x512, or 256x264. Column $T_{\rm int}$ is the total integration time, in seconds, of a single frame. Column $N_{\rm fit}$ is the number of frames used in our photometric and/or astrometric analysis, and is only given when companions are present. Column $N_{\rm stack}$ is the number of frames combined to make the contrast curve measurements. We only compute contrast curves in the K_s and K_c bandpasses so this column is not applicable for other bandpasses. In some cases, $N_{\rm fit}$ and $N_{\rm stack}$ are not equal because the companion may not be present in all frames due to the dither pattern and/or observing conditions.

In addition to the 144 RV-detected planet host stars in our main survey sample, we also obtained images of three additional transiting planet-host stars previously known to be in triple systems. Two of these triple systems (HAT-P-8, WASP-12) were previously discovered by imaging surveys (Bergfors et al., 2013; Ginski et al., 2013) and later characterized as part of our "Friends of Hot Jupiters" program (Bechter

Table 4.2: Stellar parameters for candidate multi-stellar systems

Target	Type	$T_{\rm eff}$ (K)	M ($M_\odot$)	$\log g$ (cgs)	D (pc)	References for... T	M, $\log g$	D
RV planet host stars								
HD 30856	B	4982 ± 44	1.350 ± 0.094	3.40 ± 0.06	118^{+11}_{-9}	1	1	2
HD 43691	T	6200 ± 40	1.38 ± 0.05	4.28 ± 0.13	81^{+6}_{-5}	3	3	2
HD 86081	B	6036 ± 23	1.23 ± 0.08	4.21 ± 0.04	95^{+10}_{-8}	4	4	2
HD 96167	B	5749 ± 25	1.16 ± 0.05	4.15 ± 0.06	87^{+7}_{-6}	5	5	2
HD 116029	B	4951 ± 44	1.58 ± 0.11	3.40 ± 0.06	123^{+11}_{-9}	1	1	2
HD 126614	B	5585 ± 44	1.145 ± 0.030	4.39 ± 0.08	73 ± 5	6	6	2
HD 142245	T	4878 ± 44	1.69 ± 0.12	3.30 ± 0.06	110^{+8}_{-7}	1	1	2
HD 164509	B	5922 ± 44	1.13 ± 0.02	4.44 ± 0.06	52 ± 3	7	7	2
HD 177830	B	5058 ± 35	1.37 ± 0.04	3.66 ± 0.06	59 ± 2	8	8	2
HD 187123	bg	5845 ± 22	1.037 ± 0.025	4.32 ± 0.04	48 ± 1	9	10	2
HD 188015	bg	5746[a]	1.056 ± 0.09	$4.41^{+0.05}_{-0.04}$	57 ± 3	11	7	2
HD 195019	B	5741 ± 20	1.05 ± 0.10	4.06 ± 0.04	39^{+2}_{-1}	12	12	2
HD 207832[b]	T	5736 ± 27	0.980 ± 0.070	4.51 ± 0.07	54 ± 3	4	4	2
Transiting planet host stars in triple systems								
HAT-P-8	T	6223 ± 67	1.192 ± 0.075	4.177 ± 0.022	230 ± 15	13	14	15
KELT-4A	T	6207 ± 75	1.204 ± 0.070	$4.105^{+0.029}_{-0.032}$	211^{+13}_{-12}	16	16	16
WASP-12	T	6118 ± 64	1.38 ± 0.19	4.159 ± 0.024	427 ± 90	13	17	15

Notes. The "Type" column indicates whether the candidate multi-stellar system is a bound binary (B), bound triple (T) or a background object (bg). The planetary parameters are listed only for the innermost planet in each system in our RV planet host star survey. All planetary parameters are listed as they appear in the cited reference.
[a] No uncertainty available for this temperature estimate. Since the candidate companion is a background object, the temperature was not used in any further calculation.
References. (1) Johnson et al. (2011); (2) Leeuwen (2007); (3) Da Silva et al. (2007); (4) Santos et al. (2013); (5) Jofré et al. (2015); (6) Howard et al. (2010); (7) Giguere et al. (2012); (8) Johnson et al. (2006); (9) Santos et al. (2004); (10) Takeda et al. (2007); (11) Butler et al. (2006); (12) Ghezzi et al. (2010); (13) Torres et al. (2012); (14) Mancini et al. (2013); (15) Triaud et al. (2014); (16) Eastman et al. (2016); (17) Southworth (2012)

et al., 2014; Ngo et al., 2015). The other triple system (KELT-4A, also known as HIP-51260) was recently reported by Eastman et al. (2016). Although we do not include these additional triple systems when determining the overall multiplicity rate for planet-hosting stars, we obtain and process the images of these additional systems in the same way as our survey targets. Table 4.2 lists the properties of the stars from our survey with detected companions as well as the separate sample of previously published triple systems.

4.4 Analysis

Photometry and astrometry of candidate multi-stellar systems

We detect candidate companions around 13 stars in our survey (see Figures 4.1 and 4.2). We summarize the stellar parameters for stars with detected companions as well as our determination of the companion's bound or background status in Table 4.2. As described in Ngo et al. (2015), we model the stellar point-spread function (PSF) as a combination of a Moffat and Gaussian function. We use a maximum likelihood estimation routine to find the best fit parameters of a multiple-

source PSF for each candidate multi-stellar system and determine the flux ratio of the candidate companion to the primary star, as well as the on-sky separation. On 2015 April 13, the optics in the Keck II AO bench were realigned to improve performance. We account for the NIRC2 detector distortion and rotation using astrometric solutions from Yelda et al. (2010) for data taken prior to this realignment work and from Service et al. (2016) for data taken afterwards. To determine the stability of the Yelda et al. (2010) solution (based on data from 2007 to 2009), Service et al. (2016) also computed a distortion solution for data taken just prior to the NIRC2 realignment. The Service et al. (2016) and Yelda et al. (2010) solutions are consistent within 0.5 milliarcseconds, demonstrating that the Yelda et al. (2010) solution is suitable for all of our NIRC2 data taken prior to 2015 April 13 UT. Our reported uncertainties include both measurement errors and the uncertainty contributed by the published astrometric solution. We report the fluxes and astrometry for each candidate companion in Tables 4.3 and 4.4.

Table 4.3: Photometry of confirmed stellar companions

Companion	UT Obs. Date	m_{Jc}	m_{Kc}	ΔJ_c	ΔK_c	$J_c - K_c$
RV planet host stars						
HD 30856B	2014 Oct 04	10.963 ± 0.020	10.904 ± 0.021	4.708 ± 0.020	5.247 ± 0.021	0.059 ± 0.029
	2014 Dec 07	11.160 ± 0.088	10.473 ± 0.042	4.905 ± 0.088	4.816 ± 0.042	0.687 ± 0.097
	2015 Oct 26	···	10.786 ± 0.046	···	5.129 ± 0.046	···
HD 43691B	2013 Dec 18	···	13.698 ± 0.084	···	6.998 ± 0.084	···
	2014 Dec 04	14.38 ± 0.38	13.253 ± 0.051	7.40 ± 0.38	6.553 ± 0.051	1.12 ± 0.38
	2015 Oct 26	···	13.203 ± 0.093	···	6.503 ± 0.093	···
	2016 Sep 13	···	12.94 ± 0.11	···	6.24 ± 0.11	···
HD 43691C	2013 Dec 18	···	12.895 ± 0.081	···	6.195 ± 0.081	···
	2014 Dec 04	23.0 ± 3.0	12.534 ± 0.050	16.0 ± 3.0	5.834 ± 0.050	10.5 ± 3.0
	2015 Oct 26	···	12.483 ± 0.044	···	5.783 ± 0.044	···
	2016 Sep 13	···	11.847 ± 0.084	···	5.147 ± 0.084	···
HD 86081B	2013 Dec 18	···	15.25 ± 0.35	···	7.95 ± 0.35	···
	2014 Dec 05	···	14.766 ± 0.086	···	7.467 ± 0.086	···
HD 96167B	2014 Jan 12	···	12.97 ± 0.40	···	6.41 ± 0.40	···
	2015 Jan 09	15.10 ± 0.17	12.591 ± 0.039	8.18 ± 0.17	6.037 ± 0.039	2.51 ± 0.17
HD 116029B	2013 Jul 04	···	12.513 ± 0.091	···	6.979 ± 0.091	···
	2014 Jun 09	13.63 ± 0.16	12.414 ± 0.066	7.49 ± 0.16	6.880 ± 0.066	1.22 ± 0.17
	2015 Jan 09	13.85 ± 0.11	12.55 ± 0.10	7.71 ± 0.11	7.01 ± 0.10	1.30 ± 0.15
HD 126614B	2015 Jan 09	···	11.132 ± 0.018	···	4.072 ± 0.018	···
	2015 Jun 24	11.65 ± 0.12	10.9740 ± 0.0100	4.18 ± 0.12	3.9140 ± 0.0100	0.68 ± 0.12
HD 142245B	2013 Jul 04	···	11.159 ± 0.034	···	6.049 ± 0.034	···
	2014 Jun 09	11.241 ± 0.080	10.632 ± 0.085	5.552 ± 0.080	5.522 ± 0.085	0.61 ± 0.12
	2015 Jun 24	···	10.896 ± 0.037	···	5.786 ± 0.037	···
	2016 Jun 09	···	10.988 ± 0.031	···	5.878 ± 0.031	···
HD 142245C	2013 Jul 04	···	10.794 ± 0.022	···	5.684 ± 0.022	···
	2014 Jun 09	11.164 ± 0.060	10.635 ± 0.024	5.475 ± 0.060	5.525 ± 0.024	0.529 ± 0.064

Continued on next page

Table 4.3 – continued from previous page

Companion	UT Obs. Date	m_{Jc}	m_{Kc}	ΔJ_c	ΔK_c	$J_c - K_c$
	2015 Jun 24	···	10.690 ± 0.013	···	5.580 ± 0.013	···
	2016 Jun 09	···	10.645 ± 0.025	···	5.535 ± 0.025	···
HD 164509B	2014 Jun 09	11.66 ± 0.27	10.172 ± 0.024	4.72 ± 0.27	3.586 ± 0.024	1.49 ± 0.27
	2015 Jun 24	···	10.022 ± 0.053	···	3.436 ± 0.053	···
	2016 Jun 09	10.654 ± 0.025	10.0151 ± 0.0056	3.716 ± 0.025	3.4291 ± 0.0056	0.639 ± 0.026
HD 177830B	2014 Jun 09	12.81 ± 0.19	11.861 ± 0.081	7.45 ± 0.19	7.052 ± 0.081	0.95 ± 0.21
	2015 Jul 05	···	11.897 ± 0.089	···	7.088 ± 0.089	···
	2016 Jun 09	12.339 ± 0.045	11.539 ± 0.061	6.972 ± 0.045	6.730 ± 0.061	0.800 ± 0.076
HD 195019B	2013 Aug 19	8.511 ± 0.018	7.9276 ± 0.0084	2.911 ± 0.018	2.6676 ± 0.0084	0.583 ± 0.020
	2014 Jun 09	···	7.970 ± 0.059	···	2.710 ± 0.059	···
	2014 Jul 12	8.492 ± 0.014	7.9395 ± 0.0069	2.892 ± 0.014	2.6795 ± 0.0069	0.553 ± 0.016
	2015 Jun 03	···	7.878 ± 0.040	···	2.618 ± 0.040	···
HD 207832B	2013 Aug 19	14.58 ± 0.18	13.148 ± 0.055	7.00 ± 0.18	5.941 ± 0.055	1.44 ± 0.19
	2014 Jul 12	14.336 ± 0.094	13.143 ± 0.042	6.749 ± 0.094	5.936 ± 0.042	1.19 ± 0.10
	2015 Jul 05	···	12.870 ± 0.086	···	5.663 ± 0.086	···
	2015 Oct 26	···	13.005 ± 0.077	···	5.798 ± 0.077	···
	2016 Sep 13	···	13.47 ± 0.12	···	6.26 ± 0.12	···
	2013 Aug 19	14.58 ± 0.18	13.166 ± 0.033	7.00 ± 0.18	5.959 ± 0.033	1.42 ± 0.19
HD 207832C	2013 Aug 19	14.077 ± 0.096	12.813 ± 0.048	6.490 ± 0.096	5.606 ± 0.048	1.26 ± 0.11
	2014 Jul 12	14.06 ± 0.14	12.826 ± 0.070	6.47 ± 0.14	5.619 ± 0.070	1.23 ± 0.15
	2015 Jul 05	···	12.909 ± 0.056	···	5.702 ± 0.056	···
	2015 Oct 26	···	12.921 ± 0.044	···	5.714 ± 0.044	···
	2016 Sep 13	···	12.62 ± 0.13	···	5.41 ± 0.13	···
	2013 Aug 19	14.077 ± 0.096	12.770 ± 0.054	6.490 ± 0.096	5.563 ± 0.054	1.31 ± 0.11
Transiting planet host stars in triple systems						
HAT-P-8B	2014 Oct 03	···	14.883 ± 0.082	···	5.930 ± 0.082	···
	2015 Jul 07	···	14.811 ± 0.065	···	5.858 ± 0.065	···
	2016 Sep 12	···	14.803 ± 0.058	···	5.850 ± 0.058	···

Continued on next page

Table 4.3 – continued from previous page

Companion	UT Obs. Date	m_{Jc}	m_{Kc}	ΔJ_c	ΔK_c	$J_c - K_c$
HAT-P-8C	2014 Oct 03	···	15.204 ± 0.089	···	6.251 ± 0.089	···
	2015 Jul 07	···	15.469 ± 0.025	···	6.516 ± 0.025	···
	2016 Sep 12	···	15.462 ± 0.021	···	6.509 ± 0.021	···
KELT-4A B	2015 Dec 20	···	10.70 ± 0.36	···	2.02 ± 0.36	···
KELT-4A C	2015 Dec 20	···	11.79 ± 0.15	···	3.10 ± 0.15	···
WASP-12B	2014 Dec 04	···	13.251 ± 0.077	···	3.063 ± 0.077	···
	2015 Dec 26	···	13.342 ± 0.026	···	3.154 ± 0.026	···
	2016 Sep 13	···	13.294 ± 0.035	···	3.106 ± 0.035	···
WASP-12C	2014 Dec 04	···	13.70 ± 0.10	···	3.51 ± 0.10	···
	2015 Dec 26	···	13.411 ± 0.023	···	3.223 ± 0.023	···
	2016 Sep 13	···	13.300 ± 0.041	···	3.112 ± 0.041	···

Table 4.4: Astrometric measurements of all candidate companions

Candidate[a]	UT Obs. Date	Band	ρ (mas)	PA (°)	Reference
RV planet host stars					
HD 30856 B	2014 Oct 04	K_c	789.4 ± 1.5	108.6 ± 0.1	this work
	2014 Dec 07	K_c	788.7 ± 1.5	108.7 ± 0.1	this work
	2015 Oct 26	K_c	786.3 ± 1.5	108.8 ± 0.1	this work
HD 43691 B	2013 Dec 18	K_c	4550.3 ± 1.8	40.50 ± 0.02	this work
	2014 Dec 04	K_c	4546.6 ± 2.2	40.40 ± 0.02	this work
	2015 Oct 26	K_c	4540.4 ± 2.5	40.27 ± 0.03	this work
	2016 Sep 13	K_c	4536.5 ± 2.9	39.91 ± 0.04	this work
HD 43691 C	2013 Dec 18	K_c	4452.6 ± 1.8	41.08 ± 0.02	this work
	2014 Dec 04	K_c	4456.8 ± 1.9	41.08 ± 0.02	this work
	2015 Oct 26	K_c	4462.2 ± 2.5	41.08 ± 0.03	this work
	2016 Sep 13	K_c	4463.5 ± 2.5	40.90 ± 0.03	this work
HD-43691 BC	2015 Mar 10	i'	4435 ± 16[b]	40.8 ± 0.2[b]	Ginski et al. (2016)
	2013 Dec 18	K_c	4513.5 ± 1.9	40.72 ± 0.02	this work
	2014 Dec 04	K_c	4512.7 ± 2.3	40.65 ± 0.02	this work
	2015 Oct 26	K_c	4510.9 ± 2.7	40.57 ± 0.03	this work
	2016 Sep 13	K_c	4508.9 ± 3.0	40.28 ± 0.05	this work
HD 86081 B	2013 Dec 18	K_c	2904.8 ± 2.3	89.29 ± 0.06	this work
	2014 Dec 05	K_c	2901.3 ± 2.9	89.35 ± 0.06	this work
HD 96167 B	2013 Jan 24	K_s	5873.0 ± 1.8	297.1 ± 0.1	Mugrauer and Ginski (2015)
	2014 Jan 12	K_c	5889.7 ± 3.4	297.18 ± 0.03	this work
	2015 Jan 09	K_c	5884.1 ± 2.1	297.11 ± 0.02	this work
HD 116029 B	2013 Jun 30	i'	1387.1 ± 5.8	209.1 ± 0.3	Ginski et al. (2016)
	2013 Jul 04	K_c	1391.6 ± 1.7	209.32 ± 0.07	this work
	2014 Jun 09	K_c	1393.0 ± 1.6	209.37 ± 0.06	this work
	2015 Jan 09	K_c	1391.4 ± 1.6	209.37 ± 0.07	this work
HD 126614 B	2009 Apr 13	K_s	489.0 ± 1.9	56.1 ± 0.3	Howard et al. (2010)
	2011 Jan 14	i'	499 ± 67	60.7 ± 5.6	Ginski et al. (2012)
	2015 Jan 09	K_c	486.1 ± 1.5	69.1 ± 0.2	this work
	2015 Jun 24	K_c	485.3 ± 1.5	70.4 ± 0.2	this work
HD 142245 B	2013 Jul 04	K_c	2484.7 ± 1.6	168.79 ± 0.04	this work
	2014 Jun 09	K_c	2499.5 ± 1.9	168.21 ± 0.04	this work
	2015 Jun 24	K_c	2501.3 ± 1.8	168.23 ± 0.04	this work
	2016 Jun 09	K_c	2507.5 ± 1.8	168.07 ± 0.04	this work
HD 142245 C	2013 Jul 04	K_c	2524.7 ± 1.6	169.54 ± 0.03	this work
	2014 Jun 09	K_c	2516.7 ± 1.7	169.66 ± 0.04	this work
	2015 Jun 24	K_c	2513.2 ± 1.8	169.71 ± 0.04	this work
	2016 Jun 09	K_c	2505.9 ± 1.9	169.74 ± 0.04	this work
HD-142245 BC	2012 Aug 31	K_s	2498 ± 6[b]	169.2 ± 0.2[b]	Mugrauer and Ginski (2015)
	2013 Jul 24	K_s	2494 ± 6[b]	169.1 ± 0.1[b]	Mugrauer and Ginski (2015)
	2013 Jul 04	K_c	2503.3 ± 1.6	169.14 ± 0.04	this work
	2014 Jun 09	K_c	2507.4 ± 2.0	168.89 ± 0.04	this work
	2015 Jun 24	K_c	2506.7 ± 1.8	168.92 ± 0.04	this work
	2016 Jun 09	K_c	2506.5 ± 1.9	168.85 ± 0.04	this work
HD 164509 B	2014 Jun 09	K_c	698.8 ± 1.5	202.4 ± 0.1	this work
	2014 Jul 22	880 nm	697 ± 2	202.6 ± 0.2	Wittrock et al. (2016)
	2015 Jun 24	K_c	703.3 ± 1.5	202.9 ± 0.1	this work

Continued on next page

Table 4.4 – continued from previous page

Candidate[a]	UT Obs. Date	Band	ρ (mas)	PA (°)	Reference
	2016 Jun 09	K_c	707.7 ± 1.5	203.3 ± 0.1	this work
HD 177830 B	2002 Jul 19	I	1620 ± 10	84.1 ± 1.0	Roberts et al. (2011)
	2005 May 08	K	1640 ± 10	84.6 ± 0.4	Eggenberger et al. (2007)
	2012 May 9	K_s	1670 ± 10	84.3 ± 0.2	Roberts et al. (2015)
	2012 Jun 12	YJH	1680 ± 2	86.0 ± 0.1	Roberts et al. (2015)
	2014 May 14	K_s	1670 ± 10	85.3 ± 0.2	Roberts et al. (2015)
	2014 Jun 09	K_c	1665.9 ± 1.7	84.27 ± 0.06	this work
	2015 Jul 05	K_c	1664.6 ± 1.7	84.19 ± 0.06	this work
	2016 Jun 09	K_c	1665.9 ± 1.7	84.12 ± 0.06	this work
HD 187123 bg	2008 Jul 11	i'	2926 ± 11	48.1 ± 0.3	Ginski et al. (2012)
	2009 Sep 07	i'	2917 ± 13	43.9 ± 0.3	Ginski et al. (2012)
	2013 Aug 19	K_c	2947.4 ± 7.4	29.5 ± 0.2	this work
	2015 Jun 24	K_c	3006.8 ± 4.1	22.73 ± 0.05	this work
HD 188015 bg	2013 Jun 30	i'	4063 ± 13	113.7 ± 0.2	Ginski et al. (2016)
	2013 Aug 19	K_c	4079.2 ± 1.8	113.45 ± 0.02	this work
	2014 Jul 12	K_c	3992.2 ± 1.7	112.84 ± 0.03	this work
	2014 Aug 20	i'	4006 ± 67	112.5 ± 0.8	Ginski et al. (2016)
HD 195019 B	2013 Aug 19	K_c	3416.3 ± 1.7	333.80 ± 0.03	this work
	2014 Jun 09	K_c	3406.9 ± 1.8	333.87 ± 0.03	this work
	2014 Jul 12	K_c	3403.9 ± 1.7	333.89 ± 0.03	this work
	2015 Jun 03	K_c	3391.1 ± 2.0	333.95 ± 0.03	this work
HD 207832 B	2013 Aug 19	K_c	2044.3 ± 1.6	218.24 ± 0.04	this work
	2013 Aug 19	K_s	2042.8 ± 1.5	218.23 ± 0.05	this work
	2014 Jul 12	K_c	2051.7 ± 1.6	218.25 ± 0.04	this work
	2015 Jul 05	K_c	2059.0 ± 1.9	218.26 ± 0.05	this work
	2015 Oct 26	K_c	2059.9 ± 1.8	218.21 ± 0.05	this work
	2016 Sep 13	K_c	2037.8 ± 6.4	217.3 ± 0.2	this work
HD 207832 C	2013 Aug 19	K_c	2065.0 ± 1.6	216.11 ± 0.04	this work
	2013 Aug 19	K_s	2065.3 ± 1.5	216.08 ± 0.04	this work
	2014 Jul 12	K_c	2075.3 ± 1.6	216.37 ± 0.04	this work
	2015 Jul 05	K_c	2087.5 ± 1.8	216.73 ± 0.05	this work
	2015 Oct 26	K_c	2093.6 ± 1.8	216.82 ± 0.05	this work
	2016 Sep 13	K_c	2101.2 ± 5.0	217.79 ± 0.08	this work
HD 207832 BC	2013 Aug 19	K_c	2054.4 ± 1.7	217.17 ± 0.04	this work
	2013 Aug 19	K_s	2053.8 ± 1.5	217.14 ± 0.05	this work
	2014 Jul 12	K_c	2063.3 ± 1.7	217.30 ± 0.04	this work
	2015 Jul 05	K_c	2073.2 ± 2.0	217.48 ± 0.06	this work
	2015 Oct 26	K_c	2076.7 ± 1.9	217.51 ± 0.05	this work
	2016 Sep 13	K_c	2069.7 ± 7.9	217.5 ± 0.2	this work
Transiting planet host stars in triple systems					
HAT-P-8 B	2012 Jul 27	K'	1037.9 ± 1.5	137.6 ± 0.1	Ngo et al. (2015)
	2013 Aug 19	K_s	1041.0 ± 1.5	137.8 ± 0.1	Ngo et al. (2015)
	2014 Oct 03	K_s	1043.9 ± 1.6	137.83 ± 0.09	this work
	2015 Jul 05	K_s	1044.2 ± 1.5	137.86 ± 0.08	this work
	2016 Sep 12	K_s	1045.4 ± 1.6	137.42 ± 0.09	this work
HAT-P-8 C	2012 Jul 27	K'	1047.8 ± 1.6	140.9 ± 0.1	Ngo et al. (2015)
	2013 Aug 19	K_s	1044.7 ± 1.5	141.1 ± 0.1	Ngo et al. (2015)
	2014 Oct 03	K_s	1040.3 ± 1.9	141.17 ± 0.09	this work

Continued on next page

Table 4.4 – continued from previous page

Candidate[a]	UT Obs. Date	Band	ρ (mas)	PA (°)	Reference
	2015 Jul 05	K_s	1037.5 ± 1.7	141.20 ± 0.09	this work
	2016 Sep 12	K_s	1036.7 ± 1.7	140.8 ± 0.1	this work
HAT-P-8 BC	2012 Jul 27	K'	1043.1 ± 1.6	139.5 ± 0.1	Ngo et al. (2015)
	2013 Aug 19	K_s	1042.7 ± 1.6	139.6 ± 0.1	Ngo et al. (2015)
	2014 Oct 03	K_s	1041.4 ± 2.0	139.7 ± 0.1	this work
	2015 Jul 05	K_s	1039.9 ± 1.7	139.76 ± 0.09	this work
	2016 Sep 12	K_s	1040.0 ± 1.7	139.3 ± 0.1	this work
KELT-4A B	2012 May 07	K	1562.5 ± 8.3	29.7 ± 0.2	Eastman et al. (2016)
	2015 Dec 20	K_s	1569.2 ± 1.8	29.80 ± 0.07	this work
KELT-4A C	2012 May 07	K	1584.3 ± 8.4	28.1 ± 0.1	Eastman et al. (2016)
	2015 Dec 20	K_s	1561.6 ± 2.0	28.18 ± 0.07	this work
KELT-4A BC	2012 May 07	K	1573.2 ± 1.8	28.89 ± 0.07	Eastman et al. (2016)
	2015 Dec 20	K_s	1564.7 ± 2.1	28.88 ± 0.08	this work
WASP-12 B	2012 Feb 02	K'	1058.8 ± 1.5	251.2 ± 0.1	Ngo et al. (2015)
	2013 Mar 02	K_s	1058.6 ± 1.5	251.4 ± 0.1	Ngo et al. (2015)
	2014 Dec 04	K_s	1059.5 ± 1.9	251.46 ± 0.08	this work
	2015 Dec 26	K_s	1058.3 ± 1.5	251.50 ± 0.08	this work
	2016 Sep 13	K_s	1057.7 ± 1.6	251.51 ± 0.09	this work
WASP-12 C	2012 Feb 02	K'	1067.1 ± 1.5	246.8 ± 0.1	Ngo et al. (2015)
	2013 Mar 02	K_s	1068.4 ± 1.5	246.9 ± 0.1	Ngo et al. (2015)
	2014 Dec 04	K_s	1070.1 ± 1.6	246.89 ± 0.09	this work
	2015 Dec 26	K_s	1070.2 ± 1.5	246.94 ± 0.08	this work
	2016 Sep 13	K_s	1069.1 ± 1.6	246.90 ± 0.09	this work
WASP-12 BC	2012 Feb 02	K'	1062.1 ± 1.5	248.97 ± 0.09	Ngo et al. (2015)
	2013 Mar 02	K_s	1062.7 ± 1.5	246.16 ± 0.08	Ngo et al. (2015)
	2014 Dec 04	K_s	1064.0 ± 1.9	249.14 ± 0.09	this work
	2015 Dec 26	K_s	1063.4 ± 1.5	249.19 ± 0.08	this work
	2016 Sep 13	K_s	1062.6 ± 1.7	249.17 ± 0.09	this work

Notes. Separations (ρ) and position angle (PA) measurements of candidate companions in this work and other studies with published uncertainties. For triple systems, astrometry for both individual components and their center of mass ("BC") are included. These values are also plotted in Figures 4.3 and 4.4.

[a] Candidate companions are labelled with uppercase letters (B, C) when our analysis determines that they are comoving stellar companions and as "bg" when they are distant background objects.

[b] This astrometric epoch from the literature did not resolve the individual companions, so the center of light, rather than the center of mass, are reported.

Common proper motion check

We obtained a second epoch of K_c images of all candidate companions to determine whether these companions are gravitationally bound to the primary star. As described in Ngo et al. (2015), we show the measured projected separation and position angle of each candidate companion as a function of time and compare it to the predicted tracks for a bound companion and an infinitely distant background object in Figures 4.3 and 4.4. Predicted tracks are computed using stellar proper motions from Leeuwen (2007) and start from the epoch with the smallest uncertainties. When available, we also include previously published astrometric measurements

and their corresponding uncertainties in Figures 4.3 and 4.4 and Table 4.4. After reviewing the available astrometry, we conclude that 11 out of 13 candidate multi-stellar systems are gravitationally bound. We discuss the astrometric measurements for each individual system separately in Section 4.5.

Companion star masses and separations

For the 11 confirmed multi-stellar systems, we follow the procedure described in Ngo et al. (2015) to compute the companion star's physical parameters. Here, we will describe our method briefly. We model the stars with PHOENIX synthetic spectra (Husser et al., 2013) assuming solar compositions for both stars ([Fe/H]=0, [α/H]=0) and calculate fluxes from each star by integrating the chosen spectra over the observed bandpass. For the primary star, we interpolate PHOENIX spectra to get a model with the corresponding stellar mass, radius, and effective temperature as reported in previous studies, summarized in Table 4.2. Using the published parallax and corresponding distance to each system and the flux of the primary star, we solve for the companion temperature that best fits our measured photometric flux ratio. With this best fitting effective temperature, we calculate the corresponding companion mass and radius using zero-age main sequence star models (Baraffe et al., 1998). We report the properties of each companion star in Table 4.5 with uncertainties calculated from the uncertainty in the measured flux ratio. These errors do not account for systematic uncertainties from our use of PHOENIX spectra or the zero-age main sequence model. We find that errors introduced by assuming solar metallicities and compositions are much smaller than the uncertainties on the measured contrast ratio. Similarly, some error may be introduced from using literature values for primary star mass and radius as these measurements may not have included the effects of the secondary star. Because the secondary stars are several magnitudes or more fainter, this effect is also smaller than the uncertainties. For planet population and orbit fit analyses presented in Section 4.6, we use the epoch with the smallest measurement error as the final measurement for each system.

Table 4.5: Derived stellar parameters of confirmed stellar companions

Companion	UT Obs. Date	$T_{\rm eff}$ (K)	M ($M_\odot$)	$\log g$ (cgs)	D (au)
RV planet host stars					
HD 30856B	2014 Oct 04	3940 ± 200	0.595 ± 0.070	4.693 ± 0.060	$93.2^{+8.7}_{-7.1}$
	2014 Dec 07	3945 ± 70	0.614 ± 0.022	4.688 ± 0.018	$93.1^{+8.7}_{-7.1}$

Continued on next page

Table 4.5 – continued from previous page

Companion	UT Obs. Date	$T_{\rm eff}$ (K)	M ($M_\odot$)	$\log g$ (cgs)	D (au)
	2015 Oct 26*	3731 ± 29	0.537 ± 0.013	4.759 ± 0.013	$92.8^{+8.7}_{-7.1}$
HD 43691B	2013 Dec 18	2750 ± 150	0.0964 ± 0.0091	5.265 ± 0.036	366^{+26}_{-23}
	2014 Dec 04	2900 ± 130	0.108 ± 0.013	5.225 ± 0.039	366^{+26}_{-23}
	2015 Oct 26	2940 ± 120	0.113 ± 0.015	5.211 ± 0.041	365^{+26}_{-23}
	2016 Sep 13*	3020 ± 110	0.126 ± 0.019	5.180 ± 0.042	365^{+26}_{-23}
HD 43691C	2013 Dec 18	3040 ± 110	0.128 ± 0.019	5.174 ± 0.041	358^{+25}_{-22}
	2014 Dec 04	4100 ± 1200	0.18 ± 0.18	4.35 ± 0.44	358^{+25}_{-22}
	2015 Oct 26	3162 ± 95	0.153 ± 0.025	5.128 ± 0.039	359^{+25}_{-22}
	2016 Sep 13*	3308 ± 71	0.209 ± 0.037	5.056 ± 0.042	359^{+25}_{-22}
HD 86081B	2013 Dec 18	2400 ± 1700	0.08 ± 0.54	5.34 ± 0.63	277^{+29}_{-24}
	2014 Dec 05*	2562 ± 61	0.0876 ± 0.0019	5.305 ± 0.010	276^{+29}_{-24}
HD 96167B	2014 Jan 12*	3080 ± 140	0.135 ± 0.028	5.159 ± 0.053	512^{+43}_{-37}
	2015 Jan 09	2820 ± 240	0.102 ± 0.025	5.224 ± 0.081	512^{+43}_{-37}
HD 116029B	2013 Jul 04*	3387 ± 18	0.259 ± 0.014	5.004 ± 0.014	171^{+15}_{-13}
	2014 Jun 09	3378 ± 21	0.252 ± 0.015	5.010 ± 0.015	171^{+15}_{-13}
	2015 Jan 09	3343 ± 29	0.229 ± 0.017	5.033 ± 0.019	171^{+15}_{-13}
HD 126614B	2015 Jan 09*	3382 ± 23	0.255 ± 0.017	5.008 ± 0.016	$35.3^{+2.6}_{-2.3}$
	2015 Jun 24	3434 ± 28	0.300 ± 0.028	4.966 ± 0.023	$35.2^{+2.6}_{-2.3}$
HD 142245B	2013 Jul 04*	3589 ± 14	0.455 ± 0.011	4.842 ± 0.011	273^{+20}_{-17}
	2014 Jun 09	3824 ± 63	0.573 ± 0.025	4.723 ± 0.022	275^{+20}_{-17}
	2015 Jun 24	3651 ± 20	0.501 ± 0.011	4.796 ± 0.011	275^{+20}_{-18}
	2016 Jun 09	3628 ± 14	0.484 ± 0.011	4.812 ± 0.010	276^{+20}_{-18}
HD 142245C	2013 Jul 04*	3687 ± 20	0.5172 ± 0.0091	4.7791 ± 0.0094	278^{+20}_{-18}
	2014 Jun 09	3847 ± 80	0.580 ± 0.030	4.717 ± 0.027	277^{+20}_{-18}
	2015 Jun 24	3725 ± 20	0.5343 ± 0.0090	4.7619 ± 0.0088	276^{+20}_{-18}
	2016 Jun 09	3741 ± 21	0.5417 ± 0.0097	4.7547 ± 0.0094	276^{+20}_{-18}
HD 164509B	2014 Jun 09	3403 ± 40	0.268 ± 0.035	4.990 ± 0.034	$36.6^{+2.0}_{-1.7}$
	2015 Jun 24*	3480 ± 14	0.355 ± 0.015	4.924 ± 0.013	$36.9^{+2.0}_{-1.8}$
	2016 Jun 09	3515 ± 29	0.388 ± 0.029	4.895 ± 0.023	$37.1^{+2.0}_{-1.8}$
HD 177830B	2014 Jun 09	3159 ± 33	0.1524 ± 0.0087	5.129 ± 0.014	$98.3^{+3.8}_{-3.5}$
	2015 Jul 05	3139 ± 42	0.1475 ± 0.0099	5.137 ± 0.016	$98.2^{+3.8}_{-3.5}$
	2016 Jun 09*	3260 ± 33	0.185 ± 0.014	5.083 ± 0.017	$98.3^{+3.8}_{-3.5}$
HD 195019B	2013 Aug 19	4000 ± 120	0.631 ± 0.036	4.673 ± 0.031	$131.5^{+5.1}_{-4.8}$
	2014 Jun 09*	3890 ± 100	0.599 ± 0.034	4.702 ± 0.030	$131.2^{+5.1}_{-4.8}$
	2014 Jul 12	4000 ± 130	0.632 ± 0.038	4.672 ± 0.032	$131.1^{+5.1}_{-4.8}$
	2015 Jun 03	3940 ± 110	0.614 ± 0.033	4.689 ± 0.029	$130.6^{+5.1}_{-4.7}$
HD 207832B	2013 Aug 19	2680 ± 140	0.0931 ± 0.0070	5.278 ± 0.030	$111.2^{+5.9}_{-5.3}$
	2014 Jul 12	2716 ± 90	0.0944 ± 0.0051	5.273 ± 0.021	$111.6^{+6.0}_{-5.3}$
	2015 Jul 05*	2870 ± 81	0.1053 ± 0.0076	5.234 ± 0.024	$112.0^{+6.0}_{-5.4}$
	2015 Oct 26	2819 ± 86	0.1007 ± 0.0065	5.249 ± 0.023	$112.1^{+6.0}_{-5.4}$
	2016 Sep 13	2623 ± 100	0.0894 ± 0.0040	5.295 ± 0.020	$110.9^{+5.9}_{-5.3}$
HD 207832C	2013 Aug 19	2864 ± 98	0.1049 ± 0.0094	5.234 ± 0.030	$112.3^{+6.0}_{-5.4}$
	2014 Jul 12	2838 ± 85	0.1023 ± 0.0071	5.243 ± 0.024	$112.9^{+6.0}_{-5.4}$
	2015 Jul 05*	2855 ± 80	0.1040 ± 0.0069	5.238 ± 0.023	$113.6^{+6.1}_{-5.4}$
	2015 Oct 26	2850 ± 80	0.1035 ± 0.0067	5.240 ± 0.022	$113.9^{+6.1}_{-5.4}$
	2016 Sep 13	2958 ± 75	0.116 ± 0.010	5.205 ± 0.027	$114.3^{+6.1}_{-5.5}$
Transiting planet host stars in triple systems					
HAT-P-8B	2014 Oct 03	3186 ± 26	0.1604 ± 0.0076	5.118 ± 0.011	238 ± 13

Continued on next page

Table 4.5 – continued from previous page

Companion	UT Obs. Date	$T_{\rm eff}$ (K)	M ($M_\odot$)	$\log g$ (cgs)	D (au)
	2015 Jul 07	3205 ± 23	0.1659 ± 0.0068	5.1099 ± 0.0097	238 ± 13
	2016 Sep 12*	3206 ± 22	0.1664 ± 0.0065	5.1092 ± 0.0093	238 ± 13
HAT-P-8C	2014 Oct 03	3100 ± 31	0.1393 ± 0.0065	5.152 ± 0.012	237 ± 13
	2015 Jul 07	3022 ± 21	0.1250 ± 0.0031	5.1810 ± 0.0076	236 ± 13
	2016 Sep 12*	3024 ± 21	0.1254 ± 0.0031	5.1801 ± 0.0076	236 ± 13
KELT-4A B	2015 Dec 20*	4560 ± 320	0.776 ± 0.081	4.565 ± 0.066	331^{+20}_{-19}
KELT-4A C	2015 Dec 20*	3846 ± 83	0.584 ± 0.029	4.715 ± 0.026	330^{+20}_{-19}
WASP-12B	2014 Dec 04	3861 ± 66	0.589 ± 0.022	4.711 ± 0.019	462 ± 40
	2015 Dec 26*	3820 ± 51	0.575 ± 0.019	4.723 ± 0.017	462 ± 39
	2016 Sep 13	3842 ± 55	0.583 ± 0.019	4.716 ± 0.017	461 ± 39
WASP-12C	2014 Dec 04	3690 ± 53	0.518 ± 0.024	4.778 ± 0.024	467 ± 40
	2015 Dec 26*	3791 ± 47	0.564 ± 0.019	4.733 ± 0.018	467 ± 40
	2016 Sep 13	3839 ± 56	0.582 ± 0.020	4.717 ± 0.018	466 ± 40

Notes. For observations on each date, we report error weighted averages of all measurements on $T_{\rm eff}$, M, $\log g$, and D. Our uncertainties account for measurement error and the published primary star's stellar parameters but do not include uncertainties introduced from use of stellar models and our assumptions on stellar composition. Therefore, the true uncertainties are larger than the values presented in this table. For each target, we choose the epoch with the lowest measurement error as the representative value for further dynamical analysis. This epoch is marked with an asterisk.

Contrast curves for all systems

We report the 5-sigma K_c-band detection limits for each star in our survey as a function of the projected separation. For systems with a companion, we mask out the companion before calculating this detection limit. Figure 4.5 shows the contrast curves for the stars in this work. We compute the contrast curves from the standard deviation of pixel values in a series of annuli, following the procedure described in Ngo et al. (2015), and provide a complete list of these curves for each individual system in Table 4.10. For targets imaged on the full 1024x1024 array, we do not have coverage in all directions beyond 5″ and drop to 90% directional completeness at 6″. This limit is smaller for targets imaged on smaller subarrays. This lack of directional completeness results in fewer frames imaged in that region, which increases the standard deviation of stacked pixels and leads to lower contrast.

4.5 Individual systems

Tables 4.2–4.5 summarize our survey targets' properties, measured companion photometry, measured companion astrometry and calculated companion properties, respectively. Table 4.4 also includes astrometric measurements from other studies, when available. The following paragraphs provide additional notes on each of the eleven confirmed multi-stellar systems from our survey as well as candidate com-

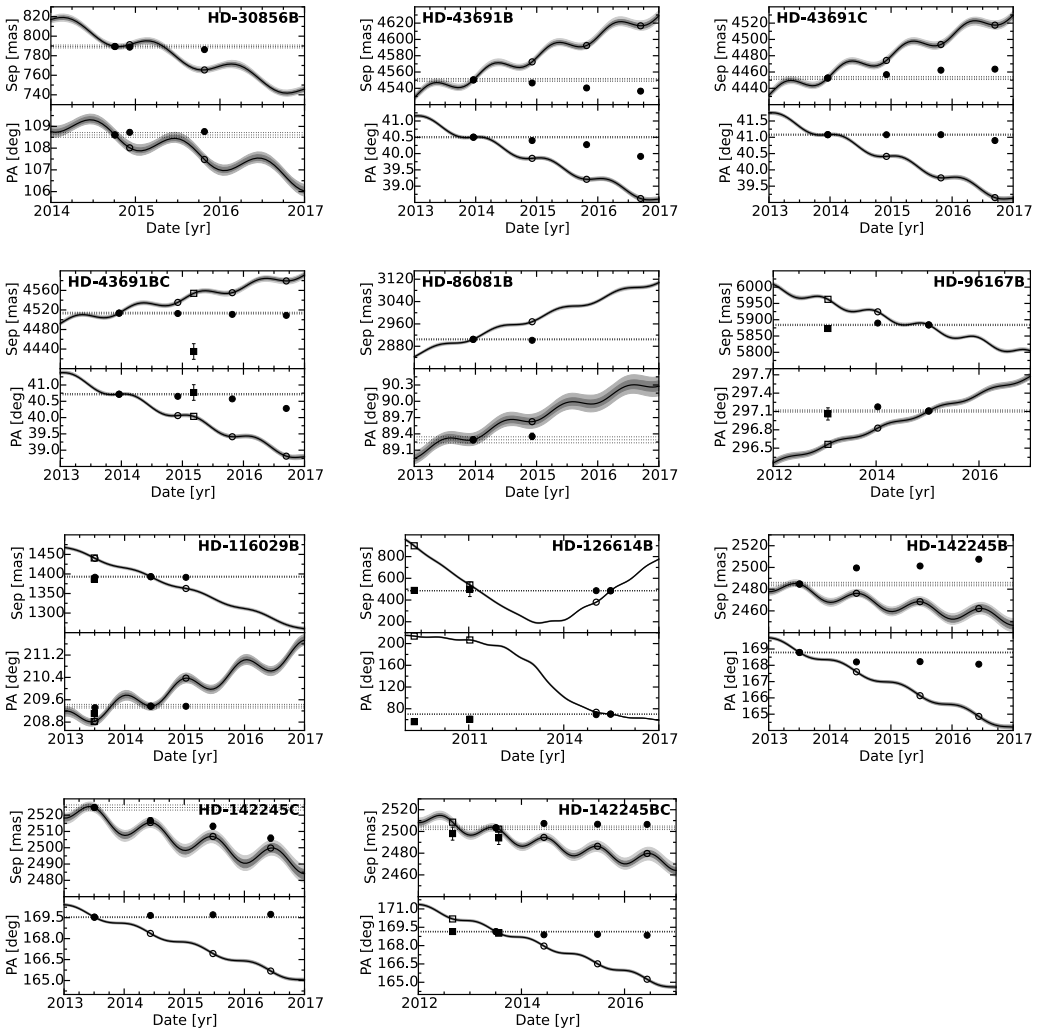

Figure 4.3: Top and bottom panels show the projected separation and position angle of each companion star relative to the primary star. This figure and the following figure include all confirmed common proper motion companions and background objects from our survey. The solid line shows the expected evolution of separation and position angle for an infinitely distant background object. The dark grey and light grey shaded regions represent the 68% and 95% confidence regions. We use a Monte Carlo routine accounting for uncertainties in our measurements, the primary star's celestial coordinates, proper motion, and parallax. The horizontal dashed lines represent a trajectory with no change in separation or position angle. Filled symbols show measured positions of companions while open symbols show the expected position of an object if it were a background source. Circles represent data from this work and squares represent data from the literature. The data used in this figure can be found in Table 4.4. Companion candidates that were determined to be physically bound are labelled as the "B" or "C" components with the center of mass of the two companions denoted as "BC".

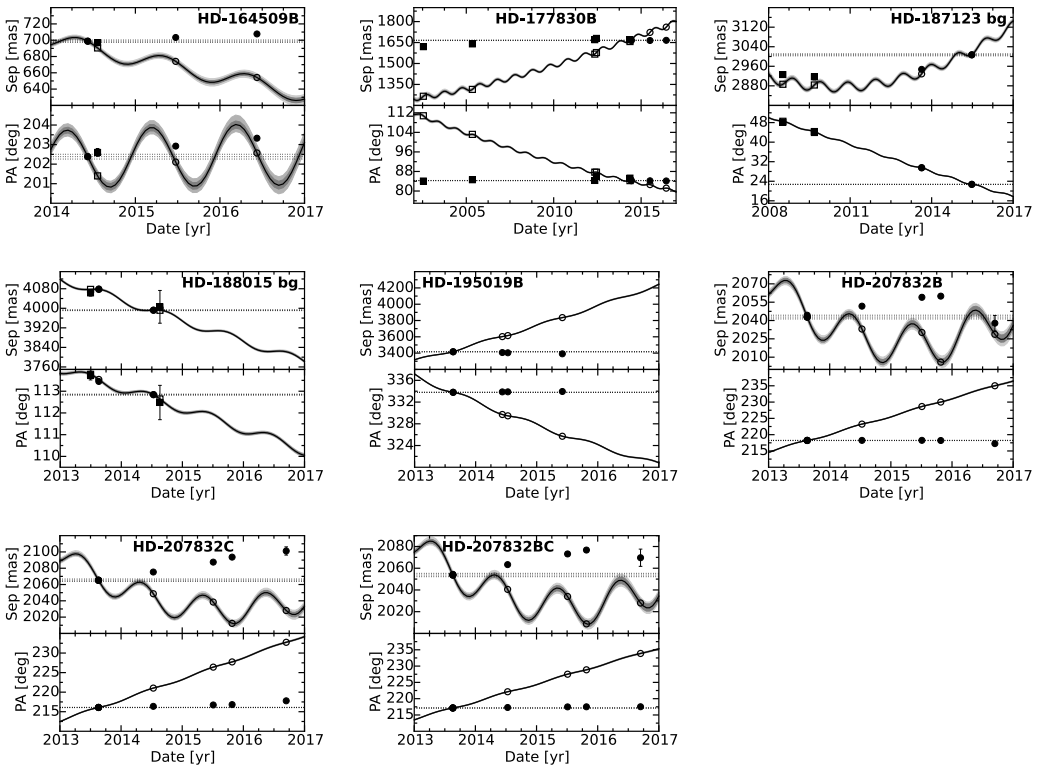

Figure 4.4: Continued from Figure 4.3. These panels also include two background objects, which are labelled as "bg".

panions that were found to be background objects. In total, we report the discovery of three new multi-stellar planet-hosting systems (HD 30856, HD 86081, and HD 207832) and the first confirmation of common proper motion for three additional systems (HD 43691, HD 116029, and HD 164509).

HD 30856. This binary system is reported for the first time in this work. Our images from 2014 and 2015 confirm this companion is comoving with its host star.

HD 43691. Our images from 2013 through 2016 provide the first confirmation that this is a comoving hierarchical triple system. The secondary and tertiary components have a projected separation of 360 au from the primary star, and a mutual projected separation of 10 au. Ginski et al. (2016) reported a single companion to this system that is consistent with our detection. They did not resolve the individual secondary and tertiary components but they did note that the companion appeared to have an elongated PSF. We are unable to use their astrometric measurements in our analysis because they did not resolve the two companion stars. We label the primary star as "A", the northernmost companion as "B" and the other companion as "C".

HD 86081. This binary system is presented for the first time in this work. In

Bryan et al. (2016), we report a long term RV trend of $-1.3 \pm 0.25\,\mathrm{m\,s^{-1}\,yr^{-1}}$ in this system corresponding to a companion with a minimum mass of 0.69 Jupiter masses at a separation of 4.6 au. Here, we report a companion with a mass of 88 ± 2 Jupiter masses ($0.0840 \pm 0.002 M_{\odot}$) and a projected separation of 280 ± 30 au. To determine whether or not our imaged companion could be responsible for the measured RV trend, we calculate the minimum companion star mass required to produce the observed RV trend at this projected separation using Equation 6 from Torres (1999). This minimum mass is $1.4^{+0.6}_{-0.5} M_{\odot}$, indicating that the companion star is not responsible for the RV trend. The non-detection of an additional companion in the AO images set an upper limit on the RV trend companion to be 72 Jupiter masses at 124 au. Our images from 2013 and 2014 indicate that the stellar companion is comoving with its host star.

HD 96167. This binary system was previously reported by Mugrauer and Ginski (2015) to be a comoving companion to its host star. Their astrometric measurements date back to 2013 and are consistent with our measurements in 2014 and 2015.

HD 116029. Ginski et al. (2016) reported this as a candidate binary system based on their 2013 image but were unable to confirm that the companion was comoving because they only had one epoch of astrometry. Our measured separation and position angle from our 2013, 2014 and 2015 images are consistent with their measurement. We provide the first confirmation that this system is a comoving binary pair.

HD 126614. The close companion star in this system was first detected in 2009 by Howard et al. (2010). Ginski et al. (2012) also imaged this system in 2011 and concluded that the companion is comoving. Our images from 2014 and 2015 agree with this assessment. We also found a long term RV trend for this system in Bryan et al. (2016) that is consistent with the imaged stellar companion. Finally, this system also has an additional distant common proper motion companion, NLTT 37349, at 41″.8 (3000 au; Lodieu et al., 2014) that is outside of our survey's field of view.

HD 142245. Our images from 2013 through 2016 provide the first images that resolve the individual stars in this hierarchical triple system. The two companion stars have a projected separation of 280 au from the primary star and a mutual projected separation of 6 au. Mugrauer and Ginski (2015) reported images from 2012 and 2013 showing a companion with an elongated PSF that is consistent with our measurements. They determined that this companion was comoving with the

host star but were unable to resolve the individual components. We label the primary star as "A", the northernmost companion as "B" and the other companion as "C".

HD 164509. Our images from 2014, 2015 and 2016 provide the first confirmation that this is a comoving binary system. Wittrock et al. (2016) also report a companion from their 2014 image that is consistent with our detection. With only one epoch, they were unable to confirm whether the companion is bound, but they noted that the color of the companion was consistent with a lower mass star at the same distance as the target star. We also found a long term RV trend for this system in Bryan et al. (2016) that is consistent with the imaged stellar companion.

HD 177830. The companion to this star was first reported by Eggenberger et al. (2007). They used images from 2004 (H-band) and 2005 (K-band) to determine that this is a comoving binary system. Roberts et al. (2011) and Roberts et al. (2015) later combined their images of this binary system with additional observations dating back to 2002. Our images in 2014, 2015 and 2016 recover the same companion reported in these previous studies and support the conclusion that the companion is bound.

HD 195019. Fischer et al. (1999) reported a companion around this star, but did not have precise measurements of its photometry or astrometry. Eggenberger et al. (2004) subsequently noted that both components are comoving based on archival data from Fischer et al. (1999), Allen et al. (2000) and Patience et al. (2002). Roberts et al. (2011) published additional images from 2002, but did not report uncertainties on their astrometry. Our images from 2013 through 2015 are consistent with all of the previous detections and also confirm that this is a comoving binary system.

HD 207832. This hierarchical triple system is reported for the first time in this work. The two companions have a projected separation of 110 au from the primary star and a mutual projected separation of 4 au, making this system the most compact RV-planet hosting triple system. Our images from 2013 through 2016 confirm that both companion stars are comoving with their host star. This system also has an extremely wide stellar companion, at $38''.6$ (Lodieu et al., 2014), which is far outside of our survey's field of view. With the fourth star at a projected separation of 126000 au, we only consider the inner hierarchical triple system for further analysis in this work. We label the primary star as "A", the northernmost companion as "B" and the other companion as "C".

Background objects. Two candidate companions were determined to be back-

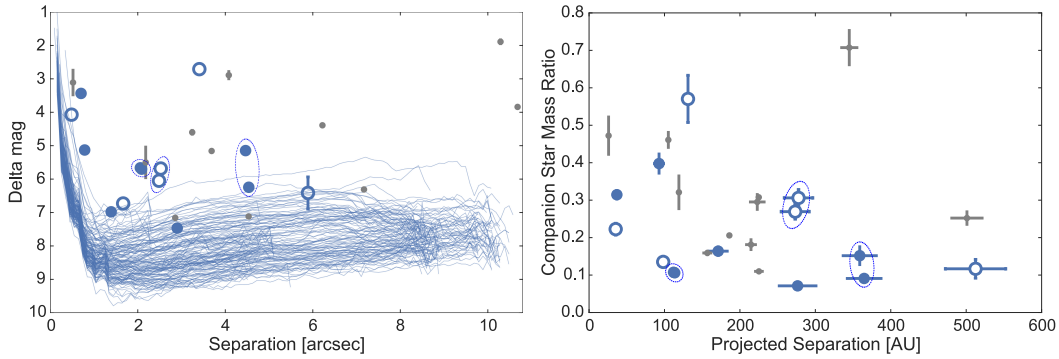

Figure 4.5: In both plots, filled blue symbols are companions that are either new or newly confirmed to be comoving in this work. Open blue symbols are companions previously reported in other studies. Dashed ellipses encompass the two components of the three triple systems in our survey (the two companions to HD 207832 are similar enough that their points almost completely overlap). Small gray symbols show confirmed comoving companions found only in other surveys (Eggenberger et al., 2007; Ginski et al., 2012; Mugrauer and Ginski, 2015; Ginski et al., 2016). Two of these surveys, Ginski et al. (2012) and Ginski et al. (2016), are conducted in i band rather than K band. Some of these studies do not report measurement uncertainties and in some cases, mass ratios are estimated based on the reported brightness difference and primary star spectral type. In the left plot, the blue lines show contrast curves for all 144 surveyed RV-host stars out to 10″. This figure excludes one companion detected by Ginski et al. (2012). With $\Delta I = 7.5 \pm 0.5$ and a separation of 1″.139 ± 0″.005, this object would be the lowest flux ratio companion on this plot. However, the target star is HD 176051, which is a previously known binary hosting an astrometry detected planet, not an RV-detected planet.

ground objects rather than comoving multi-stellar systems. HD 187123 has a background object approximately 3″to the north-east. Ginski et al. (2012) concluded that this companion was a background star based on their 2008 and 2009 images. Our new images from 2013 and 2015 independently confirm this conclusion. We found a source approximately 4″to the north-west in our 2013 and 2014 images of HD 188015 that we determined to be a background object. Ginski et al. (2016) found two candidate companions with similar projected separations, one of which was consistent with our detection, and determined both of them to be background sources. HD 188015 does have a distant comoving companion at 11″ (Raghavan et al., 2006), but this companion is outside our field of view and we therefore do not include it when calculating the frequency of stellar companions in our sample.

Companions beyond our survey's field of view. Six systems in our survey host companions that were outside of our survey's field of view, but reported in the literature. Eggenberger et al. (2007) report companions with separations of 6″.2 and 10″.3 around HD 16141 and HD 46375, respectively. The Washington Double Star Catalog (WDS; Mason et al., 2001) shows that HD 109749, HD 178911, HD 186427 (also known as 16 Cyg B) each have a companion at separations of 8″.3,

16″.1 and 39″.6, respectively. Finally, the WDS also reports three companions around GJ 667C at separations of 31″.2, 32″.5 and 36″.4.

4.6 Discussion

Stellar companion fraction

We find a raw companion fraction of 11 multi-stellar systems out of 144 surveyed stars, corresponding to a multiplicity rate of $7.6\% \pm 2.3\%$. For the typical target, we are sensitive to stellar-mass companions in all directions with projected separations between 0″.3 and 6″(at 90% directional completeness), corresponding to projected separations of 15 au and 300 au for a star at 50 pc. We are sensitive to companions in limited directions up to 10″. The most distant companion detected in our survey was found at 512 ± 43 au around HD 96167. It was found at the outer edge of our survey limit, at a separation of 5″.9. Our raw companion fraction is consistent, within 1σ, with results from other direct imaging surveys for stellar companions around RV-detected planet host stars, as reported in Table 4.6. This companion fraction is lower than the Eggenberger et al. (2007) control sample's companion fraction of $17.6\% \pm 4.9\%$, at a significance of 1.9σ. It is not certain whether the difference is by chance, is due to different companion vetting by different RV planet surveys, or if it suggests an anti-correlation between intermediate distance giant planet and a stellar companion. Figure 4.5 compares the projected separations, flux ratios, and mass ratios for the companions in our survey to those reported in these other imaging surveys.

Prior to this study there were sixteen confirmed wide-binary multiple star systems with separations less than 6″that were known to host RV planets. Our observations increase this number by six, for a total of 22 systems. This work also increases the number of confirmed multi-stellar systems with companions within 200 au by four; bringing the total number of such systems to twelve. As indicated by our contrast curves, our survey is more sensitive at small separations than these previous surveys. Figure 4.5 shows that a majority of our new confirmed multi-stellar systems have relatively small flux ratios and projected separations as compared to the sample of previously published planet-hosting multiple star systems. All known multi-stellar RV-planet hosting systems with companions within 6″ are listed in Table 4.7. For each system, we calculate ν/n, the ratio of the planet's precession due to the companion star divided by the planet's mean motion as a proxy for the companion star's ability to dynamically influence the planet. We sort the multi-stellar systems by this metric in order to highlight the most interesting systems for future dynamical

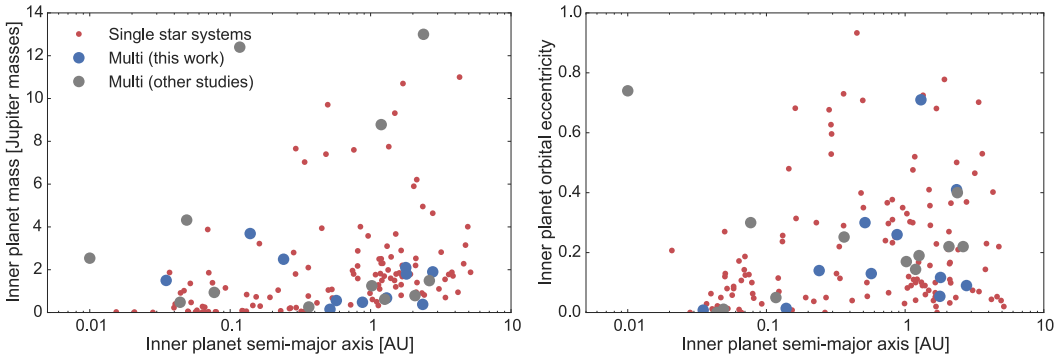

Figure 4.6: Mass and eccentricity vs. semimajor axis of the inner-most planet for single star systems (red) and multi-stellar systems from our survey (blue) and other studies listed in Table 4.7 (gray).

studies.

The stellar companion rate for our population of RV-detected giant planet host stars is much lower than the companion fraction of 47% ± 7% that we reported for transiting hot Jupiter systems (Ngo et al., 2016). This is most likely due to the relatively severe biases against multiple star systems in the target selection process for RV surveys. Unfortunately, these biases are neither well characterized nor fully reported, and we are therefore unable to report a completeness corrected stellar multiplicity rate for the RV-detected planet population. Unlike transit surveys, RV surveys such as the California Planet Survey (Howard et al., 2010) and the HARPS survey (Lagrange et al., 2009), vet potential targets for known companion stars that are close enough (generally within 2″) to fall within the spectrograph slit and are bright enough to have detectable spectral lines at the optical wavelengths where most RV surveys operate. Although it is possible to measure RV shifts for double-lined spectroscopic binaries, RV pipelines developed to search for planets are not typically designed to accommodate a second set of spectral lines and therefore avoid these kinds of systems. Nearby stars are generally identified via archival surveys such as the Washington Double Star catalog (Mason et al., 2001). RV surveys also discard targets that show large RV variations, effectively eliminating close binaries from their samples. Although RV-planet survey target selection is performed with some quantitative and objective metrics, there are also any number of subjective choices made over the years which are difficult to quantify retroactively (Clanton and Gaudi, 2014). We therefore conclude that we cannot reliably compare stellar multiplicity rates for planet-hosting stars from RV surveys with similar results for samples of planets detected by transit surveys.

Table 4.6: Stellar companion fraction of stars in RV-planet surveys

Survey	Multi-stellar systems	Companion fraction	Observatory / Instrument	Range[a](″)	Overlap
RV-detected planet host stars					
This work	11 out of 144	7.6% ± 2.3%	Keck / NIRC2	0.3–6.0	–
Eggenberger et al. (2007)	6 out of 56[b]	10.7% ± 4.4%[b]	VLT / NACO	0.2–13.0	20/56
Ginski et al. (2012)	3 out of 70	4.3% ± 2.5%	Calar Alto / AstraLux	0.5–12.0	29/70
Ginski et al., 2016	4 out of 51	7.8% ± 3.9%	Calar Alto / AstraLux	1.2–12.0	22/51
	6 out of 51[c]	11.8% ± 4.4%[c]			
Mugrauer and Ginski (2015)	2 out of 32[d]	6.3% ± 4.32%[d]	VLT / NACO	0.3–13.0	5/32
Control group (RV planet survey stars without a planet)					
Eggenberger et al. (2007)	13 out of 74[b]	17.6% ± 4.9%[b]	VLT / NACO	0.2–13.0	0/74

Notes. Companion fractions were computed from the raw number of confirmed multi-stellar systems reported by each survey, assuming Poisson uncertainties. These companion fractions are not corrected for survey completeness. Only stars that have RV-detected planet hosts are counted. The "overlap" column indicates the number of targets from the cited survey that are also in our survey. 73 out of our 144 targets have also been imaged in the other surveys; however, only 26 out of 144 targets have been previously imaged at observatories comparable to Keck.

[a] The inner limit of the range corresponds to a separation where the survey is sensitive to a contrast of $\Delta K \sim 5$ ($\Delta I \sim 7$ for the AstraLux surveys). We determine the outer limit of our survey to be the separation where we have 90% directional completeness, however our full chip size is 10″. For other surveys, we report their instrument's full chip size as the outer limit.

[b] One target in Eggenberger et al. (2007), HD 33636, was originally in our survey list until we learned the detection of HD 33636 was retracted. Therefore, we count this system as part of Eggenberger et al. (2007)'s control group instead of their planet hosting sample.

[c] Ginski et al. (2016) reported four confirmed multi-stellar systems and several candidate multi-stellar systems. Two of these ambiguous cases (HD 43691 and HD 116029) were also in our survey and we confirmed them to be co-moving systems. In this row, we report an updated companion fraction rate with these two additional systems.

[d] We were unable to confirm the planetary status for the HD 9578 system surveyed by Mugrauer and Ginski (2015) in the peer-reviewed literature. Thus, we exclude it from this count.

Table 4.7: Stellar and planetary parameters of RV-planet host systems with stellar companions within 6″

Planet host	$M_{\rm host}$ ($M_\odot$)	$a_{\rm pl}$ (au)	$e_{\rm pl}$	$m_{\rm pl}$ ($M_{\rm Jup}$)	Ref.	$M_{\rm comp}$ ($M_\odot$)	$a_{\rm comp}$ (au)	$\rho_{\rm comp}$ (″)	Ref.	ν/n
HD 164509	1.13 (2)	0.875 (8)	0.3 (1)	0.48 (9)	Gig12	**0.36 (2)**	**37 (2)**	**0.703 (2)**	**this work**	4×10^{-6}
HD 30856	1.35 (9)	1.8 (2)	0.117 ()	1.8 (2)	J11	**0.54 (1)**	**93 (8)**	**0.786 (2)**	**this work**	3×10^{-6}
HD 197037	1.06 (2)	2.07 (5)	0.22 (7)	0.79 (5)	S15,R12	0.34 (5)	119 (2)	3.688 (9)	G16	2×10^{-6}
HD 217786	1.02 (3)	2.38 (4)	0.40 (5)	13.0 (8)	Mo11	0.162 (7)	157 (7)	2.856 (7)	G16	6×10^{-7}
HD 142245[a]	1.7 (1)	2.77 (9)	0.09 ()	1.90 (2)	J11	0.97 (1)	276 (14)	2.505 (2)	this work	6×10^{-7}
HD 126614	1.15 (3)	2.35 (2)	0.41 (1)	0.38 (4)	Ho10	0.26 (2)	35 (3)	0.486 (1)	this work	5×10^{-7}
HD 142[a]	1.2 (2)	1.02 (3)	0.17 (6)	1.3 (0.2)	W12	0.59 (2)	105 (2)	4.08 (2)	E07	5×10^{-7}
HD 132563B[a]	1.01 (1)	2.62 (4)	0.22 (9)	1.49 (9)	D11	1.64 (2)	400 (50)	4.11 (2)	D11	5×10^{-7}
HD 116029	1.6 (1)	1.78 (5)	0.054 ()	2.1 (2)	J11	**0.26 (1)**	**171 (15)**	**1.392 (1)**	**this work**	2×10^{-7}
HD 87646	1.12 (9)	0.117 (3)	0.05 (2)	12.4 (7)	M16	0.6[c]	15.7 (2.1)	0.213 ()	M16, HIP	2×10^{-7}
HD 89484	1.2 (2)	1.19 (2)	0.14 (5)	9 (1)	Ha10	0.9[c]	178 (6)	4.629 ()	Ma06	2×10^{-7}
HD 207832[a,d]	0.98 (7)	0.570 (2)	$0.13^{+0.18}_{-0.05}$	$0.56^{+0.06}_{-0.03}$	S13,H12	**0.21 (1)**	**113 (4)**	**2.073 (2)**	**this work**	3×10^{-8}
HD 177830[e]	1.37 (4)	0.5137 (3)	0.3 (1)	0.15 (2)	J06,Me11	0.19 (1)	98 (4)	1.666 (2)	this work	2×10^{-8}
HD 2638	0.9 (1)	0.044[f]()	0 ()	0.48 ()	G10,M05	0.43 (1)	26 (2)	0.520 (4)	G16	2×10^{-9}
HD 96167	1.16 (5)	1.30 (7)	0.71 (4)	0.7 (2)	J15,P09	0.14 (3)	512 (43)	5.890 (3)	this work	2×10^{-9}
HD 16141	1.1 (1)	0.36 (2)	0.25 (5)	0.26 (3)	G10,B06	0.31 (2)	223 (11)	6.22 (3)	E07	1×10^{-9}
HD 195019	1.1 (1)	0.139 (8)	0.014 (4)	3.7 (3)	G10,B06	0.60 (3)	131 (5)	3.407 (2)	this work	7×10^{-10}
HD 86081	1.23 (8)	0.035[f]()	0.008 (4)	1.5 ()	S13,J06	**0.088 (2)**	**276 (29)**	**2.901 (2)**	**this work**	1×10^{-10}
HD 43691[a]	1.38 (5)	0.24 ()	0.14 (2)	2.49 ()	ds07	**0.33 (4)**	**362 (18)**	**4.500 (2)**	**this work**	7×10^{-11}
HD 41004A	0.7[c]	0.006[f](2)	0.7 (2)	2.5 (7)	S02,Z04	0.4[c]	22.5 ()	0.5 ()	S02,HIP	1×10^{-11}
HD 185269	1.3 (1)	0.077[f]()	0.23 (3)	1.03 (3)	Mo06	0.23 (1)	215 (8)	4.53 (1)	G16	8×10^{-12}
tau Boo	1.34 (5)	0.049[f](3)	0.011 (6)	4.32 (4)	B12,B15	0.4 ()	225 (1)	2.18 (1)	Gin12	3×10^{-12}

Continued on next page

Table 4.7 – continued from previous page

Planet host	$M_{\rm host}$ ($M_\odot$)	$a_{\rm pl}$ (au)	$e_{\rm pl}$	$m_{\rm pl}$ ($M_{\rm Jup}$)	Ref.	$M_{\rm comp}$ ($M_\odot$)	$a_{\rm comp}$ (au)	$\rho_{\rm comp}$ ($''$)	Ref.	ν/n

Notes. All RV-planet hosting systems with stellar companions detected within $6''$. As this is a soft limit (see text), we included HD 16141 with a companion at $6''.22$. For brevity, the number(s) in parentheses are uncertainties on the last digit(s) (i.e. 2.35 (2) is 2.35 ± 0.02). Missing values indicate no uncertainty provided by the source. References for the system and companion parameters follow each set of columns. We rank this list by a metric, $\nu/n = \frac{M_{\rm comp}}{M_{\rm host}} \left(\frac{a_{\rm pl}}{a_{\rm comp}}\right)^3$, to represent strength of the precession induced on the planet by the companion star. Systems with new or newly confirmed stellar companions have boldface names. and companion properties

[a] This is a triple system. The reported $M_{\rm comp}$ is the combined mass of both stars and $a_{\rm comp}$ is the average projected separation of each component.

[b] The innermost planet, HD 142b, is reported here. This system also hosts a second planet, HD 142c, at 6.8 au and 5.3 $M_{\rm Jup}$.

[c] These stellar masses were not measured. Instead, they were estimated from the star's spectral type.

[d] The innermost planet, HD 207832b, is reported here. This system also hosts a second planet, HD 207832c, at 2.112 au and 0.73 $M_{\rm Jup}$.

[e] The innermost planet, HD 177830c, is reported here. This system also hosts a second planet, HD 177830b, at 1.2218 au and 1.49 $M_{\rm Jup}$.

[f] This system is not included in the comparison between single and multi stellar systems described in Section 4.6 because the planet's semimajor axis is less than 0.1 au.

References. (B06) Butler et al. (2006); (B12) Brogi et al. (2012); (B15) Borsa et al. (2015); (D11) Desidera et al. (2011); (E07) Eggenberger et al. (2007); (G10) Ghezzi et al. (2010); (Gig12) Giguere et al. (2012); (Gin12) Ginski et al. (2012); (G16) Ginski et al. (2016); (Ha10) Han et al. (2010); (Ho10) Howard et al. (2010); (H12) Haghighipour et al. (2012); (HIP) Hipparcos Catalogue Perryman et al. (1997); (J06) Johnson et al. (2006); (J11) Johnson et al. (2011); (J15) Jofré et al. (2015); (M05) Moutou et al. (2005); (Ma06) Mason et al. (2004); (Mo06) Moutou et al. (2006); (Me11) Meschiari et al. (2011); (Mo11) Moutou et al. (2011); (M16) Ma et al. (2016); (P09) Peek et al. (2009); (S02) Santos et al. (2002); (dS07) Da Silva et al. (2007); (S13) Santos et al. (2013); (S15) Sousa et al. (2015); (W12) Wittenmyer et al. (2012); (W13) Wittenmyer et al. (2013); (Z04) Zucker et al. (2004)

Characteristics of RV-detected planets in multi-stellar systems

Although RV surveys are undoubtedly subject to different selection biases than transit surveys when it comes to multiple star systems, this bias is effectively removed when we limit ourselves to comparing different sub-samples within our RV planet survey population, assuming the selection biases affect all sub-samples in the same way. Previous studies have suggested that stellar companions are less common in systems with long-period planets than those with short-period planets (e.g Kaib et al., 2013; Zuckerman, 2014; Wang et al., 2015b). Here, we compare properties of planets in multi-stellar and single star systems within our survey population of RV-detected planet host stars. Figure 4.6 and Table 4.7 show the orbital properties of the innermost planet of each single and multi-stellar system in our survey. We wish to determine whether the distributions for innermost planet orbital eccentricity, orbital period and mass differ for single star systems from multi-star systems. Thus, we calculate whether a two-population (for single and multi-stellar systems) distribution is a better fit to the data than a one-population model. To avoid tidal circularization effects, we exclude 35 single and 5 multi-stellar systems with planets with semimajor axes less than 0.1 au in this analysis. Because we have a relatively small sample of multiple star systems in our survey, we also include similar multiple star systems (i.e., those with projected separations less than 6″; see Table 4.7 for a complete list) from the published literature. In total, there are 98 single star systems and 17 multi-stellar systems considered in this part of the analysis.

Assuming planet eccentricities follow a beta distribution (Kipping, 2013), we calculate the probability of obtaining an individual planet orbital eccentricity e_k to be

$$\text{prob}(e_k|a,b) = \frac{\Gamma(a+b)}{\Gamma(a)\,\Gamma(b)} e^{a-1}(1-e)^{b-1}, \tag{4.1}$$

where $\Gamma()$ denotes the Gamma function and a and b are the model parameters. We assume the planet mass and orbital period take the form of the Cumming et al. (2008) power law, so that the probability of obtaining an individual planet mass m_k and orbital period P_k is

$$\text{prob}(m_k, P_k|\alpha,\beta) \propto m^{\alpha} P^{\beta}, \tag{4.2}$$

where α and β are the model parameters. We assume that the orbital eccentricity is not correlated with orbital period and planetary mass so we can determine the probability of obtaining any individual planetary system to be the product of the above probabilities. Our goal is to compute the likelihood of a model M with a set

of parameters $\theta = (a, b, \alpha, \beta)$ for a set of planets. For an individual system, we can write

$$\text{prob}(e_k, m_k, P_k|\theta, M) \propto \frac{\Gamma(a+b)}{\Gamma(a)\,\Gamma(b)} e^{a-1}(1-e)^{b-1} m^{\alpha} P^{\beta}. \tag{4.3}$$

From Bayes' Theorem and choosing uniform priors for all model parameters, we can write the log-likelihood of a one-population model $\mathcal{L}_1$ as

$$\mathcal{L}_1 = \sum_k \ln\left[\text{prob}(e_k, m_k, P_k|M, \theta)\right] + C, \tag{4.4}$$

where the sum over k includes all RV planet host systems and C is a constant. Similarly, we can write the log-likelihood of a two-population model $\mathcal{L}_2$ as

$$\begin{aligned} \mathcal{L}_2 &= \sum_i \ln\left[\text{prob}(e_i, m_i, P_i|M_s, \theta_s)\right] \\ &+ \sum_j \ln\Big[\text{prob}(e_j, m_j, P_j|M_m, \theta_m)\Big] + C, \end{aligned} \tag{4.5}$$

where the sum over i includes all RV planet host systems with no companion star, the sum over j includes all RV planet host systems with at least one companion star, and the model parameters have subscripts s and m to denote separate sets of parameters for single and multi-stellar systems, respectively. C is the same constant from the one-population likelihood.

Using the Markov chain Monte Carlo implemented by `emcee` python package's affine-invariant sampler (Foreman-Mackey et al., 2013), we compute the posterior probability distributions for the model parameters and determine the maximum likelihoods of each model, $\hat{\mathcal{L}}_1$ and $\hat{\mathcal{L}}_2$. Figure 4.7 and 4.8 show our calculated posteriors on each model parameter for each model. We determine whether a two-population model is justified by comparing the Bayesian information criteria (BIC) for these two models and by computing the Bayesian odds ratio. First, we compute the BIC as $\text{BIC} = \ln(N)k - 2\hat{\mathcal{L}}$, where N is the number of planets in the model fit and k is the total number of parameters (i.e. four in the one-population model and eight in the two-population model). We find that the difference between the two-population model BIC and the one-population model BIC to be 17, indicating that the two-population model is very strongly disfavored (Kass and Raftery, 1995). Second, we compute the Bayesian odds ratio as the probability of a one-population model divided by the probability of a two-population model, assuming both models have equal prior likelihoods and uniform priors on all model parameters, i.e.

$$\frac{\text{prob(1pop)}}{\text{prob(2pop)}} = \frac{\exp\hat{\mathcal{L}}_1}{\exp\hat{\mathcal{L}}_2} \frac{\prod_x 2\pi\delta\theta_x/\Delta\theta_x}{\prod_y 2\pi\delta\theta_y/\Delta\theta_y}. \tag{4.6}$$

This is equal to the ratio of the evidence for each model in the case where the posteriors are n-dimensional normal distribution and when the priors are uniform. The first term on the right is the Bayes factor, and the second term is the Ockham factor to account for the model parameters. The product sum over x covers the four parameters of the one-population model and the product sum over y covers the eight parameters of the two-model population. The $\Delta\theta$ term corresponds to range in allowable parameter values from our uniform prior and $\delta\theta$ is the region in which the parameter yields a good fit. For this calculation, we calculate $\delta\theta$ as the θ interval, centered on the median value for θ, that encompasses 68% of the posterior probability. Table 4.8 shows our assumed priors and fit errors used to calculate the odds ratio. We compute the Bayes factor to be 0.64 and the Ockham factor to be 135, yielding an overall odds ratio that favors the one-population model over the two-population model 87 to 1.

We also consider whether some of these companion stars could be more influential than others by repeating the above calculation with only the top nine (i.e. the top half) systems in Table 4.7. In this case, the BIC comparison still favors the one-population model with a Δ BIC of 13. However, due to the smaller number of multi-stellar systems, the larger uncertainties on the model parameters for the multiple star component of the two-population model reduces the Ockham factor and yields an odds ratio of 2.6 to 1, indicating no strong preference for either model. This also shows that our angular separation cutoff choice does not affect our results. Finally, we also repeat the above analysis including all planets in each system instead of only the innermost planet and find no difference in our results.

Based on these calculations we conclude that there is no evidence for a difference in the eccentricity, mass and orbital period distributions of the inner giant planet between single and multi-stellar systems within $6''$. Notably, in Bryan et al. (2016), we searched for outer planetary-mass companions in these systems using long-term RV monitoring and found that the presence of such companions correlated with increased eccentricities for the inner planets in these systems, a difference significant at the 3σ level.

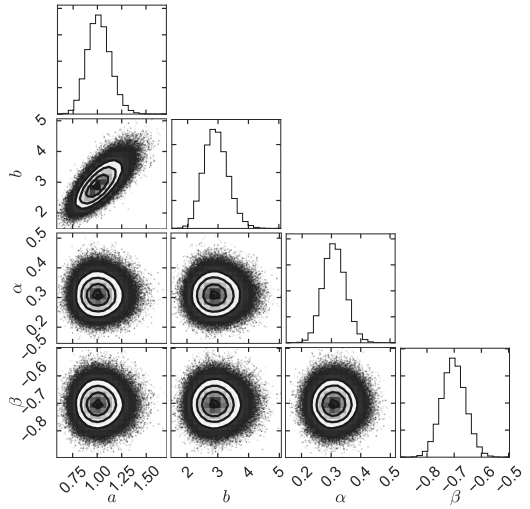

Figure 4.7: Two-dimensional posterior probability distributions on the four model parameters describing the 98 single systems and 17 multi-stellar systems as a single population of planets. The histograms represent the one-dimensional marginalized posterior probability distribution for each parameter.

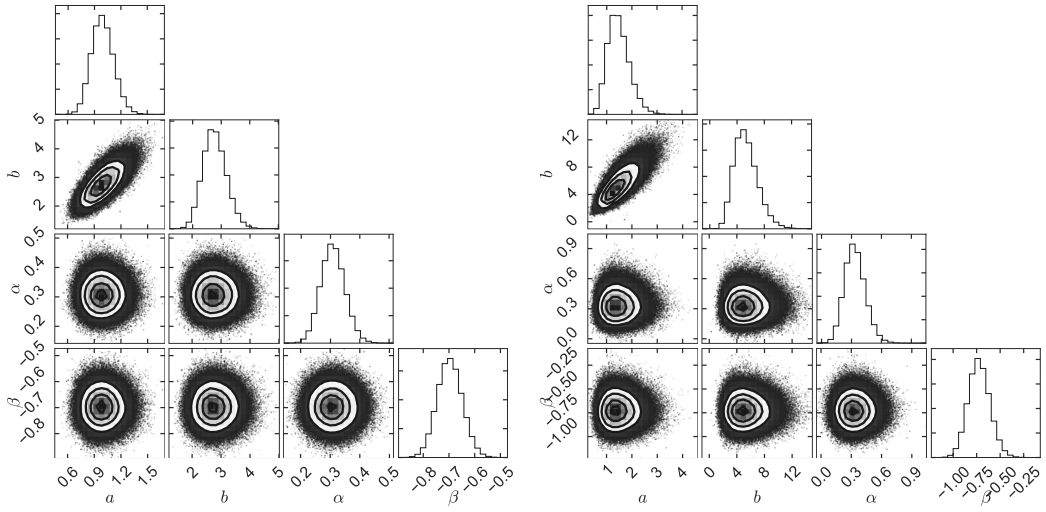

Figure 4.8: Posterior distributions on the eight model parameters describing the 98 single systems and 17 multi-stellar systems as a two distinct populations of planets. The set of plots on the left correspond to the distribution of single systems and the set on the right corresponds to multi-stellar systems. The histograms represent the one-dimensional marginalized posterior probability distribution for each parameter.

Table 4.8: Bayesian model comparison

	One-population model	Two-population model	
		single systems	multi-stellar systems
Uniform prior ranges and $\Delta\theta$			
a	(0,10), 10	(0,10), 10	(0,10), 10
b	(0,10), 10	(0,10), 10	(0,15), 15
α	(-2,2), 4	(-2,2), 4	(-2,2), 4
β	(-2,2), 4	(-2,2), 4	(-2,2), 4
Fit results and uncertainties $\delta\theta$ for all single and multi-stellar systems			
$\hat{\mathcal{L}}$	-1331	-1136	-195
N parameters	4	4	4
N systems	115	98	17
δa	0.119	0.126	0.431
δb	0.397	0.409	1.745
$\delta\alpha$	0.038	0.041	0.104
$\delta\beta$	0.044	0.048	0.114
Fit results and uncertainties $\delta\theta$ for all single and the top nine multi-stellar systems			
$\hat{\mathcal{L}}$	-1236	-1136	-97
N parameters	4	4	4
N systems	107	98	9
δa	0.125	0.125	0.852
δb	0.411	0.407	2.948
$\delta\alpha$	0.039	0.041	0.148
$\delta\beta$	0.047	0.048	0.224

Notes. Maximum likelihood, prior ranges and fit uncertainties for Bayesian model comparison of a one-population vs. two-population model of giant planets discussed in Section 4.6.

Constraining additional sub-stellar companions

For the remaining single star systems, we provide deep K-band contrast curves from our imaging campaign. The average 5-σ K_s contrast at separations of 0″.25, 0″.50, and 1″.0 are 4.96, 6.64 and 8.22, respectively. These contrasts correspond to companions with masses of 0.16, 0.09 and 0.08 solar masses, respectively, around a sun-like primary star. These upper limits on another object in a narrow field of view around these stars provide upper limits on mass and semi-major axis of any potential additional sub-stellar companions which might be detected by other techniques, such as RV (e.g. Bryan et al., 2016) or astrometry. There is a strong theoretical motivation for continued RV monitoring of these systems, as Petrovich and Tremaine (2016) present a scenario for warm and hot Jupiter formation via planet-planet interactions and predict additional giant planets at much wider separations that may be found via a long term RV survey. A recent study (Hamers, 2017) suggest that a companion star could interact with an additional planetary mass companion to induce the hot Jupiter to migrate via planetary Kozai-Lidov oscillations. Long term RV surveys (e.g. Fischer et al., 2014b; Knutson et al., 2014; Montet et al., 2014; Bryan et al., 2016) currently have RV baselines up to 25 years. Bryan et al. (2016)

report 50% completeness in their surveys for 1 Jupiter mass planets at 20 au and for 10 Jupiter mass planets at 70 au. Hamers (2017) predict Jupiter-sized planets at 40 au could cause migration. In the coming decades, RV surveys can find or rule out objects as small as a few Jupiter masses at separations up to 40 au. These published contrast curves will help constrain the masses and semimajor axes of these potential future discoveries. In the future, Gaia astrometry will reach accuracies as low as 10μas (microarcseconds) for stars with V magnitudes 7–12 and 25μas for stars with $V = 15$ (Perryman et al., 2014). This would be accurate enough to determine the mutual inclination between widely separated giant planetary companions found in transiting and RV surveys (e.g. Buhler et al., 2016) and allow for constraints on planet-planet Kozai-Lidov migration.

Astrometry of triple systems

We study six hierarchical triple systems to determine the stellar orbital architectures. In these systems, the secondary and tertiary stars (the "inner binary" orbit) are close enough that we can detect orbit motion over our survey's baseline, unlike the orbits of our widely separated binary systems. Because of the hierarchical architecture, when we consider the "outer binary" orbit, the secondary and tertiary stars behave like a single body. We fit for all the orbital parameters of both the "inner" (B and C components) and "outer" orbits (A and BC components) using the Orbits For The Impatient method (OFTI), a Bayesian rejection sampling method described in Blunt et al. (2017). As demonstrated in Rosa et al. (2015), Rameau et al. (2016), Bryan et al. (2016) and Blunt et al. (2017), OFTI calculates posterior distributions of orbital parameters that are identical to those produced by MCMC, but operates significantly faster when the input astrometry covers a short fraction of the total orbit ($< 10\%$).

OFTI generates an initial orbit with a semimajor axis a of 1 au, a position angle of nodes Ω of 0°, and other orbital parameters drawn from appropriate priors: uniform in eccentricity e, argument of periastron ω, epoch of periastron passage T_0, and uniform in $\cos(i)$ (inclination angle). System mass and distance values are drawn from Gaussian distributions with medians and standard deviations equal to the measured values and observational uncertainties, and period P is calculated from Kepler's third law. OFTI then scales a and rotates Ω to match a single observational epoch, with observational errors included by adding random values drawn from Gaussian distributions with FWHM equal to the observed uncertainties in projected separation and position angle. Finally, the orbit's probability is computed from

$p = e^{-\chi^2/2}$. This value is compared with a uniform random number in (0,1). If the chi-square probability is greater than this random number, the orbit is accepted. After many iterations of this process, probability distributions are calculated by computing histograms of the accepted sets of orbital parameters.

Table 4.9 describes the posterior distributions on the orbital inclinations of the inner (BC) and outer (ABC) orbits. One system, HD 142245, has secondary and tertiary stars with a mutual orbital plane that is misaligned with the plane of their orbit around the primary star. This misalignment is significant at the 95% confidence level. Two systems, HD 43691 and WASP-12, have well-aligned orbital planes. Out of the transiting systems where the planet's inclination is measured, KELT-4A is the only system where companion stars are misaligned with the planet at the 95% confidence level. Note that RV fits do not provide the position angle of the nodes, so we are not sensitive to any misalignment perpendicular to our line of sight. Therefore, any offset in inclination angles in RV systems represent a minimum misalignment. Figure 4.9 shows the posterior distribution on the difference between the binary inclination and the planetary inclination for the three triple star systems with transiting planets. We find that both the inner and outer binaries of these systems are no more or less likely to be aligned or misaligned with the transiting planet. The transiting planets have inclinations close to edge-on, so this implies that the outer and inner orbits favor neither an edge-on nor a face-on orbit. Although there are only three systems in our sample, it would be interesting to investigate the general distribution of $i_{ABC} - i_b$ and $i_{BC} - i_b$ with more transiting systems. Although we only discuss the inclination probability distribution here, we plot the probability contours for all seven orbital parameters for one sample system in Figure 4.10, we summarize the posteriors on all orbital elements for all triple systems in Tables 4.11 to 4.16, and we provide posterior samples of all parameters for all six triple systems online.

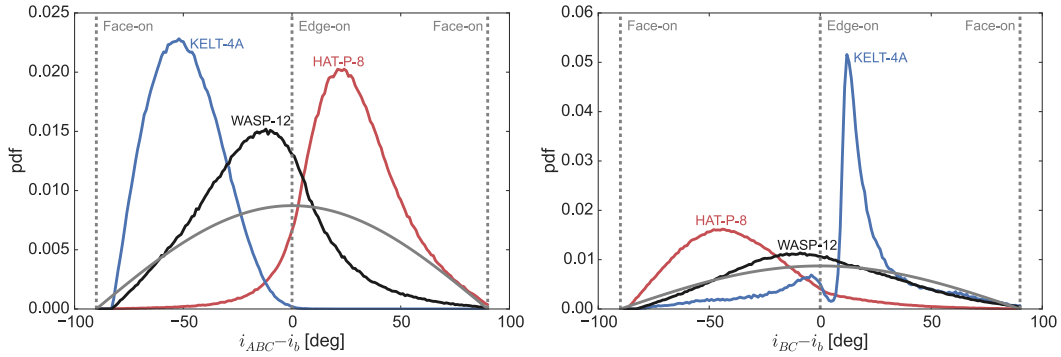

Figure 4.9: Left: Posterior distributions on the difference between the outer binary's inclination and the transiting planet's inclination. Posteriors on the outer binary's inclination are computed from OFTI while the planet's inclination comes from Latham et al. (2009), Eastman et al. (2016) and Collins et al. (2017) for HAT-P-8b, KELT-4Ab, and WASP-12b, respectively. The solid grey pdf represents the prior on Δi for an edge-on planet. Right: The same for the difference between the inner binary's inclination and the transiting planet's inclination.

Table 4.9: Orbital inclination fits of hierarchical triple systems

System	Planet inclination (deg)	Outer orbit (ABC) inclination (deg)			Inner orbit (BC) inclination (deg)		
		$i_{\mathrm{P,max}}$	68% C.I.	95% C.I.	$i_{\mathrm{P,max}}$	68% C.I.	95% C.I.
HAT-P-8	$87.5^{+1.9}_{-0.9}$	118.8	(94.8,136.3)	(69.6,161.2)	44.7	(24.9,75.6)	(9.4,118.6)
HD 43691	unknown	121.4	(131.9,163.4)	(116.4,173.9)	127.0	(131.0,162.8)	(115.2,173.6)
HD 142245	unknown	116.2	(107.3,139.7)	(97.7,162.8)	52.7	(21.8,53.9)	(8.3,64.3)
HD 207832	unknown	43.8	(18.5,53.9)	(6.8,65.0)	69.5	(54.2,75.7)	(37.7,82.6)
KELT-4A	$83.16^{+0.22}_{-0.21}$	41.2	(16.6,50.6)	(6.2,66.8)	111.0	(74.9,119.0)	(28.3,155.9)
WASP-12	$83.37^{+0.72}_{-0.64}$	76.3	(40.1,94.8)	(15.9,133.6)	84.7	(44.2,117.0)	(17.5,153.0)

Notes. The most likely value ($i_{\mathrm{P,max}}$) and 68% and 95% confidence intervals (C.I.) for orbital inclinations of the triple star systems are computed from the orbital fits described in Section 4.6. HAT-P-8, HD 142245, and KELT-4A have the orientation of the binary pair misaligned with the entire triple system. HD 43691 and WASP-12 are well aligned. HD 207832 is only marginally aligned (within the 68% confidence intervals). All of the transiting planet systems have binary companions on an orbital plane consistent with the planet's inclination at the 68% confidence interval (KELT-4A and WASP-12) or the 95% confidence interval (HAT-P-8).

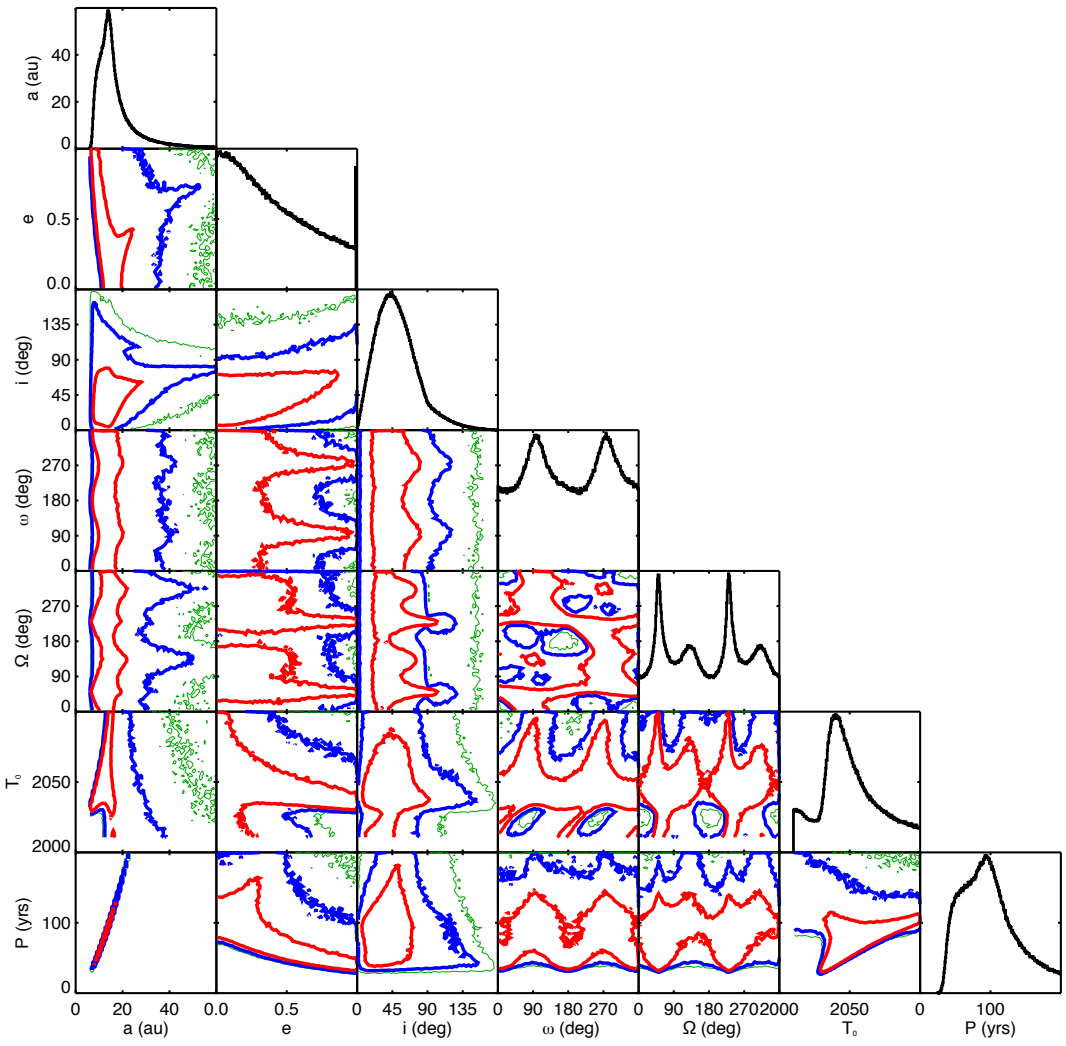

Figure 4.10: Two-dimensional probability contours for each pair of the seven OFTI-fitted orbital parameters. The red, blue and green contours represent regions containing 68%, 95% and 99.7% of the marginalized probabilities. The black histograms show the one-dimensional marginalized probability distributions for each orbital parameter. This representative set of panels are for the inner orbit of the system with the best constraints, HAT-P-8. Tables 4.11 through 4.16 summarize the fit results for this system and all triple systems.

Summary of current observational constraints on the effects of companions on giant planet formation and migration

There is a considerable body of literature focused on possible formation and migration mechanisms for hot and warm Jupiters. In this section, we review this literature and the current work to constrain these theories via surveys for planetary and stellar companions to hot and warm Jupiters. We also put the results of this work in context with these other surveys. Although there exist variations on the strict definitions of a "hot" vs a "warm" Jupiter, for brevity in this discussion, we refer to giant planets with masses greater than $0.1 M_{Jup}$ and semimajor axes less than 0.1 au as "hot" Jupiters and planets with semimajor axes between 0.1-1.0 au as "warm" Jupiters.

Possible migration mechanisms include both interactions with the protoplanetary gas disk and with other planetary or stellar companions in the system. Formation followed by gas disk migration must occur quickly, as the gas disk only survives for 1-10 million years (Pollack et al., 1996; Haisch et al., 2001; Hernández et al., 2009). This formation channel is expected to create hot Jupiters on low eccentricity orbits (e.g. Goldreich and Tremaine, 1980; Lin and Papaloizou, 1986; Tanaka et al., 2002). On the other hand, interactions such as gravitational scattering with other planets (e.g. Chatterjee et al., 2008; Wu and Lithwick, 2011; Beaugé and Nesvorný, 2012; Lithwick and Wu, 2014; Petrovich, 2015) or stars via stellar Kozai-Lidov oscillations (e.g Wu and Murray, 2003; Fabrycky and Tremaine, 2007; Naoz et al., 2012; Naoz et al., 2013; Storch et al., 2014) in the system could create hot Jupiters on more eccentric orbits.

Recent studies have used characteristics of the existing giant exoplanet population to attempt to distinguish between migration mechanisms. Dawson et al. (2015) points out a lack of high-eccentricity warm Jupiters in the *Kepler* sample, suggesting that multi-body processes are unlikely to form hot Jupiters. However, Petrovich et al. (2014) showed that planet-planet scattering at separations within 0.2 au would not excite high eccentricities. In this scenario, the giant planets could scatter off each other without creating high eccentricity warm Jupiters. Stellar Kozai-Lidov migration is expected to create misaligned hot Jupiters, but our recent stellar companion surveys (Ngo et al., 2015; Piskorz et al., 2015) find no correlation between the incidence of hot Jupiter misalignment and stellar multiplicity. In addition, we place an upper limit of 20% for systems experiencing Kozai-Lidov migration (Ngo et al., 2016). Furthermore, Schlaufman and Winn (2016) argue that a planet-planet scattering scenario for hot Jupiter migration would predict that

hot Jupiters would have fewer giant planet companions interior to the water-ice line as compared to warm Jupiters. They examined RV-detected hot and warm Jupiter systems and found that hot Jupiters are just as likely to host exterior giant planet companions as warm Jupiters. In addition, short-period giant planets found around young T Tauri stars, such as CI Tau b (Johns-Krull et al., 2016), have lifetimes too short for migration via multi-body interactions. These results disfavor high-eccentricity hot Jupiter migration and would instead suggest that disk migration or *in situ* formation scenarios are more likely for short period giant planets.

RV monitoring surveys have found that long period giant planet companions to transiting hot Jupiters (Knutson et al., 2014) and RV-detected giant planets (Bryan et al., 2016) are common. In Bryan et al. (2016), we find that 52% ± 5% of the RV giant planet systems host additional long-period planetary mass companions (5-20 au, 1-20 Jupiter masses). In addition, the gas giant planets beyond 0.1 au have, on average, higher orbital eccentricities when they have an outer companion. This finding is consistent with work by Petrovich and Tremaine (2016) showing that secular planet-planet interactions can account for most of the observed hot Jupiter population; however, these interactions fail to reproduce the known warm Jupiter planets. These types of interactions can also excite large mutual inclinations, resulting in misaligned planetary systems (e.g. see Johansen et al., 2012; Morton and Winn, 2014; Ballard and Johnson, 2016; Becker and Adams, 2016; Spalding and Batygin, 2016). Finally, these additional planets can also interact with the inner giant planets through planet-planet Kozai-Lidov effects (Dawson and Chiang, 2014).

The presence of massive planetary and/or stellar companions in these systems can also have important implications for *in situ* formation models. Some *in situ* models (e.g. Boley et al., 2016) invoke a globally enhanced disk mass or a local concentration of solids in the region of interest, both of which would affect the locations and masses of other gas giant planets formed in the same disk. Alternatively, other *in situ* models (e.g. Batygin et al., 2016) form hot Jupiters from rapid gas accretion onto super-Earth planets, which are already commonly found at short periods (Fressin et al., 2013). Batygin et al. (2016) also predict that hot Jupiters that formed *in situ* should also have additional low-mass planets with orbital periods of less than 100 days. RV surveys of known planetary systems find preliminary evidence that that hot Jupiters are more likely to host an additional companion than warm Jupiters (Bryan et al., 2016). Many theoretical studies of planet formation in binary star systems predict that the presence of a second star would be detrimental for planet forma-

tion by exciting or removing planetesimals in the protoplanetary disk (e.g. Mayer et al., 2005; Pichardo et al., 2005). Stellar companions could also eject planets after formation (e.g. Kaib et al., 2013; Zuckerman, 2014). For close (less than 50 au separation) binaries, the current observational evidence appears to support this view. Kraus et al. (2012) found that two-thirds of young stars with stellar companions within 40 au lose their protoplanetary disks within 1 million years, while systems with more distant companions have disk lifetimes that are comparable to single-star systems. In a followup study, Kraus et al. (2016) surveyed 386 *Kepler* planet host stars and showed that these stars are three times less likely to have a stellar companion within 50 au than non-planet hosting field stars. Wang et al. (2014) also came to a similar conclusion in their survey of 56 *Kepler* planet host stars.

Although current studies indicate that planet formation is suppressed in close stellar binaries, there are many examples of known planet-hosting stars in relatively wide (greater than 50 au) binaries. The two most recent directly imaged giant planet systems, 51 Eri b (Macintosh et al., 2015; Montet et al., 2015) and HD 131399 Ab (Wagner et al., 2016), are both part of hierarchical triple systems. Ngo et al. (2016) surveyed a sample of 77 transiting hot Jupiter host stars and found that 47% ± 7% of these systems have a directly imaged stellar companion. Other near-infrared diffraction-limited direct imaging surveys for stellar companions to transiting close-in giant planet systems have found companion fractions consistent with our result (Adams et al., 2013; Wöllert et al., 2015; Wöllert and Brandner, 2015; Wang et al., 2015a; Evans et al., 2016). In Ngo et al. (2016), we found that hot Jupiter host stars have fewer close-in stellar companions (projected separations less than 50 au) than field stars; however, they are three times more likely to have a wide companion star (projected separations greater than 50 au) than field stars. These companions may play some role in enhancing planet formation.

In this work, we considered the effects of stellar companions on gas giant planets at intermediate ($0.1 - 5$ au) separations. We conducted a large survey for stellar companions to RV-detected warm and cool ($a < 5$ au) Jupiters. We show that there is currently no evidence for a correlation between the incidence of a stellar companion and the gas giant planet's mass, orbital eccentricity or orbital period. This suggests that the presence or absence of a stellar companion does not significantly alter the formation or orbital evolution of gas giant planets at intermediate separations. Given the mass ratios and projected separations of the stellar companions in our sample, it seems unlikely that these companions could have induced Kozai-Lidov oscillations

in most of the systems observed. This result is consistent with the absence of increased planet eccentricities in multi-stellar systems, and lends more weight to *in situ* or planet-planet scattering theories for the formation of warm Jupiters. Our results also increase the number of known RV-planet systems with companion stars; these systems can serve as case studies for models of planet formation and migration in multiple star systems.

4.7 Summary

We carry out an AO imaging search for stellar companions around 144 stars with RV-detected giant planets. The sample is the largest survey for stellar companions around RV planet hosts to date and includes 123 stars from our previous long-term RV monitoring study (Bryan et al., 2016). We detect 11 comoving multi-stellar systems, corresponding to a raw companion fraction of 7.6% ± 2.3%. This value is consistent with other surveys for stellar companions around RV planet systems, but is much lower than the stellar companion fraction for transiting gas giant planets because of strong biases against multi-stellar systems in sample selection for RV surveys.

Three of the multi-stellar systems are presented for the first time in this work (HD 30856, HD 86081 and HD 207832). We confirm common proper motion for another three systems (HD 43691, HD 116029 and HD 164509). These six new confirmed multi-stellar RV systems increase the total number systems with known companions closer than 6″ to 22. We compare the mass, orbital eccentricity and semimajor axis distribution of the innermost planet in the multi-stellar systems with those of the innermost planet in the single star systems. Our analysis indicates that these distributions are the same for both single and multi-stellar systems. This suggests the observed stellar companions do not significantly alter the properties of the giant planet in these systems. Even when limiting our comparison to the most dynamically influential (i.e., the most massive and closest in) stellar companions, we find no evidence for any difference in the distribution of planet orbital properties. These results appear to disfavor Kozai-type migration processes, and are consistent with both *in situ* formation and planet-planet scattering.

We also compute contrast curves for all 144 surveyed targets. These provide upper limits on remaining undetected stellar and substellar companions, and can be used to constrain the masses of any additional companions found in long term RV monitoring surveys. We note that there is great value in continued RV monitoring of

these systems, as the presence or absence of more distant ($> 5 - 10$ au) planetary mass companions would provide invaluable insights into the likely formation and migration histories of these systems. Another potentially valuable study would be to obtain AO imaging data for a control sample of stars from the CPS survey which are not currently known to host planets. As in Eggenberger et al. (2007), this sample would allow us to empirically measure the selection biases against multi-stellar systems in our current planet-hosting star sample and calculate a stellar multiplicity rate for that sample that can be directly compared to that of field stars.

Finally, in our survey's hierarchical triple systems (HD 43691, HD 142245, and HD 207832), the secondary and tertiary stellar components are on very tight orbits (less than 10 au), so it is possible to measure orbital motion over the several year baseline of our survey. We fit orbital parameters for all three stars in these three triple systems as well as three additional triple systems from transiting planet surveys. We show that these orbital fits allow us to constrain the geometry of the triple system (e.g. edge-on or face-on), which has implications for the dynamical evolution of the planet orbits in these systems.

4.8 Acknowledgments

We would like to thank John A. Johnson, Christopher Spalding and Benjamin Montet for helpful discussions. We also appreciate the useful suggestions from the anonymous referee and the statistics editor. This work was supported by NASA grant NNX14AD24G. HN is grateful for funding support from the Natural Sciences and Engineering Research Council of Canada and the NASA Earth and Space Science Fellowship Program grant NNX15AR12H. HAK acknowledges support from the Sloan Foundation. ELN and SCB are supported by NASA grant NNX14AJ80G.

This work was based on observations at the W. M. Keck Observatory granted by the California Institute of Technology. We thank the observers who contributed to the measurements reported here and acknowledge the efforts of the Keck Observatory staff. We extend special thanks to those of Hawaiian ancestry on whose sacred mountain of Mauna Kea we are privileged to be guests.

Facilities: Keck:II

Software: Astropy (The Astropy Collaboration et al., 2013), OFTI (Blunt et al., 2017), emcee (Foreman-Mackey et al., 2013), corner.py (Foreman-Mackey, 2016)

4.9 Supplementary data

Contrast curves

We make the 5σ contrast curves for all 144 targets in this chapter available in the comma-separated value (CSV) format as part of the supplementary information of the online publication of Ngo et al. (2017). Table 4.10 shows sample lines of this large table.

Table 4.10: Contrast curves for all targets

Star	Bandpass	Date	Separation (arcsec)	5σ contrast (magnitudes)	Directional completeness
GJ 317	Kc	2014-11-07	0.154	2.87	100.0
			0.252	4.52	100.0
			0.350	5.53	100.0
			0.449	6.33	100.0
			...	...	...
GJ-433	Kc	2015-01-09	0.154	3.07	100.0
			0.251	4.90	100.0
			0.350	5.77	100.0
			0.449	6.52	100.0
			...	...	...
...	...	...	...	...	...

Notes. Best 5σ contrast curve for each target in the indicated bandpass. The full table is available with the online publication of Ngo et al. (2017).

OFTI orbit fits

The full orbit fit results from Section 4.6 are described in this appendix section. Figure 4.10 displays the two-dimensional probability distribution for the orbital parameters of one typical system. Tables 4.11 through 4.16 summarize the fit results for each system. Samples of the posteriors for all fit parameters for all systems are available in FITS format as part of the supplementary information of the online publication of Ngo et al. (2017).

Table 4.11: OFTI fit summary for triple system HAT-P-8

x	Median	$x_{\chi^2,\min}$	$x_{\mathrm{P,max}}$	68% C.I.	95% C.I.	99.7% C.I.
Outer orbit (min χ^2 = 25.701, χ^2 at highest probability = 25.854)						
a (au)	241.9	178.7	111.5	(160.2,491.4)	(128.3,1713.3)	(112.9,8324.6)
e	0.582	0.413	0.832	(0.210,0.868)	(0.031,0.980)	(0.002,0.990)
i (deg)	113.4	115.3	118.8	(94.8,136.3)	(69.6,161.2)	(25.6,175.2)
ω (deg)	91.3	162.6	22.4	(36.4,144.3)	(5.5,174.6)	(0.3,179.7)
Ω (deg)	128.5	134.4	327.8	(50.6,148.8)	(6.8,173.7)	(0.4,179.6)
T_0 (yr)	3312	2892	2556	(2687,6377)	(2393,30869)	(2035,325732)
P (yr)	3091	1916	942	(1665,8956)	(1191,58222)	(978,625040)
Inner orbit (min χ^2 = 0.320, χ^2 at highest probability = 0.787)						
a (au)	14.9	15.8	9.3	(10.5,25.3)	(7.9,73.4)	(6.8,366.7)
e	0.347	0.193	0.457	(0.098,0.728)	(0.014,0.955)	(0.001,0.990)
i (deg)	47.7	3.5	44.7	(24.9,75.6)	(9.4,118.6)	(2.3,160.5)
ω (deg)	94.2	242.9	288.4	(34.9,147.6)	(4.9,175.1)	(0.3,179.7)
Ω (deg)	80.3	326.6	93.4	(39.2,143.0)	(6.7,173.4)	(0.4,179.6)
T_0 (yr)	2056	2010	2034	(2035,2135)	(2014,2603)	(2010,8439)
P (yr)	105	116	52	(63,234)	(41,1159)	(32,12930)

Notes. Summary of the posteriors from OFTI orbit fitting (see Section 4.6) for this triple system's outer and inner orbits. For each parameter, we show the median value, the value with the lowest χ^2 ($x_{\chi^2,\min}$), the most likely value ($x_{\mathrm{P,max}}$) and three confidence intervals (C.I.).

Table 4.12: OFTI fit summary for triple system HD 43691

x	Median	$x_{\chi^2,\min}$	$x_{\mathrm{P,max}}$	68% C.I.	95% C.I.	99.7% C.I.
Outer orbit (min χ^2 = 7.089, χ^2 at highest probability = 7.444)						
a (au)	452.1	401.5	162.2	(341.5,709.3)	(254.5,1547.9)	(190.4,4882.8)
e	0.229	0.169	0.312	(0.068,0.474)	(0.010,0.730)	(0.001,0.909)
i (deg)	148.3	165.0	121.4	(131.9,163.4)	(116.4,173.9)	(103.1,178.5)
ω (deg)	92.0	143.5	223.4	(28.4,152.4)	(4.0,176.0)	(0.2,179.8)
Ω (deg)	98.3	210.6	49.3	(28.9,153.5)	(4.1,175.9)	(0.2,179.7)
T_0 (yr)	5071	8249	3059	(2930,11372)	(2130,34638)	(2017,187612)
P (yr)	7518	6569	1649	(4935,14775)	(3172,47655)	(2050,266357)
Inner orbit (min χ^2 = 2.256, χ^2 at highest probability = 2.974)						
a (au)	11.2	16.6	7.2	(8.5,17.9)	(6.5,39.8)	(5.0,127.7)
e	0.214	0.333	0.310	(0.064,0.456)	(0.009,0.727)	(0.001,0.910)
i (deg)	147.4	119.8	127.0	(131.0,162.8)	(115.2,173.6)	(102.3,178.5)
ω (deg)	79.1	148.6	256.2	(25.6,148.7)	(3.9,176.0)	(0.2,179.8)
Ω (deg)	79.7	278.9	272.8	(33.1,128.8)	(5.9,173.4)	(0.4,179.6)
T_0 (yr)	2029	2027	2032	(2018,2056)	(2012,2172)	(2010,2952)
P (yr)	74	138	39	(49,151)	(33,499)	(22,2863)

Notes. Summary of the posteriors from OFTI orbit fitting (see Section 4.6) for this triple system's outer and inner orbits. For each parameter, we show the median value, the value with the lowest χ^2 ($x_{\chi^2,\min}$), the most likely value ($x_{\mathrm{P,max}}$) and three confidence intervals (C.I.).

Table 4.13: OFTI fit summary for triple system HD 142245

x	Median	$x_{\chi^2,\min}$	$x_{\mathrm{P,max}}$	68% C.I.	95% C.I.	99.7% C.I.
Outer orbit (min χ^2 = 21.154, χ^2 at highest probability = 21.337)						
a (au)	273.2	309.5	111.9	(182.0,556.9)	(140.6,1694.7)	(115.1,6011.4)
e	0.543	0.568	0.711	(0.211,0.785)	(0.032,0.918)	(0.002,0.982)
i (deg)	120.4	118.3	116.2	(107.3,139.7)	(97.7,162.8)	(91.6,175.7)
ω (deg)	85.8	268.6	161.2	(38.4,139.8)	(6.0,173.9)	(0.4,179.6)
Ω (deg)	91.3	207.6	163.9	(24.2,168.6)	(2.5,177.8)	(0.1,179.9)
T_0 (yr)	3060	4428	2312	(2573,5746)	(2343,23231)	(2034,167483)
P (yr)	2747	3351	712	(1493,8005)	(1012,42425)	(749,285552)
Inner orbit (min χ^2 = 6.811, χ^2 at highest probability = 8.294)						
a (au)	6.4	44.1	5.1	(5.1,8.7)	(4.4,15.1)	(3.9,43.0)
e	0.440	0.924	0.705	(0.210,0.619)	(0.033,0.774)	(0.002,0.897)
i (deg)	39.5	64.5	52.7	(21.8,53.9)	(8.3,64.3)	(1.9,74.6)
ω (deg)	97.2	133.8	90.1	(38.9,145.9)	(5.5,174.5)	(0.4,179.6)
Ω (deg)	75.5	33.4	15.0	(37.3,115.6)	(7.7,170.7)	(0.5,179.5)
T_0 (yr)	2012	2013	2012	(2011,2021)	(2010,2030)	(2010,2060)
P (yr)	16	289	11	(11,25)	(9,58)	(8,279)

Notes. Summary of the posteriors from OFTI orbit fitting (see Section 4.6) for this triple system's outer and inner orbits. For each parameter, we show the median value, the value with the lowest χ^2 ($x_{\chi^2,\min}$), the most likely value ($x_{\mathrm{P,max}}$) and three confidence intervals (C.I.).

Table 4.14: OFTI fit summary for triple system HD 207832

x	Median	$x_{\chi^2,\min}$	$x_{\mathrm{P,max}}$	68% C.I.	95% C.I.	99.7% C.I.
Outer orbit (min χ^2 = 3.760, χ^2 at highest probability = 4.301)						
a (au)	171.5	158.0	60.8	(116.4,299.0)	(86.9,684.2)	(68.8,2131.0)
e	0.713	0.701	0.680	(0.567,0.809)	(0.359,0.900)	(0.122,0.966)
i (deg)	36.2	30.6	43.8	(18.5,53.9)	(6.8,65.0)	(1.6,72.1)
ω (deg)	64.0	232.3	20.4	(23.1,133.7)	(4.0,175.8)	(0.3,179.8)
Ω (deg)	67.9	229.8	42.1	(41.3,104.3)	(9.9,168.0)	(0.7,179.4)
T_0 (yr)	3925	3765	2357	(3007,6644)	(2604,18356)	(2057,92862)
P (yr)	2083	1900	456	(1159,4821)	(743,16659)	(522,91976)
Inner orbit (min χ^2 = 7.067, χ^2 at highest probability = 7.376)						
a (au)	6.7	21.9	5.0	(4.5,12.1)	(3.4,26.3)	(2.8,81.1)
e	0.305	0.538	0.597	(0.093,0.613)	(0.013,0.847)	(0.001,0.958)
i (deg)	65.9	75.5	69.5	(54.2,75.7)	(37.7,82.6)	(15.2,87.5)
ω (deg)	61.2	204.7	63.1	(28.1,141.0)	(4.8,175.1)	(0.3,179.7)
Ω (deg)	105.2	285.3	275.9	(89.9,120.8)	(50.6,135.9)	(7.8,170.0)
T_0 (yr)	2026	2236	2024	(2019,2051)	(2011,2160)	(2010,2852)
P (yr)	39	231	25	(22,95)	(14,302)	(10,1639)

Notes. Summary of the posteriors from OFTI orbit fitting (see Section 4.6) for this triple system's outer and inner orbits. For each parameter, we show the median value, the value with the lowest χ^2 ($x_{\chi^2,\min}$), the most likely value ($x_{\mathrm{P,max}}$) and three confidence intervals (C.I.).

Table 4.15: OFTI fit summary for triple system KELT-4A

x	Median	$x_{\chi^2,\min}$	$x_{\mathrm{P,max}}$	68% C.I.	95% C.I.	99.7% C.I.
Outer orbit (min χ^2 = 0.039, χ^2 at highest probability = 0.900)						
a (au)	425.1	478.9	369.1	(312.4,725.5)	(239.2,1657.8)	(193.5,5227.0)
e	0.406	0.561	0.229	(0.145,0.660)	(0.021,0.846)	(0.001,0.951)
i (deg)	32.7	5.8	41.2	(16.6,50.6)	(6.2,66.8)	(1.4,80.3)
ω (deg)	89.0	63.3	289.7	(29.0,150.8)	(4.2,175.8)	(0.3,179.7)
Ω (deg)	114.7	41.8	169.8	(18.9,163.6)	(2.5,177.6)	(0.1,179.9)
T_0 (yr)	2683	2408	2501	(2421,3736)	(2122,12556)	(2018,70154)
P (yr)	5467	6377	4279	(3443,12198)	(2304,42183)	(1673,236009)
Inner orbit (min χ^2 = 0.001, χ^2 at highest probability = 0.180))						
a (au)	7.4	7.9	4.6	(5.5,12.5)	(4.7,27.8)	(4.2,85.2)
e	0.865	0.460	0.894	(0.568,0.969)	(0.335,0.990)	(0.135,0.990)
i (deg)	97.8	96.1	111.0	(74.9,119.0)	(28.3,155.9)	(6.9,174.1)
ω (deg)	48.8	16.8	1.8	(13.7,163.9)	(2.0,178.0)	(0.1,179.9)
Ω (deg)	109.5	106.5	113.1	(89.5,127.8)	(44.7,151.1)	(2.5,177.6)
T_0 (yr)	2012	2010	2012	(2011,2013)	(2010,2053)	(2010,2318)
P (yr)	19	21	9	(12,42)	(9,138)	(8,739)

Notes. Summary of the posteriors from OFTI orbit fitting (see Section 4.6) for this triple system's outer and inner orbits. For each parameter, we show the median value, the value with the lowest χ^2 ($x_{\chi^2,\min}$), the most likely value ($x_{\mathrm{P,max}}$) and three confidence intervals (C.I.).

Table 4.16: OFTI fit summary for triple system WASP-12

x	Median	$x_{\chi^2,\min}$	$x_{\mathrm{P,max}}$	68% C.I.	95% C.I.	99.7% C.I.
Outer orbit (min χ^2 = 19.894, χ^2 at highest probability = 20.116)						
a (au)	512.6	432.2	122.0	(322.7,990.3)	(222.8,2992.2)	(155.2,13293.9)
e	0.531	0.202	0.858	(0.173,0.856)	(0.025,0.980)	(0.001,0.990)
i (deg)	67.9	74.6	76.3	(40.1,94.8)	(15.9,133.6)	(3.9,167.0)
ω (deg)	92.4	141.6	344.8	(32.5,148.9)	(4.7,175.4)	(0.3,179.7)
Ω (deg)	73.8	69.4	72.8	(46.9,126.8)	(8.3,171.7)	(0.5,179.5)
T_0 (yr)	5230	7474	2409	(3412,12532)	(2609,57434)	(2051,530896)
P (yr)	7364	5874	811	(3675,19784)	(2102,103755)	(1219,967232)
Inner orbit (min χ^2 = 0.106, χ^2 at highest probability = 0.600))						
a (au)	40.7	30.5	11.2	(25.8,79.3)	(18.0,251.4)	(12.9,1166.0)
e	0.521	0.736	0.976	(0.169,0.853)	(0.024,0.979)	(0.001,0.990)
i (deg)	77.9	64.7	84.7	(44.2,117.0)	(17.5,153.0)	(4.4,173.2)
ω (deg)	99.1	299.5	194.0	(35.9,148.4)	(5.1,175.0)	(0.3,179.7)
Ω (deg)	128.6	19.2	164.8	(26.5,167.9)	(2.8,177.5)	(0.2,179.8)
T_0 (yr)	2131	2086	2034	(2068,2374)	(2032,4005)	(2011,22015)
P (yr)	245	158	35	(124,666)	(72,3764)	(43,37519)

Notes. Summary of the posteriors from OFTI orbit fitting (see Section 4.6) for this triple system's outer and inner orbits. For each parameter, we show the median value, the value with the lowest χ^2 ($x_{\chi^2,\min}$), the most likely value ($x_{\mathrm{P,max}}$) and three confidence intervals (C.I.).

References

Adams, E. R., A. K. Dupree, C. Kulesa, and D. McCarthy (2013). *The Astronomical Journal* **146**, 9. DOI: 10.1088/0004-6256/146/1/9.

Allen, C., A. Poveda, and M. A. Herrera (2000). *Astronomy & Astrophysics* **356**, 529.

Ballard, S. and J. A. Johnson (2016). *The Astrophysical Journal* **816**, 66. DOI: 10.3847/0004-637X/816/2/66.

Baraffe, I., G. Chabrier, F. Allard, and P. H. Hauschildt (1998). *Astronomy & Astrophysics* **412**, 403.

Batygin, K., P. H. Bodenheimer, and G. P. Laughlin (2016). *The Astrophysical Journal* **829**.2, 114. DOI: 10.3847/0004-637X/829/2/114.

Bean, J. L., B. E. McArthur, G. F. Benedict, et al. (2007). *The Astronomical Journal* **134**, 749.

Beaugé, C. and D. Nesvorný (2012). *The Astrophysical Journal* **751**, 119. DOI: 10.1088/0004-637X/751/2/119.

Bechter, E. B., J. R. Crepp, H. Ngo, et al. (2014). *The Astrophysical Journal* **788**, 2. DOI: 10.1088/0004-637X/788/1/2.

Becker, J. C. and F. C. Adams (2016). *Monthly Notices of the Royal Astronomical Society* **455**, 2980. DOI: 10.1093/mnras/stv2444.

Bergfors, C., W. Brandner, S. Daemgen, et al. (2013). *Monthly Notices of the Royal Astronomical Society* **428**, 182. DOI: 10.1093/mnras/sts019.

Blunt, S. C., E. Nielsen, R. J. De Rosa, et al. (2017). *Astronomical Journal* **229**. arXiv: 1703.10653.

Bodenheimer, P., O. Hubickyj, and J. J. Lissauer (2000). *Icarus* **143**, 2. DOI: 10.1006/icar.1999.6246.

Boley, A. C., A. P. G. Contreras, and B. Gladman (2016). *The Astrophysical Journal* **817**, L17. DOI: 10.3847/2041-8205/817/2/L17.

Borsa, F., G. Scandariato, M. Rainer, et al. (2015). *Astronomy & Astrophysics* **578**, A64. DOI: 10.1051/0004-6361/201525741.

Bowler, B. P. (2016). *Publications of the Astronomical Society of the Pacific* **128**.968, 102001. DOI: 10.1088/1538-3873/128/968/102001.

Brogi, M., I. A. G. Snellen, R. J. de Kok, et al. (2012). *Nature* **486**, 502. DOI: 10.1038/nature11161.

Bryan, M. L., H. A. Knutson, A. W. Howard, et al. (2016). *The Astrophysical Journal* **821**, 89. DOI: 10.3847/0004-637X/821/2/89.

Buhler, P. B., H. A. Knutson, K. Batygin, et al. (2016). *The Astrophysical Journal* **821**, 26. DOI: 10.3847/0004-637X/821/1/26.

Butler, R. P., J. T. Wright, G. W. Marcy, et al. (2006). *The Astrophysical Journal* **646**, 505. DOI: 10.1086/504701.

Chatterjee, S., E. B. Ford, S. Matsumura, and F. A. Rasio (2008). *The Astrophysical Journal* **686**, 580. DOI: 10.1086/590227.

Clanton, C. and B. S. Gaudi (2014). *The Astrophysical Journal* **791**, 91. DOI: 10.1088/0004-637X/791/2/91.

Collins, K. A., J. F. Kielkopf, and K. G. Stassun (2017). *The Astronomical Journal* **153**, 78. DOI: 10.3847/1538-3881/153/2/78.

Cumming, A., R. P. Butler, G. W. Marcy, et al. (2008). *The Publications of the Astronomical Society of the Pacific* **120**, 531. DOI: 10.1086/588487.

Da Silva, R., S. Udry, F. Bouchy, et al. (2007). *Astronomy and Astrophysics* **473**, 323. DOI: 10.1051/0004-6361:20077314.

Dawson, R. I. and E. Chiang (2014). *Science (New York, N.Y.)* **346**, 212–216. DOI: 10.1126/science.1256943.

Dawson, R. I., R. A. Murray-Clay, and J. A. Johnson (2015). *The Astrophysical Journal* **798**, 66. DOI: 10.1088/0004-637X/798/2/66.

Desidera, S., E. Carolo, R. Gratton, et al. (2011). *Astronomy & Astrophysics* **533**, A90. DOI: 10.1051/0004-6361/201117191.

Duquennoy, A. and M. Mayor (1991). *Astronomy & Astrophysics* **248**, 485.

Eastman, J. D., T. G. Beatty, R. J. Siverd, et al. (2016). *The Astronomical Journal* **151**, 45. DOI: 10.3847/0004-6256/151/2/45.

Eggenberger, A., S. Udry, G. Chauvin, et al. (2007). *Astronomy and Astrophysics* **474**, 273. DOI: 10.1051/0004-6361:20077447.

Eggenberger, A., S. Udry, and M. Mayor (2004). *Astronomy & Astrophysics* **417**, 9. DOI: 10.1051/0004-6361:20034164.

Evans, D. F., J. Southworth, P. F. L. Maxted, et al. (2016). *Astronomy & Astrophysics* **589**, A58. DOI: 10.1051/0004-6361/201527970.

Fabrycky, D. and S. Tremaine (2007). *The Astrophysical Journal* **669**, 1298. DOI: 10.1086/521702.

Fischer, D. A., A. W. Howard, G. P. Laughlin, et al. (2014a). *Protostars and Planets VI*. Ed. by H. Beuther, R. S. Klessen, C. P. Dullemond, and T. Henning. University of Arizona Press, pp. 715–737. DOI: 10.2458/azu_uapress_9780816531240-ch031.

Fischer, D. A., G. W. Marcy, R. P. Butler, S. S. Vogt, and K. Apps (1999). *Publications of the Astronomical Society of the Pacific* **111**, 50. DOI: 10.1086/316304.

Fischer, D. A., G. W. Marcy, and J. F. P. Spronck (2014b). *The Astrophysical Journal Supplement Series* **210**, 5. DOI: 10.1088/0067-0049/210/1/5.

Foreman-Mackey, D. (2016). *The Journal of Open Source Software* **24**.2, 1. DOI: 10.21105/joss.00024.

Foreman-Mackey, D., D. W. Hogg, D. Lang, and J. Goodman (2013). *Publications of the Astronomical Society of the Pacific* **125**, 306. DOI: 10.1086/670067.

Fressin, F., G. Torres, D. Charbonneau, et al. (2013). *The Astrophysical Journal* **766**, 81. DOI: 10.1088/0004-637X/766/2/81.

Ghezzi, L., K. Cunha, V. V. Smith, et al. (2010). *The Astrophysical Journal* **720**, 1290. DOI: 10.1088/0004-637X/720/2/1290.

Giguere, M. J., D. A. Fischer, A. W. Howard, et al. (2012). *The Astrophysical Journal* **744**, 4. DOI: 10.1088/0004-637X/744/1/4.

Ginski, C., M. Mugrauer, M. Seeliger, and T. Eisenbeiss (2012). *Monthly Notices of the Royal Astronomical Society* **421**, 2498. DOI: 10.1111/j.1365-2966.2012.20485.x.

Ginski, C., M. Mugrauer, M. Seeliger, and T. Löhne (2013). *Astronomy & Astrophysics* **559**, A71. DOI: 10.1051/0004-6361/201322274.

Ginski, C., M. Mugrauer, M. Seeliger, et al. (2016). *Monthly Notices of the Royal Astronomical Society* **457**, 2173. DOI: 10.1093/mnras/stw049.

Goldreich, P. and S. Tremaine (1980). *The Astrophysical Journal* **241**, 425. DOI: 10.1086/158356.

Haghighipour, N., R. P. Butler, E. J. Rivera, G. W. Henry, and S. S. Vogt (2012). *The Astrophysical Journal* **756**, 91. DOI: 10.1088/0004-637X/756/1/91.

Haisch, K., E. Lada, and C. Lada (2001). *The Astronomical Journal* **553**, L153–L156. DOI: 10.1086/320685.

Hamers, A. S. (2017). *The Astrophysical Journal* **835**, L24. DOI: 10.3847/2041-8213/835/2/L24.

Han, I., B. C. Lee, K. M. Kim, et al. (2010). *Astronomy and Astrophysics* **509**, A24. DOI: 10.1051/0004-6361/200912536.

Hernández, J., N. Calvet, L. Hartmann, et al. (2009). *The Astrophysical Journal* **707**, 705. DOI: 10.1088/0004-637X/707/1/705.

Howard, A. W., J. A. Johnson, G. W. Marcy, et al. (2010). *The Astrophysical Journal* **721**, 1467. DOI: 10.1088/0004-637X/721/2/1467.

Husser, T.-O., S. Wende-von Berg, S. Dreizler, et al. (2013). *Astronomy & Astrophysics* **553**, A6. DOI: 10.1051/0004-6361/201219058.

Jofré, E., R. Petrucci, C. Saffe, et al. (2015). *Astronomy & Astrophysics* **574**, A50. DOI: 10.1051/0004-6361/201424474.

Johansen, A., M. B. Davies, R. P. Church, and V. Holmelin (2012). *The Astrophysical Journal* **758**.1, 39. DOI: 10.1088/0004-637X/758/1/39.

Johns-Krull, C. M., J. N. McLane, L. Prato, et al. (2016). *The Astrophysical Journal* **826**, 206. DOI: 10.3847/0004-637X/826/2/206.

Johnson, J. A., C. Clanton, A. W. Howard, et al. (2011). *The Astrophysical Journal Supplement Series* **197**, 26. DOI: 10.1088/0067-0049/197/2/26.

Johnson, J. A., G. W. Marcy, D. A. Fischer, et al. (2006). *The Astrophysical Journal* **647**.1, 600–611. DOI: 10.1086/505173.

Kaib, N. A., S. N. Raymond, and M. Duncan (2013). *Nature* **493**, 381. DOI: 10.1038/nature11780.

Kass, R. E. and A. E. Raftery (1995). *Journal of the American Statistical Association* **90**, 773. DOI: 10.2307/2291091.

Kipping, D. M. (2013). *Monthly Notices of the Royal Astronomical Society: Letters* **434**, L51. DOI: 10.1093/mnrasl/slt075.

Knutson, H. A., B. J. Fulton, B. T. Montet, et al. (2014). *The Astrophysical Journal* **785**, 126. DOI: 10.1088/0004-637X/785/2/126.

Kraus, A. L., M. J. Ireland, L. A. Hillenbrand, and F. Martinache (2012). *The Astrophysical Journal* **745**, 19. DOI: 10.1088/0004-637X/745/1/19.

Kraus, A. L., M. J. Ireland, D. Huber, A. W. Mann, and T. J. Dupuy (2016). *The Astronomical Journal* **152**.1, 8. DOI: 10.3847/0004-6256/152/1/8.

Lagrange, A.-M., M. Desort, F. Galland, S. Udry, and M. Mayor (2009). *Astronomy and Astrophysics* **495**, 335. DOI: 10.1051/0004-6361:200810105.

Latham, D. W., G. Á. Bakos, G. Torres, et al. (2009). *The Astrophysical Journal* **704**, 1107. DOI: 10.1088/0004-637X/704/2/1107.

Leeuwen, F. van (2007). *Astronomy and Astrophysics* **474**, 653. DOI: 10.1051/0004-6361:20078357.

Lin, D. N. C., P. Bodenheimer, and D. C. Richardson (1996). *Nature* **380**, 606. DOI: 10.1038/380606a0.

Lin, D. N. C. and J. Papaloizou (1986). *The Astrophysical Journal* **309**, 846. DOI: 10.1086/164653.

Lithwick, Y. and Y. Wu (2014). *Proceedings of the National Academy of Sciences of the United States of America* **111**, 12610. DOI: 10.1073/pnas.1308261110.

Lodieu, N., A. Pérez-Garrido, V. J. S. Béjar, et al. (2014). *Astronomy & Astrophysics* **569**, A120. DOI: 10.1051/0004-6361/201424210.

Ma, B., J. Ge, A. Wolszczan, et al. (2016). *The Astronomical Journal* **152**, 112. DOI: 10.3847/0004-6256/152/5/112.

Macintosh, B., J. R. Graham, T. Barman, et al. (2015). *Science* **350**, 64. DOI: 10.1126/science.aac5891.

Mancini, L., J. Southworth, S. Ciceri, et al. (2013). *Astronomy & Astrophysics* **551**, A11. DOI: 10.1051/0004-6361/201220291.

Mason, B. D., W. I. Hartkopf, G. L. Wycoff, et al. (2004). *The Astronomical Journal* **128**, 3012. DOI: 10.1086/425532.

Mason, B. D., G. L. Wycoff, W. I. Hartkopf, G. G. Douglass, and C. E. Worley (2001). *The Astronomical Journal* **122**, 3466. DOI: 10.1086/323920.

Mayer, L., J. Wadsley, T. Quinn, and J. Stadel (2005). *Monthly Notices of the Royal Astronomical Society* **363**, 641. DOI: 10.1111/j.1365-2966.2005.09468.x.

Meschiari, S., G. Laughlin, S. S. Vogt, et al. (2011). *The Astrophysical Journal* **727**, 117. DOI: 10.1088/0004-637X/727/2/117.

Montet, B. T., B. P. Bowler, E. L. Shkolnik, et al. (2015). *The Astrophysical Journal* **813**, L11. DOI: 10.1088/2041-8205/813/1/L11.

Montet, B. T., J. R. Crepp, J. A. Johnson, A. W. Howard, and G. W. Marcy (2014). *The Astrophysical Journal* **781**, 28. DOI: 10.1088/0004-637X/781/1/28.

Morton, T. D. and J. N. Winn (2014). *The Astrophysical Journal* **796**, 47. DOI: 10.1088/0004-637X/796/1/47.

Moutou, C., B. Loeillet, F. Bouchy, et al. (2006). *Astronomy and Astrophysics* **458**, 327. DOI: 10.1051/0004-6361:20066029.

Moutou, C., M. Mayor, F. Bouchy, et al. (2005). *Astronomy and Astrophysics* **439**, 367. DOI: 10.1051/0004-6361:20052826.

Moutou, C., M. Mayor, G. Lo Curto, et al. (2011). *Astronomy & Astrophysics* **527**, A63. DOI: 10.1051/0004-6361/201015371.

Mugrauer, M. and C. Ginski (2015). *Monthly Notices of the Royal Astronomical Society* **450**, 3127. DOI: 10.1093/mnras/stv771.

Mulders, G. D., I. Pascucci, and D. Apai (2015). *The Astrophysical Journal* **814**, 130. DOI: 10.1088/0004-637X/814/2/130.

Naoz, S., W. M. Farr, Y. Lithwick, F. A. Rasio, and J. Teyssandier (2013). *Monthly Notices of the Royal Astronomical Society* **431**, 2155. DOI: 10.1093/mnras/stt302.

Naoz, S., W. M. Farr, and F. A. Rasio (2012). *The Astrophysical Journal* **754**, L36. DOI: 10.1088/2041-8205/754/2/L36.

Ngo, H., H. A. Knutson, M. L. Bryan, et al. (2017). *Astronomical Journal* **153**, 242. DOI: 10.3847/1538-3881/aa6cac.

Ngo, H., H. A. Knutson, S. Hinkley, et al. (2015). *The Astrophysical Journal* **800**, 138. DOI: 10.1088/0004-637X/800/2/138.

Ngo, H., H. A. Knutson, S. Hinkley, et al. (2016). *The Astrophysical Journal* **827**, 8. DOI: 10.3847/0004-637X/827/1/8.

Patience, J., R. J. White, A. M. Ghez, et al. (2002). *The Astrophysical Journal* **581**, 654–665. DOI: 10.1086/342982.

Peek, K. M. G., J. A. Johnson, D. A. Fischer, et al. (2009). *Publications of the Astronomical Society of the Pacific* **121**.880, 613–620. DOI: 10.1086/599862.

Perryman, M. A. C., L. Lindegren, J. Kovalevsky, et al. (1997). *Astronomy and Astrophysics* **323**, L49.

Perryman, M., J. Hartman, G. Á. Bakos, and L. Lindegren (2014). *The Astrophysical Journal* **797**.1, 14. DOI: 10.1088/0004-637X/797/1/14.

Petrovich, C. (2015). *The Astrophysical Journal* **805**, 75. DOI: 10.1088/0004-637X/805/1/75.

Petrovich, C. and S. Tremaine (2016). *The Astrophysical Journal* **829**, 132. DOI: 10.3847/0004-637X/829/2/132.

Petrovich, C., S. Tremaine, and R. Rafikov (2014). *The Astrophysical Journal* **786**, 101. DOI: 10.1088/0004-637X/786/2/101.

Pichardo, B., L. S. Sparke, and L. A. Aguilar (2005). *Monthly Notices of the Royal Astronomical Society* **359**, 521. DOI: 10.1111/j.1365-2966.2005.08905.x.

Piskorz, D., H. A. Knutson, H. Ngo, et al. (2015). *The Astrophysical Journal* **814**, 148. DOI: 10.1088/0004-637X/814/2/148.

Pollack, J. B., O. Hubickyj, P. Bodenheimer, et al. (1996). *Icarus* **124**.1, 62–85. DOI: 10.1006/icar.1996.0190.

Raghavan, D., T. J. Henry, B. D. Mason, et al. (2006). *The Astrophysical Journal* **646**, 523–542. DOI: 10.1086/504823.

Raghavan, D., H. A. McAlister, T. J. Henry, et al. (2010). *The Astrophysical Journal Supplement Series* **190**, 1. DOI: 10.1088/0067-0049/190/1/1.

Rameau, J., E. L. Nielsen, R. J. D. Rosa, et al. (2016). *The Astrophysical Journal* **822**, L29. DOI: 10.3847/2041-8205/822/2/L29.

Roberts, L. C., R. Oppenheimer, J. R. Crepp, et al. (2015). *The Astronomical Journal* **150**, 6. DOI: 10.1088/0004-6256/150/4/103.

Roberts, L. C., N. H. Turner, T. A. ten Brummelaar, B. D. Mason, and W. I. Hartkopf (2011). *The Astronomical Journal* **142**.5, 175. DOI: 10.1088/0004-6256/142/5/175.

Rosa, R. J. de, E. L. Nielsen, S. C. Blunt, et al. (2015). *The Astrophysical Journal* **814**, L3. DOI: 10.1088/2041-8205/814/1/L3.

Sahlmann, J., D. Ségransan, D. Queloz, et al. (2011). *Astronomy & Astrophysics* **525**, A95. DOI: 10.1051/0004-6361/201015427.

Santos, N. C., G. Israelian, and M. Mayor (2004). *Astronomy and Astrophysics* **415**, 1153. DOI: 10.1051/0004-6361:20034469.

Santos, N. C., M. Mayor, D. Naef, et al. (2002). *Astronomy and Astrophysics* **392**, 215. DOI: 10.1051/0004-6361:20020876.

Santos, N. C., S. G. Sousa, A. Mortier, et al. (2013). *Astronomy & Astrophysics* **556**, A150. DOI: 10.1051/0004-6361/201321286.

Schlaufman, K. C. and J. N. Winn (2016). *The Astrophysical Journal* **825**, 62. DOI: 10.3847/0004-637X/825/1/62.

Service, M., J. R. Lu, R. Campbell, et al. (2016). *Publications of the Astronomical Society of the Pacific* **128**, 095004. DOI: 10.1088/1538-3873/128/967/095004.

Sousa, S. G., N. C. Santos, A. Mortier, et al. (2015). *Astronomy & Astrophysics* **576**, A94. DOI: 10.1051/0004-6361/201425227.

Southworth, J. (2012). *Monthly Notices of the Royal Astronomical Society* **426**, 1291. DOI: 10.1111/j.1365-2966.2012.21756.x.

Spalding, C. and K. Batygin (2016). *The Astrophysical Journal* **830**, 5. DOI: 10.3847/0004-637X/830/1/5.

Storch, N. I., K. R. Anderson, and D. Lai (2014). *Science* **345**, 1317–21. DOI: 10.1126/science.1254358.

Takeda, G., E. B. Ford, A. Sills, et al. (2007). *The Astrophysical Journal Supplement Series* **168**, 297. DOI: 10.1086/509763.

Tanaka, H., T. Takeuchi, and W. R. Ward (2002). *The Astrophysical Journal* **565**, 1257. DOI: 10.1086/324713.

The Astropy Collaboration, T. P. Robitaille, E. J. Tollerud, et al. (2013). *Astronomy & Astrophysics* **558**, A33. DOI: 10.1051/0004-6361/201322068.

Torres, G. (1999). *Publications of the Astronomical Society of the Pacific* **111**, 169. DOI: DOI:10.1086/316313.

Torres, G., D. A. Fischer, A. Sozzetti, et al. (2012). *The Astrophysical Journal* **757**, 161. DOI: 10.1088/0004-637X/757/2/161.

Triaud, A. H. M. J., A. A. Lanotte, B. Smalley, and M. Gillon (2014). *Monthly Notices of the Royal Astronomical Society* **444**, 711. DOI: 10.1093/mnras/stu1416.

Udry, S., M. Mayor, D. Naef, et al. (2000). *Astronomy and Astrophysics* **356**, 590.

Wagner, K., D. Apai, M. Kasper, et al. (2016). *Science* **353**, 673–678. DOI: 10.1126/science.aaf9671.

Wang, J., D. A. Fischer, J.-W. Xie, and D. R. Ciardi (2014). *The Astrophysical Journal* **791**, 111. DOI: 10.1088/0004-637X/791/2/111.

Wang, J., D. A. Fischer, J.-W. Xie, and D. R. Ciardi (2015a). *The Astrophysical Journal* **806**, 248. DOI: 10.1088/0004-637X/813/2/130.

Wang, J., D. A. Fischer, J.-W. Xie, and D. R. Ciardi (2015b). *The Astrophysical Journal* **813**, 130. DOI: 10.1088/0004-637X/813/2/130.

Wittenmyer, R. A., J. Horner, M. Tuomi, et al. (2012). *The Astrophysical Journal* **753**, 169. DOI: 10.1088/0004-637X/753/2/169.

Wittenmyer, R. A., S. Wang, J. Horner, et al. (2013). *The Astrophysical Journal Supplement Series* **208**, 2. DOI: 10.1088/0067-0049/208/1/2.

Wittrock, J. M., S. R. Kane, E. P. Horch, et al. (2016). *The Astronomical Journal* **152**, 149. DOI: 10.3847/0004-6256/152/5/149.

Wizinowich, P. (2013). *Publications of the Astronomical Society of the Pacific* **125**.929, 798–808. DOI: 10.1086/671425.

Wöllert, M. and W. Brandner (2015). *Astronomy & Astrophysics* **579**, A129. DOI: 10.1051/0004-6361/201526525.

Wöllert, M., W. Brandner, C. Bergfors, and T. Henning (2015). *Astronomy & Astrophysics* **575**, A23. DOI: 10.1051/0004-6361/201424091.

Wu, Y. and N. Murray (2003). *The Astrophysical Journal* **589**, 605. DOI: 10.1086/374598.

Wu, Y. and Y. Lithwick (2011). *The Astrophysical Journal* **735**, 109. DOI: 10.1088/0004-637x/735/2/109.

Yelda, S., J. R. Lu, A. M. Ghez, et al. (2010). *The Astrophysical Journal* **725**, 331. DOI: 10.1088/0004-637X/725/1/331.

Zucker, S., T. Mazeh, N. C. Santos, S. Udry, and M. Mayor (2004). *Astronomy and Astrophysics* **426**, 695. DOI: 10.1051/0004-6361:20040384.

Zuckerman, B. (2014). *The Astrophysical Journal* **791**, L27. DOI: 10.1088/2041-8205/791/2/L27.

Chapter 5

SUMMARY AND FUTURE WORK

5.1 Synthesis of dissertation results

The summary and discussion sections of the three preceding chapters, especially Section 4.6, have more detailed analyses specific to each stellar companion survey. This section will briefly discuss the results of the three studies presented in this dissertation and their constraints on four giant planet formation and migration scenarios. The first scenario does not require any sort of migration while the other three assume giant planets form at moderate distances of several au and then migrate via different mechanisms.

In-situ formation scenarios (e.g. Bodenheimer et al., 2000; Batygin et al., 2016; Boley et al., 2016) in which giant planets form where they are found today, without invoking a migration mechanism, are not directly investigated by the studies in this dissertation. Therefore, the majority of the conclusions neither support nor refute *in-situ* planet formation. The only exception is the finding that hot Jupiters are much less likely to have nearby (1-50 au) stellar companions than field stars, as presented in Chapter 3 (Ngo et al., 2016). Although these close stellar companions would disrupt planet formation at separations beyond 0.1 au, they would not directly influence any hot Jupiters forming *in-situ* at separations within 0.1 au. However, the hot Jupiter region may be fed by material falling in from outer parts of the disk and a nearby stellar companion may disrupt this process and reduce the amount of planet-forming material accessible by the proto-hot Jupiter. Therefore, the lack of stellar companions within 1-50 au of hot Jupiters is only compatible with *in-situ* formation models if stellar companions influence the outer disk enough to prevent a giant planet from forming within 0.1 au.

Disk migration scenarios (e.g. Lin et al., 1996) invoke migration without requiring another massive body. Angular momentum exchange between the forming giant planet and the gas disk results in planetary migration. This dissertation suggests that interactions with stellar companions are not the dominant formation pathway for hot Jupiters, leaving disk migration to be one possible alternative. The formation and migration scenario must also explain the observed spin-orbit misalignment and excited orbital eccentricities of hot Jupiters, however, disk migration models are

likely to produce well-aligned and circular orbits. Although Chapters 3 and 4 (Ngo et al., 2016; Ngo et al., 2017) suggest that the stellar companion does not directly misalign the planet, other works (e.g. Spalding and Batygin, 2014; Spalding and Batygin, 2015) show that a misaligned disk can cause misaligned planets.

Some models invoke migration via gravitational interactions with companion planets (e.g. Chatterjee et al., 2008; Wu and Lithwick, 2011; Dawson and Chiang, 2014; Petrovich and Tremaine, 2016) to produce the currently observed population of giant planets. This dissertation does not directly report on planetary companions, but work from our group, targeting the same stars in the surveys from this dissertation does search for planetary companions to giant planets. Knutson et al. (2014) showed that while the transiting hot Jupiter hosts from Chapters 2 and 3 (Ngo et al., 2015; Ngo et al., 2016) show no correlation between a companion planet and misaligned hot Jupiters, the majority of hot Jupiters have more distant giant planet companions. Similarly, Bryan et al. (2016) showed that the RV-detected giant planet host stars from Chapter 4 (Ngo et al., 2017) also often host additional planetary mass companions in the 5-20 au range. Bryan et al. (2016) also reported that inner gas giants have higher orbital eccentricities in multi-body systems compared to those in single planet systems. These results provide good support for the importance of planet-planet interactions in the migration history of giant planets.

Many models have also proposed gravitational interactions between the giant planet and a companion star (e.g. Fabrycky and Tremaine, 2007; Naoz et al., 2012; Naoz et al., 2013; Storch et al., 2014; Dawson et al., 2015; Petrovich, 2015; Anderson et al., 2016; Muñoz et al., 2016) to induce migration and misalignment of giant planets. Typically, these studies raise the eccentricity of the planets with the Kozai-Lidov mechanism (Kozai, 1962; Lidov, 1962), putting the planet on an orbit that has very close approaches to the host star, which raises tides on the planet that damp energy and cause inward migration. The misalignment could arise out of the exchange of eccentricity for the mutual inclination between the planet's orbital plane and a companion star. In Chapter 2 (Ngo et al., 2015), we show a lack of a correlation between a stellar companion and planetary misalignment, suggesting that a stellar companion is not required to produce a misalignment. In Chapter 3 (Ngo et al., 2016), we characterize the population of stellar companions to hot Jupiter systems and limit the influence of Kozai-Lidov migration to be less than 20% of hot Jupiter systems. In Chapter 4 (Ngo et al., 2017), we investigate whether stellar companions dynamically interact with their giant planets and found no evidence

for these interactions. However, in Chapter 3, we did find that hot Jupiters are three times more likely to be in wide (a > 50 au) multi-stellar systems than field stars, suggesting a potential connection between giant planet formation and stellar multiplicity. Hamers (2017) suggested an alternate explanation, where the stellar companion might excite a very distant giant planet (beyond 40 au and detection capabilities) which in turn produces Kozai-Lidov oscillations on the inner giant planet.

Future work involves further testing of the connection between stellar companions, the protoplanetary disk, and the formation of giant planets. One question is to determine whether protoplanetary disks in binary systems have more mass and could form into giant planets more readily. Another question is whether stellar companions may redistribute planet-building materials in the protoplanetary disks and either suppress the formation of small planets or enhance the formation of giant planets in areas with additional materials.

5.2 Work in progress: A vector vortex coronagraph survey for directly imaged giant planets around 200 young, nearby M-stars

The surveys in thsis dissertation searched for stellar companions around stars hosting giant planets with orbital semi-major axes less than 5 au. However, as demonstrated in Figure 1.1, there are many giant planets, or planetary mass objects, on orbits out to hundreds or thousands of au. These objects appear in purple on this figure because they are detected via direct imaging methods. Directly imaging planets is similar in principle to directly imaging stellar companions, however the contrast required to image a planet is much larger as these planets are orders of magnitude fainter than a companion star. While planets like hot Jupiters represent one end of the extreme for giant planet orbits, these very distant objects represent another. The mass estimates of these distant objects have large uncertainty and, due to their distance from the host star, it is not yet clear whether these objects represent the high-mass end of planet formation, or the low-mass end of star formation. One way to probe this question is to compare these objects to the RV-detected giant planets. However, current RV surveys do not find very many planets beyond 5-10 au, while imaging surveys do not find very many objects within 10 au. Discovering both classes of objects in the same environment would allow for a better comparison. For example, if the mass and separation distribution of directly imaged objects match with the distribution of RV giant planets, then we might conclude that these two objects share a formation history. This section briefly describes a survey in progress to find these close-in

directly imaged planetary mass objects in order to make this link.

The challenge of finding planets involves not only detection of a very faint object, but also being able to detect this faint object at very close separations from the very bright host star. To achieve these goals, careful choices in target selection and instrumentation are necessary. The review by Bowler (2016) covers these considerations in more detail. Young giant planets are still emitting energy from their formation processes and therefore we would receive more flux if we targeted young stars. To further increase the contrast between star and planet, smaller and dimmer stars, such as M-dwarfs, are preferred. We also choose closer stars so that our inner angular separation limit corresponds to a smaller physical separation. Combining all of these ideal qualities, the best targets are M-stars in nearby (average distance is 40 pc) young moving groups. Young moving groups also provide an extra advantage as the conversion from brightness ratio to object mass depends a lot on planet formation models, which are very sensitive to age. Therefore, constraining the age through young moving group membership will help constrain the mass of any objects that are found.

Although some studies such as Dressing and Charbonneau (2013) show that small stars are more likely to host small planets than large gas giant planets, these studies are based on planets on short-period orbits so this trend may not hold for more distant planets targeted by this survey. In addition, Bowler (2016) points out that the majority of stars known to be in young moving groups are M-stars, allowing for more target choices. Bowler (2016) also identifies stars in young moving groups as the ideal group for imaging surveys as they strike the right balance between age and distance. Young T Tauri stars may host brighter planets, but they are four to five times more distant than young moving groups. And while there may be more field stars at closer distances, they are much older. Planets that are several billion years old will be significantly fainter.

Our survey uses a new coronagraph installed on Keck/NIRC2 in 2015. The vector vortex coronagraph (Mawet et al., 2005; Femenía Castellá et al., 2016) is different from traditional occulting coronagraphs, which physically block light from the target star. Instead, the vector vortex coronagraph, also known as an "annular groove phase mask", is transparent to incoming radiation. The mask is a series of concentric gratings that introduce a phase ramp to incoming on-axis light. This results in a singularity that destructively interferes all on-axis light, that is, light from the target star. Because the vector vortex coronagraph does not physically block the light,

this allows imaging of planets at very small angular separations. The inner working angle for Keck vector vortex coronagraph is on the order of λ/D, or around 80 milliarcseconds, several times smaller than Keck's traditional spot coronagraphs. These vector vortex coronagraphs are engineered for specific wavelengths. For this survey, longer wavelengths are more favorable as the young giant planets are cooler than stars and emit more energy at longer wavelengths. We choose the Keck L' band, which has a central wavelength close to 3.8μm.

This survey is complementary to other large surveys on recently commissioned second generation adaptive optics systems, such as GPIES with the GPI instrument on Gemini-South and the SPHERE survey on the Very Large Telescope. GPIES is a 600-star survey still in progress, with one new planet, 51 Eri b, presented by Macintosh et al. (2015). The first planet discovered using SPHERE was also recently announced (Wagner et al., 2016). The Keck vector vortex survey's longer wavelength and smaller inner working angle is sensitive to different ranges of planet mass and separations. In addition, GPI and SPHERE are in the southern hemisphere while Keck/NIRC2 is in the northern hemisphere. On the other hand, GPI and SPHERE have multi-wavelength capabilities and in the case of SPHERE, also different polarimetric observing modes.

Figure 5.1 shows the detection probability for a planet of a given mass and separation averaged over all the stars selected for this survey. These are end-to-end calculations, starting with models of stellar images on the NIRC2 detector, including NIRC2 noise sources, and averaging over possible planetary orbital parameters. Combining this sensitivity analysis with occurrence rate estimates of giant planets around M-stars from microlensing surveys (Clanton and Gaudi, 2014), the expected planet yield is 1-10 planets out of 200 stars. The large uncertainty in the occurrence rate power law is partially responsible for the large range in expected planet yield.

This survey began in August 2015 and will be complete by July 2017. As of this writing, 21 out of 26 allocated nights have been completed and 148 stars have been observed. No candidate companions have been found. However, the full data reduction pipeline is not yet complete. For a typical target in our survey, we are sensitive to a $6\,M_{Jup}$ planet at 13 au (0.3 arcseconds), and a $3\,M_{Jup}$ planet at 22 au (0.5 arcseconds). We are currently working to improve our sensitivity near the inner working angle, with a goal of detecting $6\,M_{Jup}$ planets at 4 au (0.1 arcseconds).

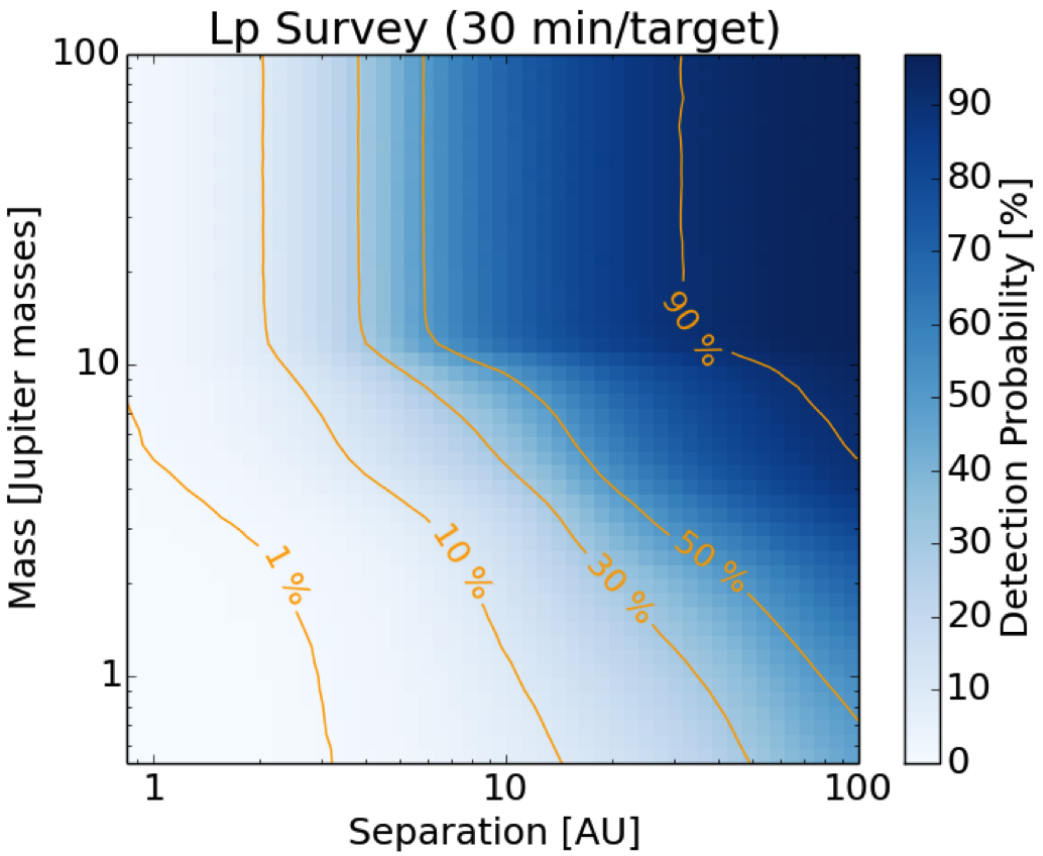

Figure 5.1: The detection probability for objects of a given mass and separation, averaged over all stars in the ongoing Keck vector vortex coronagraph survey, assuming 30 minutes of open shutter time.

References

Anderson, K. R., N. I. Storch, and D. Lai (2016). *Monthly Notices of the Royal Astronomical Society* **456**, 3671. DOI: 10.1093/mnras/stv2906.

Batygin, K., P. H. Bodenheimer, and G. P. Laughlin (2016). *The Astrophysical Journal* **829**.2, 114. DOI: 10.3847/0004-637X/829/2/114.

Bodenheimer, P., O. Hubickyj, and J. J. Lissauer (2000). *Icarus* **143**, 2. DOI: 10.1006/icar.1999.6246.

Boley, A. C., A. P. G. Contreras, and B. Gladman (2016). *The Astrophysical Journal* **817**, L17. DOI: 10.3847/2041-8205/817/2/L17.

Bowler, B. P. (2016). *Publications of the Astronomical Society of the Pacific* **128**.968, 102001. DOI: 10.1088/1538-3873/128/968/102001.

Bryan, M. L., H. A. Knutson, A. W. Howard, et al. (2016). *The Astrophysical Journal* **821**, 89. DOI: 10.3847/0004-637X/821/2/89.

Chatterjee, S., E. B. Ford, S. Matsumura, and F. A. Rasio (2008). *The Astrophysical Journal* **686**, 580. DOI: 10.1086/590227.

Clanton, C. and B. S. Gaudi (2014). *The Astrophysical Journal* **791**, 91. DOI: 10.1088/0004-637X/791/2/91.

Dawson, R. I. and E. Chiang (2014). *Science (New York, N.Y.)* **346**, 212–216. DOI: 10.1126/science.1256943.

Dawson, R. I., R. A. Murray-Clay, and J. A. Johnson (2015). *The Astrophysical Journal* **798**, 66. DOI: 10.1088/0004-637X/798/2/66.

Dressing, C. D. and D. Charbonneau (2013). *The Astrophysical Journal* **767**, 95. DOI: 10.1088/0004-637X/767/1/95.

Fabrycky, D. and S. Tremaine (2007). *The Astrophysical Journal* **669**, 1298. DOI: 10.1086/521702.

Femenía Castellá, B., E. Serabyn, D. Mawet, et al. (2016). *Adaptive Optics Systems V*. Vol. 9909. Proceedings of the SPIE, p. 990922. DOI: 10.1117/12.2233228.

Hamers, A. S. (2017). *The Astrophysical Journal* **835**, L24. DOI: 10.3847/2041-8213/835/2/L24.

Knutson, H. A., B. J. Fulton, B. T. Montet, et al. (2014). *The Astrophysical Journal* **785**, 126. DOI: 10.1088/0004-637X/785/2/126.

Kozai, Y. (1962). *The Astronomical Journal* **67**, 591. DOI: 10.1086/108790.

Lidov, M. L. (1962). *Planetary and Space Science* **9**, 719. DOI: 10.1016/0032-0633(62)90129-0.

Lin, D. N. C., P. Bodenheimer, and D. C. Richardson (1996). *Nature* **380**, 606. DOI: 10.1038/380606a0.

Macintosh, B., J. R. Graham, T. Barman, et al. (2015). *Science* **350**, 64. DOI: 10.1126/science.aac5891.

Mawet, D., P. Riaud, O. Absil, and J. Surdej (2005). *The Astrophysical Journal* **633**, 1191. DOI: 10.1086/462409.

Muñoz, D. J., D. Lai, and B. Liu (2016). *Monthly Notices of the Royal Astronomical Society* **1093**, 8. DOI: 10.1093/mnras/stw983.

Naoz, S., W. M. Farr, Y. Lithwick, F. A. Rasio, and J. Teyssandier (2013). *Monthly Notices of the Royal Astronomical Society* **431**, 2155. DOI: 10.1093/mnras/stt302.

Naoz, S., W. M. Farr, and F. A. Rasio (2012). *The Astrophysical Journal* **754**, L36. DOI: 10.1088/2041-8205/754/2/L36.

Ngo, H., H. A. Knutson, M. L. Bryan, et al. (2017). *Astronomical Journal* **153**, 242. DOI: 10.3847/1538-3881/aa6cac.

Ngo, H., H. A. Knutson, S. Hinkley, et al. (2015). *The Astrophysical Journal* **800**, 138. DOI: 10.1088/0004-637X/800/2/138.

Ngo, H., H. A. Knutson, S. Hinkley, et al. (2016). *The Astrophysical Journal* **827**, 8. DOI: 10.3847/0004-637X/827/1/8.

Petrovich, C. (2015). *The Astrophysical Journal* **799**, 27. DOI: 10.1088/0004-637X/799/1/27.

Petrovich, C. and S. Tremaine (2016). *The Astrophysical Journal* **829**, 132. DOI: 10.3847/0004-637X/829/2/132.

Spalding, C. and K. Batygin (2014). *The Astrophysical Journal* **790**, 42. DOI: 10.1088/0004-637X/790/1/42.

Spalding, C. and K. Batygin (2015). *The Astrophysical Journal* **811**, 82. DOI: 10.1088/0004-637X/811/2/82.

Storch, N. I., K. R. Anderson, and D. Lai (2014). *Science* **345**, 1317–21. DOI: 10.1126/science.1254358.

Wagner, K., D. Apai, M. Kasper, et al. (2016). *Science* **353**, 673–678. DOI: 10.1126/science.aaf9671.

Wu, Y. and Y. Lithwick (2011). *The Astrophysical Journal* **735**, 109. DOI: 10.1088/0004-637x/735/2/109.